Unraveling the mechanisms of climbing fiber synapse specificity in the cerebellum

Maëla Paul

Sorbonne Université

Ecole doctorale Cerveau, Cognition, Comportement (Ed158)

Centre de Recherche Interdisciplinaire en Biologie, Collège de France

Unraveling the mechanisms of climbing fiber synapse specificity in the cerebellum

Par Maëla Paul

Thèse de doctorat de Neurosciences

Dirigée par le Dr. Fekrije Selimi

Présentée et soutenue publiquement le 15 mai 2023

Devant un jury composé de :

Pr. Peter Scheiffele, président
Pr. Corette Wierenga, rapportrice
Pr. Joris de Wit, rapporteur
Dr. Cécile Charrier, examinatrice
Dr. Fekrije Selimi, directrice de thèse

“One, remember to look up at the stars and not down at your feet. Two, never give up work. Work gives you meaning and purpose and life is empty without it. Three, if you are lucky enough to find love, remember it is there and don't throw it away.”

— Stephen Hawking

ACKNOWLEDGEMENTS

First of all, I would like to thank the members of my jury, Pr. Corette Wierenga and Pr. Joris de Wit for taking the time to review my manuscript, Dr. Cécile Charrier for her follow-up and advice throughout my PhD and Pr. Peter Scheiffele for chairing my jury.

I would like to address my most sincere thanks to Fekrije, my PhD supervisor, I have gained so much from you. I may have found you tough with me at first, but I have grown stronger and more confident than I was! Five years ago, I joined the lab as a student and I feel like I have become a researcher. Thank you for trusting me with this ambitious project which I know is very special and important to you. This PhD has been an outstanding scientific adventure. I have always held you in high esteem, you are a great woman scientist, and I hope to be one day.

Ma très chère Séverine, je n'ai pas vraiment de mot pour décrire notre relation. Malgré nos neurones pas toujours connectés au même moment, on a toujours réussi à être sur la même longueur d'onde, c'est normal on est des « type I » ! Du projet « code » est progressivement né une profonde et sincère amitié. Tu as toujours été un véritable pilier pour moi pendant toutes ces années. Merci pour tous tes conseils, ton aide, ton soutien infini mais surtout pour ta bienveillance. Je me sens extrêmement chanceuse d'avoir pu travailler à tes côtés, ne change rien.

I would also thank all the incredible people in the lab; Shayan for your kindness, your good mood, your sympathy, your altruism and our evening, sometimes nightly, laboratory discussions; Beetsi for the guacamole, the tequila, your "french-spanish" language, but mostly for all our laughs; Léa pour ton aide précieuse pour le projet "code" et pour ta bonne humeur; Adeline, Maxime et Mélanie, avec qui j'ai eu la chance de partager mes premières années de thèse.

Je voudrai aussi remercier les Chadocs pour tous ces vendredi soirs de décompression passés au Pub Saint Hilaire, qui m'ont permis de comprendre que les hauts et les bas sont le processus normal de toute thèse.

Un immense merci à mon amoureux Romain, récemment devenu mon mari. Merci pour ton éternel support, ta compréhension, ta patience pour tous les soirs rentrés tard, pour les dimanches passés à travailler, d'avoir supporté mon stress, écouté mes inquiétudes. Tu as toujours compris que la Science pouvait prendre une part importante dans ma vie, même si je l'admets, parfois elle a pu prendre beaucoup de place. Merci d'avoir été à mes côtés, et merci de m'avoir aidé à faire la part des choses quand cela a été nécessaire.

Je voudrais aussi remercier mes amis pour la vie à côté du labo, car oui, il y a une vie en dehors du labo. Vous avez grandement contribué à mon équilibre personnel, vous êtes une vraie famille pour moi. Merci d'avoir toujours été compréhensifs quand je n'ai pas pu être présente.

TABLE OF CONTENTS

LIST OF ABBREVIATIONS

-A-

AAV: adeno-associated virus

ADAM: Disintegrin and metalloproteinase domain-containing protein

AIS: axon initial segment

AMPA: α-amino-3-hydroxy-5-methyl-4-isoxazolepropionic acid

AMPAR: α-amino-3-hydroxy-5-methyl-4-isoxazolepropionic acid receptor

ASD: autism spectrum disorders

-B-

BAI: Brain-specific angiogenesis inhibitor

Bdnf: Brain-derived neurotrophic factor

BEN: BEN/SC1/DM-GRASP

BG: Bergmann glial cells

BMP4: Bone morphogenetic protein 4

BoNT/B: *clostridial botulinum* neurotoxin serotype B-light chain

-C-

C3: Complement C3

C1Q: Complement component 1q

C1QL1: Complement C1q-like protein 1

Ca^{2+}: Calcium

CA: *Cornu Ammonis*

CAM: Cell adhesion molecule

Cas9: CRISPR associated protein 9

CBLN: Cerebellin

CF: climbing fiber

CHL1: close homolog of L1 protein

Cdh: Cadherin

CNO: clozapine-N-oxide

CNS: Central nervous system

CR3: Complement Receptor 3

Crh : Corticotropin-releasing factor

CRISPR: Clustered regularly interspaced short palindromic repeats

Crtac1: Cartilage acidic protein 1

CTL: Control

Cx3cl1: C-X3-C Motif chemokine ligand 1

CX_3CR_1: CX3C chemokine receptor 1

-D-

DCC: Netrin receptor

DCN: deep cerebellar nuclei

DEG: differentially expressed gene

DIV: *day in vitro*

dLGN: dorsal lateral geniculate nucleus

DREADD: Designer Receptors Exclusively Activated by Designer Drug

DSCAM: Down syndrome cell adhesion molecule homolog

-E-

EC: entorhinal cortex

EGL: external granular layer

Egr1: Early growth response protein 1

EphA: Ephrin type-A receptor

EphB: Ephrin type-B receptor

EPSC: excitatory postsynaptic current

-F-

Fgf13: Fibroblast growth factor 13

FLRT: Leucine-rich repeat transmembrane protein

Fstl1: Follistatin-related protein 1

-G-

GABA: γ-aminobutyric acid

$GABA_AR$: γ-aminobutyric acid type A receptor

Gαq: Gq protein alpha subunit

GC: granule cell

GCP: granule cell precursor

GFP: Green fluorescent protein

GL: granular layer

GLAST: glutamate aspartate transporter

GluA2: AMPA glutamate receptor 2

GluD: glutamate receptor δ

GPCR: G protein-coupled receptor

Gpr123: G protein-coupled receptor 123

gRNA: guide RNA

-H-

Hevin: SPARC-like protein 1

hM4Di: modified form of the human M4 muscarinic (hM4) receptor

Homer3: Homer protein homolog 3

hSyn: Human synapsin 1 gene promoter

-I-

ID: intellectual disability

IEG: immediate early genes

iEGL, inner granular layer

Ig: immunoglobulin

IGL: internal granular layer

IgSF: immunoglobulin superfamily

IO: inferior olive

ION: inferior olivary neuron

IPSC: inhibitory postsynaptic current

Ires: internal ribosome entry site

ItgB1: Integrin beta-1

-K-

KI: Knock-in

Kir2.1: inward-rectifier potassium channel

KO: Knock-out

-L-

Lphn: Latrophilin

LGI: Leucine-rich glioma-inactivated protein

LGN: lateral geniculate nucleus

LOF: Loss of function

LTP: Long-term potentiation

LTD: Long-term depression

LRG: late response gene

LRR: leucine-rich repeat family

LRRTM: Leucine-Rich Repeat-domain containing transmembrane protein

-M-

mGRASP: Mammalian GFP reconstruction across synaptic partners

MF: mossy fiber

mGluR1: Metabotropic glutamate receptor1
ML: molecular layer
mRNA: Messenger RNA
MS: mass spectrometry

-N-

NBQX: 2,3-dioxo-6-nitro-7-sulfamoyl-benzo[f]quinoxaline
NDMA: *N*-methyl-D-aspartic acid
NDMAR: *N*-methyl-D-aspartic acid receptor
NF186 : Neurofascin isoform 186
Npas4 : Neuronal PAS domain-containing protein 4
Nrcam: Neuronal cell adhesion molecule
NRXN: Neurexin
NLGN: Neuroligin

-O-

oEGL: outer external granular layer
OPC: oligodendrocyte progenitor cell
OSNs: olfactory sensory neurons
OR: olfactory receptor

-P-

PF: parallel fiber
PC: Purkinje cell
Pcdh: Protocadherin
PCL: Purkinje cell layer
PCR: Polymerase Chain reaction
PKCγ: Protein kinase Cγ
PLCβ4: 1-Phosphatidylinositol-4,5-bisphosphate phosphodiesterase beta-4
PlxnC1: Plexin-C1
PPD: paired-pulse depression
PPF: paired-pulse facilitation
PV: parvalbumin-positive neuron
PSD: Postsynaptic density
PSD95: Postsynaptic density protein 95
PSD93: Postsynaptic density protein 93

-R-

RAC1: Rac Family Small GTPase 1
RFP: red fluorescent protein
RGC: retinal ganglion cell
ROBO: Roundabout
RNA: Ribonucleic acid
RTN4R: Reticulon-4 receptor
RTqPCR: Quantitative reverse transcription PCR

-S-

SAP102: synapse-associated protein 102
SC: Schaffer collateral
Sema: Semaphorin
Shisal1: protein shisa-like-1
shRNA: short hairpin RNA
Slit: Slit homolog protein
Slitrk1: Slit and neurotrophic tyrosine kinase receptor-like protein 1
SLM: *lacunosum moleculare*
smFISH: single molecule Fluorescent *In Situ* Hybridization
SPARC: secreted protein acidic and rich in cysteine

SPARCL1: secreted protein acidic and rich in cysteine like 1

SO: *stratum oriens*

SS4: splice site 4

SST+: somatostatin positive

SR: *stratum radiatum*

SynGap1: Synaptic Ras GTPase activating protein 1 homolog

SV: synaptic vesicle

-T-

TC: Thalamo-cortical relay neurons

Thy1: Thy-1 membrane glycoprotein

Tmem: Transmembrane protein

TSP: Thrombospondin

TeNT: Tetanus toxin

TTX: Tetrodotoxin

-V-

VAMP : Vesicle-associated membrane protein

VDCC: P/Q-type voltage-dependent Ca^{2+} channels

VGAT: vesicular GABA transporter

VGLUT1: Vesicular glutamate transporter1

VGLUT2: Vesicular glutamate transporter2

-W-

WT: wild-type

LIST OF FIGURES

SUMMARY

Brain function is based on the establishment of highly stereotyped neuronal networks through precise and diverse synaptic contacts. Understanding what controls synapse specificity and identity is thus mandatory not only to understand brain functions but also the etiology of synaptopathies such as autism spectrum disorders or schizophrenia. While Sperry postulated the chemo-affinity hypothesis in the 1960s, implying a molecular combination for each synapse type in the assembly of neural circuits, the existence and nature of these combinations have not been demonstrated. To address this question, I focused on the olivo-cerebellar network involved in the control of motor function and cognitive processes. In this well characterized circuit, two different excitatory inputs, the climbing fibers and the parallel fibers, connect the same target neuron, the Purkinje cell, initially on the same territory and then on distinct and non-overlapping territories in the mature stage. It is therefore an ideal model to study the molecular basis of synapse identity. Based on previous data from our laboratory and others, the expression of a specific C1Q-related protein in each input is necessary, but not sufficient, for proper formation of climbing fibers and parallel fibers synapses on Purkinje cells. Loss of function of the specific C1Q-related protein at each input, CBLN1 at the parallel fibers and C1QL1 at the climbing fiber, result in the loss of about half of the respective synapses, suggesting the involvement of other molecules. Thus, I searched for the nature of this molecular combination, focusing on identifying the one coding for climbing fiber/Purkinje cell synapse identity. I combined neuron-specific transcriptomics and bioinformatics analyses followed by neuron-specific loss of function using genome editing *in vivo* during mouse development. I have identified a combination of presynaptic secreted molecules underlying the identity of the climbing fiber/Purkinje cell synapses. Surprisingly, I have also discovered that this specific code is generated, during postnatal development, in an afferent-specific manner starting from a common code. Climbing fibers actively and gradually specify their synaptic molecular identity while parallel fibers rely on the “original common code”. This result suggests that synapse molecular diversification follows input-specific molecular rules. Finally, I am currently testing whether the specification of the molecular code is regulated by neuronal activity during postnatal development. This study represents an unprecedented dissection of the mechanisms controlling circuit development at a single neuron type level with important consequences for our understanding of the etiology of neurodevelopmental disorders.

RÉSUMÉ

Le fonctionnement du cerveau repose sur la mise en place de réseaux neuronaux hautement stéréotypés *via* des contacts synaptiques précis mais variés. Comprendre ce qui contrôle la spécificité et l'identité des synapses est donc indispensable à la compréhension non seulement du cerveau mais aussi de l'étiologie des synaptopathies, comme les troubles du spectre autistique ou encore la schizophrénie. En 1963, Sperry propose l'hypothèse de chimio-affinité impliquant que chaque type de synapse exprime une combinaison moléculaire spécifique qui régule la connectivité du circuit. Cependant, l'existence et la nature de telles combinaisons restent toujours à démontrer. Afin de tester cette hypothèse, je me suis concentrée sur le réseau olivo-cérébelleux qui est impliqué dans de nombreux processus cognitifs ainsi que dans le contrôle des fonctions motrices. Dans ce système, les fibres grimpantes et les fibres parallèles se connectent au même neurone cible, la cellule de Purkinje, initialement sur un territoire commun, puis plus tard sur des territoires distincts. Ce modèle est ainsi idéal pour l'étude les mécanismes moléculaires à l'origine de la spécificité des synapses. Chaque afférence de la cellule de Purkinje exprime une protéine différente de la famille C1Q qui est nécessaire, mais pas suffisante, à la formation de leurs synapses sur leur cible. J'ai donc cherché à déterminer la nature de la combinaison moléculaire qui est à l'origine de l'identité de la synapse fibre grimpante/cellule de Purkinje. Pour cela, j'ai combiné des analyses de transcriptomiques et de bio-informatiques, avec des expériences de perte de fonction réalisées de manière neurone-spécifique chez la souris. J'ai identifié une combinaison de molécules présynaptiques qui sont sécrétées et qui sous-tendent l'identité de la synapse fibre grimpante/cellule de Purkinje. Étonnamment, j'ai découvert que ce code spécifique est généré, au cours du développement postnatal, à partir d'un code commun aux deux afférences. De plus, les fibres grimpantes spécifient activement leur identité moléculaire synaptique alors que les synapses des fibres parallèles conservent le "code commun" initial. Enfin, je suis actuellement en train de tester si cette spécification du code moléculaire est régulée par l'activité neuronale au cours du développement postnatal. Pour conclure, cette étude constitue une dissection sans précédent des mécanismes contrôlant le développement des circuits convergeant vers un seul type de neurone, et ouvrant la voie à notre compréhension de l'origine des troubles du neurodéveloppementaux.

INTRODUCTION

"*Unfortunately, nature seems unaware of our intellectual need for convenience and unity, and very often takes delight in complication and diversity*"

— Ramón y Cajal

Part I - The molecular complexity of synapses

1. From “the synapsis” to “synapses”

In 1873, Camillo Golgi's accidental discovery of silver staining, in which potassium dichromate and silver nitrate were applied to produce a black impregnation of neurons, marked the beginning of a new field in neuroscience. From this finding, two opposed doctrines were born. Golgi postulated the “reticular theory” where the different elements of the nervous system formed a gigantic syncytium similar to a reticulum network. Few years later, Ramón y Cajal, using the same staining method, hypothesized the "neuron doctrine" which states that the nervous system is made up of independent cells, later called neurons. He observed in the cerebellum that Baskets cells and Stellate cells terminals are ended, and do not appear in continuity with Purkinje cells (PCs) **(Figure 1)**. To support his hypothesis, he sectioned some PC axons in the cat and showed 24 hours later that, unlike PCs, Basket cells and Stellate cells do not degenerate, suggesting that they are not in continuity **(Figure 1)** (Cajal 1909).

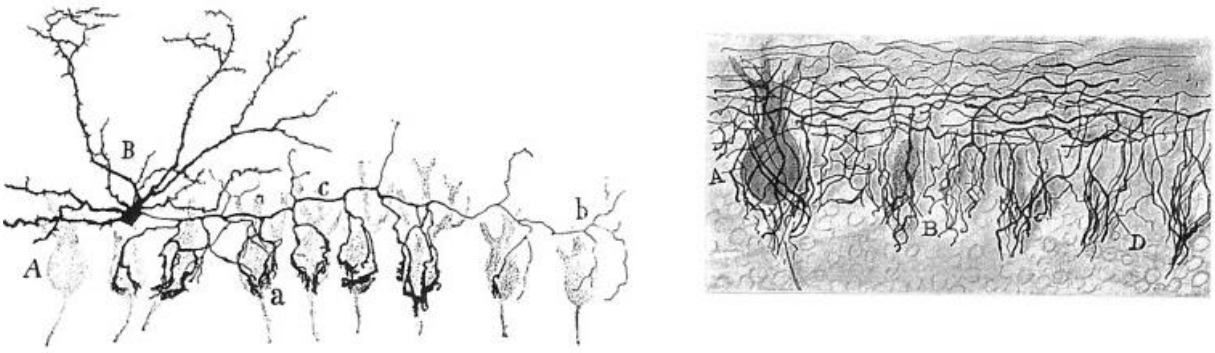

Figure 1. The “neuron doctrine”, a non-continuity between cells.
Golgi-impregnated cerebellum section by Ramón y Cajal. Left: Ending terminals of Basket cell. A, PCs stained using osmic acid staining; B, Basket cell; a, b, Basket cell ramifications around PC soma; c, Basket cell axon. Right: Ending terminals of Basket cells and Stellate cells 24 hours after PC axons were cut. A, Normal PC with intact axon; B, D, PC is atrophied but Basket cells are still around PC soma. From Bennett 1999.

In parallel, Charles Sherrington, an English physiologist who was working on spinal motor reflexes and on proprioception in the cerebellum, proposed that discontinuity would play the role of “functional boundary” with a “valve like function” allowing the conduction of information in only one direction (Bennett 1999; Sotelo 2020). In 1897, when his friend Michael Foster invited him to contribute to his “Textbook of Physiology”, he named such a

special connection “synapsis” (Foster and Sherrington 1897). The word was derived from the Greek *synaptein* “bind together, be connected with”, which comes from *syn*- “together" and *haptein* "to fasten". At that time, synapses were too small to be seen by microscopes. It was only with the advent of electron microscopy, the second great revolution in neuroscience, that these structures could be confirmed. In 1955, at the Rockefeller Institute, Sanford Palay and George Palade published the first electron microscopy of a synapse showing the existence of a presynaptic and a postsynaptic compartment separated by an extracellular space, the synaptic cleft **(Figure 2)** (Palade 1954; Palay and Palade 1955).

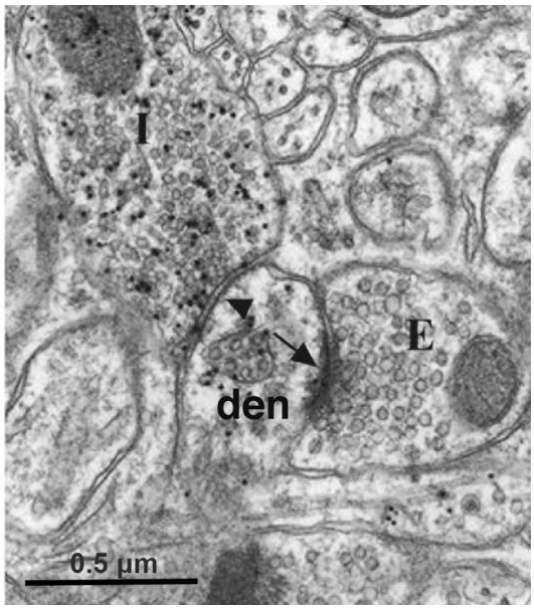

Figure 2. Electron micrograph of two presynaptic axonal terminals synapsing on a dendrite in the abducens nucleus.

The two arrow-heads show the two synaptic complexes. Pre- and postsynaptic membranes are distinct, synaptic vesicles and presynaptic mitochondria are visible. Den, dendrite; I, inhibitory synapse; E, excitatory synapse. From Palay 1958; adapted from Sotelo 2020.

Gray’s investigation on the ultrastructural characteristics of the pre- and the postsynaptic terminals identified two major types of synapses in the brain: asymmetric called “Gray type I” and symmetric called “Gray type II” **(Figure 3 A, B)** (Gray 1959). In electron microscopy images, the type I synapses are characterized by a thick density at the postsynaptic membrane, the postsynaptic density (PSD), and contain rounded vesicles. Type I synapses were later confirmed to be excitatory synapses. In opposition, type II synapses do not possess a thick PSD, have flattened vesicles and underly inhibitory transmission. Both type I and II synapses are made between the axon and the dendrites (axo-dendritic). However, inhibitory synapses can be

also made between the axon and the soma (axo-somatic), as well as the axon and the axon initial segment (axo-axonic). The postsynaptic compartment of these two types of synapses is composed of different scaffolding proteins. PSD95 is known to preferentially localize at glutamatergic synapses and interact with NMDA and AMPA receptors (Kornau et al. 1995; Hunt et al. 1996; Kennedy 2000; Schnell et al. 2002) while gephyrin is localized at inhibitory synapses and interact with GABAergic and glycinergic receptors **(Figure 3 C, D)** (Kirsch et al. 1996; Essrich et al. 1998; Lévi et al. 1999). In addition to GABAergic and glycinergic synapses, numerous neurotransmitters (e.g., acetylcholine, dopamine, serotonin) as well as neuromodulators (e.g., endocannabinoids, retinoic acid, nitric oxide) were discovered, thereby increasing the complexity and diversity of synapses.

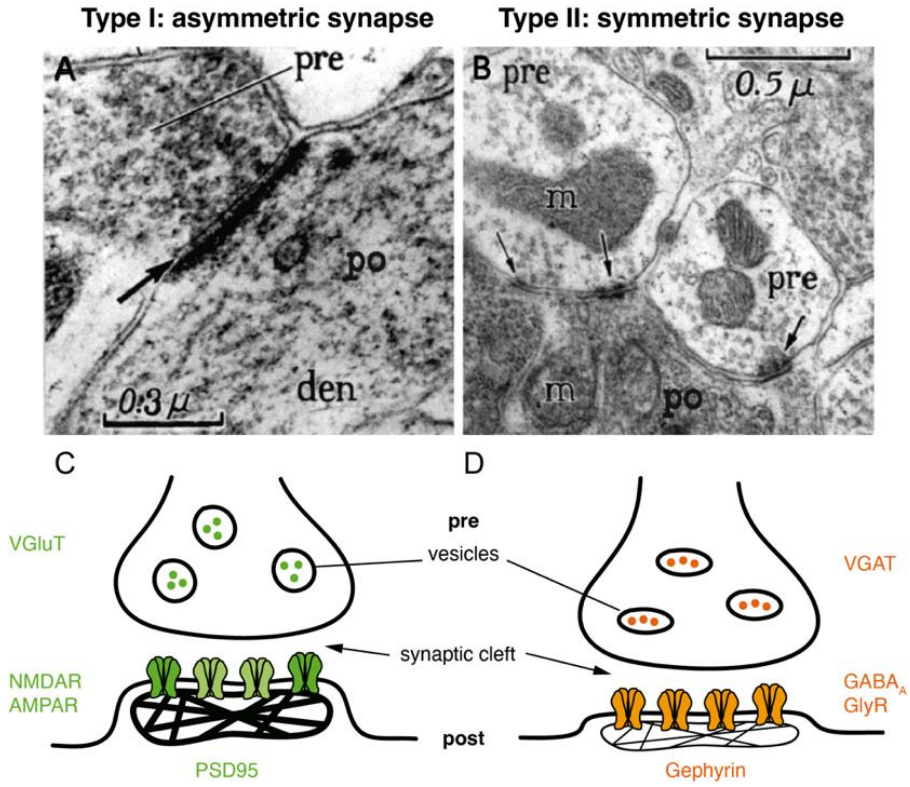

Figure 3. Excitatory (asymmetric) synapse vs inhibitory (symmetric) synapses.
Electronic microscopy of (A) type I synapse with a postsynaptic structure thicker than the presynaptic membrane, (B) type II synapse that shows an equal thickness of the pre- and postsynaptic membranes. Den, dendrite; m, mitochondria; po, postsynaptic; pre, presynaptic. Schematic representation of (C) an excitatory synapse and (D) are inhibitory synapse. Adapted from Gray 1959 and González-Calvo 2018).

2. Synapse diversity, specific connectivity and function

The advent of proteomic approaches as well as of mass spectrometry has revealed a degree of synaptic molecular diversity that is far more complex than one might have imagined **(Figure 4)**. Synaptosomes preparation, from biochemically isolated synapses through subcellular fractionation, revealed the presence of more than 2,000 differentially expressed proteins (Gray 1960; De Robertis et al. 1961; Gray and Whittaker 1962; Whittaker 1993; Peng et al. 2004; Collins et al. 2006). Moreover, differential splicing and post-translational modification increase the complexity of synapses (Trinidad et al. 2008; Schreiner et al. 2014).

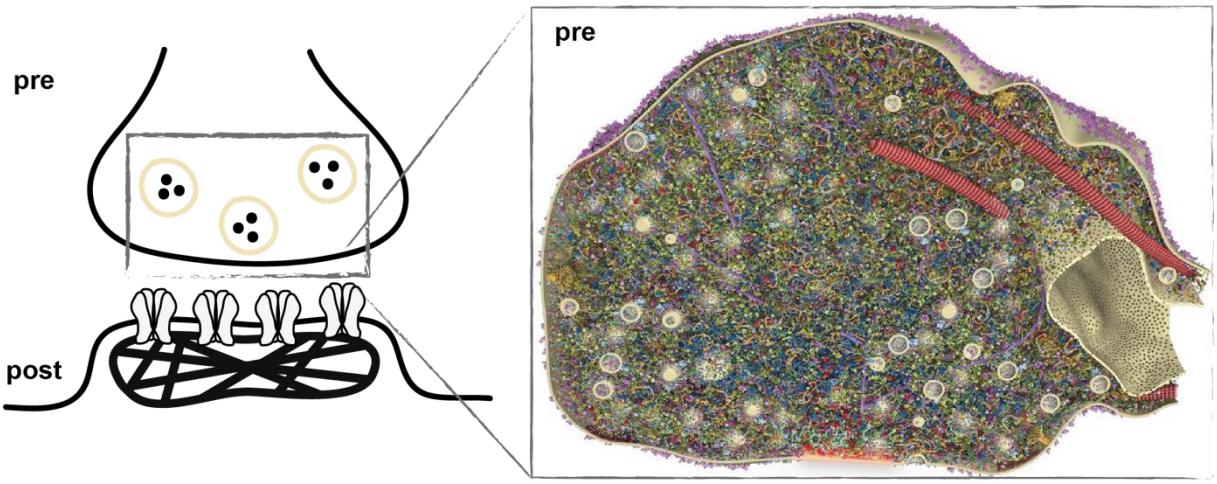

Figure 4. A total average of 300,000 molecules per single synapse.
Section of a synaptic bouton after 3D reconstruction of its molecular architecture. Only 60 proteins are shown here but represented in copy number, revealing a crowded synaptic active zone. The yellow circles represent neurotransmitters vesicles, actin filaments can be seen in purple and tubulin in red. Adapted from Wilhelm et al. 2014.

Synaptic molecular diversity generates a large range of synaptic functions, allowing different computational processing of information in a synapse-specific manner. Synapses can manifest a wide variety of synaptic transmission, strength, kinetics or even plasticity. They can have different vesicle release probability with either short-term facilitation or depression, respectively referring to an increase or decrease of synaptic strength after a short train of repeated stimuli. Synapses can also exhibit different long lasting synaptic plasticity, a fundamental process for learning and memory according to the Hebbian theory (reviewed in Malenka and Bear 2004). Long-term potentiation (LTP) is a persistent strengthening of synaptic transmission while long-term depression (LTD) results in a decrease of synaptic transmission.

This diversity of molecularly distinct synapses is present at different scales of the brain, between different regions, neurons and domains of the same neuron **(Figure 5)**. A study of PSD protein profile demonstrates differences between forebrain and cerebellum synaptic molecular composition (Cheng et al. 2006). Zhu and colleagues genetically labeled two postsynaptic proteins at excitatory synapses, PSD95 and SAP102, by fusing a genetically encoded fluorescent protein onto their C-terminus in mice. These two proteins are assembled into physically distinct complexes, with synapses expressing only PSD95 or SAP102, and some expressing both. They observed that each region of the brain is characterized by a "signature" of synapse composition (Zhu et al. 2018). Moreover, synapse diversity is also present between different neuron types. Cell-type specific proteomics on synaptosome preparation revealed a wide range of physiological and molecular signatures among different neuron types (Selimi et al. 2009; Heller et al. 2012; Uezu et al. 2016; Uezu and Soderling 2019; Apóstolo et al. 2020; Marcassa et al. 2023). In the parallel fiber/Purkinje cell synapses of the cerebellum, among the 65 proteins identified, some were common between the different types of cerebellar neurons and others were specific to this synapse type (Selimi et al. 2009). Finally, molecularly distinct synapses have been also identified along a single neuron. For instance in CA1 hippocampal neurons, synaptic molecules were found to be differentially distributed along CA1 dendritic arborization (reviewed in Apóstolo and de Wit 2019). Zhu et al. also identified a differential distribution of PSD95 and SAP102 radially and tangentially within CA1 dendrites. In the cerebellar cortex, different subcellular localization of Gephyrin isoforms were found between the axon initial segment (AIS), dendrites and soma of PC (Dos Reis et al. 2022).

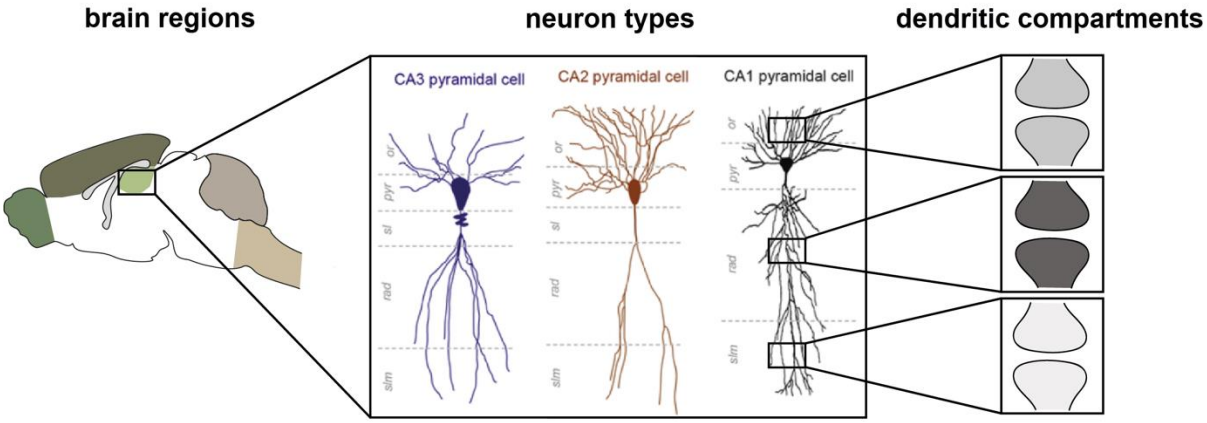

Figure 5. Synapse molecular diversity is present at three distinct levels in the brain.
Molecularly distinct synapses are differentially distributed within brain regions, neurons types and dendritic segment on the same neuron. Adapted from Pignatelli and Rockland 2020.

Evolutionary studies indicate a link between increased synaptic molecular diversity and the sophistication of neuronal architecture in mammals. A huge enlargement of the synaptic proteomes between invertebrates and vertebrates due to genome duplications has been documented (Emes et al. 2008). Interestingly, a more recent diversification occurred in mammals most likely to support the expansion and the complexification of the central nervous system. Indeed, the mammalian central nervous system is composed of hundred billions of neurons, and each neuron makes an average of a thousand connections (Herculano-Houzel 2012). Electron microscopy reconstruction from layer 4 of the mouse cerebral cortex illustrates this dense and compact connectomic characterizing neuronal circuitry **(Figure 6)**. Within 500,000 μm^3 of cortical tissue, Motta and colleagues counted 89 neurons, 2.7 m of neural cables and approximately 400,000 synapses (Motta et al. 2019). The adult human brain is made up of 10 billions of these small cubes. Nevertheless, the connectome is highly organized and is assembled in a very reproducible way. For instance in the fly visual system, the "core connectome" which is composed of 20 neuron types organized in 7 columns in the medulla exhibits less than 1% wiring variations between neighboring columns (Takemura et al. 2015). Thus, it is suggested that synaptic molecular diversity would enable the generation of a variety of identities that are specific and unique to each synapse type, allowing the specification of the connectivity (Zhu et al. 2018).

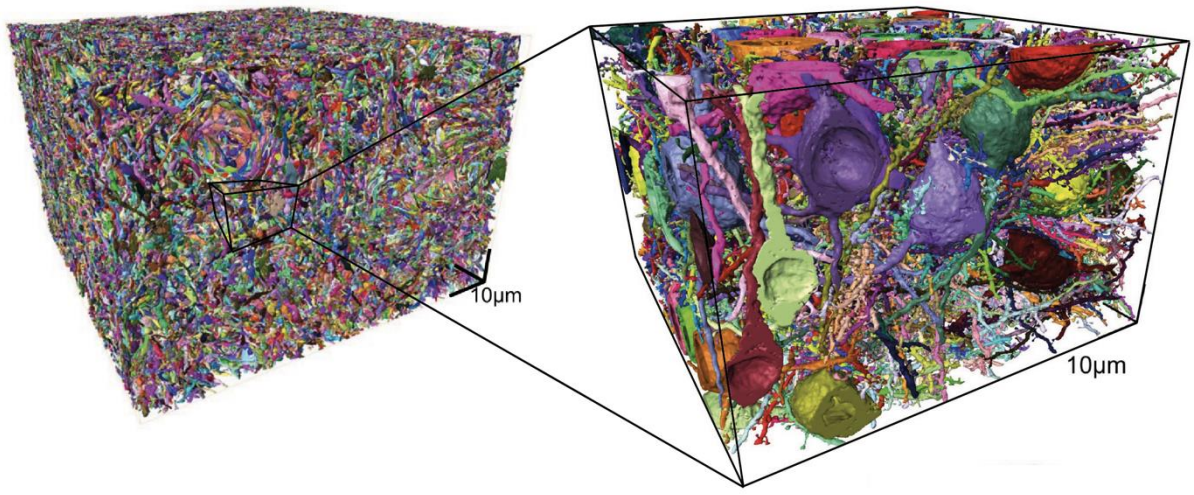

Figure 6. A very dense and compact primary somatosensory cortical circuitry.
3D electron microscopy reconstruction of the upper layer 4 of primary somatosensory cortex of a 28-day old mouse. Modified from Motta et al. 2019.

Therefore, synapse molecular diversity is observed at different levels in the CNS: across different brain areas, different types, subtypes of neurons and between different dendritic

compartments. Interestingly, the different levels of synapse heterogeneity correlate with the different stages of specificity required for brain development. After differentiation, neurons migrate to their final position, their axon reaches their appropriate target areas, contact specific partners (cellular specificity) on a specific subcellular localization (subcellular specificity), and finally form functional synapses. Although this is a great challenge for neuroscientists, it is necessary to characterize not only synaptic molecular diversity but also how and when it is generated to elucidate the formation of the specific brain "connectome."

Part II - The Purkinje cell, a well characterized model to study synaptic diversity and specificity

The olivo-cerebellar network is composed of the cerebellum and the inferior olive (IO), located in the brainstem. Its stereotyped circuitry is evolutionary conserved in all vertebrates making it the most highly conserved structure of the brain. Despite its relatively small size, the cerebellum contains half of the brain's neurons, thus explaining its name the "little brain". In 1967, Eccles, Ito and Szentagòthai were the first to compare the olivo-cerebellar system to a “neuronal machine” supporting motor control and learning (Eccles 2013). Thanks to neuroimaging and new anatomical techniques, the cerebellum has been increasingly recognized for its involvement in higher cognitive processes such as language, learning and emotional control (Buckner 2013).

1. The olivo-cerebellar topography

The Purkinje cell (PC) is the sole output of the cerebellar cortex and sends projections to deep cerebellar nuclei (DCN) embedded in the white matter in the center of the cerebellum. The DCNs are connected to sensorimotor areas, associative cortices and the limbic system, thus constituting the main output of the cerebellum. At the same time, the cerebellum receives two main inputs: the mossy fibers (MFs) and the climbing fibers (CFs). MFs innervate DCNs and granule cells (GCs) forming synapses called “rosettes” because of their large grape-like terminals. The MFs innervate specific areas of the cerebellum depending on the CNS regions from which they originate. CFs, the other main inputs of the cerebellum, are the axons of inferior olivary neurons (IONs) arriving from the brainstem. The IONs receive afferents from different regions in the CNS such as the superior colliculus, the red nucleus, the raphe nuclei, the sensory trigeminal nuclei, and the spinal cord. Sugihara et al. demonstrated that the different regions of the inferior olive (IO) specifically innervate different compartments of the cerebellar cortex and are themselves innervated by different inputs **(Figure 7)**. The connection between PCs, the IO and the DCN follows a precise topography and defines cerebellar “modules” considered as the functional units of the cerebellum (Sugihara and Shinoda 2004; Sugihara and Shinoda 2007; Reeber et al. 2013). Each cerebellar module is characterized by Zebrin II (Aldolase C) positive or negative staining forming in total 24 bands **(Figure 7)** (Brochu et al.

1990). Interestingly, Zebrin II pattern is highly reproducible between individuals and conserved across mammalian specifies suggesting that one IO region will always target the same PC clusters to form the functional unit of the cerebellar cortex (Sillitoe et al. 2005). This constitutes a very interesting example of cell specificity among heterogenous PCs.

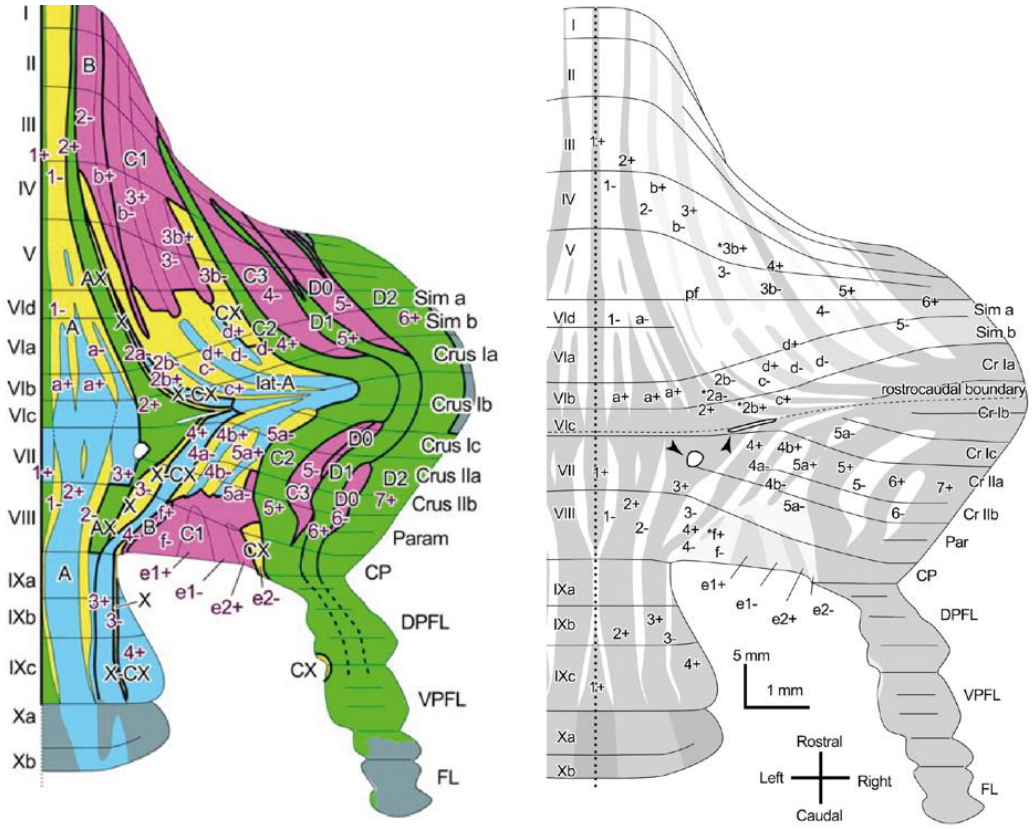

Figure 7. Topography of the olivo-cerebellar tract.

A close correspondence is observed between the representation of IONs innervation to the cerebellar cortex where each color corresponds to different IO region and the Aldolase C map, supporting the functional cerebellar "module" hypothesis. Representation of the Aldose C positive (Zebrin II+) in gray and Aldose C negative (Zebrin II-) in white in the unfolded cerebellum. Modified from Sugihara and Shinoda 2004.

2. Synaptic connectivity on Purkinje cells

The cerebellar cortex is organized in three different layers: the molecular layer (ML) (adjacent to the pia matter), the PC layer (PCL) and the granular cell layer (GCL). It is composed of a limited number of cell types connected in a very precise and stereotyped manner. PC receives direct inputs from different cell populations, inhibitory and excitatory, on different subcellular domains, making this neuron a perfect example of subcellular specificity **(Figure 8)**.

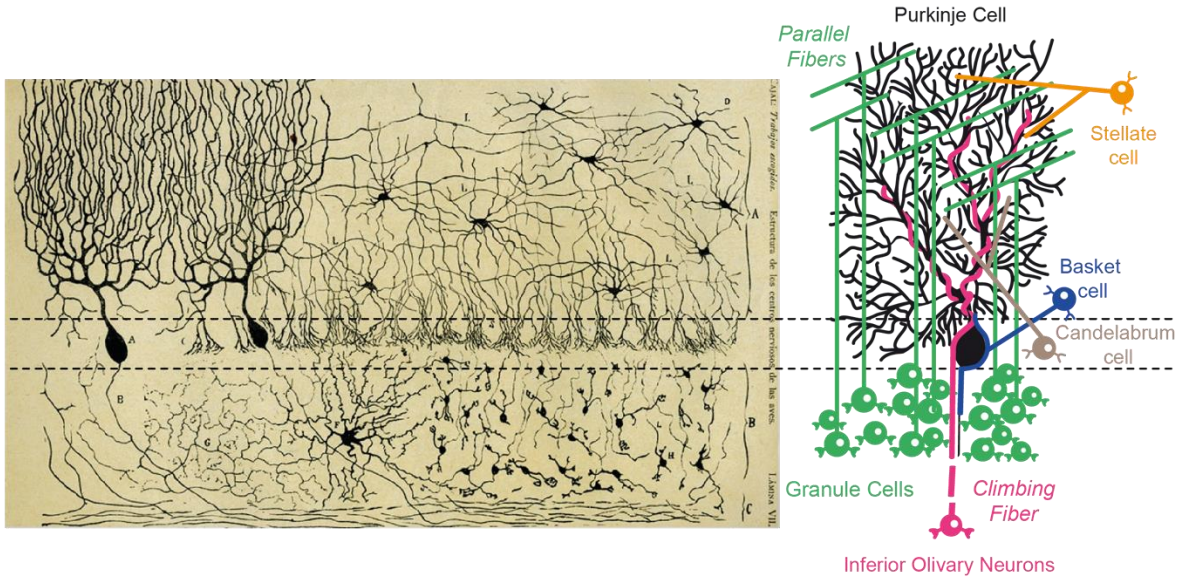

Figure 8. The cerebellar cortex.
Left panel: First illustration from a Golgi impregnation (silver staining) of the cerebellum by Santiago Ramón y Cajal in 1888. Original legend states: "Vertical section of a cerebellar convolution of a hen. Impregnation by the Golgi method. A, represents the molecular layer, B, designates the granular cell layer, the two dotted lines delimit the Purkinje cell layer and C, the white matter." Right panel: Schematic representation of a PC receiving four different inputs: two inhibitory (from the Stellate, the Basket cells and Candelabrum cells) and two excitatory (from the granule cells and the inferior olivary neurons, through the parallel fibers and climbing fibers, respectively).

Stellate cells, located in the upper molecular layer, innervate the superior dendritic arborization of PC whereas Basket cells, localized in the molecular layer but very close to PC layer, forms "pinceau" synapses on the axon initial segment of 5 to 7 PCs (Somogyu and Hámori 1976) **(Figure 8)**. Candelabrum cells are sandwiched between the soma of PCs. They do not contact specific compartment of PC dendrites like Basket or Stellate cells, but extend their axon towards the ML and make numerous synapses (Lainé and Axelrad 1994; Osorno et al. 2022). PC also directly receives two types of glutamatergic excitatory afferents: parallel fibers (PFs), axons of GCs, and CFs, axons of IONs whose soma are located in the brainstem. GCs are very small cells (5-8 µm of diameter) and are located in the granular layer of the cerebellar cortex. Similar to Stellate and Basket cells, CF and PFs have very distinct subcellular specificity on PC with PFs connecting the distal dendrites of PC and CF contacting only PC proximal compartment **(Figure 9A)**. CFs and PFs intensively compete for their own territory on PC dendritic tree. This stereotyped connectivity is achieved thanks to molecular and activity-dependent mechanisms that occurred during the course of postnatal cerebellar development which I will describe in details later. Each PC receives approximately 200,000 PFs that occupy the majority of its

dendritic tree **(Figure 9A)** (Harvey and Napper 1991). PFs are perpendicular to the sagittal plane and to the PC dendritic tree. In the ML, the axon of the GC splits into two PFs and is characterized by a “T-shape” morphology. Thereby, one GC can contact several hundred PCs but each PF forms approximately 0 to 2 "en passant" synapses with each PC. However, PCs have one-to-one relationship with CF but each ION innervates about 7 PCs in adulthood (Sugihara et al. 2001). A single CF forms about 300 synapses on each PC (Harvey and Napper 1991).

PCs are characterized by two types of action potential output, simple and complex spikes. Simple spikes are very weak action potentials and occur spontaneously. They could be driven by PF inputs which required 50 simultaneous active GCs, and are smoothly graded with the increase of stimulus intensity (Barbour 1993). In contrast, complex spikes exhibit strong depolarizations with an all-or-none burst of several action potentials driven by CF inputs **(Figure 9B)** (Eccles et al. 1966; Davie et al. 2008). In parallel, Basket and Stellate cells play complementarity function in modulating PC activity. Basket cells decrease simple spike frequency and increase the frequency of complex spike firing, while Stellate cells control simple spike regularity and decrease the frequency of complex spike firing (Brown et al. 2019). The distribution of PC spines in the proximal and distal dendrites are functionally linked to the different synaptic properties of PFs and CFs. In fact, the proximal compartment has about 0.07 spines/μm^2 which are organized in clusters contacted by CF, while the distal compartment has about 3 spines/ μm^2 and each spine is contacted by a PF presynaptic bouton **(Figure 9C)** (Strata 2002). However, 85% of the PF/PC synapses are silent (Isope and Barbour 2002). A low spine density at the proximal dendrites is sufficient to generate a gigantic EPSC in the PC. Moreover, PF/PC synapses exhibit short-term facilitation during bursts of high-frequency activity (Valera et al. 2012) whereas CF/PC synapses exhibit short-term depression (Konnerth et al. 1990; Hashimoto and Kano 1998; Pätz et al. 2019). In cerebellar slices, PF/PC synapses undergo long-term potentiation (LTP) when CF is not activated. However, co-activation of CF and PF leads to long-term depression (LTD) **(Figure 9B)** (Coesmans et al. 2004). This LTD is induced by a large Ca^{2+} influx through voltage-gated Ca^{2+} channels in PC followed by a molecular cascade that ends with the endocytosis of AMPA receptors at PF/PC synapses leading to a reduction of PF/PC synaptic strength.

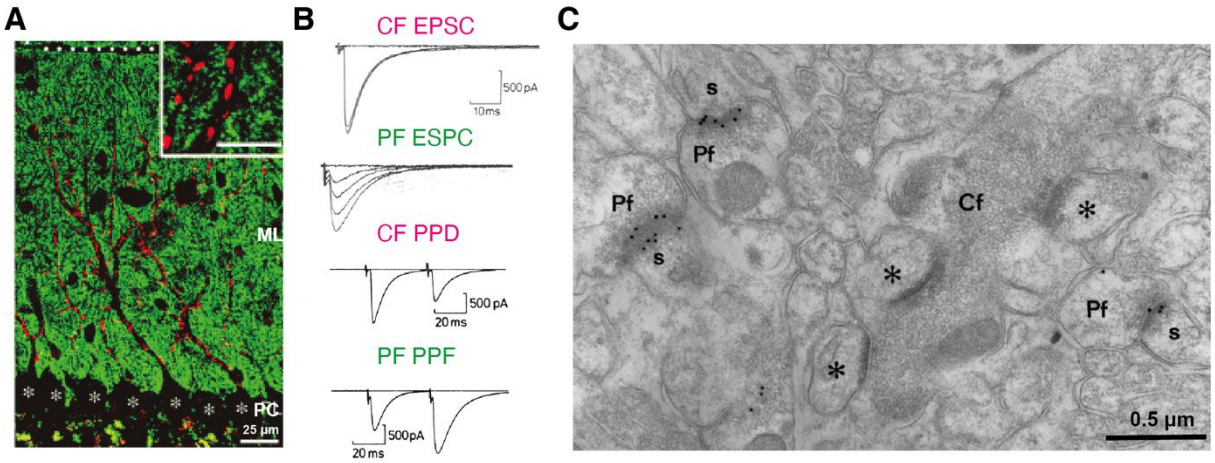

Figure 9. Distinct properties of Purkinje cell excitatory inputs.
(A) Immunohistochemistry of CF/PC synapse labeled by VGLUT2 (red) shows that CFs occupy the proximal compartment of PC dendrites while PF/PC synapses, labeled here by VGLUT1 (green) innervate the distal dendrites of PC. Adapted from Miyazaki et al. 2003. (B) CF activation produces a gigantic EPSC in PC with an all-or-none characteristic. CF is characterized by a paired-pulse depression (PPD), where the second CF-EPSC presents a smaller amplitude. PF-EPSC amplitude increases with the strength of stimulation thanks to the recruitment of a bigger number of PFs. PF/PC synapse exhibit paired-pulse facilitation (PPF). (C) Electron micrograph of the rat cerebellum. Cf, Climbing fiber Pf, Parallel fibers; s, Purkinje cell spines. Adapted from Landsend et al. 1997.

3. Development of Purkinje cell afferents, a comprehensive framework to understand the establishment of synaptic specificity

Besides its stereotypy, the development of the cerebellar circuitry is mainly postnatal in rodents, making it an ideal brain structure to study the different mechanisms regulating synapse formation.

3.1 Basket cell and Stellate cell synapses

Basket and Stellate cells are generated from postnatal day 1 (P1) to P15 (Miale and Sidman 1961). For a long time, it was proposed that they might be generated from the EGL, the only germinal zone at this age in the cerebellum. Three decades later, retrovirus injection of β-galactosidase in the cerebellar cortex demonstrates that these two types of interneurons are generated from the cerebellar white matter, where neuronal progenitors reside (Zhang and Goldman 1996). They reach their final position between P7 and P21, Basket cells in the lower third of the ML and Stellate cells at upper two-thirds of the ML. As early as P10, inhibitory

postsynaptic currents (IPSCs) are identified in PCs (Crepel 1974). Contrary to Basket cells, Stellate cell branches are guided towards PC dendrites thanks to Bergmann glial cells (Ango et al. 2008). Basket cells start to innervate PC soma around P7 (Sotelo 2008). They start to innervate the PC AIS around P9 and establish axo-axonic synapses. At P20, Basket cells are mature and their axons exhibit "pinceaux" shape like morphology around the PC soma and AIS.

3.2 Climbing fiber synapses

In 1911, Ramón y Cajal was the first to describe the different stages of the CF/PC connection in rat. In the mouse, it is important to note that these sequential steps are advanced by 1 to 2 days compared to the rat.

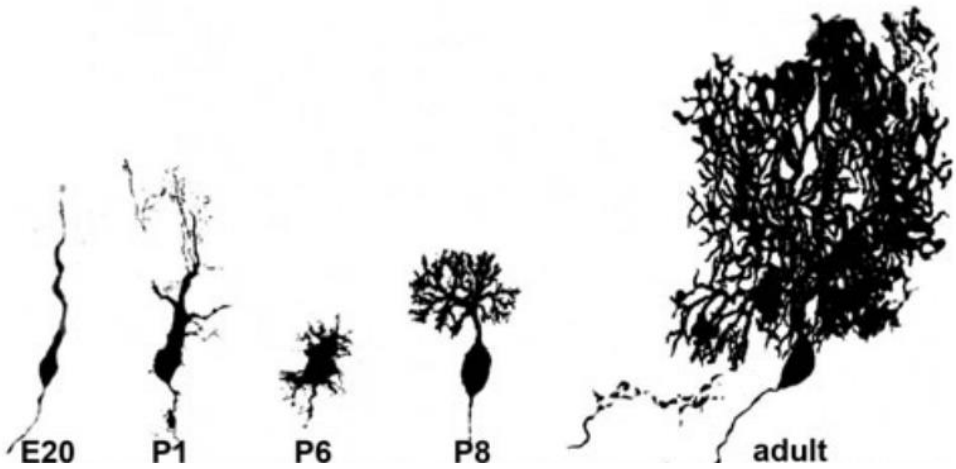

Figure 10. Development of Purkinje cell in rat cerebellum.
The adult stage corresponds to P60. From Sotelo and Rossi 2013.

PCs are born around embryonic day 11 (E11) and E13, and are the first neurons of the cerebellum to be generated. They migrate to the cerebellar plate between E12 to E15. From E20 to P1, PC switches from a "fusiform" to a "complex-fusiform" shape. At P6, PC regresses to "stellate cell with disoriented dendrites", then at P8, PC starts to grow its dendritic arborization **(Figure 10)** (Mason et al. 1990a; Armengol and Sotelo 1991; Chedotal and Sotelo 1993).
In parallel, IONs proliferate between E12-E13 in rat, and migrate around the edges of the brainstem to their final location near the ventral midline (Altman and Bayer 1987; Bourrat and Sotelo 1988; Bourrat and Sotelo 1991). CFs form synapses with PC as soon as they enter the cerebellum around E15-E16 in mouse (Kita et al. 2015). At birth, each ION produces about 100 CFs creeping over PC apical dendrites (Sugihara 2005). During the "creeper stage", the synaptic

contacts between PCs and CFs are transient, since the "bipolar shape" of PC regresses, and disappear between P1 and P5 in rat (Chedotal & Sotelo, 1993). Only 10 CFs out of 100 CFs in the creeper stage finally develop and form "pericellular nests" around PCs **(Figure 11)**. From P5 to P9, the pericellular nest develops and the number of CF perisomatic synapses peaks at P9. Perisomatic innervation of PC then shifts from glutamatergic CF to GABAergic Basket cells (Ichikawa et al. 2011). During this switch, CFs begin to connect the apical part of PC somata and the main dendrites forming a cone-shaped hat-like appearance, hence the "capuchon stage" (Chedotal and Sotelo 1992). During this step, only one CF will translocate and then gradually extend its connections along the PC dendrites, growing in parallel, to finally extend at P20 to 76% of the PC height (Kouichi Hashimoto et al. 2009).

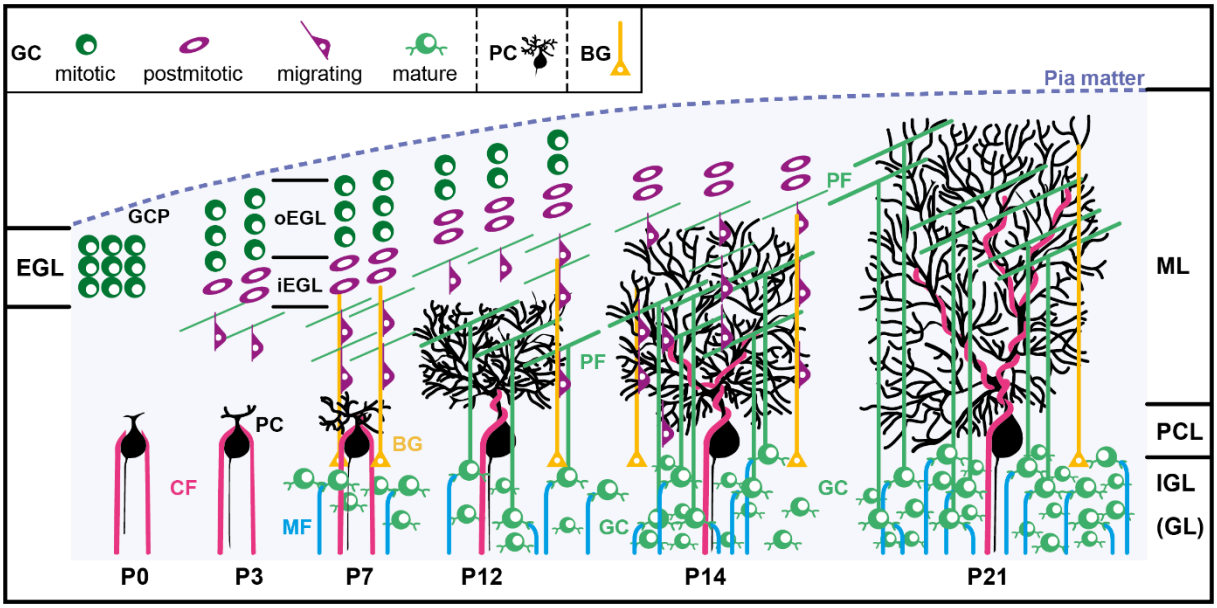

Figure 11. Schematic illustration of the postnatal development and maturation of granule cells and inferior olivary neuron connectivity on Purkinje cells in the cerebellar cortex.
At P0, CFs start to contact PC somata. From P3 to P7, one CF is selectively strengthened and translocate around P9. In parallel, granule cells are generated from granule cell precursors and migrate thanks to Bergmann glia. Granule cells receive inputs from mossy fibers. GC, granule cell; PC, Purkinje cell; BG, Bergmann glial cells; CF, climbing fiber; MF, mossy fiber; PF, parallel fiber; GCP, granule cell precursor; EGL, external granular layer; oEGL, outer external granular layer; iEGL, inner external granular layer; ML, molecular layer; PCL, Purkinje cell layer; IGL, internal granular layer; GL, granular layer. Adapted from Cerebellar development transcriptome database, Japan Node.

3.3 Parallel fibers synapses

GCs are generated between E15 and P15 from granule cell precursors, localized in the superficial zone of the cerebellar cortex above the ML, in the external granular layer (EGL) (Miale and Sidman 1961). As these precursors replicate, they also migrate tangentially in rostro-caudal direction and mediolateral axes (Komuro et al. 2001). Once post-mitotic GCs are generated, they migrate radially from the EGL along Bergmann glia to form the internal granular layer (IGL) below the PC layer **(Figure 11)**. GCs are organized in an "inside-out" manner with later born GCs in superficial layer and earlier born GCs in deeper layer of the IGL. It has been hypothesized that during their migration, they start to connect PC dendrites in the growing molecular layer starting at P7, although there is no clear evidence yet. A substantial increase of PF/PC synapses is observed during the second postnatal week (Altman 1972). PF terminals initially express the vesicular glutamate transporter2 (VGLUT2). Then, as they mature, PFs switch to VGLUT1, whereas CFs express VGLUT2 throughout the postnatal development and in adult **(Figure 12)** (Miyazaki et al. 2003). Through reconstruction of dendritic innervation by serial electron microscopy, Ichikawa and colleagues demonstrated that supernumerary PFs synapses on PC proximal dendrites are eliminated during the third postnatal week, shortening the overlap region between CF and PF connections (Kano and M. Watanabe 2019). The EGL then finally disappears by P20 (Altman et al. 1997).

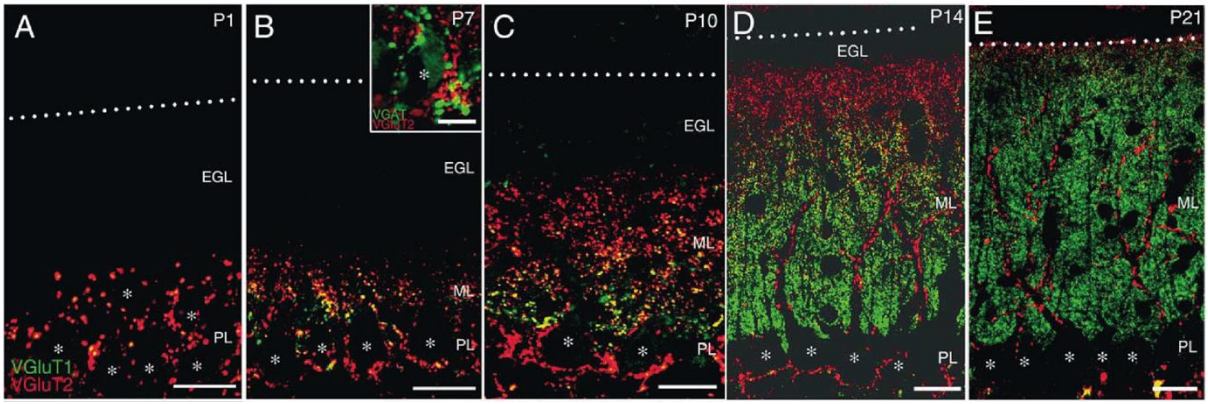

Figure 12. Developmental switching of VGLUT2 to VGLUT1 in parallel fiber terminals.
At P1, only VGLUT2 staining is observed around PC soma from CFs. At this stage, GCs number is very low. At P7, big CF-VGLUT2 puncta are still localized around PC soma but tiny puncta from PFs start to be seen in the ML. At P14, as the ML expands, there is a switch in PF terminals from VGlut2 to VGlut1, while immature PFs at the top of the ML still express VGLUT2 until complete maturation. EGL, external granular layer; ML, molecular layer; PL, Purkinje cell layer. From Miyazaki et al. 2003.

Part III - Mechanims underlying cellular partner specificity: in the cerebellum and other systems.

1. Neuron birth timing in partner selectivity

Proper circuit wiring first begins with neural cell fate specification. The contribution of neuronal lineage and birth timing in partner selection is not yet clear and appears to be circuit-dependent. For instance, in the cerebellum, a study by Bourrat and Sotelo demonstrated that IONs generated at the same time but not at the same location in the neuroepithelium are packed together in the IO (Bourrat and Sotelo 1991). They suggested that the sequence of ION generation might play a role in the acquisition of the olivo-cerebellar topography since an ION cluster would target the same region of the cerebellum (Sugihara and Shinoda 2004). Moreover, it was suspected that GCs generated at the same time would receive connections from mossy fibers arising from a common brain region. However, a recent study showed that early- and late-born GCs receive mossy fiber inputs from the same brainstem nuclei (Shuster et al. 2021). This indicates that birth timing does not regulate MFs-GCs wiring specificity.

One of the most evident examples of the role of neuronal birth timing in the regulation of partners specificity is in the mammalian cortex. Consecutive asymmetric division of radial glial cells in the developing neocortex results in ontogenic columns of sister excitatory neurons. Recent studies using retroviral lineage tracing and mouse genetics have shown that excitatory neuron clones are more likely to be connected with each other than with their unrelated neighbors, at the beginning through gap-junction and then *via* chemical synapses **(Figure 13)** (Yu et al. 2009; Yu et al. 2012; Cadwell et al. 2020). This vertical arrangement has a functional role in the development of response selectivity since clonally related neurons had similar orientation preferences in the visual cortex (Li et al. 2012; Ohtsuki et al. 2012; Ko et al. 2013). Work from Pico Caroni's lab has also demonstrated this idea in the hippocampus where granule cells and pyramidal cells wire more likely, according to their time of neurogenesis (Deguchi et al. 2011). As in the neocortex, pyramidal cells are generated in an "inside-out" manner with later born neurons in superficial layers and earlier born neurons in deeper layers. Interestingly, different birthdates could also be a driver for generating neuronal diversity inside CA1 subpopulations of two distinct sublayers (Cavalieri et al. 2021).

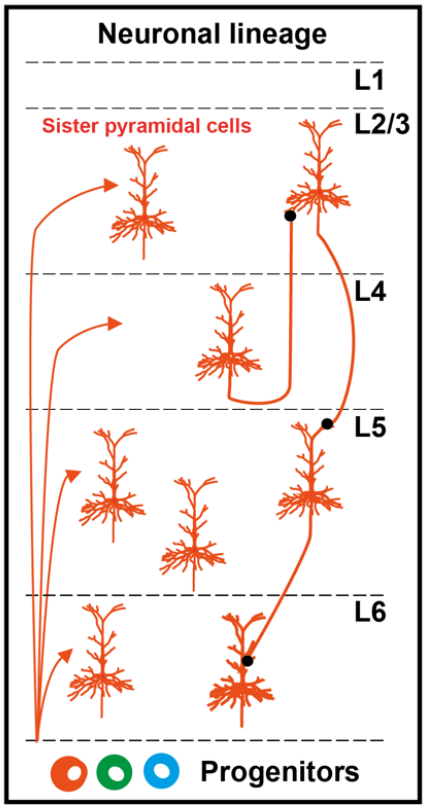

Figure 13. Neuron birth timing regulates partners selectivity.
Birth order and neuronal lineages could affect synaptic connectivity. Cortical pyramidal related cells are preferentially connected around P10. Adapted from Gutman-Wei and Brown 2021.

2. Limitation of encounters between potential partners

One possibility to ensure proper neuronal connectivity is to control the interaction between potential partners. Thus, the matching of pre- and postsynaptic cells could be modulated by pre-ordering their axons, controlling their overlap as well as the approach angle of axons and dendrites, and the kinetics of their axonal filopodia.

The mouse olfactory system is a typical illustration where olfactory sensory neuron axons are pre-sorted in the bundle to reduce the number of postsynaptic choice in the glomeruli, and helps in topographic map formation (Imai et al. 2009). Then, when neurites are sufficiently close, axo-dendritic overlap was hypothesized to likely determine synapse density as a function of the surface area between pre- and postsynaptic partners **(Figure 14)**. This idea is known as “Peter’s rule” and was first described to explain the connectivity between thalamocortical axons from the lateral geniculate nucleus to the granular layer 4 of the primary visual cortex (Peters and Feldman 1976). Peter's rule was studied extensively in the brain over the past four decades,

particularly in the neocortex, with many studies in favor or against this hypothesis (Garey 1999; Stepanyants and Chklovskii 2005; Rees et al. 2017). One relevant example of this observation is in the hippocampus formation. The connectivity between the presynaptic CA3 Schaffer collaterals, the postsynaptic CA1 pyramidal cells and inhibitory CA1 parvalbumin-positive neurons (PVs) was mapped using mammalian GFP reconstitution across synaptic partners (mGRASP)(Kwon et al. 2018; Agi et al. 2020). Interestingly, Kwon and colleagues found that connections between CA3 axons and dendrites of CA1 PVs are predicted by Peter's rule, leading to a more random wiring pattern, while connection between CA3 Schaffer collaterals and CA1 pyramidal cells, with a more structured pattern, do not fit this rule. These results suggest that different mechanisms underly different connectivity profiles on two postsynaptic partners in the same circuit.

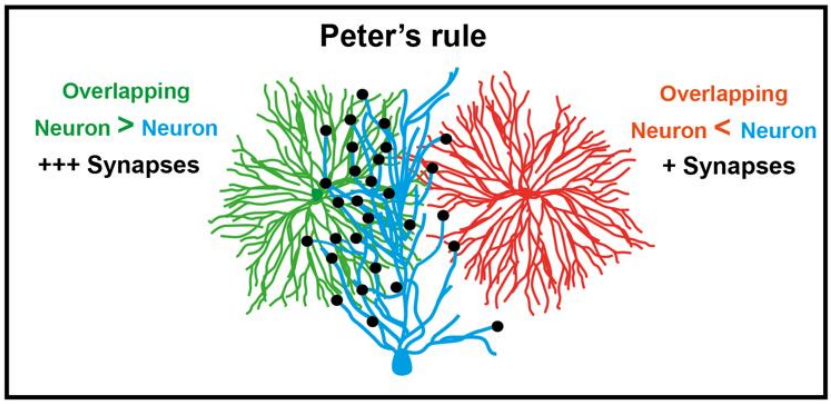

Figure 14. Peter's rule predicts synaptic connectivity based on the average axodendritic overlapping.
The overlapping between axons and dendritic arborization could influence the number of synapses between different neurons. Adapted from Gutman-Wei and Brown 2021.

In addition to Peter's rule, specific angle of axo-dendritic approach seems to modulate the connectivity of proprioceptive sensory axons to motor neuron dendrites in the mouse spinal cord (Balaskas et al. 2019). They observed that the probability of synapse formation between these two neurons is dependent on the angle of which sensory axons approach to their target. According to them, their model could generate highly selective pattern of connection but could not account for the full selectivity observed (Balaskas et al. 2019). Additionally, in the drosophila visual system, a study demonstrated that photoreceptor neurons connectivity to lamina and medulla neuropils of the optic lobe relies on the kinetics of synaptogenic axon filopodia (Kiral et al. 2020). The loss of autophagy specifically in these neurons leads to an increase of the overlapping territory between axons and dendrites, and thus to the recruitment

of incorrect postsynaptic partners followed by an increase in the number of synapses. In summary, all these data suggest other mechanisms than the Peter's rule to allow for a more hardwired and structured pattern of connectivity, especially in the case of equally proximate partners.
So far, from Peter's rule to specific approach angles and axon kinetics, none of these various mechanisms have been tested in the cerebellum for partners specificity.

3. Cell-adhesion molecules in partner selectivity

Molecular recognition and adhesion mechanisms are known to be critical in establishing complex and stereotyped pattern of synaptic connections among different target neurons. This molecular view was actually established first by John Langley in 1895 and then by Roger Sperry in the sixties. Langley studied cat's peripheral nervous system and more particularly spinal cord neurons that innervate specific peripheral organs. After sectioning a single axon and waiting for regeneration, Langley observed that this neuron managed to form connection with their original partners (Langley 1895). This experiment inspired Roger Sperry who started to work on the retinotectal system of amphibians. He cut the optic nerves and demonstrated the restoration of a functional visual system, suggesting that axons regenerate and are able to form synapses with the appropriate target (Sperry 1943; Sperry 1944). Surprisingly, Sperry noticed that when the eye is turned 180°, the frog sees the world upside down, implying that the axons reconnected to the original target and do not reconnect based on function (Sperry 1963). Based on these observations, Sperry postulated that "the cells and fibers of the brain and cord must carry some kind of individual identification tags", hence giving rise to the chemoaffinity hypothesis. In other words, this means that each type of neuron expresses a specific combination of proteins that gives it an "affinity" for its synaptic partners. Since then, an increasing number of molecules have been identified and classified as cell adhesion molecules (CAM). CAMs are cell surface molecules that can be membrane and secreted proteins, and are capable of trans-cellular interactions to promote cell adhesion or cell signaling (Zipursky and Sanes 2010).

3.1 Target recognition in the olivo-cerebellar system

Many studies suggest that olivo-cerebellar topography is established by the specific expression of CAMs, allowing precise and reproducible targeting of IONs to different PC populations. In

co-culture explants containing the cerebellum and the brainstem of chick embryo, normal anteroposterior topography of the olivo-cerebellar was observed. Moreover, after anteroposterior rotation of the cerebellum, rostromedian IONs still properly target the posterior vermis as well as caudolateral IONs to the anterior vermis of the cerebellum (Chédotal et al. 1997). The first potential candidate identified was the BEN/SC1/DM-GRASP protein from the immunoglobulin superfamily (Chédotal et al. 1996). Nevertheless, even if BEN is expressed transiently and only in a subset of PC and IONs, its role in the formation of the cerebellar maps was never demonstrated. Type- II cadherins are known to play a role in the topography of other brain regions and are differentially expressed in the cerebellum and in different IONs subpopulations. They have therefore also been suggested to control cerebellar topography, but as with BEN, there is still no clear evidence in favor of these molecules in controlling the targeting of IONs to PC subpopulations (Reeber et al. 2013). Partner selectivity could be achieved non only *via* cell adhesion but also *via* cell repulsion mechanism. For instance, EphA receptors and ephrin-A ligand are differentially expressed in PCs and IONs. IONs with high EphA receptor level project to cerebellar domains with no or low ephrin-A expression (Nishida et al. 2002). Ephrin-A2 or EphA3 overexpression in IONs or in PC respectively resulted in the disruption of the olivo-cerebellar map by preventing theses axons to invade their ectopic domains. Therefore, Eph/Ephrin could provide specific positional information. However, given the complexity of the olivo-cerebellar map, it seems likely that other adhesion molecules may be involved in target selection of specific subsets of IONs and PCs.

MFs, originating from several areas in the brainstem, convey information to the cerebellum *via* their specific connections to GCs which synapse on PC. However, during development, some MF axons emerging from the pontine nucleus form transient contacts with PCs before switching to GCs (Mason and Gregory 1984; Takeda and Maekawa 1989). MFs arrive in the cerebellum around birth and stop their growth to not enter the EGL where GCs are generated. Once GCs migrate to form the IGL, mossy fibers establish synaptic connection with them. Cell-type specific target recognition mechanism was suggested to instruct MF and GCs innervation. In *Sema6a* KO mice, GCs migration is impaired with GCs localized in the ML, however these ectopic GCs are still innervated by MFs (Kerjan et al. 2005). An *in vitro* study of co-culture explants demonstrates that GCs preferentially establish contact with MFs rather than with ION axons suggesting the existence of cell-surface cues (Ito and Takeichi 2009). Few years later, *cadherin7* (Cdh7) which is expressed in GCs and MFs was shown to mediate specific connection between them (Kuwako et al. 2014). Besides, BMP4 was identified as a retrograde

PC-derived signal that negatively regulates MF-PC contact (Kalinovsky et al. 2011). Thus, MF-GC specific connectivity is also achieved after the elimination of MF-PC connections.

3.2 Classical cell-cell recognition molecules in partner specificity

A recent and elegant study in *Drosophila* illustrates the remarkable partner selectivity underlying circuit connectivity (Valdes-Aleman et al. 2021). The position of mechanosensory neurons was altered in larvae by shifting them laterally from the midline. To this end, the chimeric receptor FraRobo, composed of the Frazzled ectodomain and the intracellular domain of Robo, was overexpressed thereby enhancing the sensitivity of mechanosensory neurons to Netrin and thus shifting them to the lateral edge of the neuropil. In this context, their postsynaptic partners extended branches to the ectopic territory and formed synaptic connections, suggesting that cell-surface cues instruct partner specificity rather than the target's location.

Many studies have suggested that Cdh contribute to partners specificity, first because they are differentially expressed between neurons and second, because they can generate a large number of molecules. Cdh are divided into 2 types, the classical and type II Cdh encoded by 20 different genes (Takeichi 2007). Type II cadherins were shown to regulate specific circuit assembly in the hippocampus in which knock-down of *Cdh9* caused a specific reduction of dentate gyrus-CA3 synapses (Williams et al. 2011). In the mouse retina, *Cdh8* and *Cdh9*, which are expressed by distinct populations of bipolar cells, enable specific synaptic targeting to retinal ganglion cells (RGCs) (Duan et al. 2014). Additionally, subpopulation of RGCs expressing *Cdh6* selectively innervate *Cdh6* retinorecipient target (Osterhout et al. 2011). Protocadherins (Pcdh), a subgroup of the Cdh family, were also shown to regulate partner specificity. In *Pcdh-α* mutant mouse, the axons of olfactory sensory neurons, which project to the glomeruli of the olfactory bulb, are mistargeted (Hasegawa et al. 2008).

The Eph/Ephrin molecules can regulate partner specificity in ways other than cell adhesion, by repelling neurons and thus prohibiting the formation of synapses between two neurons. For instance, in the fly mushroom body, Dscam1 from immunoglobulin (IgSF) plays a role in axon guidance *via* the selective repulsion between two axons from the same type of neurons. Homophilic binding of DSCAM1 ensures proper segregation of theses axons and thus their proper targeting (Wang et al. 2002). In addition to its role in axon guidance, DSCAM also

contribute to cellular synaptic specificity (Millard et al. 2010). In *Drosophila* and *C.elegans*, the majority of presynaptic site has 2 to 5 postsynaptic elements. In tetrad synapses, photoreceptors presynaptic site contacts 2 postsynaptic elements of lamina neurons. There are 6 photoreceptor terminals (R1–R6) and each photoreceptor axon makes about 50 tetrad synapses containing an invariant pair of L1 (lamina neuron 1) and L2 (lamina neuron 2) **(Figure 15)**. In *Dscam1* and *Dscam2* mutant, tetrads do not contain any more L1 and L2 pair but L1 or L2 pair.

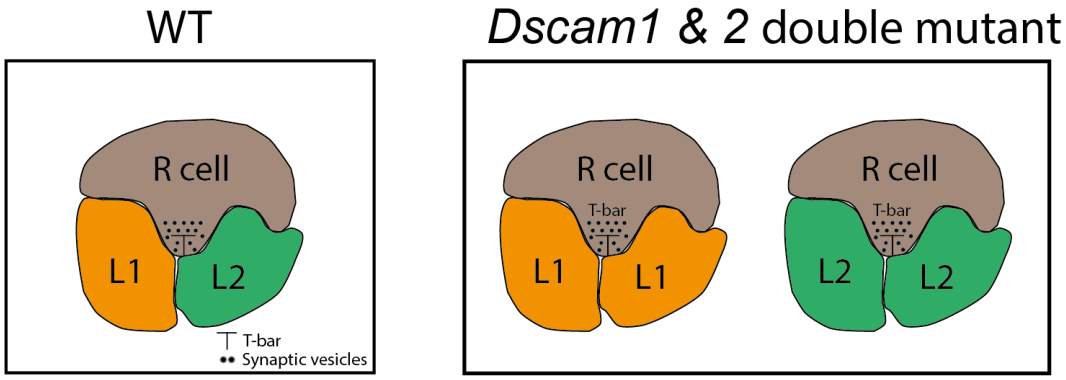

Figure 15. The specificity of tetrad synapses is mediated by DSCAM1 and 2.
Photoreceptor axon (R cell) form tetrad synapses with an invariant pair of L1 and L2 neurons. In Dscam1 and 2 double mutant, tetrad synapses are composed of a pair of L1 or L2 neurons only. Modified from Zipursky and Sanes 2010.

4. Activity-dependent mechanisms in partners selection

Neuronal activity can sculpt developing circuits by acting at different levels, from the establishment of the circuit to its refinement by selectively strengthening or weakening inputs. Inspired by the development of the CF and PF synapses on the PC, Jean-Pierre Changeux postulated that after synapse formation, "selective synapse stabilization" occurs where some synapses are strengthened while weakened ones are eliminated, thereby refining the specificity of the developing circuit **(Figure 16)** (Changeux and Danchin 1976). An important number of synapses during brain development are pruned. For instance in the human prefrontal cortex, there is a 2-to-3-fold decrease in the number of synapses from childhood to adulthood (Petanjek et al. 2011). In fact, another way to generate specific wiring is to form a large number of synapses even if they are aberrant and then refine them (Rakic et al. 1986). The intrinsic primary function of a neuron is to make synapses. Autapses, synapses from a neuron onto itself, are found in a variety of brain region such as in the neocortex, hippocampus and in the cerebellum

(Van Der Loos and Glaser 1972). It can be seen as inefficient but it could allow the optimization of the circuit.

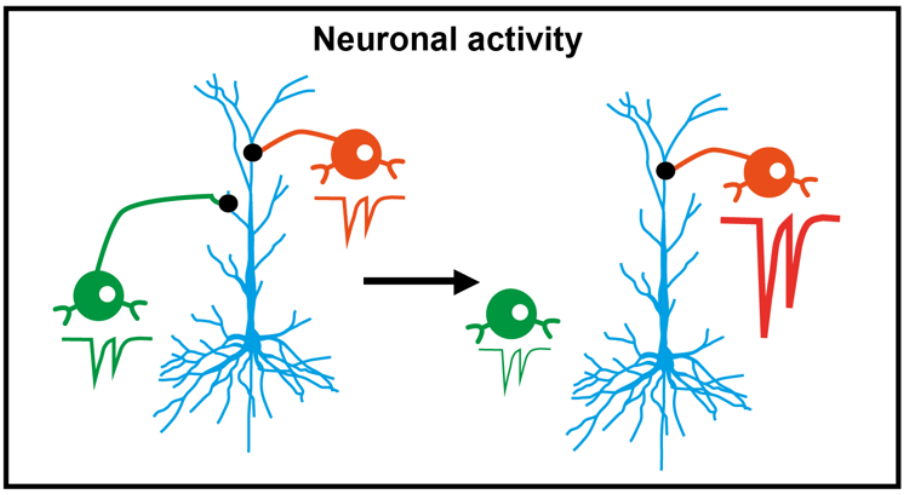

Figure 16. Neuronal activity regulates circuit specificity.
Inputs can be selectively strengthened (orange input) or weakened (green input) through activity-dependent mechanisms, leading to synapse stabilization or elimination, respectively. Adapted from Gutman-Wei and Brown 2021.

Experiments in which neurotransmitter release was blocked resulted in normal synapse formation overall and stereotyped connectivity (Verhage et al. 2000; Varoqueaux et al. 2002; Sando et al. 2017; Sigler et al. 2017). In mouse olfactory sensory neurons, conditional expression of tetanus toxin light chain (TeNT) which prevents calcium-dependent presynaptic release, has no effect on their proper targeting (Wang et al. 1998). However, the effect of blocking neurotransmission appears to be circuit-dependent, with some clear evidences suggesting that neurotransmission is essential for the refinement of wiring specificity (Kerschensteiner et al. 2009; Okawa et al. 2014). Thus, I decided here to mainly discuss the role of global neuronal activity and not only neurotransmission.

4.1 "Fire together, wire together"

The importance of late-stage neural activity in the formation of developing circuits was first demonstrated by the pioneering work of David Hubel and Torsten Wiesel on the cat visual system. They demonstrated that visual stimuli are necessary for the formation of the ocular dominance column, that is, the preference of cortical cells to respond to visual input from one eye or the other (Wiesel and Hubel 1963; Hubel and Wiesel 1970; Le Vay et al. 1980). Since then, it has become clear that sensory driven experience, during specific time windows of

postnatal development (i.e., critical period), is essential in fine-tuning neuronal connectivity (Hensch 2005; LeBlanc and Fagiolini 2011; Park and Fine 2020). Shortly thereafter, Carla Shatz demonstrated the role of spontaneous activity through retinal waves during early brain development, *in utero*, in the formation of specific patterns of connectivity (Katz and Shatz 1996). The projections of retinal ganglion cells from the two eyes are initially intermixed in the dorsal lateral geniculate nucleus (dLGN) but segregate into eye-specific layers during early development. Blocking of activity by tetrodotoxin (TTX) in one eye in juvenile ferrets results in an increase in the territory of the active retina over the one of the inactive eye, suggesting that concomitant spontaneous retinal action potentials drive competition between the two eyes (Penn et al. 1998). Other publications followed this discovery (McLaughlin et al. 2003; Luhmann et al. 2016; Antón-Bolaños et al. 2019; Akin and Zipursky 2020; Baines and Landgraf 2021), giving birth to the statement " fire together, wire together", i.e. coordinated neuronal activity regulates the establishment of neuronal circuits. To summarize, retinogeniculate synapse development takes place in 3 different stages. First, thalamo-cortical (TC) relay neurons are innervated by supernumerary retinal ganglion cell (RGC) axons that are segregated into eye-specific layers before the eyes open. Then, thanks to retinal spontaneous activity, the number of RGCs axons per TC neuron decreases. Finally, sensory driven visual experience strengthens and maintains RGCs axon on TC neurons.

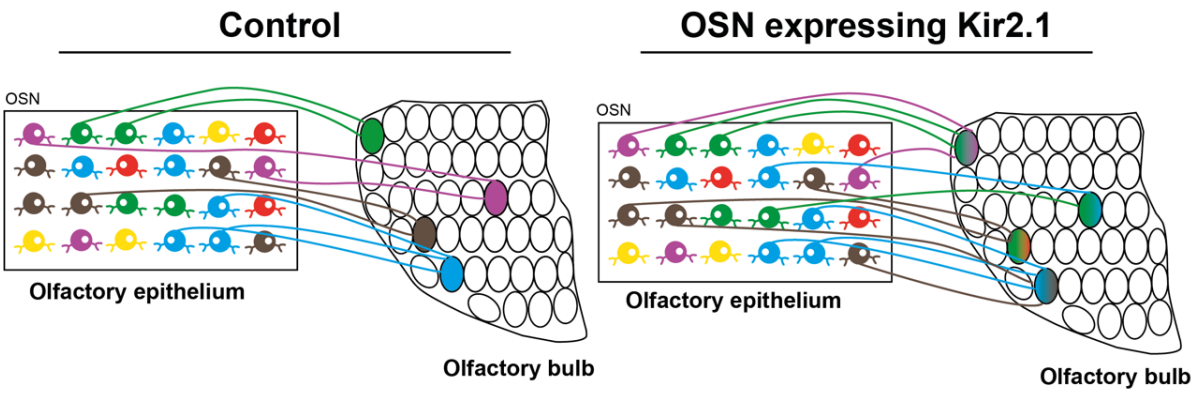

Figure 17. Schematic diagram of the mouse olfactory system in the olfactory epithelium and the olfactory bulb.

In control condition, olfactory sensory neurons (OSNs) expressing the same olfactory receptors, indicated here by the same colors, converge to the same glomeruli in the olfactory buld (OB). When Kir2.1 is expressed, OSNs territory in glomeruli is not anymore segregated. Adapted from Redolfi & Lodovichi, 2021.

I have just described that activity can specify developing circuits by selectively strengthening or weakening inputs, leading to synapse stabilization or elimination, respectively. However, it also seems that neuronal activity can itself specify contacts between partners. In the mouse olfactory bulb, individual olfactory sensory neurons (OSNs) express a single type of olfactory receptor (OR) out of 1,000 different types. OSNs expressing the same OR converge onto the same glomerulus generating an olfactory glomerular map in the olfactory bulbs **(Figure 17)**. This segregation or convergence of OSNs axons to their appropriate target is dependent on the ORs themselves (Wang et al. 1998). Interestingly, overexpression of the inward rectifying potassium channel (Kir2.1), leading to hyperpolarization of OSNs, delays the axon entry and affect the precise connectivity in the olfactory bulbs (Yu et al. 2004) **(Figure 17)**.

4.2 Formation of the olivo-cerebellar connectivity

At E17, the topography of the olivo-cerebellar connectivity is broad **(Figure 18)**. This topography is thought to be established by molecular mechanisms as discussed earlier and by neuronal activity mechanisms. Indeed, postnatal remodeling of CFs from supernumerary to a single one per PC might also play a role in the precise zonal boundaries in adult. As the cerebellum matures, the divergence of connection between IONs and PCs decreases with an average of 5 CFs per PC to one (Mason et al. 1990a; Chedotal and Sotelo 1993; Sugihara 2005). This decrease of CF number per PC is regulated by neuronal activity, which will be explained in details after. Thus, since neuronal activity controls CF synapse elimination, it is suggested that neuronal activity regulates the olivo-cerebellar topography. However, there is still no clear evidence for this.

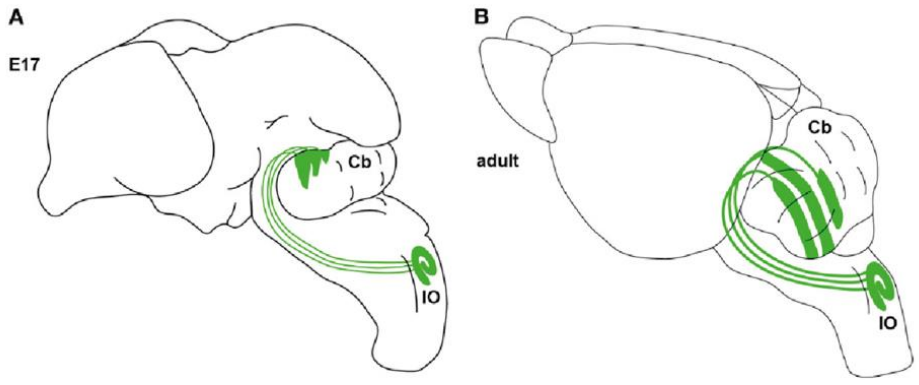

Figure 18. Schematic illustration of the olivo-cerebellar topography during the development.
(A) At E17, the organization of CF projections to the cerebellum is crude contrary to (B) adult stage where it is well-defined.

Similar to the connection of RGCs in the dLGN, an intense activity-dependent remodeling of CF/PC synaptic connections occurs during postnatal development, leading to the loss of the weaker CFs and the selection of the strongest one. Interestingly, each step, from the selection to the early and late phase of CFs removal, depends on the activity of different cerebellar neurons. All the different steps and mechanisms, from the selection to the destabilization of CFs, are described in more details below **(Figure 19)**.

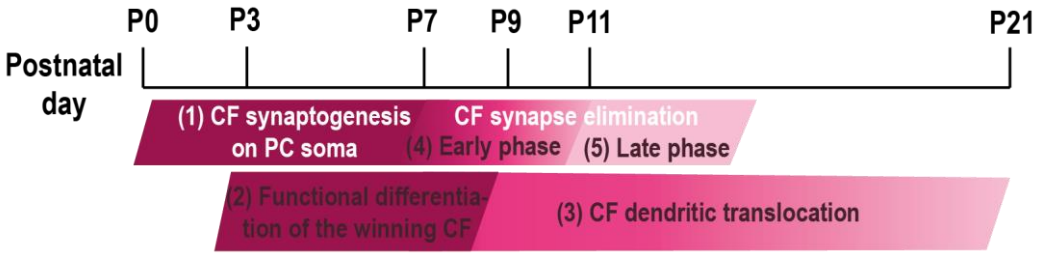

Figure 19. Time course of climbing fiber synapse formation and elimination on Purkinje cell.

(1) The formation of CF/PC synapses on PC soma arises between P0-P7; (2) from P3 to P7 a single CF is selectively strengthened among the others, this phase is called "the functional differentiation"; (3) around P9 , the "winning CF", which is the strongest one, translocates on PC dendrites; (4) CF somatic synapses of the "winner CF" and "looser CFs" are then eliminated between P7 to P11, this phase is called the "early phase" of CF elimination; (5) finally from P12 to P17, CF supernumerary synapses are eliminated during the "late phase" that is dependent on PF/PC synapse formation. Adapted from Kano & Watanabe, 2019.

Between P3 and P7, a severe competition between multiple CFs on a single PC soma occurs. This step is called the **"functional differentiation"** and enables the strengthening of one single CF for each PC. At P3, in whole-cell recordings on cerebellar slices, progressively increase of the stimulus strength of the stimulation pipette generates several discrete CF-mediated currents corresponding to the gradual recruitment of multiple CFs on a single PC (Hashimoto and Kano 2003). At this stage, 90-95% of PC are multi-innervated with similar EPSCs amplitude. From P3 to P7, the amplitude of a single CF-EPSC is increased gradually compared to the other CF-EPSCs suggesting that one CF is selectively strengthened among the others. This selection of the winning CF seems to occur *via* spike-timing dependent plasticity since when a single CF input is closest in time to a PC spike output, this CF then becomes stronger (Kawamura et al. 2013). Thus, the "functional differentiation" of CFs clearly depends on the increase of intracellular Ca^{2+}concentration in PC. After the "functional differentiation" of CFs, the synapses of the "looser CFs" are eliminated while the "winner CF" maintains its perisomatic synapses. This elimination step is called the **"early phase" of CF elimination** and occurs

between P7 and P12 **(Figure 19)**. CF and PC activity seems to play an important role in this process. The synchronous activation of IONs *via* the injection of harmaline, from P9 to P12 leads to the maintenance of CF multi-innervation in the adult (Andjus et al. 2003). In addition, PC activity and Ca^{2+} intracellular increase was also suggested to play a role in the early CF elimination. In mouse mutant where P/Q-type VDCC was deleted selectively in PC, the decrease of Ca^{2+} mediated current resulted in impairment of CF elimination before P12, in addition to the translocation of multiple CFs (Hashimoto et al. 2011). Lorenzetto *et al*. observed the maintenance of CF multi-innervation after PC hyperpolarization thanks to the overexpression of the Kir2.1 channel in PC, an inward rectifying K^+ channel (Lorenzetto et al. 2009). Interestingly, blocking PC neurotransmission using a PC-specific KO of the vesicular GABA transporter (VGAT) results in changes in the pattern of cerebellar "modules" characterized by Zebrin II positive or negative staining (White et al. 2014). Thus, this study suggests impairments in the organization of CF projections to the cerebellum, supporting the hypothesis that neuronal activity regulates the olivo-cerebellar topography.

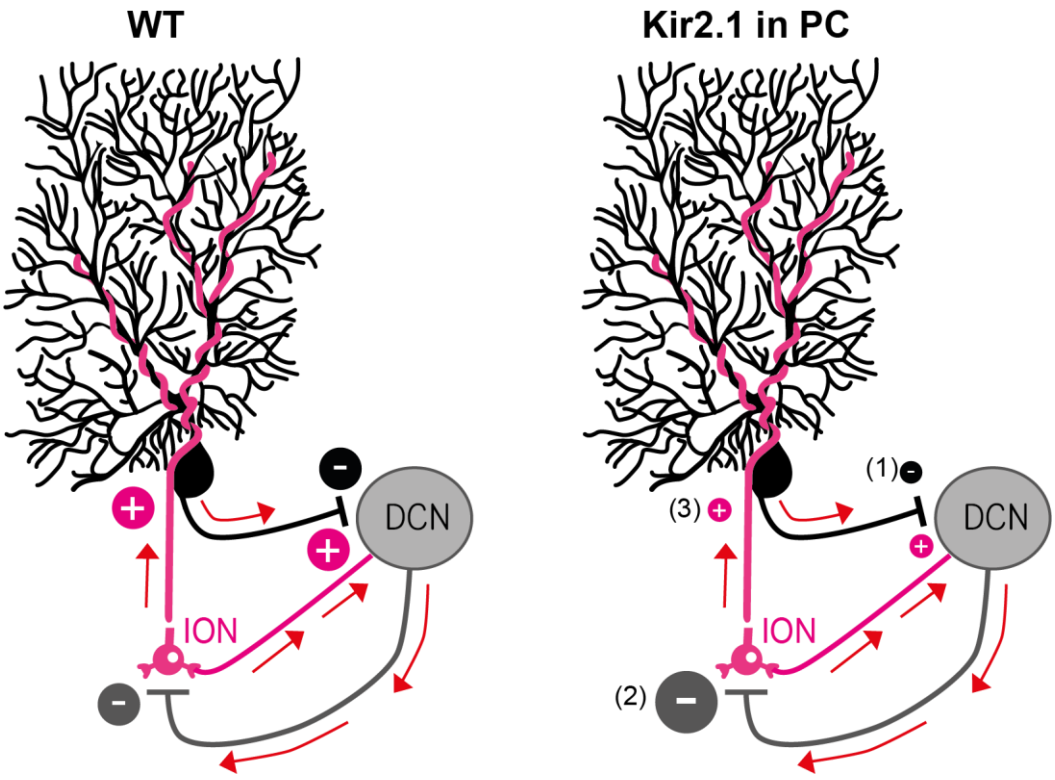

Figure 20. Inferior olivary neurons, Purkinje cell and deep cerebellar nuclei closed-loop.
Excitatory synapses are denoted by (+) and inhibitory synapses by (-). When Kir2.1 is expressed in PC, DCN inhibition is decreased leading to a stronger inhibition of IONs and a decrease in CF activity.

However, since the olivo-cerebellar circuit is a loop, the decrease in PC activity and neurotransmission result in the withdrawal of the inhibition on the DCN, and thus increases the inhibition on the IONs **(Figure 20)**. In these two last models, it is thus difficult to say whether or not the observed phenotype is specific to the decrease in PC activity itself and not to the decrease of CF activity.

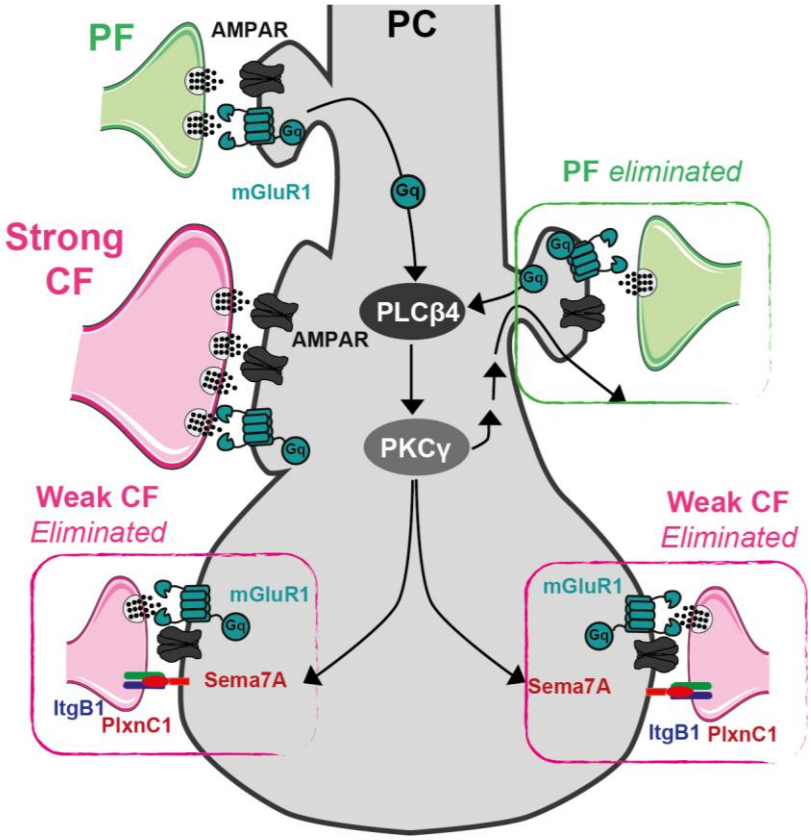

Figure 21. Illustration of mGluR1 signaling pathway involved in the late phase of climbing fiber and parallel fiber elimination in Purkinje cell.
PFs activate mGluR1 to PKCγ pathway and triggers the elimination of weakened CFs and PFs. Sema7A interaction with Plexin C1 (PlxnC1)-Integrin B1 (ItgB1) eliminates CF at PC soma. Adapted from Kano and Watanabe 2017.

The late phase of the CF elimination is known to be dependent on PF neurotransmission to PC. The use of spontaneous agranular mouse models, X-irradiated granule cell precursors and GluRδ2 knockout mice, where PF/PC synapses are decreased about 50%, demonstrated that the "early phase" of CF elimination is not impaired contrary to the late phase (Crepel and Mariani 1976; Crepel et al. 1980; Crepel et al. 1981; K. Hashimoto et al. 2009). The activation by PFs inputs of type 1 metabotropic glutamate receptor (mGluR1) expressed by PCs, is crucial for the "late phase" of CFs elimination **(Figure 21)** (Batchelor et al. 1994; Finch and Augustine 1998; Takechi et al. 1998). In mouse KO for mGluR1 or other downstream signaling molecules such

as Gαq, PLCβ4, and PKCγ, CF elimination during the early phase occurs normally whereas the late phase is impaired (Kano et al. 1995; Kano et al. 1997; Levenes et al. 1997; Offermanns et al. 1997; Hashimoto et al. 2000). A more recent study demonstrated that Sema7A, a membrane-anchored Semaphorin, at PC and its receptors ItgB1 and PlxnC1 at CFs are involved in the cascade downstream of mGluR1 **(Figure 21)** (Uesaka et al. 2014). Similarly, during the last step of retinogeniculate inputs remodeling, mGluR1 signaling is also essential for visual-experience-dependent maintenance of RGCs on TC neurons (Narushima et al. 2016). Finally, GABAergic inhibition of PC by basket cells, synapsing on PC somata and AIS, is also involved in perisomatic CF elimination. In a mouse model in which a deletion of a single allele of Gad67, a GABA synthesizing enzyme, was done, GABAergic inhibition of PCs by basket cells was attenuated in the second postnatal week (Nakayama et al. 2012). Consequently, Nakayama *et al*. observed an increase in CF-induced Ca^{2+} transients in PCs resulting in the deficit of CF synapses removal from P10 to P16. This impairment could be reversed by local application of diazepam, a $GABA_AR$ agonist.

5. Implication of glia in partners specificity

Over the past two decades, numerous studies have shown that astrocytes play a major role in the formation and maturation of synapses while microglia and more recently oligodendrocyte progenitor cells (OPCs) contribute to synapse removal, and thus to circuit refinement (Schafer et al. 2012; Auguste et al. 2022).

In the cerebellum, Bergmann glia, a specialized astrocyte enwrapping PC dendrites and synapses, play an essential role in the formation of proper synaptic wiring in PCs. In addition to guiding Stellate cell axons to their right localization towards PC dendrites, they are also involved in CF synapses remodeling on PC. Deletion of L-glutamate/L-aspartate transporter GLAST in Bergmann glial cells, which is important for the rapid clearance of glutamate released at synapses, leads to Bergmann glial processes retractation from PC dendrites (Miyazaki et al. 2017). In this context, CF innervation on PC was partially impaired. Similarly, conversion of Ca^{2+}-permeable AMPARs to Ca^{2+}-impermeable receptors using virus mediated delivery of GluA2 which is normally not expressed in Bergmannglia, results in the retraction of its processes and the multi-innervation of CFs (Iino et al. 2001).

Microglia are known to play a role in sculpting circuit rewiring through engulfment of cells and materials (Paolicelli et al. 2011). In the developing brain, microglia have ‘‘generic macrophage’’ like shape allowing the phagocytosis of synapses (Stevens et al. 2007). In the retinogeniculate system, microglia engulfment is dependent upon neural activity where extra-numeric synapses are tagged by complement protein C3 for elimination *via* C3 receptor (CR3)-mediated phagocytosis (Schafer et al. 2012). However, the general contribution of microglial cells in the selective elimination of synapses has been recently challenged. Recently, OPCs were shown to contribute to thalamocortical synapse elimination in the visual cortex in a sensory-dependent manner since OPCs receive thalamocortical inputs (Auguste et al. 2022). Moreover, microglia engulfment seems to be mainly circuit-dependent (Lowery et al. 2017). For instance in the cerebellum, contrary to the thalamus, the cortex and the hippocampus (Stoessel and Majewska 2021), microglia do not seem to engulf PC afferent synapses (Nakayama et al. 2018). Deficit in fractalkine signaling by genetic ablation of the CX_3CR_1 receptor in microglia did not affect the development of excitatory and inhibitory synapses with PC (Kaiser et al. 2020). Nevertheless, in mouse lacking microglia, Nakayama *et al*. observed a severely impaired GABA synaptic transmission in PC leading to deficits in CF synapse elimination, as discussed earlier. Because microglia are known to release neurotrophic factors and because this deficit could be restored by diazepam, an indirect role for microglia in CF elimination was suggested (Nakayama et al. 2018).

Part IV - Mechanims underlying subcellular specificity: in the cerebellum and other systems

In the previous section, I described the different mechanisms underlying cellular specificity, i.e., the preference of a neuron to connect to one type of neuron rather than another. In addition to the fact that the neurons must connect to the correct target, their axons must also connect to one or more specific domains of that target neuron, allowing the proper formation and function of neuronal circuits. In this next section, I will review the different mechanisms that have been demonstrated for subcellular specificity in the cerebellum and in other parts of the CNS.

1. The axo-dendritic overlap in subcellular specificity

As mentioned previously, Peter's rule as well as axon kinetics and their different angles of approach to target dendrites, were shown to regulate partner selectivity, however none of these mechanisms have been directly tested in the cerebellum for cellular and subcellular specificity. Since PFs are involved in the PC dendritogenesis (Sotelo 1978; Baptista Mary E.Hatten et al. 1994), one could ask in a purely hypothetical way whether this mechanism would not control the overlap between PFs and PC dendrites, and thus their connectivity. Besides, we can also wonder whether the angle of approaches of the PC excitatory afferents could regulate their connectivity. In fact, once GCs are generated, they migrate radially through the ML, their axons divided into two PFs that are then perpendicular to the PC dendritic tree (Harvey and Napper 1991). In contrast, once ION axons originating from the brainstem reached the cerebellum, CFs are positioned parallel to the PCs (Mason et al. 1990b). Thus, the orientation of the PFs and the CF relative to PC dendrites could regulate their connectivity. In this case, PFs would preferentially connect PC distal dendrites unlike CF which would connect more easily the proximal dendrites. Hence, the approach angle could play a role in subcellular specificity and not in partner selection, contrary to what has been seen previously. Similarly, if axodendritic overlap regulates synapse density, with greater overlap between CF-PC than PF-PC, we would expect CF to form more synapses than PF, which is the case with 300 synapses for CF contrary to 0-2 synapses for PF.

2. Neuronal lineage in dendritic subdomain targeting

GCs birth date determines their connectivity along PC dendrites, and thus their subcellular specificity, in contrast to what has been observed in other brain areas where birth timing controls partner selection. GCs migrate radially along Bergmann glia from the mitotic active region at the pial surface, the EGL, to the IGL. As in the neocortex, the cerebellar cortex is organized in an "inside-out" manner with later born GCs projecting to more superficial depths of the ML and earlier born GCs to deeper layer (Altman 1972). Using lineage tracing of single GC precursors, Liqun Luo's lab was able to visualize the projections of GC clones to PC at a very early stage (Zong et al. 2005). They confirmed that clonally-related GC restrict their PFs to nearby dendritic region of a given PC with early born GCs contacting PC dendrites at deeper layer than later born GC. However, contrary to what have been previously published, they argued that GC-clones are dispersed across the IGL **(Figure 22)** (Zong et al. 2005).

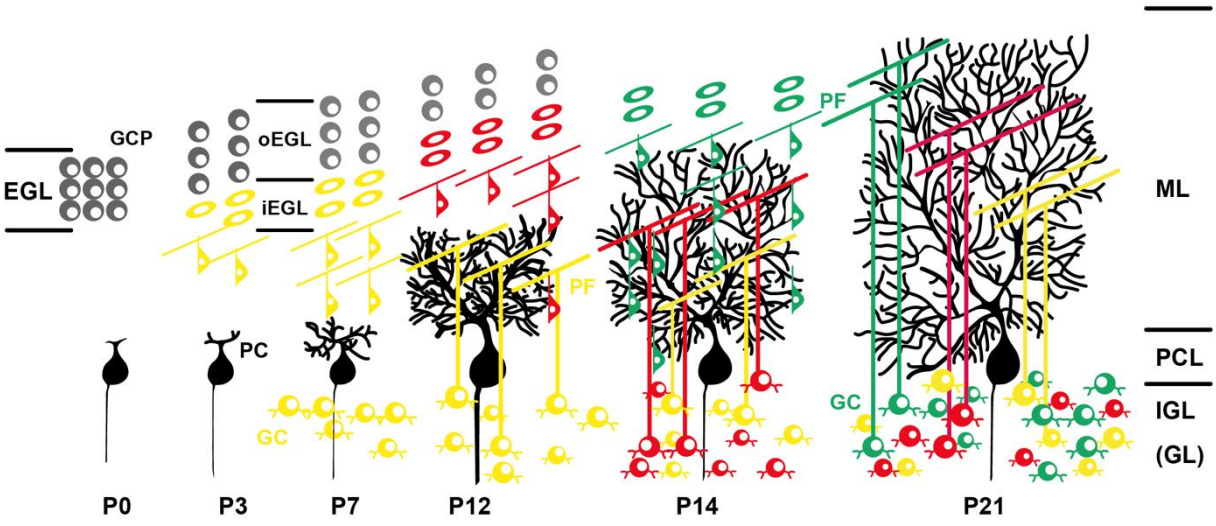

Figure 22. Parallel fibers' contacts on the Purkinje cell dendritic tree are chronologically ordered from deep to superficial sublayers.
Early generated GCs (yellow) stack their axons to deep sublayers in the ML, whereas GCs that differentiate later (red and then green) stack their axons to more superficial sublayers. GC, granule cell; PC, Purkinje cell; CF, climbing fiber; PF, parallel fiber; GCP, granule cell precursor; EGL, external granular layer; oEGL, outer external granular layer; iEGL, inner granular layer; ML, molecular layer; PCL, Purkinje cell layer; IGL, internal granular layer; GL, granular layer. Adapted from Espinosa and Luo 2008.

The exact functional significance of PFs clustering on PC is not yet clear. Nevertheless, a study published in the late 1970s in rats shows that the lower molecular layer is implicated in action coordination while the upper molecular layer is involved in motor coordination (Pellegrino & Altman, 1979). In this paper, they exposed GC precursors to X-irradiation during postnatal development to ablate either early or late-born GCs. Experiment using *in vivo* calcium imaging of neighboring GCs suggested spatially clustered activation of PFs during sensory processing (Wilms and Häusser 2015). This could facilitate generation of dendritic spikes and thus have consequences for PF transmission to PC. More recently, Straub and colleagues demonstrated that deeper GCs had higher firing thresholds and could sustain firing with larger current inputs than superficial GCs, thus improving spike-timing precision of PC (Straub et al. 2020).

3. Synapse specific CAM repertoires regulate subcellular specificity

In addition to their contribution to cellular specificity, CAMs can also promote subcellular synaptic specificity through different families of CAMs or different isoforms from the same CAM.

3.1 Excitatory neurons subcellular connectivity on Purkinje cell and CA1 pyramidal neuron

Serial electron microscopy demonstrated that at early stages of cerebellar development, CF and PFs territory are overlapped and mixed (Ichikawa et al. 2016). However, in the adult, PFs innervate the distal portions of PC dendrites while CF innervate the proximal ones. This segregated territory of PC excitatory afferents is the result of an intense competition that occurs not only during development but continues during adulthood. This contest is called the "heterosynaptic competition" in opposition to the "homosynaptic competition" which takes place among multiple CFs for the translocation on PC dendrites. Any impairment in the connection of CF or PFs with PC would provide an opportunity for PFs or CF, respectively to seize the other's assigned territory.

At the PF/PC synapses, the trans-synaptic interaction between the presynaptic NRX, the secreted Cerebellin1 (CBLN1) and the postsynaptic glutamate receptor δ2 (GluRδ2) are essential for their proper formation and maintenance (Matsuda et al. 2010a; Uemura et al. 2010; Ito-Ishida et al. 2012). GluRδ2 is expressed predominantly in PCs and localizes on spines contacting PFs (Takayama et al. 1995; Landsend et al. 1997). It is an ionotropic glutamate

receptor but does not function as a glutamate-gated ion channel (Kakegawa et al. 2008; Kakegawa et al. 2009). The first description of GluRδ2 mutant mice was done in the spontaneous GluRδ2 mutant *hotfoot* characterized by severe ataxia due to the loss of nearly half of PF/PC synapses, associated with the emergence of free spines and the mismatch of pre- and postsynaptic specializations at PF synapses (Guastavino et al. 1990; Kurihara et al. 1997). CBLN1 is highly expressed in the cerebellum, and more specifically in GCs. CBLN1 is part of the C1Q tumor necrosis factor family. It is secreted into the synaptic cleft and forms autonomous homo-hexamers. Because *Cbln1* KO and *GluRδ2* KO strikingly mimic behavioral, physiological, and anatomical phenotypes, a shared common pathway was suggested (Kashiwabuchi et al. 1995; Kishimoto et al. 2001; Hirai et al. 2005). Matsuda *et al.* demonstrated that CBLN1 act as presynaptic organizer at PF/PC synapses by promoting the clustering of GluRδ2 at the postsynaptic site as well as the clustering of NRX at the presynaptic site. CBLN1 directly interacts with the N-terminal extracellular domain of GluRδ2 while GluRδ2 C-terminus domain recruits, multiple scaffold proteins at the postsynaptic site such as Shank2, PSD-93, Homer3 and AMPA glutamate receptor 2 (GluA2) (Roche et al. 1999; Uemura et al. 2004; Matsuda et al. 2010a). Interestingly, CBLN1-GluRδ2 interaction is not only important for the proper formation of PF/PC synapses but also for the maintenance of these synapses. When recombinant CBLN1 was injected directly into the subarachnoid supracerebellar space above the cerebellar vermis, in adult *Cbln1* KO mouse, it fully recovers motor dysfunction and PF/PC synapse density within 2 days (Matsuda et al. 2010b). In the mouse model of *GluRδ2* KO in PC resulting in the loss of half of PF/PC synapses, CF invade the PF territory and extends to the distal dendrites (Ichikawa et al. 2002; Miyazaki et al. 2010). Moreover, in models of denervation of PCs by CFs, the loss of CFs was associated with the proliferation of spines, expressing GluRδ2 in the proximal compartment of PC which are contacted by PFs (Rossi and Strata 1995; Cesa and Strata 2009). PC can generate in a cell-autonomous manner a high number of spines according to the "Sotelo model" (Sotelo 2004). However, CFs repress spines formation at the proximal compartment through the Eph/ephrin signaling (Cesa et al. 2011). In this mouse model of denervation of PCs by CFs, only a subpopulation of adult IONs were lesioned, and surprisingly the neighboring CFs were able to sprout and reinnervate denervated PCs (Rossi and Strata 1995; Cesa and Strata 2009). When CFs sprout on previously denervated PC, both CF/PC and PF/PC synapses express GluRδ2, then few days later, PFs appear again to be restricted to the distal dendrites and GluRδ2 disappears from the proximal dendritic domain.

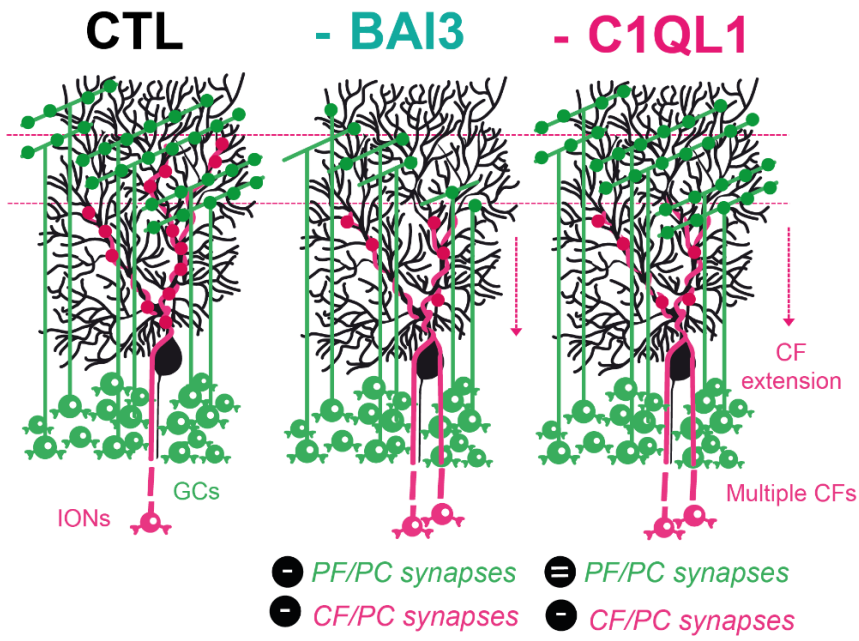

Figure 23. C1QL1 is a synaptogenic molecule at climbing fiber/Purkinje cell synapse and BAI3 promotes excitatory synaptogenesis on Purkinje cell.
BAI3 is present at both PF and CF synapses but interact with C1QL1 only at CF/PC synapses. In the absence of BAI3 and C1QL1 signaling, a loss of CF/PC and PF/PC synapses are observed. The same phenotype is observed in C1QL1-deficient mouse, except that the number of PF/PC synapses seems not changed. GCs, granule cells; IONs, inferior olivary neurons; PF, parallel fibers; CF, climbing fiber.

The complement component 1q subcomponent-like 1 (C1QL1) is a secreted member of the innate immune system, similar to CBLN1, and has a C-terminal globular domain. *C1ql1* is highly expressed in IONs during development as well in adult, and plays a major role in CF/PC synapse formation (Sigoillot et al. 2015). C1QL1 was shown to bind to brain-specific angiogenesis inhibitor 3 (BAI3), a cell-adhesion G protein-coupled receptor (GPCR) (Bolliger et al. 2011). BAI3 was initially identified at PF/PC synapses (Selimi et al. 2009). BAI3 receptor is present at both PF and CF synapses, and promotes both PF and CF connectivity on PC **(Figure 23)**. BAI3 also regulates PC dendrite morphogenesis (Lanoue et al. 2013; Sigoillot et al. 2015). At P7-P8, no differences were observed in the number of CFs per PC between the *C1ql1*-null and wild-type mouse, with a single CF-EPSC already dominant. The amplitude of the largest CF-EPSCs increases with mouse age except in *C1ql1* KO mice where it remains constant. Therefore, C1QL1 seems to not play a role at early stages in the selection of the winning CF since one CF seems to be strengthened initially. Nevertheless, at later stages this CF was not further strengthened in the absence of C1QL1 resulting in the translocation of other CFs with stronger EPSCs (**Figure 23)**. The misexpression of C1QL1 in the ML at P7 leads to

a decrease in CF synaptic territory on PC dendrites from 60% to 45% PC height (Sigoillot et al. 2015). C1QL1 overexpression in the ML might leads to the occupancy of BAI3 receptors, then disfavoring CF connection to PC. Because BAI3 is located postsynaptically at both PF/PC and CF/PC synapses, a possibility is that the proper territory of innervation on PCs is controlled by the "heterosynaptic competition" between PF and CF for a limited amount of BAI3 receptors.

To conclude, the secretion of two different complement C1Q-related proteins at each input, CBLN1 at the PF and C1QL1 at the CF, are fundamental for the proper formation and maintenance of these two synapse types on PC **(Figure 24)**. CBLN1 and C1QL1 have distinct and non-overlapping expression pattern such as their respective inputs. Indeed, initially CF and PF connect PCs on the same territory during development, and then their territories become distinct and non-overlapping in adult. This suggests that *C1ql1* and *Cbln1* contribute to synapse identity and thus specificity of connection on PC. In fact, in *Cbln1* KO or *C1ql1* KO, CF and PF territory on PC are both impaired. Taking together this support the ''chemoaffinity code'' postulated by Roger Sperry in the 1960s that stated that each type of neuron expresses a specific molecular combination that gives an "affinity" for its synaptic partners. However, it seems that C1QL1 and CBLN1 are not sufficient to define the presynaptic identity since in both KO, 50% of the synapses are still formed. Hence, the existence and nature of this molecular combination encoding synaptic identity remains to be demonstrated.

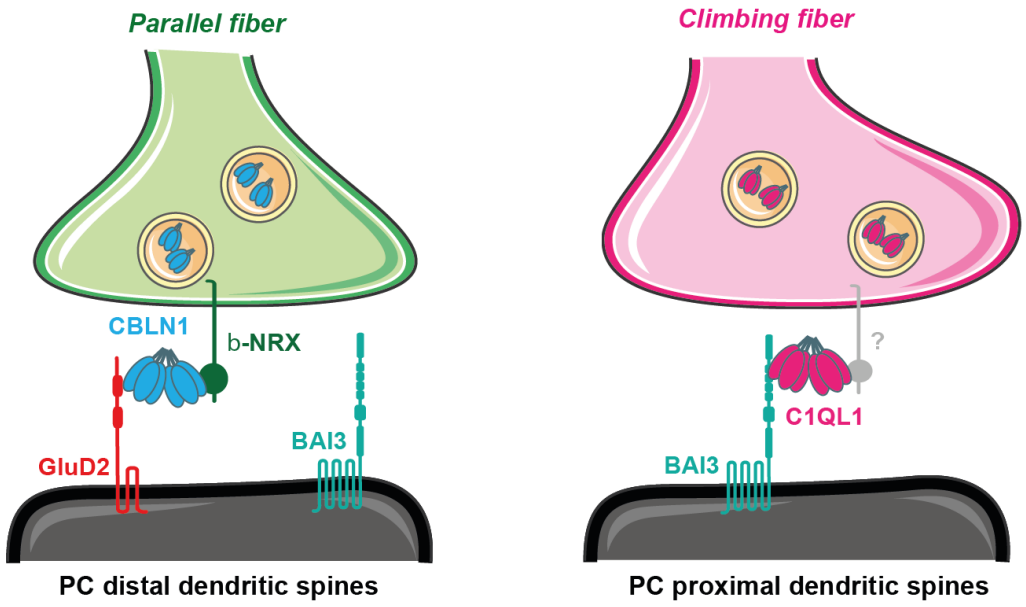

Figure 24. A partial molecular code for excitatory connectivity on Purkinje cell.

Expression of a specific C1Q-related protein in each PC input is necessary, but not sufficient, for proper connectivity.

An example other than the cerebellum that perfectly illustrates the role of CAMs in the subcellular synaptic specificity is the CA1 pyramidal neurons connectivity. CA1 connectivity is well-characterized: entorhinal cortex (EC) axons connect CA1 distal apical tuft dendrites in the *stratum lacunosum moleculare* (SLM) region and Schaffer collaterals (SCs), axons of CA3 neurons, innervate dendritic compartments both in the *stratum radiatum* (SR) and in *stratum oriens* (SO) (**Figure 25**). Differential expression patterns of several CAMs were identified across CA1 laminae and explained, in part, this stereotyped connectivity (**Figure 25**) (reviewed in Apóstolo & de Wit, 2019; Blockus & Polleux, 2021). Among these CAMs, one of the best characterized synaptogenic protein family, the Leucine-Rich Repeat-domain containing transmembrane proteins (LRRTMs) were identified. Leucine-rich repeat 2 (FLRT2) and NTRK-like protein 1 (Slitrk1) are localized in CA1 neurons at SR and SLM domains whereas LRRTM1 is only localized at SLM domain **(Figure 25)** (Schroeder et al. 2018). In SO, the presynaptic Cdh9 binds to Cdh6 and Cdh10, both expressed in CA1 dendrites. These interactions are required to give the identity of CA1-SO synapses that are characterized by more mushrooms spines **(Figure 25)** and higher magnitude of long-term potentiation (LTP) compared to CA1-SR synapses (Basu et al. 2017). SO synapses can no longer undergo this high magnitude of LTP when Cdh6 and Cdh10 are lost but no effect on LTP in the SR layer was observed. Moreover, work from Thomas Südhof's lab showed a non-overlapping expression of Latrophilin-2 (Lphn2) and Latrophilin-3 (Lphn3), postsynaptic adhesion GPCRs, on dendritic domains of CA1 neurons. Using mouse genetics to localize them endogenously and conditional knock-out, they were able to demonstrate that Lphn2 is at the SLM domain and is needed for EC/CA1 synapses formation whereas Lphn3 is at the SO and SR domains, and is needed for CA3/CA1 synapse formation (Sando et al. 2019). This synaptogenic process is dependent on the transcellular interactions between Lphn, Teneurins and FLRT proteins (Schroeder et al. 2018; Sando et al. 2019). In addition, a recent work identified a role for the trans-synaptic interaction between the postsynaptic Robo2, the secreted Slit and the presynaptic Nrxn in the establishment of synaptic specificity between CA3 axons and CA1 pyramidal neurons (Blockus et al. 2021). Robo2 is absent in the SLM region but present in the SO and the SR domains. Conditional deletion of Robo2 in CA1 neurons leads to a decrease in synapse formation only in SO and SR regions. Because CA1 neurons encode location-specific information, they assessed, using *in vivo* 2-photon Ca^{2+} imaging in awake behaving mice, place cells properties and found an increase in silent place cells.

These studies provide clear evidence that different CAMs at the SLM region *vs* SO and SR, could explain the specificity of connections on CA1 neurons. In addition to their role in

instructing synapse connectivity, they can also contribute to specify synapse function and identity (e.g., Cdh6, Cdh9). Finally, two different molecular complexes were identified in SR and SO dendrites: Nrxn-Slit-Robo2 and Teneurin/FLRT3-Lphn3 which raise interesting question: Are they present at the same synapses in the SR and SO domain? If so, do they work in combination? Further experiments are needed to elucidate these questions. A recent paper in the prefrontal cortex demonstrated a cooperation and concerted roles between LRRTM1 and SynGAP1, since the double LOF substantially lowered dendritic spine number more than the sum of single LOF (de Arce et al. 2023).

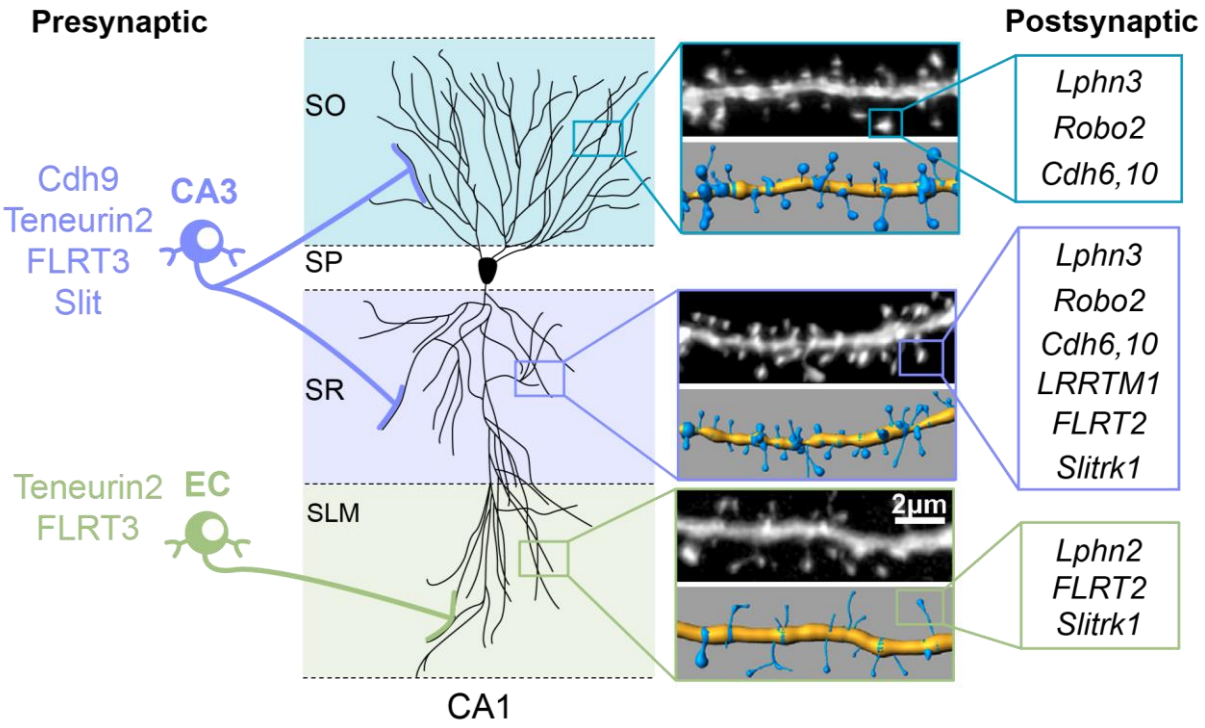

Figure 25. Principal CAMs contributing to CA1 pyramidal neurons connectivity.
CA1 neuron receives inputs from CA3 neurons and from the EC. SLM spine densities are lower and spine lengths longer compare to SR and SO. However, SO has higher densities of stubby and mushroom spines compared to SR. CAMs are differentially distributed along CA1 dendrites and regulate synapse specificity and identity, allowing proper connectivity on CA1 pyramidal neurons. Adapted from Apóstolo and de Wit 2019 and Basu et al., 2017.

3.2 Interneurons subcellular connectivity on Purkinje cell and cortical Pyramidal cell

One classical example of subcellular specificity is the connection of Stellate and Basket cells to PC. Bergmann glia are used as a guidepost for Stellate cells to reach their right subcellular localization towards PC dendrites. It was shown that this process is dependent on the close

homolog of L1 protein (CHL1) from the IgSF family (Ango et al. 2008). Indeed, in the absence of CHL1, Stellate cells show aberrant branching and orientation, and impairment in synapse formation with PCs. Moreover, targeting of Basket cells to PC AIS is dependent on a subcellular gradient of neurofascin isoform 186 (NF186), another member of the L1 immunoglobulin family (Ango et al. 2004). In ankyrinG KO mouse, NF186 gradient is abolished and localized along PC axons, leading to mistargeting of Basket cells to PC distal axon segments. In fact, ankyrinG is a membrane adaptor and is necessary to restrict NF186 to the AIS. Using a dominant-negative approach to disrupt NF186 and ankyrinG complexes, Ango and colleagues observed a severe reduction of "pinceau" synapse, suggesting that NF186 and ankyrinG might play synaptogenic function (Ango et al. 2004). These studies demonstrate that different members from the same L1 family are expressed at different GABAergic synapses and instruct synapse subcellular specificity for proper circuit wiring in the cerebellum. Finally, more recently, they demonstrated that semaphorin-3A (SEMA3A) which is secreted by PC soma, instructs Basket cell axon branching through the stabilization Neuropilin1 and thus facilitating its interaction with NF186 at the AIS (Cioni et al. 2013; Telley et al. 2016).

In the cortex, the expression of different subsets of genes by different interneuron subtype mediates their specific subcellular location on cortical pyramidal cells (Favuzzi et al. 2019). Innervation of the dendritic compartment of Pyramidal cell by Martinotti somatostatin-positive cells (SST+) involves the secretion of LGI2, a leucine-rich glioma inactivated family member. The expression of *Cbln4* in Basket PV+ cells and *Fgf13* in Chandelier PV+ cells specify soma targeting and AIS targeting respectively (**Figure 26A**). CBLN4, a member of the C1Q family, is a secreted protein and FGF13 is an intracellular protein and a microtubule stabilizer. Knock-down of these genes in each interneuron subpopulations using shRNA leads to a decrease in the number of synapses formed on pyramidal cells (**Figure 26B**). They also demonstrated that the overexpression of *Cbln4* in SST+ and Chandelier cells results in a specific increase of dendritic inhibitory synapses, suggesting that these molecules mediate subcellular synaptic specificity (**Figure 26C**). This work raises an important question: How do these proteins specify subcellular connectivity, especially FGF13? CBLN4 and LGI2 are considered as CAMs, they are secreted molecules and act as bidirectional synaptic organizer. The trans-synaptic interactions between the glutamate receptor delta-1 (GluD1), a postsynaptic organizer, and CBLN4, trigger synapse formation between SST+ and pyramidal neurons (Fossati et al. 2019). LGI2, like the LGI1 closely related protein, binds to metalloproteinase-lacking members of the ADAM family of neuronal receptors (Seppälä et al. 2011). LGI1 has been shown to

promote synapse formation and maturation by antagonizing Nogoreceptor (Thomas et al. 2018). However, FGF13 is a microtubule-stabilizing protein regulating neuronal polarization and migration in the cerebral cortex and the hippocampus (Wu et al. 2012). Thus, FGF13 is not a CAM *per se* and further investigation needed to determine whether or not FGF13 may act downstream in a signaling pathway that is specific to Chandelier cells.

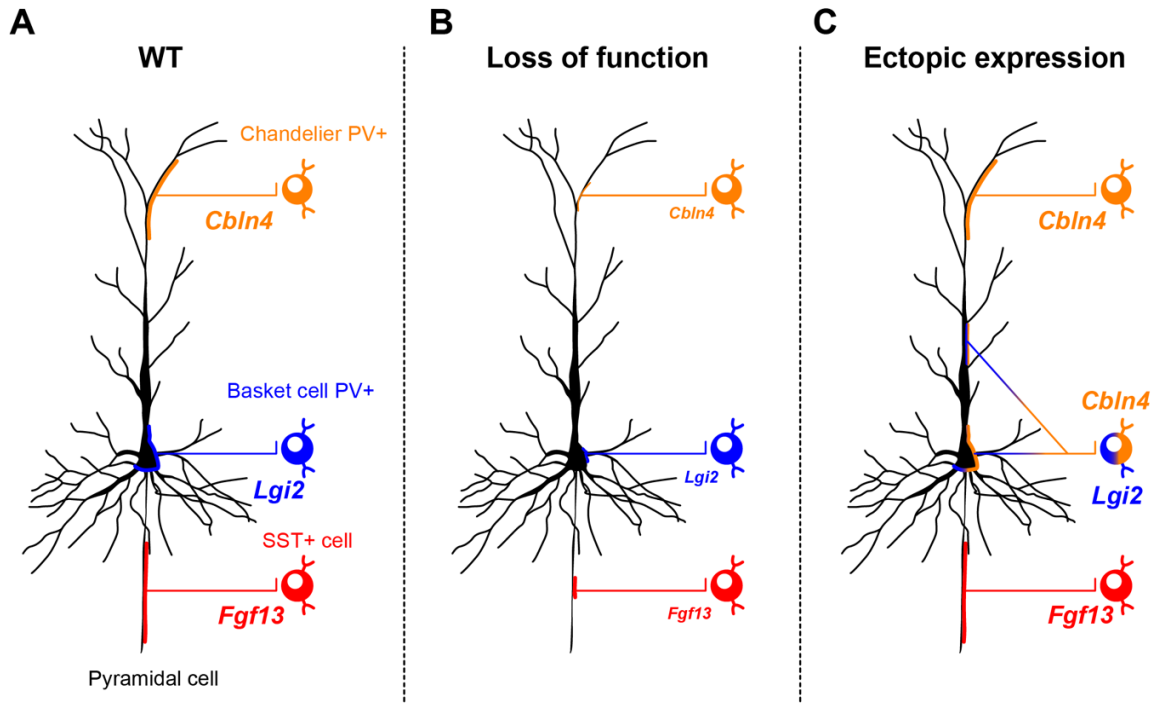

Figure 26. Differential gene expression regulates the synaptic targeting of SST+, basket and chandelier cells on Pyramidal cell.
Cbln4 in SST+ cell, Lgi2 in Basket cell and Fgf13 in Chandelier cells are required for proper synaptogenesis at specific subcellular location on Pyramidal cells. Loss of function of Cbln4, Lgi2 or Fgf13 causes a decrease in synapse density at the dendritic domain, soma and AIS respectively. Overexpression of Cbln4 in Basket cells increase the number of aberrant synapses formed on the dendritic compartment without changing the connectivity on the soma. Adapted from Llorca & Deogracias, 2022.

4. Subcellular territory specification of Purkinje cell excitatory afferents is activity-dependent

As described earlier, PC specific deletion of $Ca_V2.1$, which constitutes the major Ca^{2+} current in PC, induces deficit in the "homosynaptic competition" between multiple CFs, leading to deficits in CF elimination during the "early phase" (Hashimoto et al. 2011). Moreover, in this

mutant mouse model, CF innervation territory is decreased to the basal part of the dendrites and to the PC somatodendritic compartment. Consequently, PFs territory extends to proximal dendrites, suggesting that PFs take over the putative territory of CFs (Miyazaki et al. 2004). Similarly, infusion of TTX or NBQX, a selective antagonist of the AMPA-R, in the adult rat for 7 days leads to the expansion of PFs' territory (Kakizawa et al. 2005; Cesa et al. 2007). PFs invade the proximal dendritic arborization which is characterized by the loss of a large number of CF synaptic contacts on PC. Surprisingly, CF regression on the PC is accompanied by the appearance of newly formed spines at the proximal dendritic domain harboring GluRδ2, normally restricted to PF/PC synapses **(Figure 27)** (Bravin et al. 1999; Cesa et al. 2007). These newly formed synapses are then innervated by PFs. Two weeks after the TTX minipump removal, CFs retake their territory, GluRδ2 is localized only at PF/PC synapses and PFs are restricted to distal dendrites. These studies reinforced the idea that neuronal activity is a key player not only for the refinement of CF and PF connectivity on PC but also for their maintenance. Interestingly, they also suggest that neuronal activity might drive synaptic subcellular specificity through the expression and/or the localization of cell adhesion molecules (i.e., GluRδ2). Thereby, neuronal activity could instruct and/or repel indirectly the localization of CF and PF on PC. Such a phenomenon does not seem to have been described in other regions of the CNS.

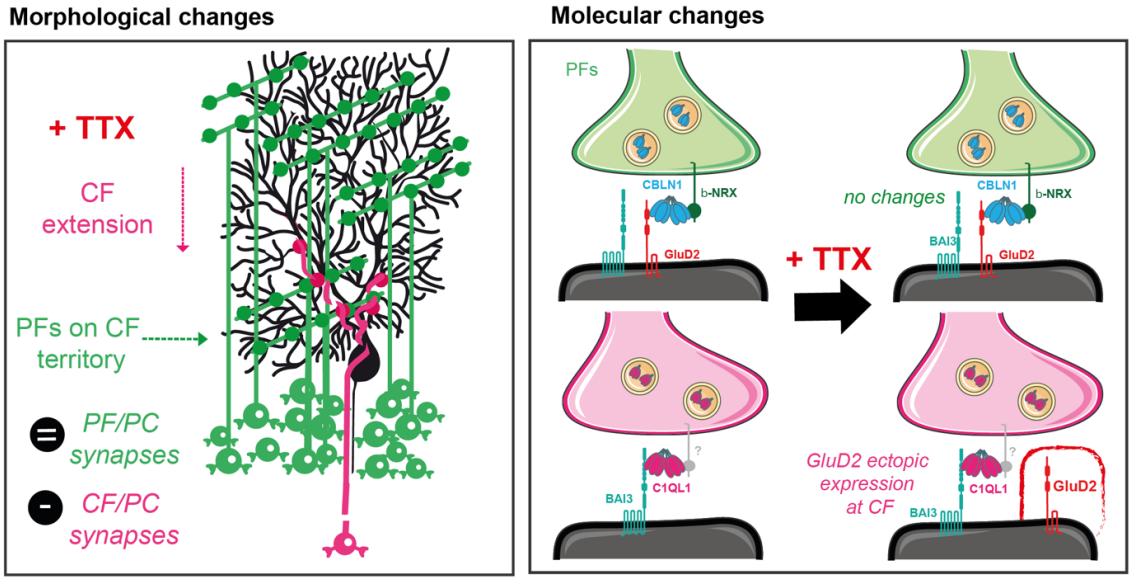

Figure 27. Schematic illustration of parallel fiber and climbing fiber innervation on Purkinje cell after TTX infusion in the cerebellum.

After TTX infusion, CFs have lost its synaptic contact on PC and new spines proliferate at the proximal dendritic domain which are innervated by PFs. GluRδ2 starts to be expressed at all PC synapses.

RESULTS

"*What mysterious forces precede [...] a skilfully arranged architectural plan, to finally establish those protoplasmic kisses [...] which seem to constitute the final ecstasy of an epic love story?*"

— Ramón y Cajal

Preamble

Understanding how the establishment of specific synaptic connections occurs during brain development is challenging. Using the olivo-cerebellar system as a model, we investigated whether each excitatory afferent of PC expresses a unique combination of proteins that could contribute to specific synapse formation and function. By combining neuron-specific transcriptomics and synapse-specific proteomics techniques *in vivo*, my team has identified novel molecular determinants involved in synapse formation and maturation in the cerebellum (Selimi et al. 2009; Lanoue et al. 2013; Sigoillot et al. 2015; González-Calvo et al. 2021). In particular, the study of C1QL1 function at CF synapses, compared to data on CBLN1 at PF synapses, revealed that the expression and specific secretion of a different member of the complement C1Q family by each afference is essential, but not sufficient, to define CF and PF presynaptic identity (Ito-Ishida et al. 2012; Kakegawa et al. 2015; Sigoillot et al. 2015). This is in support of the "chemoaffinity code" hypothesis that stated that each type of neuron expresses a specific molecular combination that instructs its specific connectivity. However, the existence and nature of this molecular combination coding for synaptic identity remained to be demonstrated. Thus, my work was organized around three axes: (1) determining the combination of presynaptic synaptogenic proteins that underlie the specificity of PC excitatory synapses by focusing more particularly at the CF/PC synapses, (2) determining when this molecular combination is established and (3) how it is regulated.

For the first and second aims (1) (2), the main results are included in a preprint deposited in Biorxiv and presented in Part I of the results. In this study, we demonstrated that the proper formation of CF/PC synapses rely on the specific expression of a combination of secreted molecules by CFs. We also discovered that at early stages the synaptic code is common between CF and PF inputs which could explain the overlapping territory observed on PC dendritic tree at early stages. Interestingly, as the circuit matures, CFs specify their synaptic molecular identity, in contrast to PFs, suggesting that the molecular diversification of synapses may follow input-specific molecular rules.

The third aim of my PhD (3) was to determine the mechanisms regulating the molecular specification of CF/PC synapses during development. It has been shown that cerebellum activity blockade in adult leads to CF loss on PC (Bravin et al. 1999) and that different neuronal activity patterns induce different gene expression program (Tyssowski et al. 2018). Thus, we

wondered whether IONs activity could control the switch between the common and specific combination of synaptogenic proteins that occurs in IONs. To test this hypothesis, I tested several strategies to specifically block activity of IONs during the first weeks of postnatal development. A summary of these experiments as well as the results obtained using Kir2.1 driven blockade of activity are described in Part II.

Part I. Article: Stepwise molecular specification of excitatory synapse diversity on a target neuron

Title: Stepwise molecular specification of excitatory synapse diversity on a target neuron

Authors: Maëla A. Paul[1†], Séverine M. Sigoillot[1†], Léa Marti[1], Marine Delagrange[2], Philippe Mailly[1], Fekrije Selimi[1*]

Affiliations:

[1]Center for Interdisciplinary Research in Biology (CIRB), College de France, CNRS, INSERM, Université PSL; Paris, France.
[2]Plateforme qPCR-HD-GPC, Institut de Biologie de l'Ecole Normale Supérieure; Paris, France
*Corresponding author. Email: fekrije.selimi@college-de-france.fr
[†]Equal contribution

Abstract:

Brain function relies on the generation of a large variety of morphologically and functionally diverse, but specific, neuronal synapses. Here, we show that, initially, synapse formation on a common target neuron, the cerebellar Purkinje cells, involves a presynaptic secreted protein common for all types of excitatory inputs. The molecular program then evolves only in one of the inputs with the additional expression of a combination of presynaptic secreted proteins that specify the mature pattern of connectivity on the target. These results show that some inputs actively and gradually specify their synaptic molecular identity while others rely on the "original code". Thus, the molecular specification of excitatory synapses, crucial for proper circuit function, is acquired in a stepwise manner during mouse postnatal development and obeys input-specific rules.

One Sentence Summary:

The molecular code specifying excitatory connectivity on a target neuron evolves with postnatal circuit maturation.

Keywords:

Brain, development, synaptogenesis, excitatory synapse, cerebellum, Purkinje cell, inferior olivary neuron, granule cell, transcriptomics, mouse

Introduction

Morphologically, molecularly and functionally distinct types of neurons need to be connected in a stereotyped manner to form the short-range and long-range circuits that underlie complex behaviors in mammals. This requires not only the recognition of the proper neuronal partners, via the molecular control of cell migration and axon guidance in particular, but also the formation of specific synapses on a given target neuron (1, 2). Each neuron receives multiple types of inputs that form synapses with specific identities determined by their subcellular localization and their degree of connectivity on the target neuron, as well as their specific molecular composition and functional properties. Indeed, synaptome mapping using two excitatory postsynaptic markers and unsupervised classification has revealed thirty-seven synaptic types (3). Given that more than a thousand synaptic proteins have been identified, the mammalian brain thus likely contains a large diversity of synapses (3) supporting information processing, learning and memory.

Various principles have been proposed to control the specific wiring of neurons during development (1, 2, 4–6). Neuronal activity sculpts circuits via selective stabilization or elimination of synapses (7). On the other hand, the chemoaffinity hypothesis states that the specificity of connectivity is regulated by "specific cytochemical affinities" (8) and implies the existence of different molecular combinations for each synapse type. While the chemoaffinity hypothesis has received much attention in the case of neuronal partner selection, to what extent it also relates to synapse specificity on a given target neuron remains to be demonstrated (2). Many adhesion complexes of transmembrane proteins with roles in synaptogenesis have been identified (see (2, 6) for review). Different surface proteins have been shown to underlie excitatory versus inhibitory synapse formation (4, 6, 9–15). However, synapse diversity goes well beyond these two broad functional classes and generally, a given neuron receives synapses from several types of glutamatergic or inhibitory inputs. While individual molecular complexes have been identified to participate in the formation of certain synapses (9, 10, 16), whether and how a combination of proteins controls the formation of a specific synapse type remains to be tested. In addition, whether the rules underlying the specification of different excitatory synapse types on a given neuron during development are identical remain unknown.

Cerebellar Purkinje cells (PCs) are a perfect example of the type of specific and stereotyped connectivity that must be generated for proper network function and information coding. They are at the center of computation of the cerebellum (17), an organ that is well known for its control of motor coordination and learning, but also increasingly recognized for its broader role

in many cognitive processes (6) (17, 18). PCs receive direct synapses from two excitatory inputs, the parallel fibers (PFs) and climbing fibers (CFs), axons of cerebellar granule cells (GCs) and inferior olivary neurons (IONs) of the brainstem respectively. Their activity is further modulated by local inhibitory neurons, the stellate cells and basket cells. The PF and CF synapses are made on separate subcellular territories on a given PC, distal dendritic spines versus proximal dendrites respectively, with a different degree of connectivity, and different functional properties. This mature connectivity is established during the first three postnatal weeks in rodents (19). The formation of each excitatory synapse type depends on signaling pathways that involve a different member of the C1Q protein family (9). Parallel fiber/Purkinje cell (PF/PC) synapses are dependent on the formation of a tripartite complex between presynaptic neurexin-1, secreted CBLN1 and postsynaptic GluD2 receptors (11, 20), while climbing fiber/Purkinje cell (CF/PC) synapses rely on secreted C1QL1 and postsynaptic adhesion GPCR BAI3 (9, 21). Both CBLN1 and C1QL1 loss of function (LOF) experiments result in the loss of about half of PF/PC or CF/PC synapses, respectively (9, 22). Thus, either compensation by other synaptic proteins can prevent complete loss of synapses, or several molecular signaling pathways might be at work at each synapse type, in support of the chemoaffinity hypothesis.

Using the cerebellar PCs as a model, we searched for the combination of membrane and secreted proteins underlying the specificity of excitatory connectivity on a single neuron type. Neuron-specific gene expression profiling and LOF analysis during postnatal development revealed that the CF relies on a combination of cell surface proteins belonging to different signaling pathways for its mature connectivity on PCs. These proteins, in particular LGI2 and CRTAC1, could play a function similar to the one of C1QL1, the well-known CF/PC synaptogenic molecule. Surprisingly, we discovered that the cerebellar GC marker Cbln1 is also expressed by IONs and that, in addition to its known role at PF/PC synapse, it also regulates synaptogenesis between CFs and PCs at early stages. Thus, a common molecular code is shared initially, and a specific molecular combination is acquired progressively in selected input types during postnatal development to establish the final connectivity pattern on a given target neuron.

Results

Purkinje cell excitatory inputs are characterized by different surfaceome expression dynamics during postnatal development

Synapse specificity and identity involves the recognition and adhesion between the pre- and postsynaptic domains of neuronal partners. Thus, molecules that regulate synapse formation and specification are expected to be part of the "surfaceome", defined as the set of genes coding for membrane and secreted proteins. In a previous study (23), neuron-specific expression profiling in vivo and comparative analysis identified the differentially expressed genes (DEGs) specific for each adult PC excitatory input (401 for cerebellar GCs versus 598 for IONs of the brainstem). Amongst these DEGs, 74 and 250 genes code for membrane and secreted proteins and thus constitute the specific adult surfaceome of GCs and IONs, respectively (Fig. 1A). As expected, these genesets contained genes coding for proteins with known function in the formation and stabilization of excitatory synapses on PCs: Cbln1 for synapses from GCs and C1ql1 for synapses from IONs. Because the pattern of expression of Cbln1 and C1ql1 is highly correlated with the respective timing of synaptogenesis on PCs (Fig. 1A), we reasoned that other genes with similar roles in synapse specification should have similar expression pattern dynamics during development. High-throughput expression analysis of the GC and ION genesets was performed at different postnatal developmental stages using RNA extracts from the cerebellum and brainstem (Data S1 and S2): from E17, a time when IONs and PCs have already been generated and have started to connect, to adult when all the connectivity between GCs and IONs onto PCs has been established (19). Clustering analysis showed a fundamental difference in the postnatal dynamics of the surfaceome that characterizes each PC excitatory input (Fig. 1B and 1D). In GCs, only one major cluster was identified containing 70 genes with a developmental pattern similar to the one of the synaptogenic gene Cbln1: they were expressed at very low levels during the first two postnatal weeks, and then, expression synchronously increased starting at P14 (Fig. 1B), in correlation with the timing of synaptogenesis between GCs and PCs (Fig. 1C). In the brainstem, clustering analysis of ION-specific surfaceome resulted in two groups: a group of 117 genes that were expressed at higher levels during the two first postnatal weeks and then decreased (cluster 1, Fig. 1D), and a second group of 125 genes, which included C1ql1, that were expressed at increasingly higher levels starting during the second postnatal week (cluster 2, Fig. 1D). Because this developmental period is essential for the establishment of mature ION-PC connectivity (Fig. 1C), we searched amongst the 125

genes of cluster 2 for candidates that would play a functional role similar to C1ql1. Fifteen genes were selected based on high expression levels (fig. S1A) and database and literature curation looking for predicted structural domains with roles in recognition. The correlation of their expression pattern with the synaptogenic gene C1ql1 was then determined using single molecule Fluorescent In Situ Hybridization (smFISH) in the inferior olive region at three ages of interest. At P4, CF, but not PF synaptogenesis, has begun on PCs with several CFs synapsing on their somata. At P14 the single wining CF has already started to translocate (24) and CF and PF inputs compete for their subcellular synaptic territory on the growing PC dendrites (25). Finally, the adult mature stage is reached when the final territory of innervation and functional properties of excitatory synapses on PCs have been acquired. Interestingly, computation of a pixel-based Pearson correlation coefficient (see methods section) allowed the classification of the candidate genes in groups that corresponded to the different developmental stages of ION-PC connectivity. Four genes, Nrcam, Lgi2, Crtac1 and Sema4f, were highly correlated with C1ql1 (Pearson coefficient > 0.6) at every stage (Fig. 1E), suggesting a synaptogenic role similar to C1ql1 during the postnatal development of ION-PC connectivity. Five genes (Shisal1, Thy1, Adam11, Crh and Gpr123) were less correlated at P4 but highly correlated starting at P14 (Fig. 1E), suggesting a role at later stages than C1ql1, potentially in the functional maturation of CF/PC synapses. The other six candidates (Tmem184b, Fstl1, Cx3cl1, Adam23, Cd151, Tmem179) did not reach the threshold of correlation with C1ql1 in the adult (fig. S1B), and might play roles in other processes than the control of CF/PC synaptogenesis and functional maturation. Overall, our high-throughput RTqPCR and smFISH analyses reveal a multi-step postnatal acquisition of the adult gene expression pattern specific for IONs for the combination of genes coding secreted and membrane proteins. Thus, the acquisition of the adult-specific surfaceome characterizing the two PC excitatory inputs, GCs and IONs, follows different time courses during postnatal development. GCs acquire their “surface” adult identity in one step during their differentiation, while the surfaceome of IONs changes progressively to acquire the adult combination. Indeed, a first set of genes (Fig. 1D, cluster 1) is highly, but transiently, expressed during the first stage of immature ION connectivity on PC somata and the reduction of CF/PC multi-innervation by synapse elimination. The expression of a second set of genes (Fig. 1D, cluster 2) increases during the second postnatal week. This set comprises genes that will participate in the control of CF translocation, synaptogenesis on PC dendrites and competition with PFs (Fig. 1C), and other genes that will participate later in the functional maturation of the CF/PC synapses like Crh (26) (Fig. 1E, lower correlation with C1ql1 at the single cell level at P4).

A combination of secreted proteins controls the establishment of Climbing fiber/Purkinje cell connectivity

If synapse specification is controlled on a given target by a specific combination of presynaptic recognition proteins, the combination coding for CF/PC synapse development should include other ION DEGs with an expression pattern highly correlated to C1ql1 at the single cell level. Using a second analysis pipeline (cf. materials and methods available as supplementary materials), we thus analyzed smFISH experiments at the single-cell level (Fig. 2A and 2B) and computed the Pearson correlation coefficient of Nrcam, Lgi2, Crtac1 or Sema4f with C1ql1 in IONs. This analysis confirmed very high correlation for Nrcam, Lgi2 and Crtac1 at every stage, but showed a relatively lower correlation for Sema4f transiently at P14 (Fig. 2B). Interestingly, Crtac1 and Lgi2 both code, like C1ql1, for extracellular matrix proteins, while Nrcam codes for an Ig domain containing single-pass transmembrane protein (Fig. 2C). While C1QL1 is characterized by a globular C1q domain known to interact with the BAI3 synaptic adhesion-GPCR (21, 27), LGI2 is part of a family of secreted proteins containing Leucine Repeat Rich domains and a beta-propeller domain (Fig. 2C), and binds to the ADAM family of synaptic receptors (28). CRTAC1 is also part of the beta-propeller domain containing family of proteins (Fig. 2C), and binds to NOGO receptors (29) that have been recently shown to promote synaptogenesis in addition to neuronal morphogenesis (30).

To uncover the function of Nrcam, Lgi2 and Crtac1 in excitatory synaptogenesis and test their involvement in synapse specification on PCs, we set up an in vivo assay to perform ION-specific LOF of each candidate gene during postnatal development. To enable CRISPR/Cas9 based genome editing specifically in IONs during postnatal development, we developed an intersectional strategy by injecting in the cerebellum of Cas9 knock-in P0 mouse pups (31) a retrograde AAV driving the expression of the CRE recombinase under the CamKII promoter, which is not expressed in GCs, thus enabling conditional expression of CAS9 and soluble GFP specifically in IONs (Fig. 3A and 3B). Several guide RNAs were selected for each candidate gene using CRISPOR web-based tool, except the Nrcam gRNA that was previously characterized (32) (fig. S2). Transduction of cultured cortical neurons was used to assess efficiency and specificity using sequencing and RT-qPCR (fig. S2, data S3 and materials and methods available as supplementary materials). No mutation in protein coding regions was detected by sequencing, and RTqPCR showed a 50% (Nrcam and Lgi2) and 75% (Crtac1) decrease in mRNA levels for each of our targeted candidate. No effects on the expression of

other candidate genes analyzed in our study was detected. The more efficient guide RNA was selected for each candidate gene, subcloned in the AAV construct together with the CamKII-Cre to simultaneously drive the expression of guide RNAs under the control of the U6 promoter and the conditional expression of CAS9 to edit the genomic region of interest in IONs. Consequences of ION-specific LOF of each candidate gene were assessed at P21, an age when the final pattern of connectivity between PCs and its excitatory inputs has been attained. Thanks to the co-expression of soluble GFP with CAS9 after recombination, we could readily identify CFs from genome edited IONs in the cerebellar cortex (Fig. 3B). VGLUT2 is a specific marker of CF/PC synapses in the cerebellum and deficits in CF/PC synapse numbers and function have been shown consistently to be accompanied by a decrease in VGLUT2 cluster extension or numbers (9, 33). We thus used anti-GFP and anti-VGLUT2 immunolabeling followed by high resolution 3D imaging using spinning disk confocal microscopy, to quantify the morphology and the extension of the transduced GFP expressing (GFP+) CFs and, using a custom plugin, the number, and size of associated VGLUT2 presynaptic boutons (Fig. 3B and C, and methods). CF branching was significantly diminished in the case of Nrcam LOF, but not for the other candidates and total cumulative length of the CF was unchanged (Fig. 3C). In controls, CFs extend to about 70% of the molecular layer height, a value that is coherent with previously published data (9). Small but significant changes in this extension were detected for all three candidates: Lgi2 and Crtac1 LOF led to a 11% and 6% decrease respectively, while Nrcam LOF led to a 6% increase (Fig. 3C). Thus, amongst the three candidates, NRCAM plays a specific role in CF morphogenesis promoting their branching along the PC dendrites. At the synaptic level, an increase in about 17% in the number of VGLUT2 clusters per GFP labelled CF was observed after Nrcam LOF (mean 123.7 ± SEM 4.731 *versus* CTL: 105.9 ± 4.705, $p = 0.012$, Student's unpaired t test), accompanied by a significant 9% decrease in the mean volume of those clusters (mean 1.068 ± SEM 0.038 versus 0.9694 ± 0.034, $p = 0.029$, Mann-Whitney test). On the contrary, Lgi2 LOF and Crtac1 LOF led to a 20% and 29% significant decrease in the mean VGLUT2 number per transduced CF, respectively (*Lgi2*: mean 90.85 ± SEM 4.399 *versus* CTL: 112.9 ± 4.504, $p < 0.001$, Student's unpaired t test; *Crtac1*: mean 104.8 ± SEM 5.889 *versus* CTL: 134.9 ± 5.001, $p < 0.001$, Student's unpaired t test). This decreased mean number of presynaptic boutons was accompanied by a tendency to decreased mean volumes for Lgi2 LOF and a 15% significant increase for Crtac1 LOF (Fig. 3C). Thus, LGI2 and CRTAC1 both promote, while NRCAM inhibits, CF/PC synaptogenesis during the second developmental phase corresponding to CF synaptogenesis on PC dendrites and competition with PFs. NRCAM plays an additional role in controlling CF morphogenesis in accordance with expression data

showing a precocious strong expression of Nrcam in IONs (Fig. 2A and (34)). LGI2 and CRTAC1 are thus synaptogenic molecules forming together with C1QL1 a specific secreted combination underlying CF/PC synapse identity.

The combination of secreted molecules regulating climbing fiber synaptogenesis acts via partially non-redundant signaling pathways

LGI2, CRTAC1 and C1QL1 could function in parallel to modulate different signaling pathways promoting synapse formation since they bind different receptors. CRTAC1 and C1QL1 also converge on the BAI3 pathway and could thus play redundant functions: C1QL1 directly binds BAI3 (35) and CRTAC1 interacts with the NOGO receptor (36), recently shown to trans-synaptically bind BAI3 and control synapse formation (30). To test the potential synergy between these three synaptic signaling pathways at the CF/PC synapse, we performed C1ql1 single, C1ql1/Crtac1 double and C1ql1/Crtac1/Lgi2 triple LOF, specifically in IONs, using the previously described strategy of CRISPR/Cas9 genome editing. Single C1ql1 LOF led to a 15% and 30% significant decrease in the CF extension and the VGLUT2 cluster number per GFP+ CF respectively, compared to CTL (CF extension, C1ql1: mean 61.14 ± SEM 0.973 versus CTL: 72.12 ± 0.892, $p < 0.0001$, Student's unpaired t test; VGLUT2 number, C1ql1: mean 79.96 ± SEM 3.396 versus CTL: 110 ± 5.282, $p < 0.001$, Mann-Whitney test), while the volume of VGLUT2 clusters was increased by 34% (VGLUT2 cluster volume, C1ql1: mean 1.339 ± SEM 0.0582 versus CTL: 1.000 ± 0.0434, $p < 0.0001$, Student's unpaired t test), recapitulating the previously characterized phenotypes in the C1ql1 knockout mouse and after C1ql1 knockdown (Fig. 3A and 3B, fig. S3, data S3, and (9,21)). To perform double Crtac1/C1ql1 LOF, we generated retrograde AAV particles enabling the simultaneous expression of C1ql1 and Crtac1 more efficient guide RNAs under the control of their respective U6 promoter. Compared to single C1ql1 LOF, a 22% decrease in the number of VGLUT2 clusters per GFP+ CF was observed in the double C1ql1/Crtac1 LOF (C1ql1: mean 85.19 ± SEM 3.501 versus C1ql1/Crtac1: 66.56 ± 3.280, $p < 0.001$, Student's unpaired t test). No changes in CF extension and VGLUT2 cluster volume were detected. These results suggest that C1QL1 and CRTAC1 play non-redundant functions in regulating the number of CF presynaptic boutons, while they converge on the same pathway for the regulation of VGLUT2 cluster volume and extension. We then performed triple C1ql1/Crtac1/Lgi2 LOF by co-injecting retrograde AAVs driving the expression of C1ql1 and Crtac1 guide RNAs on one hand, and Lgi2 guide RNA on another hand, and compared the phenotype with the double C1ql1/Crtac1 LOF. An additional 18%

decrease was found in the mean number of CF presynaptic boutons, with no change in CF extension (VGLUT2 number, C1ql1/Crtac1/Lgi2: mean 61.47 ± SEM 3.884 versus C1ql1/Crtac1: 74.65 ± 3.827, p = 0.006, Mann-Whitney test). Interestingly, a 19% decrease of the mean volume of VGLUT2 clusters was detected in the triple LOF when compared to double C1ql1/Crtac1 LOF (VGLUT2 cluster volume, C1ql1/Crtac1/Lgi2: mean 0.812 ± SEM 0.451 versus C1ql1/Crtac1: 1.000 ± 0.044, p = 0.004, Student's unpaired t test). LGI2 thus plays non-redundant functions with CRTAC1 and C1QL1, both in terms of promotion of synaptogenesis and maturation of the presynaptic boutons, suggesting that these pathways might operate in parallel. Interestingly, in the triple LOF, the magnitude of the effect on the number of VGLUT2 clusters per GFP+ CF is consistent with the sum of the individual effect of single C1ql1, Crtac1 and Lgi2 LOF. LGI2 and CRTAC1 are thus synaptogenic molecules, forming together with C1QL1, a specific secreted combination underlying CF/PC synapse identity.

Cbln1 expression in inferior olivary neurons is necessary for proper climbing fiber connectivity on Purkinje cells

Our developmental expression analysis showed a multi-step determination of ION identity with a set of cell surface molecules that are expressed highly during the first two postnatal weeks, when CF synapses are made on the somata of PCs (Fig. 1D, cluster1). Surprisingly, by analyzing all 324 DEGs including those that are specific to cerebellar GCs, we found Cbln1 in the cluster of genes highly expressed in the brainstem during the first two postnatal weeks (fig. S3A, cluster 1; and data S4). Cbln1 is a well-known marker of PF/PC synapses and is essential for their formation and stabilization (37). We confirmed expression of Cbln1 in IONs using smFISH: our quantitative analysis shows that Cbln1 mRNA numbers in single IONs are comparable to the number of C1ql1 mRNAs at P4 but then start to diminish by P14 while C1ql1 expression on the contrary increases at the single cell level (Fig. 5A). This raised the question of the role of Cbln1 in IONs and prompted us to perform ION-specific Cbln1 LOF at P0 and analyze the consequences on CF/PC innervation (Fig. 5B). At P7, CFs lacking Cbln1 function had started to translocate in about 29% of contacted PCs in comparison to 11% for control GFP+ CFs. Cbln1 LOF also led to a 52% significant decrease of the mean number of VGLUT2/GFP clusters on PC somata compared to controls (mean 0.94 ± SEM 0.1038 versus 0.45 ± 0.0667, p = 0.029, p<0.001, Student's unpaired t test). No effect on the mean VGLUT2 cluster volume was detected (Fig. 5C and fig. S3C). When analyzed at P14, Cbln1 LOF led to an increase in CF branching and decreased CF extension. The total cumulative length of CF is

not changed by loss of Cbln1. This decreased extension of the territory of innervation along the PC dendritic arbor is accompanied by a decrease in synaptogenesis since a significant 21% decrease in VGLUT2 cluster numbers on PC dendrites was also observed, with no change in the mean VGLUT2 cluster volume, after Cbln1 LOF (Fig. 5D and fig. S3C). These results show that CBLN1 plays several roles during the establishment of CF/PC connectivity. It prevents precocious translocation of the winning CF on the growing PC dendrites, controls CF morphogenesis by directing its branching, and promotes CF synaptogenesis both on PC somata and dendrites. Given that CBLN1 is a secreted protein of the C1q family, these results finally establish CBLN1 as a common synaptogenic secreted factor for both types of excitatory inputs, GCs and IONs, connecting Purkinje cells.

Discussion

Synaptome mapping using two excitatory postsynaptic markers has revealed that a large part of synapse diversity across brain regions is acquired during the first three postnatal months in rodents (3, 38). In particular, the first month is the stage of large increases in both numbers and types of synapses in many brain regions (38). Analyzing the mechanisms regulating the development of excitatory connectivity on cerebellar PCs, we show that the increase in synapse diversity relies on specific molecular rules that control the formation of each synapse type on a given target neuron. GCs acquire their mature surfaceome, including the expression of synaptogenic genes, in one step during their differentiation, while IONs go through a multi-step definition of both their surfaceome and their mature connectivity on the PC target.

Many protein-receptor complexes have been shown individually to control synapse formation and maturation across the brain, including neurexins and their various ligands (LRRTMs, neuroligins…), secreted cerebellins and their GluD receptors, and secreted C1QL proteins and their receptors, the adhesion GPCRs of the BAI family (6, 39). However, to what extent does a combination of different signaling pathways contribute to defining the “cytochemical affinities” that underlie synapse specificity, as postulated by Sperry? Are these pathways functionally redundant for a single-synapse type? Our results demonstrate that at least five different molecular complexes contribute to CF/PC specific connectivity and identity (Fig. 5E). Some molecular pathways regulate the development of mature connectivity at different levels: in axon and dendrite morphogenesis on one hand, and synapse formation and stabilization on the other hand. In the case of CFs, NRCAM and CBLN1 regulate in opposite direction CF

morphogenesis in addition to regulating the number of synapses, in accordance with previous data (32, 40, 41). The BAI synaptic receptors or the NOGO signaling pathway also control both morphogenesis and synaptogenesis in cerebellar PCs and other neuronal types across the brain (9, 30, 42, 43). Interestingly, we show that, in addition to the BAI3-ligand C1QL1, the cell surface proteins LGI2 and CRTAC1 control synapse numbers and maturation specifically without affecting CF morphogenesis. LGI2 is part of a family of secreted proteins that binds to ADAM receptors. CRTAC1 is an extracellular matrix protein that inhibits NOGO signaling and promotes synaptogenesis in cultured hippocampal neurons (44). Thus, secreted proteins could play dual roles during synapse formation and specification: they could directly promote synaptogenesis via their specific receptors, but also inhibit other functions of their receptors by competing with other ligands, for example those regulating neuronal morphogenesis. Are these pathways redundant? Double and triple loss of function experiments show an additive phenotype for synapse numbers but not for the volume of VGLUT2 clusters, demonstrating that these three molecules, at least partially, play non-redundant functions for synapse specification. Binding of LGI1 to NOGO receptors inhibits NOGO signaling and promotes binding of LGI1 to its ADAM receptor (45). Recently interactions between the NOGO receptors and the BAI adhesion GPCRs were revealed to promote synaptogenesis in cultured human neurons (30). This raises the possibility that C1QL1, like LGI and CRTAC1, also modulates NOGO signaling. These cell surface proteins could play partially redundant function by inhibiting NOGO signaling at the same synapse but in addition promote other signaling pathways via their specific receptors: BAI3 for C1QL1, ADAMs for LGI2 and other yet to be identified receptors for CRTAC1 (Fig. 5E). This partial redundancy would be essential to maintain a certain robustness of circuit formation and function in the face of mutations in genes underlying synapse specificity.

Unexpectedly, both PC inputs rely initially on the same signaling pathway, via CBLN1 expression, for proper connectivity on their common target. The CBLNs constitute a subfamily of the C1Q family of secreted proteins that act as synaptic organizers throughout the brain (13, 46, 47). CBLN1 is well known for promoting the formation and stabilization of PF/PCs synapses through the formation of a tripartite complex with presynaptic neurexin-1 and postsynaptic GluD2 (11, 20, 48). In addition, we show that CBLN1 promotes CF synapses on PC somata and that in its absence, the winning CF translocates faster on the growing PC dendritic arbor, but the number of synapses that it makes on the dendrites is still reduced. This correlates with previous observations that the receptor for CBLN1, GluD2, is transiently present

at CF/PC synapses during development and adult reinnervation (49, 50). An original model postulated that the innervation of PCs on dendritic spines by PFs was a “default mode” (19). Here, we show that a first step for PC connectivity is the recognition by the excitatory inputs, regardless of their type, via CBLN1/GluD2 complexes, constituting a sort of “default molecular code” for connectivity. Other genes that we found in our study could be part of this default molecular code such as the NOGO receptors that are found both in granule cells and immature IONs (Data S4). During a second phase, molecular specification occurs selectively in the ION input: IONs start adding the expression of a specific combination of cell surface proteins that promotes the formation of synapses and their mature territory of innervation on the growing PC dendrites, in the face of competition with the PFs for their territory. Interestingly, many of the molecular pathways identified in our study are expressed in many regions of the brain and could control synapse specificity in other neuron types with synaptic organizations resembling the one observed for cerebellar PCs. Indeed, in the hippocampus, CA3 pyramidal neurons receive several types of excitatory inputs including one from dentate gyrus GCs that form a very specialized connection on the proximal dendrites via mossy fiber boutons. NRCAM, CRTAC1, LGI1 and C1QL proteins have been found at this particular synapse (51, 52). It is thus tempting to postulate that similar molecular rules control the development of excitatory connectivity in other neurons across the brain. For example, is the molecular identity of dentate gyrus-CA3 synapses acquired actively during development, while other synapses made on CA3 hippocampal neurons rely on a “default molecular code”?

What regulates the multi-step acquisition of the molecular identity of certain synapse types while in others synapse molecular specification occurs in a single step? The transcriptional program underlying the change in the gene expression pattern would need to be controlled by either an internal program or actively regulated. If it is active, it could be due to molecular factors, as recently described in Drosophila (53), or due to changes in neuronal activity in the network (54). The postnatal developmental period of circuit formation would thus be very sensitive to modulation by external factors for certain types of synapses but not others. This would imply specific consequences on circuit development by environmental changes in terms of computation and symptom etiology. The facts that many human brain disease genes code for synaptic proteins, and that synapse diversity can be modulated by mutations relevant to neurodevelopmental disorders, highlight the importance of understanding the molecular rules generating synapse diversity during development (55, 56).

References and Notes:

1. J. R. Sanes, M. Yamagata, Many paths to synaptic specificity. Annu. Rev. Cell Dev. Biol. 25, 161–195 (2009).
2. J. R. Sanes, S. L. Zipursky, Synaptic Specificity, Recognition Molecules, and Assembly of Neural Circuits. Cell. 181, 536–556 (2020).
3. F. Zhu, M. Cizeron, Z. Qiu, R. Benavides-Piccione, M. V. Kopanitsa, N. G. Skene, B. Koniaris, J. DeFelipe, E. Fransén, N. H. Komiyama, S. G. N. Grant, Architecture of the Mouse Brain Synaptome. Neuron. 99, 781-799.e10 (2018).
4. J. de Wit, A. Ghosh, Specification of synaptic connectivity by cell surface interactions. Nat. Rev. Neurosci. 17, 4–4 (2016).
5. B. A. Hassan, P. R. Hiesinger, Beyond Molecular Codes: Simple Rules to Wire Complex Brains. Cell. 163, 285–291 (2015).
6. T. C. Südhof, Towards an Understanding of Synapse Formation. Neuron. 100, 276–293 (2018).
7. J.-P. Changeux, A. Danchin, Selective stabilisation of developing synapses as a mechanism for the specification of neuronal networks. Nature. 264, 705–712 (1976).
8. R. W. Sperry, CHEMOAFFINITY IN THE ORDERLY GROWTH OF NERVE FIBER PATTERNS AND CONNECTIONS. Proc. Natl. Acad. Sci. U. S. A. 50, 703–710 (1963).
9. S. M. Sigoillot, K. Iyer, F. Binda, I. González-Calvo, M. Talleur, G. Vodjdani, P. Isope, F. Selimi, The Secreted Protein C1QL1 and Its Receptor BAI3 Control the Synaptic Connectivity of Excitatory Inputs Converging on Cerebellar Purkinje Cells. Cell Rep. 10, 820–832 (2015).
10. A. Schroeder, J. Vanderlinden, K. Vints, L. F. Ribeiro, K. M. Vennekens, N. V. Gounko, K. D. Wierda, J. de Wit, A Modular Organization of LRR Protein-Mediated Synaptic Adhesion Defines Synapse Identity. Neuron. 99, 329-344.e7 (2018).
11. T. Uemura, S. J. Lee, M. Yasumura, T. Takeuchi, T. Yoshida, M. Ra, R. Taguchi, K. Sakimura, M. Mishina, Trans-synaptic interaction of GluRδ2 and neurexin through Cbln1 mediates synapse formation in the cerebellum. Cell. 141, 1068–1079 (2010).
12. S. Früh, J. Romanos, P. Panzanelli, D. Bürgisser, S. K. Tyagarajan, K. P. Campbell, M. Santello, J.-M. Fritschy, Neuronal Dystroglycan Is Necessary for Formation and Maintenance of Functional CCK-Positive Basket Cell Terminals on Pyramidal Cells. J. Neurosci. 36, 10296–10313 (2016).

13. M. Fossati, N. Assendorp, O. Gemin, S. Colasse, F. Dingli, G. Arras, D. Loew, C. Charrier, Trans-Synaptic Signaling through the Glutamate Receptor Delta-1 Mediates Inhibitory Synapse Formation in Cortical Pyramidal Neurons. Neuron. 104, 1081-1094.e7 (2019).

14. E. a Heller, W. Zhang, F. Selimi, J. C. Earnheart, M. a Ślimak, J. Santos-Torres, I. Ibañez-Tallon, C. Aoki, B. T. Chait, N. Heintz, The biochemical anatomy of cortical inhibitory synapses. PloS One. 7, e39572–e39572 (2012).

15. F. Selimi, I. M. Cristea, E. Heller, B. T. Chait, N. Heintz, Proteomic Studies of a Single CNS Synapse Type: The Parallel Fiber/Purkinje Cell Synapse. PLoS Biol. 7 (2009), doi:10.1371/journal.pbio.1000083.

16. E. Favuzzi, R. Deogracias, A. Marques-Smith, P. Maeso, J. Jezequel, D. Exposito-Alonso, M. Balia, T. Kroon, A. J. Hinojosa, E. F. Maraver, B. Rico, Distinct molecular programs regulate synapse specificity in cortical inhibitory circuits. Science. 363, 413–413 (2019).

17. M. Ito, Control of mental activities by internal models in the cerebellum. Nat. Rev. Neurosci. 9, 304–313 (2008).

18. R. L. Buckner, The cerebellum and cognitive function: 25 years of insight from anatomy and neuroimaging. Neuron. 80, 807–815 (2013).

19. C. Sotelo, Cellular and genetic regulation of the development of the cerebellar system. Prog. Neurobiol. 72, 295–339 (2004).

20. K. Matsuda, E. Miura, T. Miyazaki, W. Kakegawa, K. Emi, S. Narumi, Y. Fukazawa, A. Ito-Ishida, T. Kondo, R. Shigemoto, M. Watanabe, M. Yuzaki, Cbln1 is a ligand for an orphan glutamate receptor delta2, a bidirectional synapse organizer. Science. 328, 363–368 (2010).

21. W. Kakegawa, N. Mitakidis, E. Miura, M. Abe, K. Matsuda, Y. H. Takeo, K. Kohda, J. Motohashi, A. Takahashi, S. Nagao, S. Muramatsu, M. Watanabe, K. Sakimura, A. R. Aricescu, M. Yuzaki, Anterograde C1ql1 Signaling Is Required in Order to Determine and Maintain a Single-Winner Climbing Fiber in the Mouse Cerebellum. Neuron. 85, 316–329 (2015).

22. A. Ito-Ishida, E. Miura, K. Emi, K. Matsuda, T. Iijima, T. Kondo, K. Kohda, M. Watanabe, M. Yuzaki, Cbln1 Regulates Rapid Formation and Maintenance of Excitatory Synapses in Mature Cerebellar Purkinje Cells In Vitro and In Vivo. J. Neurosci. 28, 5920–5930 (2008).

23. M. Veleanu, B. Urrieta-Chávez, S. M. Sigoillot, M. A. Paul, A. Usardi, K. Iyer, M. Delagrange, J. P. Doyle, N. Heintz, C. Bécamel, F. Selimi, Modified climbing fiber/Purkinje

cell synaptic connectivity in the cerebellum of the neonatal phencyclidine model of schizophrenia. Proc. Natl. Acad. Sci. 119, e2122544119–e2122544119 (2022).

24. C. A. Mason, S. Christakos, S. M. Catalano, Early climbing fiber interactions with Purkinje cells in the postnatal mouse cerebellum. J. Comp. Neurol. 297, 77–90 (1990).

25. R. Ichikawa, K. Hashimoto, T. Miyazaki, M. Uchigashima, M. Yamasaki, A. Aiba, M. Kano, M. Watanabe, Territories of heterologous inputs onto Purkinje cell dendrites are segregated by mGluR1-dependent parallel fiber synapse elimination. Proc. Natl. Acad. Sci. 113, 2282–2287 (2016).

26. M. T. Schmolesky, M. M. De Ruiter, C. I. De Zeeuw, C. Hansel, The neuropeptide corticotropin-releasing factor regulates excitatory transmission and plasticity at the climbing fibre-Purkinje cell synapse: CRF function at the climbing fibre-Purkinje cell synapse. Eur. J. Neurosci. 25, 1460–1466 (2007).

27. M. F. Bolliger, D. C. Martinelli, T. C. Südhof, The cell-adhesion {G} protein-coupled receptor {BAI3} is a high-affinity receptor for {C1q}-like proteins. Proc. Natl. Acad. Sci. U. S. A. 108, 2534–2539 (2011).

28. E. H. Seppälä, T. S. Jokinen, M. Fukata, Y. Fukata, M. T. Webster, E. K. Karlsson, S. K. Kilpinen, F. Steffen, E. Dietschi, T. Leeb, R. Eklund, X. Zhao, J. J. Rilstone, K. Lindblad-Toh, B. A. Minassian, H. Lohi, Lgi2 truncation causes a remitting focal epilepsy in dogs. PLoS Genet. 7 (2011), doi:10.1371/journal.pgen.1002194.

29. Y. Sato, M. Iketani, Y. Kurihara, M. Yamaguchi, N. Yamashita, F. Nakamura, Y. Arie, T. Kawasaki, T. Hirata, T. Abe, H. Kiyonari, S. M. Strittmatter, Y. Goshima, K. Takei, Cartilage Acidic Protein–1B (LOTUS), an Endogenous Nogo Receptor Antagonist for Axon Tract Formation. Science. 333, 769–773 (2011).

30. J. Wang, Y. Miao, R. Wicklein, Z. Sun, J. Wang, K. M. Jude, R. A. Fernandes, S. A. Merrill, M. Wernig, K. C. Garcia, T. C. Südhof, RTN4/NoGo-receptor binding to BAI adhesion-GPCRs regulates neuronal development. Cell. 184, 5869-5885.e25 (2021).

31. R. J. Platt, S. Chen, Y. Zhou, M. J. Yim, L. Swiech, H. R. Kempton, J. E. Dahlman, O. Parnas, T. M. Eisenhaure, M. Jovanovic, D. B. Graham, S. Jhunjhunwala, M. Heidenreich, R. J. Xavier, R. Langer, D. G. Anderson, N. Hacohen, A. Regev, G. Feng, P. A. Sharp, F. Zhang, CRISPR-Cas9 Knockin Mice for Genome Editing and Cancer Modeling. Cell. 159, 440–455 (2014).

32. T. Takano, J. T. Wallace, K. T. Baldwin, A. M. Purkey, A. Uezu, J. L. Courtland, E. J. Soderblom, T. Shimogori, P. F. Maness, C. Eroglu, S. H. Soderling, Chemico-genetic discovery of astrocytic control of inhibition in vivo. Nature. 588, 296–302 (2020).

33. L. Y. Chen, M. Jiang, B. Zhang, O. Gokce, T. C. Südhof, Conditional Deletion of All Neurexins Defines Diversity of Essential Synaptic Organizer Functions for Neurexins. Neuron. 94, 611-625.e4 (2017).

34. S. Backer, T. Sakurai, M. Grumet, C. Sotelo, E. Bloch-Gallego, Nr-CAM and TAG-1 are expressed in distinct populations of developing precerebellar and cerebellar neurons. Neuroscience. 113, 743–748 (2002).

35. M. F. Bolliger, D. C. Martinelli, T. C. Südhof, The cell-adhesion G protein-coupled receptor BAI3 is a high-affinity receptor for C1q-like proteins. Proc. Natl. Acad. Sci. U. S. A. 108, 2534–2539 (2011).

36. Y. Kawakami, Y. Kurihara, Y. Saito, Y. Fujita, T. Yamashita, K. Takei, The Soluble Form of LOTUS inhibits Nogo Receptor-Mediated Signaling by Interfering with the Interaction Between Nogo Receptor Type 1 and p75 Neurotrophin Receptor. J. Neurosci. 38, 2589–2604 (2018).

37. H. Hirai, Z. Pang, D. Bao, T. Miyazaki, L. Li, E. Miura, J. Parris, Y. Rong, M. Watanabe, M. Yuzaki, J. I. Morgan, Cbln1 is essential for synaptic integrity and plasticity in the cerebellum. Nat. Neurosci. 8, 1534–1541 (2005).

38. M. Cizeron, Z. Qiu, B. Koniaris, R. Gokhale, N. H. Komiyama, E. Fransén, S. G. N. Grant, A brainwide atlas of synapses across the mouse life span. Science. 369, 270–275 (2020).

39. A. M. Gomez, L. Traunmüller, P. Scheiffele, Neurexins: molecular codes for shaping neuronal synapses. Nat. Rev. Neurosci. 22, 137–151 (2021).

40. G. P. Demyanenko, V. Mohan, X. Zhang, L. H. Brennaman, K. E. S. Dharbal, T. S. Tran, P. B. Manis, P. F. Maness, Neural Cell Adhesion Molecule NrCAM Regulates Semaphorin 3F-Induced Dendritic Spine Remodeling. J. Neurosci. 34, 11274–11287 (2014).

41. P. Han, Y. She, Z. Yang, M. Zhuang, Q. Wang, X. Luo, C. Yin, J. Zhu, S. R. Jaffrey, S.-J. Ji, Cbln1 regulates axon growth and guidance in multiple neural regions. PLOS Biol. 20, e3001853 (2022).

42. V. Lanoue, A. Usardi, S. M. Sigoillot, M. Talleur, K. Iyer, J. Mariani, P. Isope, G. Vodjdani, N. Heintz, F. Selimi, The adhesion-GPCR BAI3, a gene linked to psychiatric disorders, regulates dendrite morphogenesis in neurons. Mol. Psychiatry. 18, 943–950 (2013).

43. M. M. Petrinovic, R. Hourez, E. M. Aloy, G. Dewarrat, D. Gall, O. Weinmann, J. Gaudias, L. C. Bachmann, S. N. Schiffmann, K. E. Vogt, M. E. Schwab, Neuronal Nogo-A negatively regulates dendritic morphology and synaptic transmission in the cerebellum. Proc. Natl. Acad. Sci. U. S. A. 110, 1083–1088 (2013).

44. R. Nishida, Y. Kawaguchi, J. Matsubayashi, R. Ishikawa, S. Kida, K. Takei, LOTUS, an endogenous Nogo receptor antagonist, is involved in synapse and memory formation. Sci. Rep. 11, 1–9 (2021).

45. R. Thomas, K. Favell, J. Morante-Redolat, M. Pool, C. Kent, M. Wright, K. Daignault, G. B. Ferraro, S. Montcalm, Y. Durocher, A. Fournier, J. Perez-Tur, P. A. Barker, LGI1 Is a Nogo Receptor 1 Ligand that Antagonizes Myelin-Based Growth Inhibition. J. Neurosci. 30, 6607–6612 (2010).

46. M. Yuzaki, Cbln1 and its family proteins in synapse formation and maintenance. Curr. Opin. Neurobiol. 21, 215–220 (2011).

47. E. Seigneur, T. C. Südhof, Genetic Ablation of All Cerebellins Reveals Synapse Organizer Functions in Multiple Regions Throughout the Brain. J. Neurosci. 38, 4774–4790 (2018).

48. J. Elegheert, W. Kakegawa, J. E. Clay, N. F. Shanks, E. Behiels, K. Matsuda, K. Kohda, E. Miura, M. Rossmann, N. Mitakidis, J. Motohashi, V. T. Chang, C. Siebold, I. H. Greger, T. Nakagawa, M. Yuzaki, A. R. Aricescu, Structural basis for integration of GluD receptors within synaptic organizer complexes. Science. 353, 295–299 (2016).

49. H. M. Zhao, R. J. Wenthold, R. S. Petralia, Glutamate receptor targeting to synaptic populations on Purkinje cells is developmentally regulated. J. Neurosci. Off. J. Soc. Neurosci. 18, 5517–5528 (1998).

50. R. Cesa, L. Morando, P. Strata, Glutamate Receptor ʕ2 Subunit in Activity-Dependent Heterologous Synaptic Competition, 8.

51. N. Apóstolo, S. N. Smukowski, J. Vanderlinden, G. Condomitti, V. Rybakin, J. ten Bos, L. Trobiani, S. Portegies, K. M. Vennekens, N. V. Gounko, D. Comoletti, K. D. Wierda, J. N. Savas, J. de Wit, Synapse type-specific proteomic dissection identifies IgSF8 as a hippocampal CA3 microcircuit organizer. Nat. Commun. 11 (2020), doi:10.1038/s41467-020-18956-x.

52. K. Matsuda, T. Budisantoso, N. Mitakidis, Y. Sugaya, E. Miura, W. Kakegawa, M. Yamasaki, K. Konno, M. Uchigashima, M. Abe, I. Watanabe, M. Kano, M. Watanabe, K. Sakimura, A. R. Aricescu, M. Yuzaki, Transsynaptic Modulation of Kainate Receptor Functions by C1q-like Proteins. Neuron. 90, 752–767 (2016).

53. S. Jain, Y. Lin, Y. Z. Kurmangaliyev, J. Valdes-Aleman, S. A. LoCascio, P. Mirshahidi, B. Parrington, S. L. Zipursky, A global timing mechanism regulates cell-type-specific wiring programmes. Nature. 603, 112–118 (2022).

54. H. Stroud, M. G. Yang, Y. N. Tsitohay, C. P. Davis, M. A. Sherman, S. Hrvatin, E. Ling, M. E. Greenberg, An Activity-Mediated Transition in Transcription in Early Postnatal Neurons. J. Clean. Prod. 107, 874-890.e8 (2020).

55. S. G. N. Grant, Synapse diversity and synaptome architecture in human genetic disorders. Hum. Mol. Genet. 28, R219–R225 (2019).

56. L. Tomas-Roca, Z. Qiu, E. Fransén, R. Gokhale, E. Bulovaite, D. J. Price, N. H. Komiyama, S. G. N. Grant, Developmental disruption and restoration of brain synaptome architecture in the murine Pax6 neurodevelopmental disease model. Nat. Commun. 13, 6836 (2022).

Acknowledgments: We would like to thank Adeline Boyreau for her help with some of the experimental procedures, Yves Dupraz for the development of tools for stereotaxic injections in neonates, France Maloumian for her help with infographics and the personnel from the CIRB animal and imaging facilities. In particular, we thank Héloïse Monet for her help in developing the plugin for VGLUT2 quantification. High throughput qPCR was carried out on the qPCR-HD-Genomic Paris Centre platform supported by grants from Région Ile-de-France.

Funding:

This work was supported by funding from:

Fondation pour la Recherche Médicale Equipe FRM DEQ20150331748 (FS)

European Research Council ERC consolidator grant SynID 724601 (FS)

Q-life ANR-17-CONV-0005 (FS)

ANR-10-LABX-54 MEMO LIFE (FS)

Sorbonne Université ED158 (MAP)

Collège de France (MAP)

Author contributions:

Conceptualization: FS, MAP, SMS

Methodology: FS, MAP, SMS

Investigation: MAP, SMS, LM, MD, PM

Visualization: MAP, SMS, FS

Funding acquisition: FS, MAP

Project administration: FS

Supervision: FS, SMS

Writing – original draft: FS

Writing – review & editing: FS, MAP, SMS

Competing interests: Authors declare that they have no competing interests.

Data and materials availability: All data are available in the main text or the supplementary materials (plugins are available on github via the provided links).

Figures:

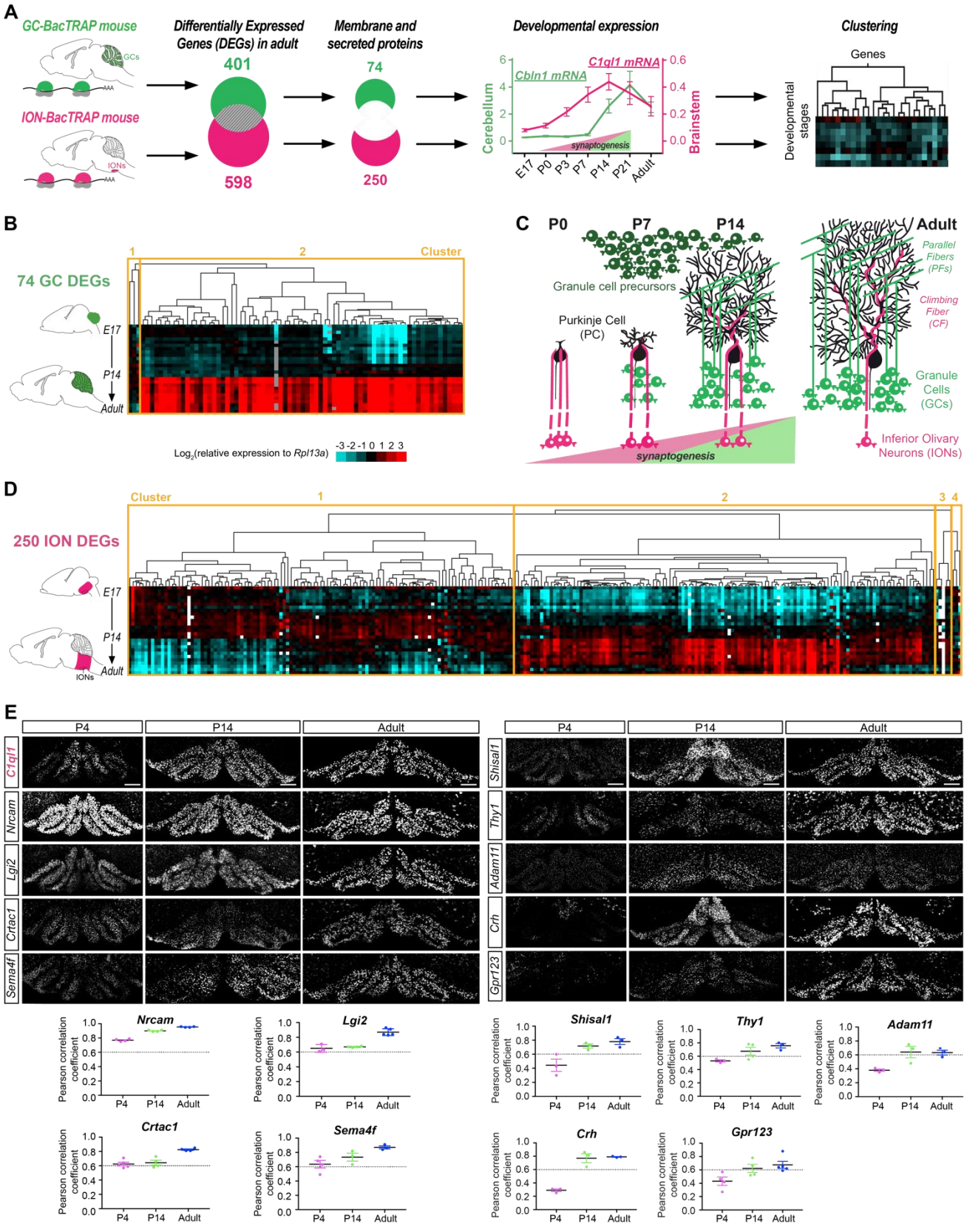

Fig. 1. Purkinje cell excitatory inputs are characterized by different surfaceome expression dynamics during postnatal development.

(A) Workflow for the identification of candidate synaptogenic genes for each input type. A previous analysis using neuron-specific BacTRAP mouse lines identified the adult gene expression profile specific for GCs or IONs, including 74 and 250 DEGs coding for membrane and secreted proteins, respectively (23). The developmental expression patterns of GC and ION surfaceomes were assessed at different stages using high-throughput RT-qPCR on cerebellar and brainstem RNA extracts (Embryonic day, E17; Postnatal days, P0, P3, P7, P14 and P21; and adult). Developmental expression profiles of *Cbln1* and *C1ql1* are shown as references for synaptogenic molecules for GCs and IONs, respectively. Clustering analysis was then performed using the Spearman rank correlation method to group the genes according to their pattern across developmental stages. (**B)** *Left panel:* Heatmap of the 74 GC DEGs in the cerebellum between E17 and adult. *(C):* Schematic illustration of postnatal development and maturation of GC and ION connectivity on PC in the cerebellar cortex. **(D)** Heatmap of the 250 ION DEGs in the brainstem between E17 and adult. **(E)** Duplex smFISH for *C1ql1* and candidate mRNAs in coronal sections from brainstem at P4, P14 and in adult. The degree of correlation of expression between *C1ql1* and candidate mRNAs in the brainstem was determined by computing the Pearson correlation coefficient (coefficient >0.6 corresponding to high correlation). *Left panel:* candidates highly correlated with *C1ql1* at all developmental stages. *Right panel:* candidates highly correlated with *C1ql1* from P14 to adult. Data are presented as mean ± SEM. n = 3-5 animals per condition, 2-4 independent experiments. Scale bars, 150 µm.

See also fig. S1.

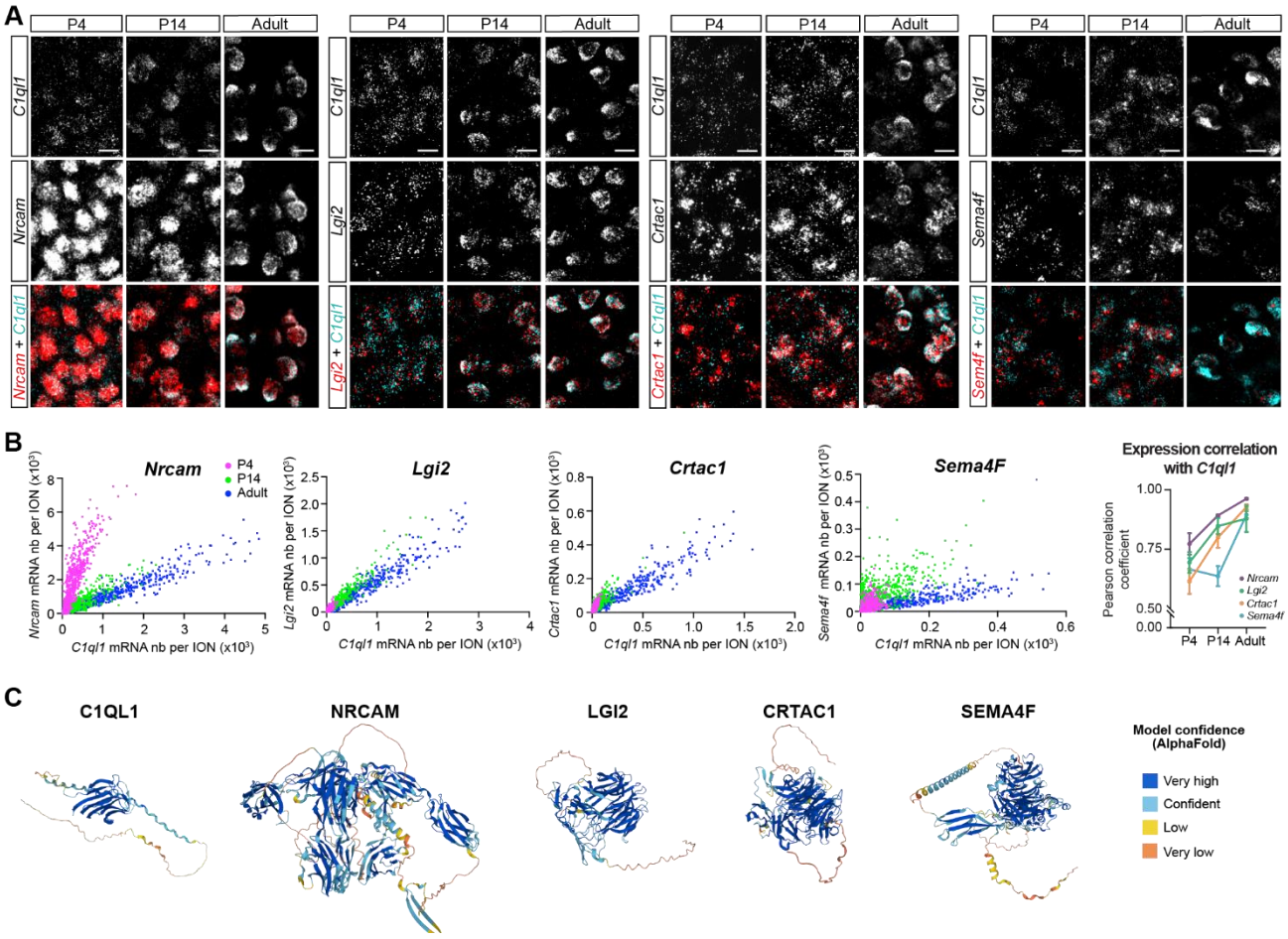

Fig. 2. A combination of cell surface molecules characterizing IONs during postnatal development.

(A) Duplex smFISH for *C1ql1* mRNAs and the four highly correlated candidate mRNAs, *Nrcam, Lgi2, Crtac1* and *Sema4f* in IONs at P4, P14 and in adult. Scale bars, 25 µm. **(B)** Quantification of the number (nb) of *C1ql1* and candidate gene mRNAs per ION for *Nrcam, Lgi2, Crtac1* or *Sema4f* at P4, P14 and in adult. n = 568-682 cells (1 cell corresponding to 1 dot on the graphs), one representative experiment is shown. Correlation between the expression of *C1ql1* and candidate mRNAs was determined at the single cell level (Pearson correlation coefficient >0.6 corresponding to high correlation). Data are presented as mean ± SEM. n = 3-6 animals, 2-4 independent experiments. **(C)** AlphaFold structure prediction of C1QL1 and candidate proteins NRCAM, LGI2, CRTAC1 and SEMA4F (Database: https://alphafold.ebi.ac.uk/).

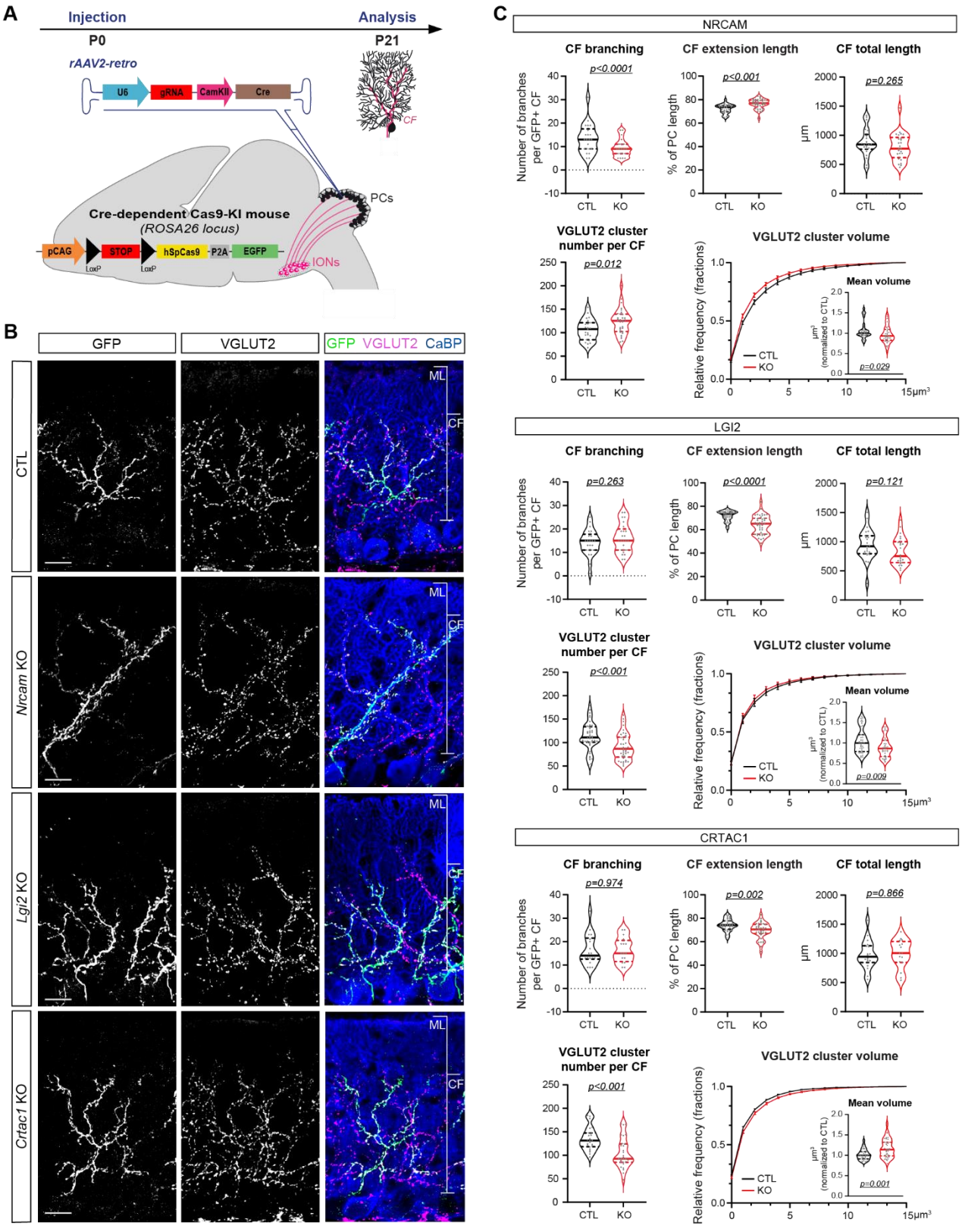

Fig. 3. A combination of cell surface proteins controls the establishment of Climbing fiber/Purkinje cell connectivity.

(A) Schematic illustration of the strategy of CRISPR/Cas9-mediated loss of function of candidate genes specifically in IONs. P0 stereotaxic injection of retrograde rAAVs expressing guide RNA (gRNA) targeting a candidate gene or a non-targeting control gRNA (CTL), under the U6 promoter, as well as the Cre recombinase, under the CamKII promoter, were performed in the cerebellum of Cre-dependent Cas9 knock-in (KI) mice. Analyses of the morphology and connectivity of GFP positive (GFP+) CFs (from Cas9-recombined IONs) were performed at P21 in parasagittal cerebellar sections from KO or CTL injected animals. **(B)** GFP+ CF and CF presynaptic boutons were immunostained for GFP (green) and VGLUT2 (magenta), respectively, and immunostaining for calbindin was used to label PCs and their dendritic tree (blue) in CTL and *Nrcam*, *Lgi2* or *Crtac1* KO. Molecular layer (ML) and CF extensions are indicated on the merge image. Scale bars, 20 µm. **(C)** GFP+ CF morphology was assessed measuring 3 parameters: the number of branches per CF, the percentage of CF extension length on PC dendrite and the total length of each CF. VGLUT2 cluster number, and distribution and mean of the VGLUT2 cluster volume were also quantified in GFP+ CFs. Data are presented as violin plot with the median and quartiles. CF morphology and VGLUT2 cluster number: n = 16-26 CFs per condition, 5-6 animals per condition; VGLUT2 cluster volume: $n \geq 33$ images per condition, 9-10 animals per condition; 3-5 independent experiments. Statistics: unpaired Student's test for CF branching (*Lgi2* or *Crtac1* KO), CF extension (*Nrcam* or *Crtac1* KO), CF total length, VGLUT2 cluster number, VGLUT2 cluster volume (*Crtac1* KO) and Mann-Whitney test for CF branching (*Nrcam* KO), CF extension (*Lgi2* KO), VGLUT2 cluster volume (*Nrcam* or *Lgi2* KO).

See also fig. S2.

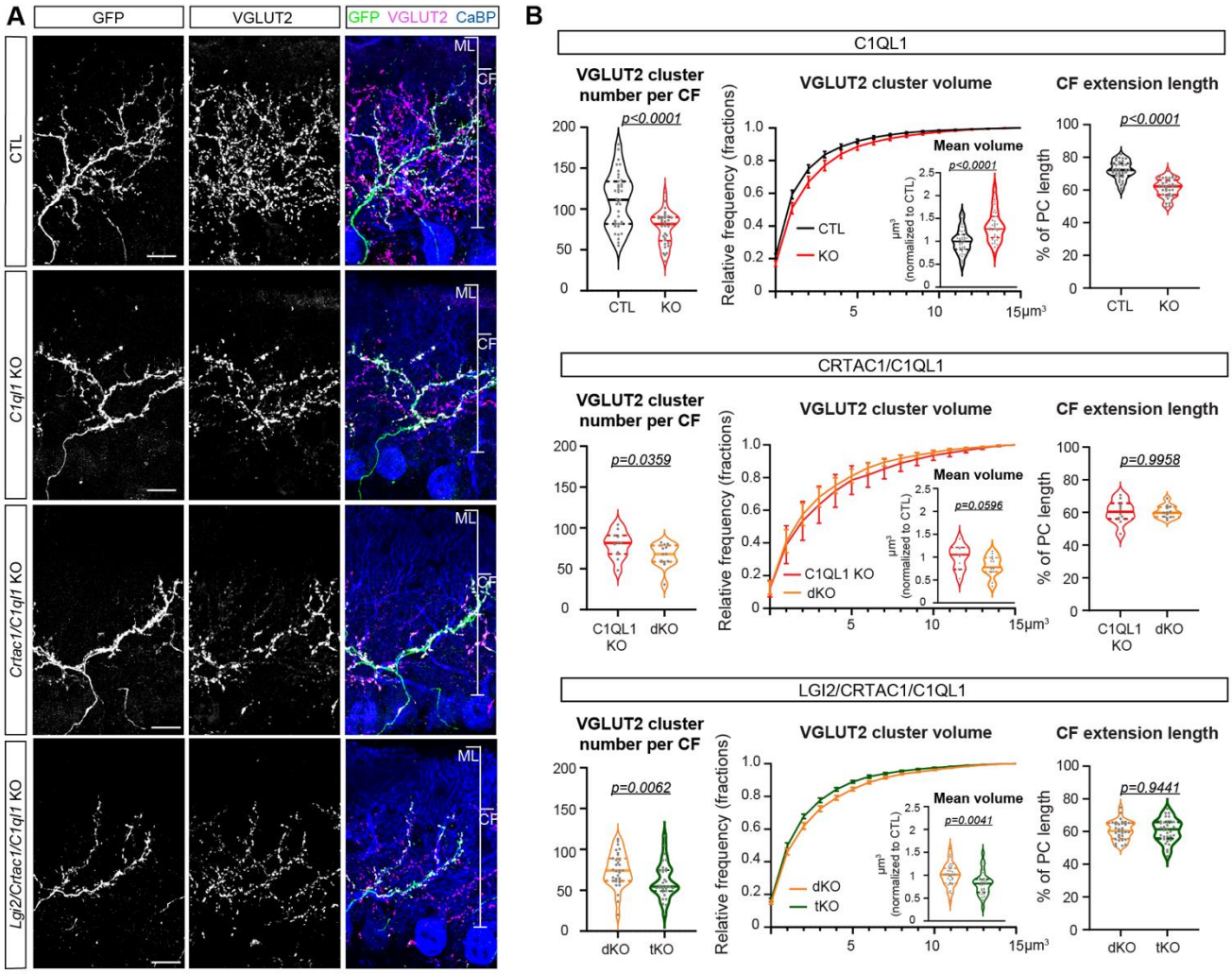

Fig. 4. CF synaptogenesis depends on a combination of cell surface proteins belonging to different signaling pathways.

(A) GFP+ CF and CF presynaptic boutons were immunostained for GFP (green) and VGLUT2 (magenta), respectively, and immunostaining for calbindin was used to label PCs and their dendritic tree (blue) in CTL and *C1ql1 KO, C1ql1-Crtac1 double KO and C1ql1-Crtac1-Lgi2 triple* KO**.** Molecular layer (ML) and CF extensions are indicated on the merge image. Scale bars, 20 µm. **(B)** GFP+ CF morphology was assessed by measuring the percentage of CF extension length on PC dendrite. VGLUT2 cluster number, and distribution and mean of the VGLUT2 cluster volume were also quantified in GFP+ CFs. Data are presented as violin plot with the median and quartiles. CF morphology and VGLUT2 cluster number and volume: n ≥ 12 images per condition, 3-10 animals per condition; 1-4 independent experiments. Statistics: unpaired Student's test for CF extension, VGLUT2 cluster number (dKO), VGLUT2 cluster volume and Mann-Whitney test for VGLUT2 cluster number (*C1ql1* KO or tKO).

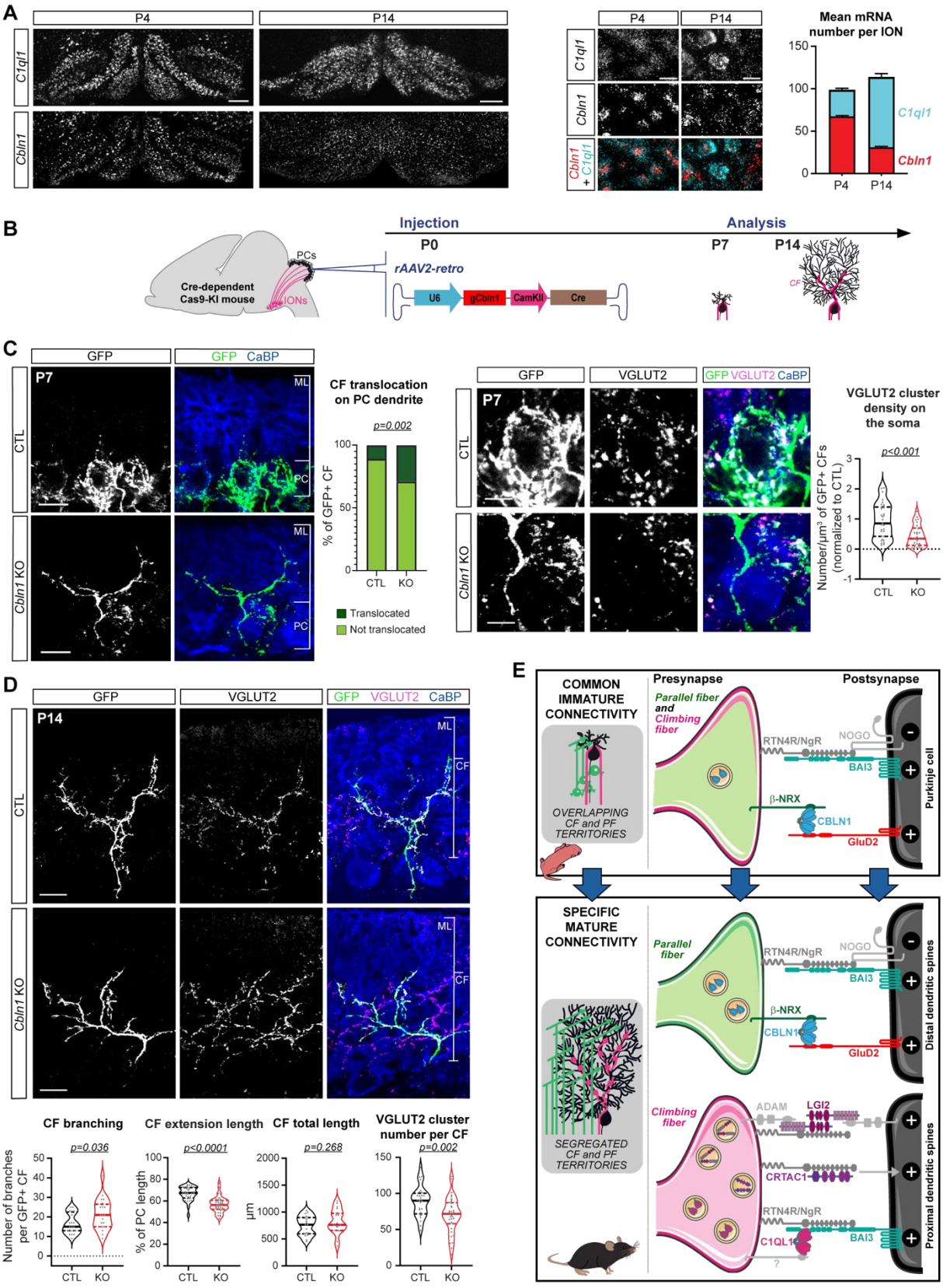

Fig. 5. *Cbln1* expression in inferior olivary neurons is necessary for proper climbing fiber connectivity on Purkinje cells.

(A) Duplex smFISH for *C1ql1* and *Cbln1* mRNAs in coronal sections from brainstem at P4 and P14. *Left panel:* Low magnification showing the inferior olive. *Right panel:* High magnification showing IONs and quantification of the mean number of both *C1ql1* and *Cbln1* mRNAs per ION at P4 and P14. Data are presented as mean ± SEM. n = 864-3910 cells, 4 animals per condition, 3 independent experiments. **(B)** Schematic illustration of the strategy of CRISPR/Cas9-mediated loss of function of *Cbln1* specifically in IONs. Stereotaxic injection of retrograde rAAVs expressing gRNAs targeting *Cbln1* or non-targeting control (CTL), under the U6 promoter, as well as the Cre recombinase, under the CamKII promoter, were performed in the cerebellum of Cre-dependent Cas9 knock-in (KI) mice at P0. Analyses of the morphology and connectivity of GFP positive (GFP+) CFs were performed at P7 or P14 in parasagittal cerebellar sections from CTL or *Cbln1* KO injected animals. **(C and D)** GFP+ CF and CF presynaptic boutons were immunostained for GFP (green) and VGLUT2 (magenta), respectively, and immunostaining for calbindin was used to label PCs and their dendritic tree (blue) in CTL and *Cbln1* KO. *(C) Left panel:* Quantification of the percentage of GFP+ CF translocated on PC dendrite in the molecular layer (ML). n≥ 87 CFs per condition. Statistics: Chi-square. Molecular layer (ML) extension and PC somata are indicated on the merge image. Scale bars, 20 µm. *Right panel:* High magnification of the GFP+ CF on the PC soma and quantification of the density of VGLUT2 clusters per GFP volume. Data are presented as violin plot with the median and quartiles. n ≥ 28 images, 8 animals per condition, 4 independent experiments. Statistics: unpaired Student's test. Scale bars, 7 µm. *(D)* GFP+ CF morphology was assessed measuring 3 parameters: the number of branches per CF, the percentage of CF extension length on PC dendrite and the total length of each CF. VGLUT2 cluster number per GFP+ CFs was also quantified. Data are presented as violin plot with the median and quartiles. n = 20 CFs per condition, 6-8 animals per condition, 3 independent experiments. Statistics: unpaired Student's test, Mann Whitney for CF branching. Scale bars, 20 µm. **(E)** Model of the change in the acquisition of molecular synapse identity of PC excitatory synapses during postnatal development.

See also fig. S3.

Supplementary Materials

Materials and Methods

Animals, mouse lines genotyping and AAV injections

All animal protocols and animal facilities were approved by the Comité Régional d'Ethique en Expérimentation Animale (#22406) and the veterinary services (D-75-05-12). OF1 (Charles River Laboratories, Massachusetts, USA) were used for the determination of developmental expression patterns or smFISH. The Cre-dependent Cas9-KI mouse line (Cas9-KI) was obtained from The Jackson Laboratory (B6J.129(B6N)-Gt (ROSA)26Sor$^{tm1(CAG-cas9*,-EGFP)Fezh}$/J, strain #026175). The NeuroD1Cre mouse line (Tg(Neurod1-cre)RZ24Gsat/Mmucd) was obtained from Pr. Mary Beth Hatten (The Rockefeller University, USA). Both lines are maintained on the C57Bl6/J background, and homozygous mice were crossed with C57Bl6/J wild-type animals to generate heterozygous animals used in our experiments. Transgene detection was performed using the following primers: F-WT 5'- AAG GGA GCT GCA GTG GAG TA -3', R-WT 5'- CAG GAC AAC GCC CAC ACA -3', F-mutant 5'- TCC CCA TCA AGC TGA TCC -3' and R-mutant 5'- CTT CTT CTT TGG GGC CAT CT -3' for Cas9-KI mice; Fw 5'- TAG GAT TAG GGA GAG GGA GCT GAA -3' and Rev 5'- CGG CAA ACG GAC AGA AGC ATT -3' for NeuroD1Cre mice. Both males and females were used for experiments.

Injections of AAV particles were performed in the cerebellar vermis of ice-anesthetized P0 Cas9-KI heterozygous mice at 1 mm depth from the skull and at 3.2 mm relative to Bregma, to target Purkinje cell layer. AAV2/retrograde serotype was used to target IONs. 0.25µl of AAV was injected per animal using pulled calibrated pipets.

Gene expression analysis

RNA extraction: The cerebellum and the brainstem were dissected in cold Hanks balanced salt solution (HBSS; Gibco, Thermo Fisher Scientific, Massachusetts, USA). After removal of the meninges, the tissues were frozen in liquid nitrogen and stored at -80°C. The cell cultures were washed with phosphate buffer saline (PBS), scraped in RLT buffer (Qiagen, Hilden, Germany) complemented with 2-mercaptoethanol and stored at -80°C. Total RNA was extracted using the Qiagen RNeasy mini kit (Qiagen) following tissue or cell homogenization, according to manufacturer's instruction.

High-throughput RTqPCR: High-throughput quantitative RT-PCR was performed as previously described (23). Briefly, cDNAs were synthesized using 100 ng of total RNAs with

high quality and integrity (mean RNA Quality Number of 9.6) using Reverse Transcription Master Mix from Fluidigm™ (California, USA) on a Nexus Thermocycler (Eppendorf®, Hambourg, Germany; protocol: 5min at 25°C, 30min at 42°C, heat-inactivation of the reverse transcriptase 5min at 85°C and then 4°C). cDNA samples were diluted 5 times in low TE buffer (10mM Tris; 0.1mM EDTA; pH = 8.0; TEKNOVA®, Fisher Scientific, Massachusetts, USA) and used for specific target multiplex pre-amplification using Fluidigm® PreAmp Master Mix and pooled TaqMan® Gene Expression assays (Life Technologies, California, USA) with a final concentration of 180nM for each assay (protocol: 95°C for 2min, followed by 18 cycles at 95°C for 15s and 60°C for 4min). Pre-designed Taqman Gene Expression assays are listed in (23).

Quantitative PCR was performed using the high-throughput platform BioMark™ HD System and the 96.96 GE Dynamic Arrays (Fluidigm®). The expression of target genes was quantified in the 5 times diluted pre-amplified cDNAs by quantitative PCR on 96.96 microfluidic chips. The loaded Dynamic Array was transferred to the Biomark™ real-time PCR instrument and amplified by PCR (25°C for 30min and 70°C for 60min for thermal mix; 50°C for 2min and 95°C for 10min for hot start; 40 cycles at 95°C for 15s and 60°C for 1min). ROX was used as a passive reference and single probe FAM-MGB as a fluorescent detector. To determine the quantification cycle Ct, data were processed by automatic threshold for each assay, with linear derivative baseline correction using BioMark Real-Time PCR Analysis Software 4.0.1 (Fluidigm®). The quality threshold was set at the default setting of 0.65.

The raw data from gene expression analysis were extracted and analysed using MATLAB. For the systematic fold change and statistical test analysis, a script was written using the R opensource software. For each dataset, a multiple *t* test comparison was performed on the 324 genes, assuming a normal distribution and the equality of variances. Benjamini-Hochberg procedure for multiple correction was performed. The delta Ct method ($2^{-\text{deltaCt}}$) was used to determine the relative gene expression, where deltaCT = CT(gene) - CT(geometric mean of reference gene). The data were normalized to *Rpl13a*, which showed the most stable expression among all the samples.

Unsupervised clustering of log2 relative gene expression during postnatal development was performed using Cluster 3.0 program. Each gene expression value was adjusted, so that the median (more robust against outliers) value of each raw is 0, to reflect their variation compare to the *Rpl13a* reference gene. Agglomerative hierarchical clustering was performed using complete linkage to compute the distance matrix between gene expression data. Hierarchical clustering methods assemble genes and time points in a tree structure, where the size of the

branches increases when their similarity decreases to each other. Treeview allowed the visualization of the data.

Droplet Digital™ PCR (ddPCR™, BioRad): ddPCR™ was performed as previously described (*23*). Briefly, 100ng of total RNA were reverse-transcribed using SuperScript® VILO™ cDNA Synthesis kit (Life Technologies), according to manufacturer's instructions. The cDNA samples diluted 5 times were mixed with the FAM-labeled fluorescent probes to target each candidate gene along with the VIC-labeled *Rpl13a* reference (pre-designed Taqman Gene Expression assay are listed in (23) and ddPCR™ Supermix for Probes (No dUTP) (BioRad, California, USA). The samples were then fractionated into 12.000 to 20.000 droplets in water–oil emulsion using the automatic droplet generator (Bio-Rad). The template molecules from each droplet were PCR amplified in a thermocycler (BioRad; protocol: one cycle of 95°C for 10 minutes, 40 cycles of 94°C for 30 seconds and 60°C for one minute, and one cycle of 98°C for 10 minutes). The fluorescence (FAM, VIC) in each droplet was then digitally counted using QX200 droplet reader (Bio-Rad). QuantaSoft analysis software (Bio-Rad) was used for data acquisition and analysis. For each assay, identical manual threshold was selected, and relative expression was determined doing the ratio of the copy number of template molecules/µl of reaction to the copy number of the *Rpl13a* reference gene/µl of reaction.

Plasmids, CRISPR/Cas9 gRNAs and validation of gRNAs efficiency and specificity

Plasmids: the pAAV-U6-guideRNA-CamKII-CRE-WPRE was designed as follow: (1) the CRE cassette from the pAAV-CMV-CRE (VB7060, Vector Biolabs, Pennsylvania, USA) was subcloned in the pAAV-CamKII-eGFP-WPRE (VB5396, Vector Biolabs), after removing the eGFP; (2) the U6-gRNA cassette from the plasmid pX333 (a gift from Andrea Ventura (57), RRID:Addgene_64073, Massachusetts, USA) was subcloned before the CamKII promoter by homologous recombination using the In-Fusion kit (Takara, Shiga, Japan). The U6-guideRNA cassettes for all our candidate genes were obtained as follow: *Nrcam*, *Lgi2* or *Crtac1* CRISPR/Cas9 guide RNAs were cloned in the plasmid pX333 (Addgene, #64073) in the *BbsI* site; the two gRNAs targeting *Cbln1* or CTL KO were cloned in the plasmid pX333 in the *BbsI* site for the first guide and in the *BsaI* site for the second guide.

Genomic sequences targeted by the CRISPR gRNA: Nrcam (exon4): 5'- GTG CCA GAT GAT CAG CGC GC -3' (58); *Lgi2* guide1 (exon1): 5'- GGG GAC CCG GCA TGG CGC TA -3'; *Lgi2* guide2 (exon1): 5'- CCG GCA TGG CGC TAT GGA G -3'; *Crtac1* guide1 (exon1): 5'-

ATG GCT CCG AGC GCT GAC CC -3'; *Crtac1* guide2 (exon2): 5'- ACT TCG AGA TCG TTG TGG CG -3'; *Cbln1* guide1 (exon1): 5'- CTT CGG GCA CAC GGC ACG CG -3'; *Cbln1* guide2 (exon3): 5'- GGA CGA AGT TGG ACC GCC GG -3'; *Control* guide1: 5'- CCA GTT GCT CTG GGG GAA CA -3' and *Control* guide2: 5'- TCA GCA AAG GAC GAA ACA AA -3' which do not target any genomic sequences.

Primary neuronal cultures: Cortical cell cultures were prepared from E14.5 mouse embryos resulting from crossbreeding between Cas9-KI and C57Bl6/J mice (analysis of CRISPR/Cas9 KO efficiency on RNA extracts) or Cas9-KI and NeuroD1Cre mice expressing the Cre recombinase mainly in GCs (analysis of CRISPR/Cas9 KO specificity on genomic DNA extracts). Cortices were dissected in cold HBSS (Gibco), washed once in cHBSS (HBSS containing HEPES (2,5mM, pH7.4), D-glucose (300 mM), $CaCl_2$ (1 mM), $MgSO_4$ (1 mM) and $NaHCO_3$ (4mM)), and incubated in cHBSS containing trypsin (1X; Gibco) and DNase I (100 µg/ml; Roche, Basel, Switzerland) for 15min at 37°C. Then, cortices were washed 3 times with cHBSS containing DNase I, and gently dissociated by pipetting. Dissociated cells were plated on poly-D-lysine (0,1mg/ml; Sigma-Aldrich, Missouri, USA) -coated coverslips (18mm diameter) in Neurobasal media (Gibco) supplemented with FBS (2,5%; Sigma-Aldrich), B27 (1X; Gibco), L-Glutamine (1X; Gibco) and penicillin/streptomycin (1X; Gibco) (LifeTechnologies). After 7 days, supplemented Neurobasal medium was added to the cultures. Cerebellar mixed cultures were prepared from P0 mouse pups resulting from crossbreeding between Cas9-KI and NeuroD1Cre mice (analysis of *Cbln1* CRISPR/Cas9 KO efficiency on RNA extracts or specificity on gDNA extracts). Cerebella were dissected and dissociated according to a previously published protocol (59). Neurons were seeded at a density of $5x10^6$ cells/ml.

Genomic DNA extraction and PCR amplification: Cortical cell cultures or mixed cerebellar cultures were washed and resuspended in PBS and stored at -80°C. Genomic DNAs (gDNAs) were extracted using the PureLink™ Genomic DNA Mini Kit (Thermo Fisher Scientific), according to the manufacturer's instructions for mammalian cell lysate. gDNAs were then used for PCR amplification targeting the *Cbln1* gene or the three first off-targets of each candidate CRISPR gRNA selected for the KO experiments. *Cbln1:* Fw primer: 5'- CGC CCG CTG CAT CAA TAA TTC -3', Rev primer: 5'- CGG GTC GGG AGA AAC ATT TCA C -3'; *Cbln1* KO g1 Offtarget1, Fw primer: 5'- TGA GCA AGC AGG TTT CAG GAT GG 3', Rev primer: 5'- AGC ATG GCT GTC TTT AGC ATC CA 3'; *Cbln1* KO g1 Offtarget2, Fw primer: 5'-

TACAGAGTTGGGGTGGGCTGTTA -3', Rev primer: 5'- CGC GAG CCA ATC CTT TAC AAG CA -3'; *Cbln1* KO g2 Offtarget1, Fw primer: 5'- GTC ATG TTC TTC CTC ACT GAA GG -3', Rev primer: 5'- CCT ACT AGG GCG ACA ACT GTC AT -3'; *Cbln1* KO g2 Offtarget2, Fw primer: 5'- TCT CCC TGG CTT GAA ACT T -3', Rev primer: 5'- GCT GAA GTC CAA AGG CAG AAA ACC -3'; *Cbln1* KO g2 Offtarget3, Fw primer: 5'- GGG GTC AGC TTC TCT ACA GAT AA -3', Rev primer: 5'- GCT TCT TTC TGT CTG CTG ATG TC -3'; *Lgi2* KO g3 Offtarget1, Fw primer: 5'- AAT TGA CAG TGT GGC TCT GCT GT -3', Rev primer: 5'- AAG AGA AGC ACC CCA TCC CAA AG -3'; *Lgi2* KO g3 Offtarget2, Fw primer: 5'- TGA CGT CAG AGG AGG ACA ATG GA -3', Rev primer: 5'- ATA TGC TCC ACC ATC CGT CCA GA -3'; *Lgi2* KO g3 Offtarget3, Fw primer: 5'- TAG AAC ACT GAC CGG CAC ATT CG -3', Rev primer: 5'- GTC TCT CTC CCT CAG CTC TTC CA -3'; *Crtac1* KO g2 Offtarget1, Fw primer: 5'- GGC CAAT GTT CAG AGA TTA AGA GAC C -3', Rev primer: 5'- GGG GAA CAA AAT ACC CAT GGA GG -3'; *Crtac1* KO g2 Offtarget2, Fw primer: 5'- ATT GTT TCC AGG AGG CTG GGT TC -3', Rev primer: 5'- CCA GGA AGG TGA TTT GAC CCT T -3'; *Crtac1* KO g2 Offtarget3, Fw primer: 5'- CTT GAA GAC CTC TGC AGG CAT CC -3', Rev primer: 5'- ATA CCA GAG AGC AAG CCA GAA GC -3'.

Production of AAV particles and transduction of cells

AAV production: HEK293T cells (ATCC, Virginia, USA; #CRL-3216) were plated in DMEM containing glutamine (Gibco, #11965-092), supplemented with 10% FBS (Sigma-Aldrich) and 1% Penicillin-Streptomycin (Gibco), and co-transfected with pAdDeltaF6 helper (pAdDeltaF6 was a gift from James M. Wilson; RRID:Addgene_112867), rAAV2-retro helper plasmid (rAAV2-retro helper was a gift from Alla Karpova & David Schaffer (60); RRID:Addgene_81070) and pAAV-U6-guideRNA-CamKII-CRE-WPRE in HBS (Sigma-Aldrich)/$CaCl_2$, to produce retrograde AAV particles, after reaching 60% to 80% confluency. 293T cells were then incubated in DMEM (Gibco, #11960-044), supplemented with 10% FBS (Sigma-Aldrich) and 1% Glutamax (Gibco) after the addition of chloroquine diphosphate at a final concentration of 25 µM in the cell medium. 293T cells were harvested 3 days after transfection. For small-scale AAV production, the supernatant medium was collected, filtered through a cellulose acetate membrane with Spin-X centrifuge tube filter (Corning® Costar®, New York, USA) and were stored at 4°C for maximum 2 weeks or frozen at -80°C. For big-scale AAV production, 293T cell plates were purified using the AAVpro Purification Kit (Takara), following the manufacturer's instruction. 150 to 200 µl of AAVs were obtained and aliquoted for storage at -80°C. Real-time PCR reactions were performed with AAVpro Titration

Kit, following manufacturer's protocol. Titers of purified AAVs used in this study were > 9.10^11 genome copies/mL (GC/ml).

Transduction in vitro: Primary neuronal cultures were transduced with 100µl of small-scale AAV2/2 or AAV2/8 supernatants, or with purified AAV2/retrograde at a final concentration of 0.25.10^10 to 2.10^10 GC/mL per virus directly added in the culture medium. AAV2/1-CMV-CRE supernatants or purified AAV2/8-CMV-CRE (Vector Biolabs, VB7060) were used to target the CRE in neurons expressing candidate genes.

Histology/Immunocytochemistry

Single molecule Fluorescent In situ Hybridization (smFISH): Animals at P4, P14 or P>60 (adult) were perfused with fresh 4% paraformaldehyde (PFA) in PBS and post-fixed at 4°C for 24 hours. Brains were cryopreserved in sucrose 10%, 20% and then 30% until the tissue sunk to the bottom of the tube, cut in parasagittal sections (30 µm-thick) and stored at -20°C in antifreeze solution. Fixed frozen sections were processed using the RNAscope Multiplex Fluorescent Assay kit V2 (Advanced Cell Diagnostics, New Jersey, USA) according to manufacturer's instructions with minor modifications: free-floating sections were rinsed two times with 0.1% Tween20 in PBS (TBST), incubated 10 min with RNAscope Hydrogen Peroxide (Advanced Cell Diagnostics) at room temperature and then rinsed two times in TBST before mounting them on Superfrost Plus slides. Slides were dried overnight, rehydrated in distilled water, baked for one hour at 60°C in dry oven and rehydrated again in water before immersion of the slides in EtOH. Probes were designed to target all predicted transcripts variants for each candidate gene: *C1ql1* #465081, *Nrcam* #581001, *Lgi2* #580991, *Crtac1* #517971, *Sema4f* #581021, *Shisal1* #586881, *Crh* #316091, *Thy1* #430661, *Gpr123* #317301, *Adam11* #580971, *Tmem184b* #516371, *Fstl1* #534121, *Cx3cl1* #426211, *Cd151* #580981, *Adam23* #580971, *Tmem179* #581011, *Cbln1* #538491. DAPI was used to stain nuclei and sections were mounted with ProLong Gold Antifade Reagent (Life Technologies).

Immunohistochemistry: Immunostaining were performed on 30 µm-thick parasagittal cerebellar sections obtained using a freezing microtome after intracardiac perfusion of mice with fresh 4% PFA in PBS. Sections were blocked with 4% normal donkey serum in PBS containing 1% Triton X-100 for 45 min at room temperature. The primary antibodies were diluted in PBS supplemented with 1% Triton X-100, 1% normal donkey serum, and incubated two hours at room temperature under agitation. The following antibodies were used: rabbit

polyclonal anti-GFP (1:2000; Abcam, Cambridge, UK; #ab13970), anti-CaBP mouse antibody (1:2000; Swant, Marly, Switzerland; #300), anti-VGluT2 guinea pig antibody (1:5000; Millipore, Molsheim, France; #AB2251). The sections were then washed three times for five minutes in PBS supplemented with 1% Triton X-100 and incubated for 45 min at room temperature in the secondary antibody diluted in PBS containing 1% Triton X-100 and 1% normal donkey serum (1:1000; Invitrogen, Thermo Fisher Scientific; anti-rabbit Alexa Fluor 488 #A21206, anti-mouse Alexa Fluor 568 #A10037, anti-guinea pig Alexa Fluor 647 #A21450). The sections were mounted with ProLong Gold Antifade Reagent (Life Technologies).

Image acquisition and analysis

All image stacks were acquired using a spinning-disk confocal CSU-W1 microscope with a 25X or 63X objective. The mosaic images of the smFISH experiments were reconstructed using the Metamorph software (Fig. 1E and Fig. 4A, left panel).

smFISH experiments: For mosaic images of smFISH in the brainstem (Fig. 1E), the Pearson correlation was obtained using a modified version of the Correlation_J Fiji plugin. Quantifications of the smFISH at 63X (Fig. 2B) were performed using a custom-made plugin for unbiased 3D detection of individual RNA puncta and DAPI nucleus (https://github.com/orion-cirb/RNA_Scope).

The number of mRNA dot per nucleus was estimated by dividing the integrated intensity of each nucleus, after background subtraction, by the corrected integrated intensity of one single mRNA dot.

Corrected integrated intensity of one single dot

$$= \frac{\sum_1^n \text{ dot integrated Intensity} - \sum_1^n \text{ mean dot background integrated intensity x } \sum_1^n \text{ dot volume}}{\text{n}}$$

where n represent the number of dots.

Mean dot background integrated intensity

$$= \frac{\sum_{\text{dot z min}}^{dot\ z\ max} \text{ dot integrated Intensity}}{\sum_{\text{dot z min}}^{dot\ z\ max} \text{ dot volume}}$$

For the nucleus identification, 3D ImageJ suite library (61) was used. Intense heterochromatin puncta were removed by using remove outliers Fiji function (62). A difference of Gaussian filter followed by a binary mask (Otsu threshold), and a three-dimensional watershed were used to separate nuclei. Finally, segmented nuclei were dilated by 3 µm in x, y and z to capture mRNAs that are at the periphery of the nucleus. A threshold of nucleus size was used to remove nuclei that could not be separated.

Morphology quantifications: For CF and VGLUT2 stainings, all the images were normalized using the quantile-based normalization plugin on Fiji. A custom-made plugin was developed based on the 3D Weka Segmentation plugin to allow semi-automatic detection of GFP positive CFs and, to count and measure VGLUT2 clusters (https://github.com/orion-cirb/Vglut2_GFP_Weka_Maela.git). Selection of signal and background were done manually. CF morphology was assessed using SNT toolbox on ImageJ for tracing and quantification.

Statistical analysis

All statistical analyses were performed using GraphPad Prism8. Normality was assessed using D'Agostino and Pearson, Shapiro-Wilk or Kolmogorov-Smirnov normality tests. When groups fit to the normal distribution, the differences between the two groups were assessed using two-tailed Student's t-test. When the populations did not fit the normal distribution, the non-parametric Mann-Whitney test was used. Differences in distribution were tested using the chi-squared test. Data are presented as mean ± SEM or as violin plots with median and quartiles.

References

57. D. Maddalo, E. Manchado, C. P. Concepcion, C. Bonetti, J. A. Vidigal, Y.-C. Han, P. Ogrodowski, A. Crippa, N. Rekhtman, E. de Stanchina, S. W. Lowe, A. Ventura, In vivo engineering of oncogenic chromosomal rearrangements with the CRISPR/Cas9 system. Nature. 516, 423–427 (2014).

58. T. Takano, J. T. Wallace, K. T. Baldwin, A. M. Purkey, A. Uezu, J. L. Courtland, E. J. Soderblom, T. Shimogori, P. F. Maness, C. Eroglu, S. H. Soderling, Chemico-genetic discovery of astrocytic control of inhibition in vivo. Nature. 588, 296–302 (2020).

59. T. Tabata, S. Sawada, K. Araki, Y. Bono, S. Furuya, M. Kano, A reliable method for culture of dissociated mouse cerebellar cells enriched for Purkinje neurons. Journal of Neuroscience Methods. 104, 45–53 (2000).

60. D. G. R. Tervo, B.-Y. Hwang, S. Viswanathan, T. Gaj, M. Lavzin, K. D. Ritola, S. Lindo, S. Michael, E. Kuleshova, D. Ojala, C.-C. Huang, C. R. Gerfen, J. Schiller, J. T. Dudman, A. W. Hantman, L. L. Looger, D. V. Schaffer, A. Y. Karpova, A Designer AAV Variant Permits Efficient Retrograde Access to Projection Neurons. Neuron. 92, 372–382 (2016).

61. J. Ollion, J. Cochennec, F. Loll, C. Escudé, T. Boudier, TANGO: a generic tool for high-throughput 3D image analysis for studying nuclear organization. Bioinformatics. 29, 1840–1841 (2013).

62. J. Schindelin, I. Arganda-Carreras, E. Frise, V. Kaynig, M. Longair, T. Pietzsch, S. Preibisch, C. Rueden, S. Saalfeld, B. Schmid, J.-Y. Tinevez, D. J. White, V. Hartenstein, K. Eliceiri, P. Tomancak, A. Cardona, Fiji: an open-source platform for biological-image analysis. Nat Methods. 9, 676–682 (2012).

Supplementary figures:

Figs. S1 to S3

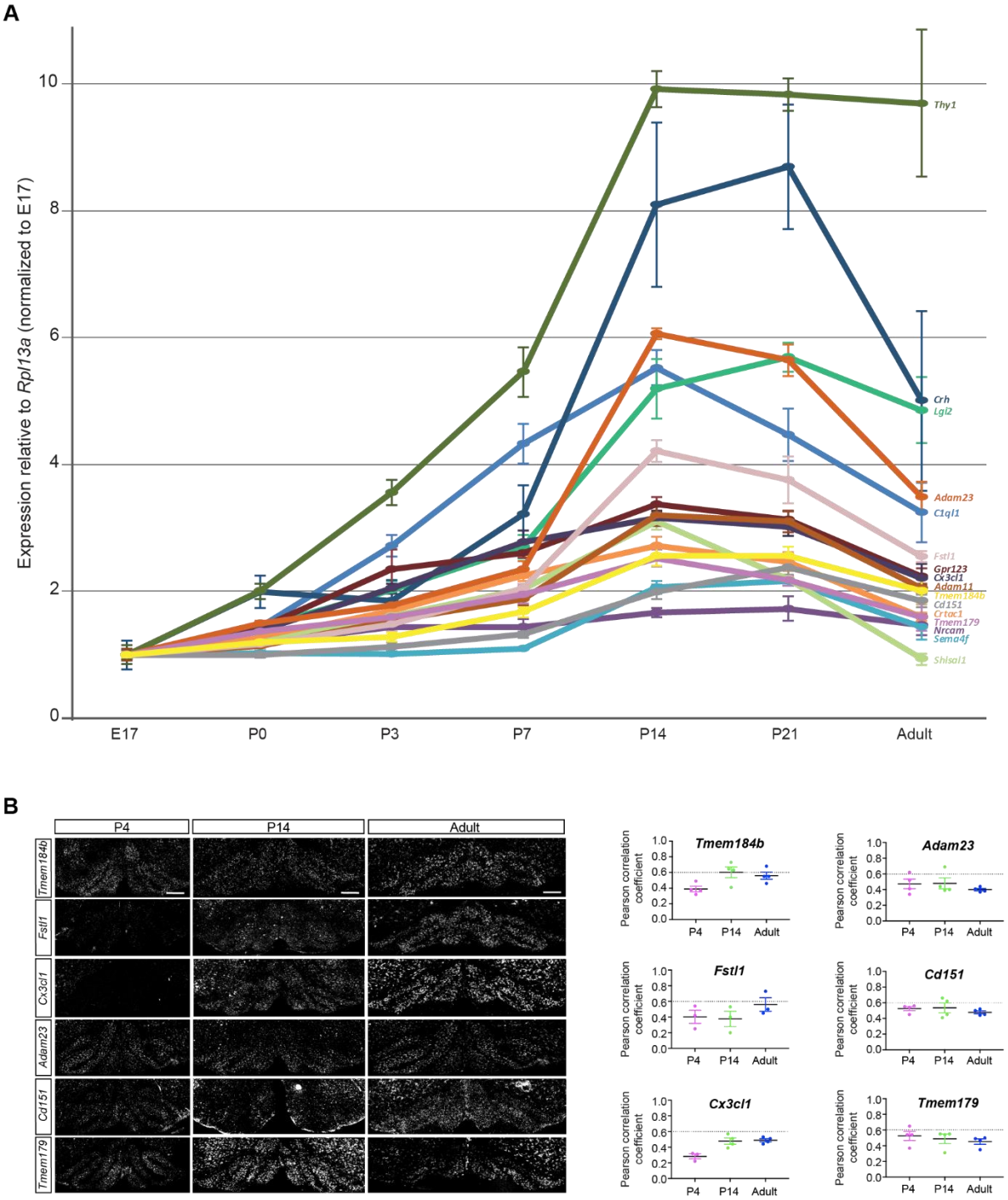

Fig. S1. Developmental expression pattern of ION candidate genes.

(A) Expression pattern of the fifteen ION DEGs selected as candidate and assessed using high-throughput RT-qPCR on brainstem RNA extracts at different stages of development (Embryonic day, E17, Postnatal days, P0, P3, P7, P14, P21) and in adult. Expression levels were normalized to *Rpl13a* gene. Data are presented as mean ± SEM. n = 4 animals per stage. **(B)** *Left panel:* duplex smFISH for *C1ql1* and six candidate mRNAs in coronal sections of the brainstem at P4, P14 and in adult. *Right*

panel: correlation between *C1ql1* and candidate mRNAs were determined at the brainstem level using the Pearson correlation coefficient, revealing ION DEGs slightly correlated with *C1ql1* (coefficient >0.6 corresponding to high correlation). Data are presented as mean ± SEM. n = 3-4 animals per condition, 2-3 independent experiments. Scale bars, 150 µm.

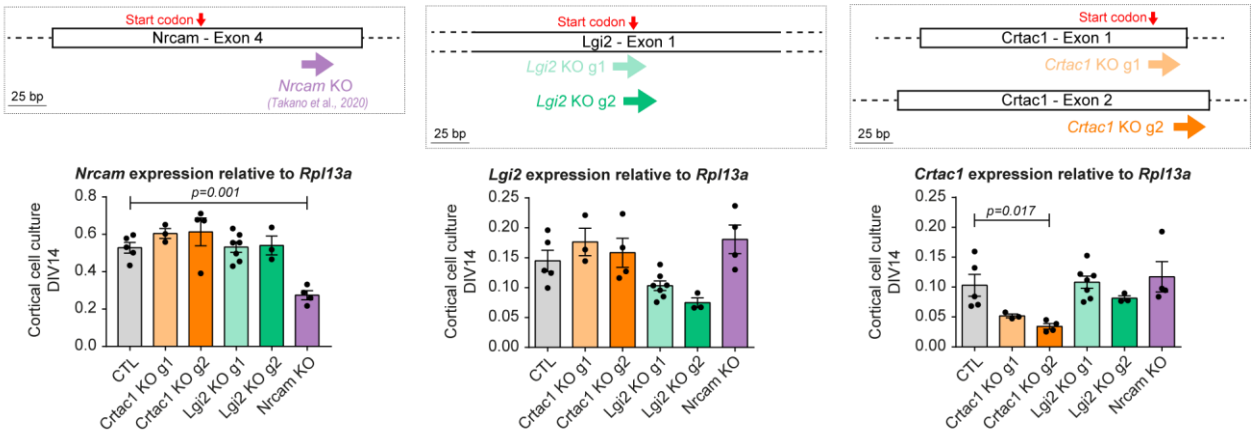

fig. S2. Validation of CRISPR/Cas9 gRNAs for *Nrcam*, *Lgi2* and *Crtac1* KO.

Top panel: illustration of the genomic sequence of mouse *Nrcam*, *Lgi2* and *Crtac1* with the location of the CRISPR/Cas9 gRNAs tested for each gene. *Bottom panel:* To test CRISPR/Cas9 efficiency, expression of *Nrcam*, *Lgi2* and *Crtac1* mRNAs was assessed using quantitative RT-PCR on RNA extracts from cortical cell cultures transduced at 3 days *in vitro* (DIV3) with AAVs driving the expression of each gRNA directed against candidate genes or non-targeting control gRNA (CTL). Analysis was done at DIV14. Expression levels were normalized to the *Rpl13a* gene. Data are presented as mean ± SEM. n = 3-7 independent experiments. Statistics: one-way ANOVA with multiple comparisons.

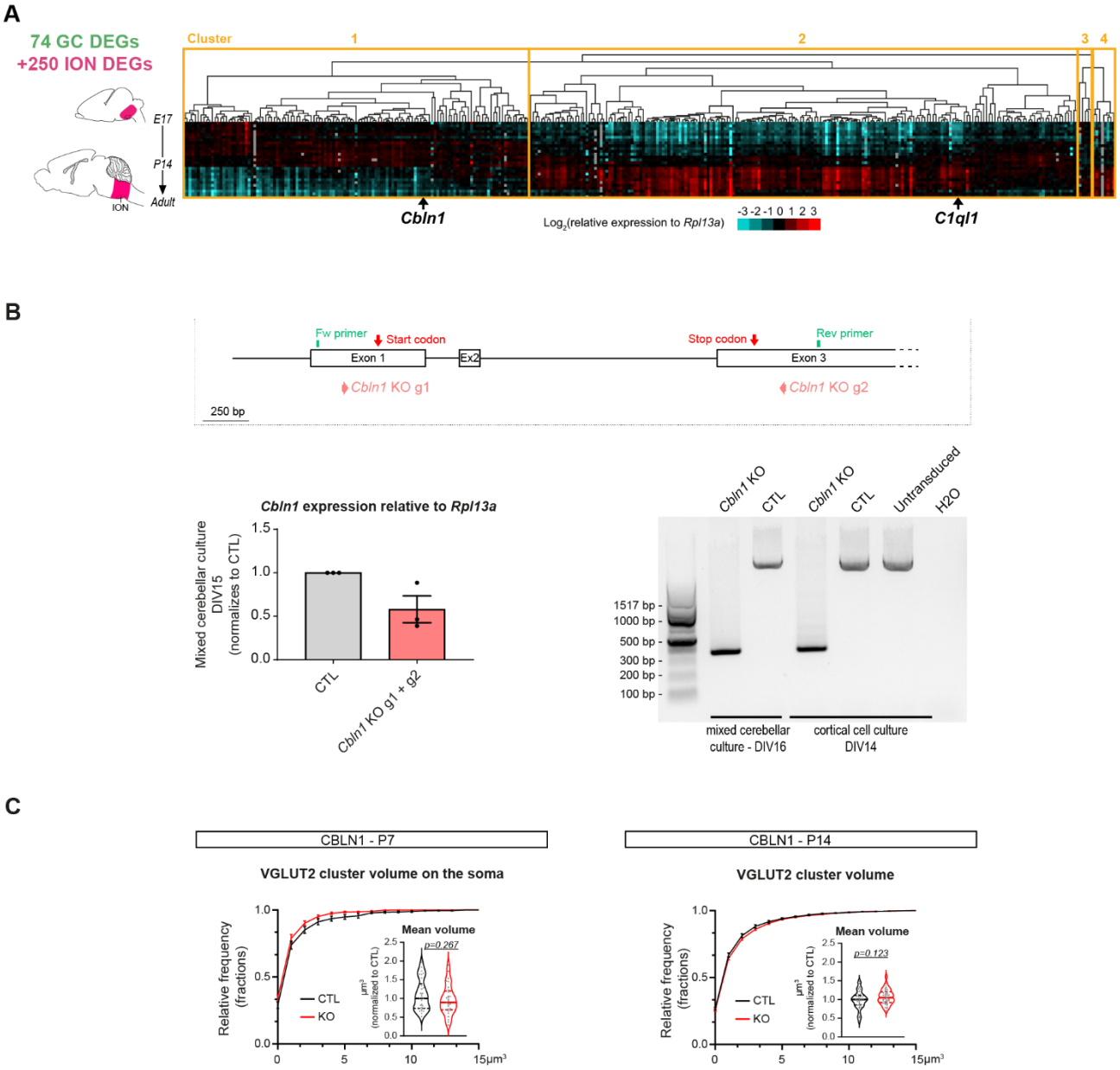

fig. S3. Cbln1 expression dynamics in the brainstem and validation of CRISPR/Cas9 gRNAs for *Cbln1* KO.

(A) Heatmap of the 74 GC DEGs and 250 ION DEGs in the brainstem between E17 and adult revealing *Cbln1* as an early-expressed gene. **(B)** *Top panel:* illustration of the genomic sequence of mouse *Cbln1* with the location of the CRISPR/Cas9 KO guide RNAs (*Cbln1* KO g1 and g2) as well as forward (Fw) and reverse (Rev) primers targeting non-coding regions of *Cbln1* exon1 and exon 3, respectively. *Bottom left panel:* to test CRISPR/Cas9 efficiency, the expression of *Cbln1* mRNAs was assessed using quantitative RT-PCR on RNA extracts from mixed cerebellar cultures transduced at days *in vitro* 2 (DIV2) with AAVs driving the expression of *Cbln1* gRNAs or non-targeting control gRNA (CTL) Analysis was done at DIV15. Expression levels were normalized to *Rpl13a* gene. Data are presented as mean ± SEM. n = 3 independent experiments. *Bottom right panel:* CRISPR/Cas9 efficiency was tested

by PCR analysis of endogenous *Cbln1* in purified genomic DNA from mixed cerebellar cultures or cortical cell cultures at DIV16 or DIV14, respectively. Transduction was performed at 2 days *in vitro* (DIV2) for cerebellar mixed cultures and DIV3 for cortical cell cultures with AAVs driving the expression of each gRNA directed against *Cbln1* or non-targeting control gRNA (CTL). Wild-type size of the fragment is expected at 2663 bp and KO fragment at 380 bp. **(C)** Distribution and mean of the VGLUT2 cluster volume, presented as violin plot, were quantified in GFP+ CFs both at P7 and P14 in CTL and *Cbln1* KO. P7 VGLUT2 cluster volume: $n \geq 29$ images per condition; 8 animals per condition, 4 independent experiments; statistics: Mann-Whitney. P14 VGLUT2 cluster volume: $n \geq 33$ images per condition; 8-9 animals per condition, 3 independent experiments; statistics: unpaired Student's test.

Supplementary data:

Data S1.
Gene clustering - Log2 of DEGs from GCs in Cerebellum extracts.

Cluster 1 Cluster 2

GENE NAME	Cb_set1_E17	Cb_set2_E17	Cb_set4_E17	Cb_set3_E17	Cb_set1_P0	Cb_set3_P0	Cb_set1_P3	Cb_set2_P0	Cb_set4_P0	Cb_set2_P3	Cb_set4_P3	Cb_set3_P3	Cb_set2_P7	Cb_set3_P7
slc30a10	-0.192726	0.148451	0.115884	0.250336	-0.052191	0.189684	0.139198	0.119069	0.076526	0.183082	-0.349658	-0.279347	0.484973	0.186999
Vps37b	-1.059715	0.0	0.036868	-0.57401	-0.684815	-0.176659	-0.453395	0.308534	0.495655	0.704569	0.230972	-0.169485	0.679352	0.154021
slc24a5	0.0	-1.764585	-2.049691	-1.490996	-0.872316	-0.707411	2.355632	-1.451023	-0.788716	-0.087898	-1.331322	-0.1593	1.45757	0.62492
Gpr22	-0.086543	0.130432	-0.053601	0.18899	0.0	-0.271369	-0.644895	-0.389342	-0.769666	-0.578786	-0.873448	-0.826749	-0.489256	-0.55221
Cdon	-0.041485	0.0	0.111839	0.056107	-0.639565	-0.785747	-0.37329	-0.825885	-1.465061	-1.125199	-1.812401	-1.40053	-0.997209	-1.312921
Tnfsf9	-0.229253	0.341181	0.26478	0.275788	-0.606201	-0.44237	-0.370765	-0.415665	-0.646209	-0.578838	-0.826101	-1.107783	-0.437114	-0.719098
Cnr1	-0.326692	0.095857	-0.076267	-0.048033	-0.389288	0.204247	-0.421278	-0.086898	-0.083568	0.0	-0.59772	-0.4289	-0.056789	-0.476675
Tspan9	-0.253643	0.024398	-0.023459	0.0	-0.216454	-0.061599	-0.297392	0.04328	-0.10593	-0.120377	-0.683319	-0.474407	-0.079173	-0.597534
Nrxn3	-0.445865	0.0	0.056803	0.015623	-0.494343	-0.100843	-0.431976	-0.026544	-0.223271	-0.265991	-1.038584	-0.767609	-0.115697	-0.604254
Rtn4r	-0.428459	0.175811	0.124425	0.0	-0.434308	-0.043091	-0.524198	-0.10849	-0.191232	-0.197648	-0.64734	-0.609326	-0.013831	-0.352063
Trhde	-0.278126	0.0	0.014725	0.285422	-0.486369	-0.150234	-0.485333	-0.345257	-0.17369	-0.193475	-0.936879	-0.615973	-0.232221	-0.433731
Dlg4	-0.143978	0.330676	0.150081	0.0	-0.501702	-0.054923	-0.570894	-0.061284	-0.188118	-0.191401	-0.750775	-0.586565	-0.209359	-0.489726
Igfbp5	-0.11364	0.319515	0.378162	0.175787	-0.490765	0.0	-0.517474	-0.182068	-0.217495	-0.168866	-0.606235	-0.51187	-0.288499	-0.5813
Aqp6	-0.53199	0.080143	0.0	-0.10143	-0.52888	-0.189131	-0.179023	-0.688547	-0.508976	-0.461503	-0.567322	-0.656692	-0.262002	-0.609917
Ramp3	-0.183553	0.251532	-0.013433	0.098741	0.0	-0.078238	-0.544423	-0.336087	-0.518714	-0.702038	-0.965578	-0.673666	-0.756193	-0.601645
Gpr25	-0.603934	0.064743	0.028453	0.0	-0.710876	-0.02936	-0.886677	-1.089778	-0.367057	-1.266728	-1.460191	-0.940359	-1.136152	-0.799105
Spint2	-0.036943	0.151802	0.151378	0.0	-0.230484	-0.108762	-0.315436	-0.2392	-0.271247	-0.576901	-0.878892	-0.929122	-0.783927	-0.898508
Jup	-0.468624	0.0	0.062978	0.036235	-0.495787	-0.048373	-0.572294	-0.411887	-0.382353	-0.661182	-1.057828	-0.619093	-0.555547	-0.680107
Ntm	-0.243579	0.0	0.089404	0.049112	-0.422902	-0.35319	-0.990256	-0.360487	-0.424938	-0.58928	-1.009603	-0.927175	-0.449674	-0.734268
Olfm3	-0.038061	0.0	0.102731	0.057714	-0.127744	-0.078162	-0.747621	-0.163568	-0.255081	-0.287009	-0.733386	-0.680185	-0.231072	-0.504414
Pard6b	-0.054594	0.0	0.234987	0.116431	-0.434015	-0.084344	-0.82815	-0.685794	-0.373339	-0.849341	-1.100648	-0.998942	-0.704744	-0.733229
Sdc1	-0.008285	0.264708	0.031803	0.150188	-0.223355	0.042823	0.0	-0.070662	-0.23927	-0.043349	-0.233079	-0.166328	-0.475057	-0.207979
Inadl	-0.79149	-0.220162	-0.01055	-0.083671	-0.11323	0.269038	-0.383354	0.206111	-0.040531	0.0	-0.343153	-0.205234	-0.426567	-0.398707
Ntf3	-0.521628	-0.180791	-0.034809	-0.044538	-0.163303	0.058145	-0.181392	0.166391	0.0	-0.102377	-0.281434	-0.376936	-0.050816	0.058258
Crlf1	-0.550722	-0.037465	-0.134812	-0.261576	-0.062443	0.630047	0.009936	0.567626	0.392425	0.007679	0.0	-0.04558	-0.197305	-0.760432
Gprc5c	-0.538437	0.012986	-0.347297	-0.358189	-0.684415	-0.033918	0.096906	-0.436597	-0.497644	-0.010118	-0.533698	0.0	-0.210194	-0.408183
Stap2	-0.759344	0.163974	-0.382938	-0.603134	-1.031873	-0.442885	-0.266016	-0.700166	-0.900796	0.070583	-0.277714	0.0	-0.025258	-0.180827
Boc	-0.374109	0.088462	-0.021298	0.012542	-0.386648	-0.113788	-0.015105	-0.096044	-0.189872	0.0	-0.378899	-0.173883	-0.109274	-0.318079
Rock2	-0.772415	0.0	-0.047934	-0.047849	-0.635379	-0.22746	-0.386005	-0.028643	-0.084993	0.0133	-0.555003	-0.458812	0.210605	-0.394308
Cnksr2	-0.697977	0.118528	-0.184086	-0.146729	-0.499464	-0.015609	-0.074767	0.0	-0.352604	-0.139276	-0.430581	-0.325444	0.400656	-0.178736
Kcnc1	-0.67115	-0.070794	-0.129719	-0.030222	-0.568822	0.029348	-0.111597	-0.334981	-0.258534	-0.41197	-0.803442	-0.472722	0.0	-0.209278
Dock4	-0.337565	-0.015616	-0.042053	-0.079053	-0.571219	0.0	0.086764	-0.027408	-0.051831	-0.073744	-0.249171	-0.118265	0.269614	-0.127519
Kcnd2	-0.665637	-0.401407	-0.472472	-0.268243	-0.563227	0.0	-0.093314	-0.170682	-0.241887	-0.098208	-0.427423	-0.283478	0.080818	-0.158991
Comp	-4.077426	-3.305219	-2.657517	-2.321697	-1.942815		0.0							
Dlgap1	-0.768733	-0.247418	-0.394227	-0.252276	-0.518082	0.001538	-0.117138	-0.278162	-0.032648	0.0	-0.421293	-0.186489	0.092969	-0.101032
Gprin1	-0.325486	0.111832	-6.37E-4	-0.015269	-0.444338	0.085814	-0.436624	-0.015	-0.085795	-0.071072	-0.697189	-0.491118	0.0	-0.408132
Rnf19b	-0.285443	0.034614	0.0	-0.130588	-0.260637	-0.096444	-0.431651	-0.039492	-0.041197	-0.148564	-0.377844	-0.432739	0.125875	-0.175416
Ehd1	-0.214032	0.0	-0.07906	-0.161056	-0.408139	-0.104263	-0.324868	-0.033662	-0.235558	0.061033	-0.463156	-0.372909	0.068097	-0.231242
Ap2a2	-0.501117	-0.059139	-0.010518	0.0	-0.323224	-0.15141	-0.354736	-0.022821	-0.128793	0.042821	-0.500734	-0.424975	0.070649	-0.307052
Lin7c	-0.360077	-0.026077	0.0	0.004701	-0.366913	-0.196982	-0.653864	-0.165647	-0.327528	-0.095626	-0.644664	-0.463598	0.017793	-0.300373
Dgcr2	-0.285346	-0.036137	-0.01996	0.0	-0.317062	-0.170697	-0.334818	-0.08414	-0.265964	0.150752	-0.443619	-0.379205	0.101931	-0.176543
Stxbp5	-0.617402	-0.263255	-0.21559	-0.229213	-0.527308	-0.098775	-0.259419	-0.059889	-0.159027	0.03916	-0.475464	-0.448122	0.409856	-0.120413
Unc13c	-0.561817	-0.234273	-0.06535	-0.237645	-0.733026	-0.213933	-0.666344	-0.052306	-0.363621	0.393795	-0.891182	-0.603617	0.384754	-0.294137
Twsg1	-0.352723	-0.050445	0.011742	-0.135813	-0.183629	-0.079105	-0.209977	-0.172353	-0.057297	0.254034	-0.174142	-0.239376	-0.087812	-0.1009
Sln	-3.885736	-3.096105	-3.259952	-3.352571	-0.968292	-1.733786	0.181669	-1.417934	-1.696454	-0.179002	0.046469	0.0	-0.349355	-0.700019
Clec10a		-3.739191		-3.700675	-2.868669	-0.911052	0.0	-2.550325	-3.257166	0.15772	-0.507799	-0.108118	-0.110433	-0.574825
Ipcef1	-0.518551	-0.487456	-0.78273	-0.131133	-0.430715	-0.054629	-0.74169	-0.252604	-0.926182	-0.232231	-1.040222	-0.29345	0.201383	0.054629
Cdh15	-0.77495	-0.574195	-2.553829	0.574537	-0.227059	-1.079081	-1.109015	-1.374586	-0.561469	-0.107032	-0.34714	-0.206557	-0.11322	-0.85899
Chn2	-0.935218	-0.511545	-0.625434	-0.64693	-0.653293	-0.794717	-0.600129	-0.754455	-0.94095	-0.331603	-0.944059	-0.687763	0.218277	-0.259809
Wnt7a	-0.539394	-0.39849	-0.39084	-0.261607	-0.904881	-0.738718	-0.619348	-0.796193	-1.067908	-0.641929	-0.803399	-0.948811	0.406088	-0.172024
Crtam	-1.327841	-0.549049	-0.862442	-0.760637	-0.738432	-0.783819	-0.576998	-1.533289	-0.258785	-0.438982	-0.49844	-0.774141	0.275576	-0.23142
Tmem159	-0.52757	-0.307573	-0.334549	-0.440776	-0.691559	-0.781913	-0.233363	-0.720653	-0.467902	-0.29752	-0.226835	-0.555428	0.236485	-0.06345
Fzd7	-1.502262	-1.106125	-1.19259	-1.163602	-0.978417	-0.838295	-0.147303	-0.714065	-0.500067	-0.163238	-0.070409	-0.311155	0.353801	0.0
Itgav	-1.256418	-1.072645	-1.243792	-0.854177	-1.207167	-0.759626	-0.212471	-1.172047	-1.103462	-0.554854	-0.574219	-0.522862	0.139219	0.012369
Grm4	-1.946732	-1.909008	-2.028641	-1.654486	-1.724841	-1.452562	-0.64043	-2.10011	-1.894349	-1.431577	-2.05571	-1.183803	0.004242	0.0
Gabrd	-4.559574	-4.700931	-4.292532	-3.959107	-3.946024	-3.91671	-2.738936	-4.038654	-4.298519	-3.060537	-3.384665	-3.464089	0.0	-0.772806
Slc17a7	-3.351256	-3.001991	-2.996697	-3.058062	-2.413497	-2.304994	-1.689397	-2.431743	-2.308245	-1.063754	-1.615728	-1.478795	0.0	-0.243182
Syt12	-2.788224	-2.729095	-2.774254	-2.334321	-2.234029	-1.844304	-1.244902	-2.160361	-2.004658	-0.94284	-1.361053	-1.252754	0.0	-0.634635
Il16	-4.151476	-4.114645	-4.221327	-4.515569	-3.727587	-3.713794	-2.430575	-3.814655	-3.983714	-2.14526	-2.687781	-2.421879	0.0	-0.760738
Bmp5	-2.755157	-2.483202	-2.586323	-2.524423	-1.898923	-1.634195	-0.576146	-2.080497	-1.769963	-0.20251	-0.74152	-0.844813	0.0	-0.085657
Cbln3	-3.15128	-3.150762	-3.475413	-3.181523	-2.837975	-2.090261	-1.540441	-2.415811	-2.340186	-0.990967	-1.516473	-1.493924	0.138163	-0.422314
Gabra6	-4.773839	-7.729487	-7.073084	-8.358421	-5.971798	-5.474126	-2.861574	-5.213743	-5.100191	-3.450122	-4.110747	-3.740801	0.0	-0.792474
Il17re	-3.474492	-4.380562	-3.640269	-4.788363	-3.913593	-3.005955	-0.800064	-1.871841	-3.140069	-0.842802	-1.832376	-1.767557	0.086855	-0.251586
Diras2	-0.214761	-0.389405	-0.588273	-0.548871	-0.708168	-0.038481	-0.372835	-0.086914	-0.174837	-0.001748	-0.47438	-0.351073	0.375699	-0.272818
Kcnk12	-2.011406	-0.738702	-1.620405	-0.821006	-0.995214	-0.70126	-0.878688	-0.652173	-0.726525	-0.402043	-1.13913	-0.935198	0.318934	-0.269377
Grik2	-0.827423	-0.354408	-0.504033	-0.431047	-0.674692	-0.057813	-0.326311	-0.302263	-0.352667	-0.26949	-0.636143	-0.441957	0.362258	0.0
Sh3gl2	-1.046626	-0.841578	-0.798565	-0.886326	-0.838871	-0.718182	-0.725968	-0.53998	-0.50972	-0.337378	-0.693717	-0.744048	0.384019	-0.082928
Asph	-0.802005	-0.552023	-0.415859	-0.570849	-0.590216	-0.236381	-0.195972	-0.215923	-0.38883	-0.115118	-0.261414	-0.323267	0.22239	-0.191105
6430571L13F	-0.884739	-0.598347	-0.461499	-0.623887	-0.601008	-0.139305	-0.284155	-0.310958	-0.464136	-0.052696	-0.487924	-0.363394	0.331586	-0.036855
Cbln1	-0.69951	-0.541854	-0.522209	-0.597926	-0.526501	-0.090177	-0.44446	-0.113852	-0.304368	-0.106384	-0.476894	-0.390906	0.364926	-0.037128
Cadps2	-1.027971	-1.314943	-1.294998	-1.182493	-0.871215	-0.646422	-0.714002	-0.641639	-0.851803	-0.665086	-0.809221	-0.793413	0.269611	-0.115501
Elmo1	-0.584473	-0.297757	-0.356438	-0.503161	-0.445177	-0.125165	-0.179362	-0.18784	-0.200164	0.075329	-0.391826	-0.36051	0.261721	-0.175507
Syt9	-1.107877	-0.727186	-0.56692	-0.797023	-0.83234	-0.563699	-0.61486	-0.578029	-0.641606	-0.19258	-0.642963	-0.664542	0.357633	-0.082808
Cbln1	-0.827275	-0.679182	-0.695772	-0.66251	-0.475601	-0.295188	-0.679456	-0.226321	-0.324943	-0.103153	-0.626878	-0.483087	0.232891	-0.091278
Cbln1	-0.863603	-0.789358	-0.62059	-0.6921	-0.676845	-0.095138	-0.722281	-0.285711	-0.341338	-0.135785	-0.496275	-0.37814	0.155837	-0.163607
Cbln1	-0.883998	-0.634356	-0.549272	-0.672798	-0.510647	-0.226877	-0.664337	-0.289657	-0.173684	-0.106658	-0.474688	-0.50231	0.330635	-0.157341

Cluster 1 Cluster 2

GENE NAME	Cb_set1_P7	Cb_set4_P7	Cb_set2_P14	Cb_set1_P21	Cb_set1_P14	Cb_set3_P14	Cb_set4_P14	Cb_set2_P21	Cb_set3_P21	Cb_set4_P21	Cb_set1_Adu	Cb_set3_Adu	Cb_set4_Adult
slc30a10	-0.356572	-0.051653	-0.121093	-0.070557	0.519987	0.45673	0.12799	-0.091488	0.0	-0.160146	-0.607564	-0.299568	-0.084247
Vps37b	0.062274	0.324233	0.449137	0.249849	0.430786	0.069007	-0.37623	-0.271289	-0.41589	-0.412468	-1.019014	-0.975904	-1.037153
slc24a5	1.520004	0.637288	0.331879	0.361222	0.854937	0.144585	0.03889	0.98247	0.137308	0.69316	-1.761382	-2.085375	-1.230943
Gpr22	-0.746333	-0.721398	3.316349	4.661366	2.70301	3.206978	3.287862	4.622665	4.501411	4.68179	4.591621	4.687249	4.780192
Cdon	-1.053422	-1.235325	2.744486	3.648693	2.516224	2.645065	2.335583	3.351521	3.044676	3.308469	4.078518	3.392952	4.007159
Tnfsf9	-0.836769	-1.06481	0.219795	1.079295	0.0	0.216406	0.259672	0.755431	1.090984	0.883021	0.374622	0.244862	0.520008
Cnr1	-0.434212	-0.451715	2.076073	3.423386	1.755089	1.911916	1.972537	2.644488	2.310346	2.543625	2.853598	2.877312	2.729472
Tspan9	-0.164355	-0.367775	3.231854	3.824402	2.944069	3.031244	2.866062	3.963246	3.395774	3.775744	3.051382	3.028041	2.992526
Nrxn3	-0.861148	-0.867002	3.160255	3.306915	2.354804	2.886838	2.709415	3.08964	2.92608	3.167409	3.758184	3.549054	3.568175
Rtn4r	-0.376817	-0.779385	2.938113	3.69867	2.538316	2.576691	2.583484	3.104612	3.360341	3.192089	2.804906	2.784285	3.002909
Trhde	-0.676548	-0.38205	2.947184	3.404372	2.314403	2.874646	2.81908	3.079008	2.949159	2.951551	3.754293	3.561661	3.531303
Dlg4	-0.604414	-0.507771	2.273549	3.17433	1.762942	2.142403	2.080864	2.362804	2.254846	2.167536	2.119305	2.138532	2.119662
Igfbp5	-1.140016	-0.722195	0.322441	1.345441	-0.085076	0.234531	0.369842	0.825347	0.664814	0.63503	0.944181	0.928073	0.995016
Aqp6	0.100037	-0.850713	3.188927	5.528364	2.883312	3.175354	3.086723	4.7416	4.774234	4.63121	5.396413	5.116482	5.300429
Ramp3	-0.559074	-0.697558	1.596428	3.047018	1.629308	1.949114	1.799868	2.847661	2.976381	2.747049	1.73315	1.824507	1.865727
Gpr25	-0.457495	-1.0805	1.591124	2.15059	0.965742	1.008704	1.119492	1.248284	1.021575	1.264919	1.767033	1.730536	2.004278
Spint2	-0.869784	-0.686814	0.830382	1.178696	0.544943	0.766683	0.670112	0.871847	1.037597	1.017537	0.635759	0.377836	0.708502
Jup	-0.52694	-0.522155	2.660929	3.941015	2.272162	2.603873	2.559276	3.156476	3.003283	2.995599	2.955752	2.986375	3.083896
Ntm	-0.478145	-0.537871	2.495834	2.870238	2.0743	2.371427	2.283551	2.529914	2.269775	2.497387	2.013804	1.970792	1.955731
Olfm3	-0.451972	-0.707714	5.089883	5.921582	4.376266	4.903611	4.894903	5.698672	5.586809	5.776459	5.249593	5.058657	5.124691
Pard6b	-0.947609	-1.0461	1.546814	2.250765	1.054496	1.631547	1.626167	2.104043	1.737571	1.841226	1.717433	1.872518	1.748285
Sdc1	-0.871469	-0.459626	0.155	1.674468	-0.419581	0.075241	-0.135561	1.707072	1.183184	1.607221	0.729543	0.88342	1.150979
Inadl	-0.859827	-0.610425	3.479335	4.586063	2.528816	3.053845	2.918257	3.952591	4.239176	4.000017	5.576279	5.348032	5.29634
Ntf3	0.342114	-0.166326	1.821766	2.008352	1.972096	1.946365	1.841224	1.572049	1.632026	1.847854	0.050579	-0.325821	-0.464558
Crlf1	-1.166889	-0.983311	2.005781	2.55473	1.842245	1.228834	0.157777	0.593502	0.705809	1.345457	-0.26165	-0.392698	-0.042334
Gprc5c	-0.155914	-0.501075	5.281988	6.239814	4.736267	5.075009	5.237543	5.67997	5.651665	5.667891	5.565132	5.333103	5.6774
Stap2	-0.396267	-0.179484	2.540803	4.329771	2.170467	2.895321	2.624636	4.146815	4.10023	4.042348	4.595176	4.699045	4.963844
Boc	-0.48154	-0.184572	1.689811	1.888498	1.327065	1.477705	1.485218	1.847279	1.600224	1.85796	1.402351	1.431075	1.470196
Rock2	-0.785031	-0.409025	2.816578	3.145755	1.694352	2.550189	2.646863	2.733794	2.750236	2.690246	3.065384	3.120064	2.916342
Cnksr2	-0.222181	-0.186797	3.175409	4.100663	2.610704	3.065906	3.151128	3.558958	3.306596	3.407784	4.15897	4.076253	4.011085
Kcnc1	0.160277	-0.150236	3.905196	5.039093	3.272801	3.638091	3.725286	4.340746	4.15952	4.365421	5.003525	4.73183	4.833425
Dock4	-0.063144	-0.027456	2.965819	4.031628	2.503853	2.725901	2.834356	3.236207	3.061704	3.093288	3.885507	3.788144	3.676653
Kcnd2	0.184343	-0.057653	2.913951	3.947852	2.558919	2.765183	2.883368	3.201199	3.099356	3.221793	3.583493	3.190027	3.434498
Comp	-0.688789					1.082233	1.945104	2.818352	2.133063	2.903918			4.438094
Dlgap1	-0.123965	-0.028818	3.31529	5.832903	2.990839	3.250259	3.257567	3.716118	3.364153	3.457111	3.554526	3.573212	3.552751
Gprin1	-0.297547	-0.31246	1.03398	1.44419	0.647737	1.039183	0.877881	0.820796	0.670368	0.634868	0.363839	0.218047	0.382171
Rnf19b	-0.031299	-0.132015	2.420225	3.100869	2.223178	2.52253	2.370565	2.593574	2.8441	2.623781	2.104989	2.241766	2.122464
Ehd1	-0.341271	-0.229873	1.302267	2.120893	1.057802	1.326437	1.072531	1.61137	1.356558	1.523888	0.910997	0.94864	1.091778
Ap2a2	-0.384004	-0.133626	2.118109	2.338451	1.567901	1.85215	1.82451	2.189389	1.909627	2.167722	1.548301	1.595752	1.643986
Lin7c	-0.339158	-0.177399	1.56638	1.317247	1.017547	1.285174	1.311198	0.964349	1.006999	1.184012	0.531195	0.505612	0.564581
Dgcr2	-0.244382	-0.177874	1.555558	1.704651	1.065295	1.372248	1.388401	1.648912	1.480236	1.754754	1.338803	1.279652	1.341007
Stxbp5	-0.162545	0.0	2.672531	2.986323	2.002624	2.531238	2.382708	2.742511	2.712177	2.784503	3.09034	3.077395	3.05056
Unc13c	-0.231564	0.0	4.570761	5.168073	3.723363	4.667784	4.612689	4.938055	4.759864	5.221521	5.170437	4.86902	5.121893
Twsg1	-0.349683	0.0	0.590679	1.28972	0.35357	0.768145	0.493291	0.617244	0.548129	0.580229	0.816103	0.929151	0.895821
Sln	-0.31681	-0.653686	4.486302	6.435047	5.436286	5.061203	5.03478	5.656574	5.212833	5.479911	4.920875	5.048875	5.012702
Clec10a	-0.029803	-0.49144	1.91517	2.022684	2.175552	2.139658	2.123472	1.895734	1.758805	1.820552	0.708253	1.486762	1.665738
Ipcef1	0.081657	-0.619028	4.101225	5.407813	3.886712	4.379229	4.382337	5.006517	4.878962	4.905431	4.955388		5.131558
Cdh15	1.174841	0.0	5.57488	6.895804	5.511611	5.805999	5.717304	6.555737	6.354316	6.541103	6.438119	6.04461	6.437635
Chn2	0.351958	0.0	4.730596	5.324423	4.091228	4.458876	4.278377	5.09573	5.073592	5.272342	5.058485	4.875499	5.0834
Wnt7a	0.906557	0.0	4.784635	5.433922	4.199597	4.622823	4.424763	5.157811	5.19265	5.128276	4.397667	4.352625	4.619741
Crtam	0.088667	0.0	6.363353	8.845042	5.441644	5.917623	5.975881	8.455579	8.542267	8.526548	9.048631	8.829407	9.003991
Tmem159	0.174951	0.0	1.802598	2.002505	1.194171	1.570857	1.295724	1.461188	1.441159	1.300264	0.270539	0.533673	0.6721
Fzd7	-0.01099	0.054921	2.285903	3.560413	2.053832	2.219779	2.307703	2.513183	2.226663	2.440813	2.516709	2.457773	2.488061
Itgav	-0.308965	0.0	2.256075	2.268488	1.426408	1.934581	1.565708	0.948817	0.978506	1.132939	2.633473	2.603107	1.620502
Grm4	0.748469	-0.236203	5.590962	6.838343	4.950758	5.352825	5.270263	6.025829	5.585506	5.852501	5.362565	5.185704	5.194924
Gabrd	1.248547	0.00209	5.821757	6.627785	5.899069	5.527467	5.520115	6.264871	6.232062	6.235692	6.116237	5.981517	5.985809
Slc17a7	0.443627	0.193086	4.691838	5.001187	3.964407	4.465359	4.462335	4.725626	4.71976	4.684422	3.555426	3.542368	3.711857
Syt12	0.519976	0.090147	4.817068	5.265958	4.324074	4.692643	4.449353	5.146274	5.109383	4.975852	4.016855	4.113799	4.115951
Il16	0.450831	0.048462	4.551599	4.717208	3.792069	4.462065	4.313659	4.466646	4.278006	4.49713	4.193706	4.114449	3.980385
Bmp5	0.188105	0.058615	1.937014	3.162811	2.089856	2.175446	2.366317	2.531117	2.881119	2.611269	2.59757	2.662987	1.856583
Cbln3	0.308189	0.0	6.427601	7.372889	5.465641	6.123816	5.783684	7.087418	6.611179	7.046669	6.469295	6.680809	6.747061
Gabra6	1.356634	0.036065	6.782349	7.459181	6.301204	6.808525	6.637753	7.251732	7.225746	7.385872	6.757933	6.808419	6.948461
Il17re	0.436321	0.0	3.700637	5.402711	4.206796	4.101666	4.140671	4.800328	4.580869	4.525393	5.49911	5.470082	4.947706
Diras2	8.0E-5	0.0	3.063337	3.763485	2.677637	2.813336	3.046692	3.102964	2.934696	2.93384	3.147055	3.267713	3.255694
Kcnk12	0.720119	0.0	4.383249	5.084495	3.95912	3.640867	4.280079	4.895442	4.366038	4.581187	4.413872	3.880686	4.445627
Grik2	0.052065	-0.096115	2.136774	2.511081	1.760956	2.012205	1.993918	1.883947	1.685444	1.654823	2.400556	2.200877	2.221814
Sh3gl2	0.077519	0.0	2.806052	3.520592	2.479268	2.859106	2.748765	3.196766	3.082777	3.171601	2.747407	2.812791	2.762071
Asph	0.0	0.025643	2.823319	4.181561	2.236296	2.86418	2.768704	3.555271	3.726098	3.565876	3.668722	3.911371	3.711235
6430571L13F	0.133688	0.0	1.636274	2.300198	1.328037	1.610283	1.41594	2.066336	1.991269	2.055289	2.161961	1.911516	2.076814
Cbln1	0.289343	0.0	2.859274	3.983453	2.427569	2.448229	2.465654	3.171434	2.908371	3.063172	2.610506	2.548229	2.539194
Cadps2	0.211433	0.0	2.696231	2.164861	1.944754	2.32414	2.266477	2.250823	1.988872	2.416212	1.943191	1.410959	1.6141
Elmo1	-0.061059	0.0	1.220664	2.059608	1.188654	1.274702	1.288429	1.13929	0.95906	1.112135	0.933874	1.044356	0.995567
Syt9	0.0	0.083578	3.13299	3.00154	2.459157	2.981745	2.690175	2.606097	2.586572	2.504075	2.307584	2.114228	2.279056
Cbln1	0.071278	0.0	2.798155	3.341875	2.339497	2.49737	2.381067	3.090905	2.794533	3.203587	2.448516	2.396472	2.419548
Cbln1	0.1213	0.0	2.656737	3.50003	2.285728	2.607686	2.537833	3.088785	2.999264	3.12825	2.564709	2.488641	2.479577
Cbln1	0.048441	0.0	2.850438	3.561841	2.367699	2.495422	2.50811	3.179371	2.910401	3.171763	2.379972	2.489347	2.503996

Data S2.
Gene clustering - Log2 of DEGs from IONs in Brainstem extracts.

Cluster 1	Cluster 2	Cluster 3	Cluster 4

Gene names	IO_set0_P0	IO_set0_E17	IO_set2_E17	IO_set1_E17	IO_set1_P0	IO_set2_P0	IO_set3_E17	IO_set3_P0	IO_set1_P3	IO_set2_P3	IO_set0_P3	IO_set3_P3	IO_set0_P7
Gab2	0.059977	0.078639	0.0	0.052724	0.144675	0.376053	0.19922	0.140326	0.082312	0.08939	0.047363	0.185987	0.016495
Cd24a	1.701702	2.716735	2.640181	2.154336	1.519319	1.66414	2.092454	1.586591	1.238282	1.095322	0.762832	1.140296	0.047989
Igsf3	0.869601	0.356546	0.207111	0.353334	0.397463	0.509711	0.097608	0.053997	0.200965	0.114834	0.044834	0.197915	-0.199767
Ctxn1	0.873983	0.549028	0.370476	0.212863	0.20735	0.667406	0.297552	0.397031	0.213201	0.301283	0.21583	0.240037	-0.144629
Panx1	0.452487	0.610638	0.567565	0.5498	0.600357	0.72837	0.64155	0.495855	0.359895	0.618729	0.352526	0.299578	-0.024562
Tspan6	0.309798	0.330151	0.348348	-0.160426	0.156065	0.325822	0.22583	0.189799	0.178626	0.223423	0.389928	0.41479	-0.072404
Tmeff1	0.173216	0.306484	0.336957	0.209376	0.185339	0.50836	-0.150953	0.228113	0.153656	0.258309	0.363654	0.172619	0.005515
Scn3b	0.0	0.165993	0.18459	0.170555	0.208382	0.361136	0.301647	0.079724	0.06144	0.366871	0.052628	0.187988	-0.047672
Odz3 = Tenm2	6.34E-4	-0.021997	0.041475	0.004526	0.259068	0.170683	0.441074	0.425712	0.308138	0.146007	0.132381	0.096912	-0.270514
Plp2	0.0	-0.209458	0.428512	0.151407	-0.008251	0.660579	0.900368	0.621684	0.50168	0.957363	0.541316	0.707821	0.394934
Stx1a	0.068497	-0.06719	0.130424	-0.156259	0.073241	0.334397	0.703108	0.404186	0.19999	0.390989	0.247895	0.367743	0.0
F2r	0.179265	0.296837	0.614295	0.453937	0.300642	0.601352	-0.136195	0.412531	0.329818	0.0	0.261778	0.530993	-0.147956
Ly6h	0.804862	-0.050552	0.157624	0.156216	0.305082	0.34385	-0.475556	0.17268	0.271804	0.0	0.390687	0.45629	0.148684
Lrfn5	0.030265	-0.016571	0.133241	0.07959	0.0	0.440817	-0.27004	0.129534	0.503601	0.531905	0.185345	0.325557	0.008128
Olfm2	0.091468	0.021431	0.072561	0.069425	0.0	0.30108	-0.255308	0.019119	0.154308	0.436974	0.212714	0.158538	-0.031977
Cklf	0.948946	-0.129092	0.410007	-0.183031	-0.17065	0.628741	0.351823	0.529604	0.124428	0.086617	0.504912	0.64876	0.111685
Stbd1	0.134034	0.379089	0.302959	0.0	-0.210472	0.096762	0.234609	-0.322194	0.21064	0.559259	0.449121	0.477271	0.100766
Rtn4rl2	0.182972	-0.090899	0.10845	0.0	0.370699	0.708185	0.194508	-0.094048	0.112699	0.679235	0.450011	0.333701	0.304818
Slc1a4		0.327093	0.36426										0.555869
Cyb561d2	0.70434	0.120913	0.24961	0.005084	-0.055947	0.249291	0.068493	-0.005084	0.2353		0.330405	0.433882	0.206082
Crlf2	1.006147	-0.15971	0.210047	0.03526	0.190028	0.449726	-0.453767	0.154114	0.356735	0.444709	0.276239	0.680966	0.183155
Cgref1	0.903276	0.072686	0.0	0.004673	0.290611	0.405772	-0.124457	-0.038267	0.295103	0.307198	0.335101	0.334511	0.127263
Gpr125	0.626461	0.138074	0.057998	0.0	-0.039581	0.078575	-0.022329	-0.107438	0.040047	0.278632	0.12802	0.227394	-0.009742
Znrf2	0.251711	0.36401	0.067122	-0.224997	0.130959	0.304257	-0.199486	0.14176	0.173827	0.069488	0.350878	0.256614	-0.020005
2200002K05Rik = Vstm5	0.240035	0.212025	0.0	-0.032208	-0.04876	0.360366	-0.370194	0.073293	0.229519	0.290957	0.346379	0.416351	0.030397
Cdh9	0.167878	0.0	-0.046874	0.146662	0.364744	0.524751	-0.347127	0.292253	0.113902	0.19519	0.459662	0.424271	0.321712
Scarb1	0.08502	-0.011232	0.0	0.112714	0.212177	0.450382	-0.345668	0.227153	0.318979	0.493783	0.298782	0.275253	0.324632
Dner	0.220528	-0.036825	0.031103	0.07996	0.071388	0.255596	-0.134115	0.0	0.236298	0.575137	0.304868	0.380073	0.238922
Efna3	0.069571	0.0	0.070134	0.076671	-0.079073	0.260503	-0.161968	0.035703	0.241076	0.414089	0.235285	0.357598	0.227387
Kit	0.234389	0.214192	0.009747	0.190235	0.216628	0.124049	-0.131796	-0.166331	0.0	0.224249	0.297689	0.193615	0.308327
Grin3a	0.939478	0.35133	-0.145524	0.082554	0.354986	0.243194	-0.171661	0.0	0.371639	0.374303	0.377522	0.443908	0.428916
Cacna1g	0.216308	-0.093135	-0.004985	-0.082489	-0.113154	0.50553	-0.135681	0.290232	0.320162	0.309417	0.261972	0.537348	0.444413
Fam189a1	1.008542	0.163084	0.068505	-0.28537	-0.017333	0.278141	-0.530516	0.026288	0.314349	0.075305	0.298143	0.274769	0.344139
Igf1	1.112065	0.161332	0.0	-0.137824	0.235541	0.49566	-0.554325	0.474861	0.629636	1.043793	0.915312	0.767623	0.946016
Cbln4	0.280756	0.102615	-0.010121	0.010121	0.257736	0.273276	-0.328349	0.178245	0.259617	0.663594	0.690521	0.614904	0.653544
Pvrl2	0.163264	0.047416	0.0	-0.122665	0.078121	0.350858	-0.178535	0.246439	0.413737	0.232781	0.208875	0.57268	0.011613
Epha4	0.096965	-0.062279	-0.055743	0.078342	-0.07186	0.083782	-0.187004	0.189974	0.151255	0.0733	0.269196	0.215969	0.1893
Nell1	0.154284	-0.032455	0.121502	0.0	0.091093	0.322704	-0.540322	0.197767	0.530599	0.379037	0.490266	0.527643	0.382029
Gng4	0.797693	0.0	-0.038547	0.023882	0.188789	0.552261	-0.152086	0.083259	0.236211	0.652484	0.230334	0.547629	0.310663
Fam20c	0.638768	0.007627	0.078205	-0.035296	0.065716	0.278246	-0.145532	0.0	0.12474	0.396629	0.121609	0.32845	0.164566
Gabra5	1.026639	0.0	-0.046428	0.140586	0.45538	0.595619	-0.218756	0.353733	0.749219	0.986917	0.647977	0.909534	0.785032
Rasgrp2	0.241208	-0.112443	-0.202712	0.057639	0.211769	0.498138	0.0	0.157627	0.424298	0.753561	0.616513	0.700511	0.502264
Scn3a	0.212725	0.041004	-0.080498	0.0	0.307952	0.500642	-0.033151	0.282228	0.070642	0.264901	0.248994	0.279352	0.05956
Lphn2 = Adgrl2	0.864288	0.214653	-0.090856	0.170457	0.131346	0.341984	0.120194	0.016006	0.0	0.534193	0.276428	0.321625	-0.089007
Vstm2l	0.466809	0.352965	-0.016564	-0.120579	0.446693	0.02304	0.192787	0.085013	0.0	0.252381	0.638176	0.362475	0.104553
Rgs19	-0.009332	-0.096086	-0.308871	0.246082	0.482118	0.688021	0.442366	0.451245	-0.037277	0.315552	0.487354	0.81171	0.213816
H2-Aa	-0.969329	-2.953262	0.333792	0.015134	0.046823	0.217004	0.329854	0.0	-2.120732	-1.238595	0.354518	1.546601	1.222625
Ajap1	0.639477	0.430722	0.142288	0.146233	0.934175	0.829758	-0.438697	0.633177	-0.376392	0.19499	0.829187	0.610994	0.897561
BC048546	-0.376141	1.385169	-0.762703	-0.797897	-0.578675	-0.095836	0.615953	0.059856	0.54219	0.518731	2.358805	0.588624	4.078236
Cnih3	-0.003568	-0.276958	-0.188615	-0.264699	-0.153557	0.103928	-0.616232	-0.413723	-0.105412	0.44794	0.358267	-0.175847	0.411818
Gpr64	0.166747	-0.470146	-0.497749	-0.34248	-0.080565	0.0	-0.51624	-0.294819	0.270273	0.26351	0.261571	0.242102	0.647169
Ecel1	0.428967	-0.270869	-0.405679	-0.286959	-0.194791	0.047585	-0.49095	-0.122711	-0.093175	0.378876	0.13272	0.447528	0.512283
Btbd11	0.189205	-0.237537	-0.595211	-0.493961	-0.32883	0.0	-1.165141	-0.234616	0.262117	0.083659	0.34345	0.256714	0.589827
Kcnq5	0.684456	-0.294826	-0.774326	-0.746632	-0.602927	-0.83749	-1.334076	-0.331309	0.394942	0.039813	0.573374	0.403379	0.985168
Adcyap1	0.023917	-0.6813	-0.936092	-0.656161	-0.220733	-0.090427	-1.099183	-0.31453	0.242648	0.310357	0.369732	0.248335	0.477768
Cacng5	0.271697	-0.43085	-0.522141	-0.484614	-0.530065	0.281492	-1.057002	-0.144562	0.514858	0.258295	0.70458	0.754401	0.89463
Gpr26	0.226216	-0.473666	-0.634015	-0.581519	-0.6853	-0.299368	-0.782032	-0.644628	-0.433287	-0.326119	0.079488	0.043992	0.188969
Gabra4	0.686175	-0.293616	-0.422053	-0.504911	-0.341633	-0.114319	-1.06839	-0.523509	-0.079108		0.416075	0.341514	0.624057
Pcdh20	-0.37713	-0.687444	-0.728969	-0.798431	-0.616246	-0.327271	-1.183306	-0.387743	-0.25803	0.112917	0.0	0.099263	0.357278
A930038C07Rik = Ndnf	-0.024445	-0.161709	-0.666266	-0.279413	-0.13888	-0.067602	-0.758576	-0.55846	-0.222243	0.080744	0.187761	0.177278	0.502605
A730017C20Rik	-0.221782	-0.121487	-0.075654	-0.259473	0.003611	0.008877	-0.128203	-0.148776	0.0	0.097691	0.039414	0.11537	-0.055767
Casc4	-0.340205	-0.577662	-0.110457	-0.10782	0.192723	0.184515	-0.213997	-0.196299	0.259195	0.405345	-0.172163	0.318664	0.340205
Atp13a2	-0.218086	-0.514201	-0.440145	-0.545411	-0.165528	0.068276	-0.65888	-0.237718	-0.004241	0.201728	-0.014144	0.164396	0.058965
Qpctl	-0.248561	-0.58493	-0.23039	-0.397096	-0.03075	0.367245	-0.425707	-0.037728	0.079185	0.274508	-0.060416	0.113816	0.105465
Rab6b	-0.121885	-0.424757	-0.665682	-0.289205	-0.030626	-0.020838	-0.298068	-0.262511	-0.01866	0.423241	0.124069	0.155695	-0.037064
Slc24a3	0.157739	-0.294264	-0.40547	-0.258256	-0.033682	0.107154	-0.673097	-0.22857	0.255034	0.443734	0.480107	0.253744	0.646227
Prmt8	0.161424	-0.124695	-0.25391	-0.211223	0.0	0.116821	-0.197925	-0.138947	0.104901	0.361848	0.482314	0.303704	0.70211
Oprl1	-0.065715	-0.024403	-0.186769	0.032814	-0.295129	-0.161132	-0.021796	-0.428085	-0.150637	0.320477	0.247705	0.261809	0.384499
Lhfpl5	0.26711	-0.813097	-0.428454	-0.43784	-0.272106	-0.138443	-0.476009	-0.23199	0.226227	0.562908	0.00539	0.31332	0.295318
Gpx3	-0.022656	-0.531873	-0.412441	-0.32888	-0.329014	-0.153306	-0.744461	-0.403172	0.0607	0.368932	0.209369	0.235678	0.340972
Cthrc1	-0.09027	-0.614154	-0.436676	-0.896601	-0.639866	-0.772217	-1.286512	-0.032791	0.384426	0.491193	0.622139	0.028571	0.729759
Syngr3	-0.129504	-0.57538	-0.535311	-0.87473	-0.103588	-0.083391	-0.33733	-0.437159	0.010196	0.366759	0.211922	0.068256	0.358283
Bgn	-0.483998	-0.937092	-1.110791	-0.973624	-1.201534	-0.741555	-0.834594	0.24411	0.0	0.240265	0.184672	0.204896	0.519255
Pde2a	-0.169942	-0.42581	-0.300646	-0.703528	-0.371216	-0.038836	0.0	-0.406263	0.013891	0.315716	0.120324	-0.197301	0.20406
Vstm2a	-0.048747	-0.214445	-0.700721	-0.325861	-0.229039	0.273899	-0.279604	-0.474729	-0.163335	0.322713	0.275852	-0.115359	0.287432
Lypd6b	0.733528	-0.231309	-0.095487	-0.808172	-0.359398	-0.178523	-0.99758	0.097177	-0.211209	0.265584	0.93006	0.566615	0.196254
E130311K13Rik	0.590797	-0.298479	-0.134432	-0.470595	-0.513487	0.022426	-0.486098	0.10225	0.420185	0.388747	0.509868	0.460697	0.582862
Mboat7	0.083624	-0.271187	-0.339728	-0.288885	0.24225	0.138298	-0.492362	-0.106164	0.242586	0.432426	0.31023	0.307967	0.108823
Kcnip2	0.781161	-0.033155	-0.11661	-0.27442	-0.140949	0.389205	-0.519963	0.006743	0.332319	0.498385	0.454107	0.652397	0.765819
Fam174b	0.556631	0.110686	0.019835	-0.192831	-0.16374	0.020989	-0.1672	-0.13041	0.063932	0.206955	0.228477	0.212647	0.302331
Gjd2	0.912541	-0.12542	-0.173503	-0.121811	0.007719	0.184808	-0.779062	-0.018776	0.144333	0.290156	0.429673	0.449448	0.580751
Igfbp3	0.622488	-0.053448	-0.261255	-0.337702	0.0	0.334814	-0.50659	0.505486	-0.139803	0.130585	0.435217	0.281205	0.488279
Lypd1	-0.01507	-0.103629	0.0	0.045963	0.053093	0.363859	-0.185407	0.084545	0.285259	0.55109	0.307131	0.25528	0.35718
Ifngr2	0.103135	-0.140772	0.069625	0.030402	-0.084184	0.398018	-0.494021	0.175353	0.172346	0.5666	0.286232	0.567539	0.087221
Cdh13	0.188579	-0.11245	0.0	0.140035	0.213677	0.670938	-0.202744	0.304376	0.601866	0.772026	0.408451	0.612764	0.411431
Vstm2b	0.528352	0.127512	-0.038818	-0.286633	-0.220877	0.234172	-0.532826	0.123972	0.437798	1.028945	0.798694	0.656597	0.745713
Nell2	0.0	0.032137	-0.155087	-0.003263	0.103183	0.191567	-0.29917	0.019587	0.107673	0.508592	0.230879	0.166078	0.222152
Npnt	0.259155	0.021994	-0.284162	-0.004882	0.324995	0.412339	-0.109943	0.046102	0.350818	0.653546	0.624633	0.407405	0.512943
Nptx2	0.527705	-0.031532	-0.230539	0.217161	0.345882	0.837419	-0.097613	0.223996	0.597521	1.026229	0.626304	0.406169	0.93118
Pcsk5	0.015086	-0.380267	-0.263812	-0.261381	0.0	0.221403	-0.081611	0.231241	0.23251	0.488029	0.240763	0.28893	0.691485
Fxyd7	0.714716	-0.169074	-0.090346	-0.026421	0.091139	0.466069	-0.418402	0.072036	0.421895	0.706497	0.535179	0.639159	0.629534
Fam3c	0.59615	-0.162969	-0.022178	-0.153882	0.070605	0.273073	-0.41856	0.13619	0.143093		0.352591	0.488349	0.468091
Lypd6	0.911212	-0.005149	-0.628466	-0.250368	0.005149		-0.774118	0.220551	0.544174	0.820846	0.840221	0.480462	0.890991
Ptn	0.060163	-0.084039	-0.167705	-0.11493	4.91E-4	0.209959	-0.325513	-0.034864	0.0	0.203754	0.267343	0.245965	0.255113
Lyz1	-0.510591	0.187548	-1.249513	-1.017438	-1.016099	0.093609	-1.169859	0.119339	0.036465	0.272242	1.199567	0.199953	0.479374
Tmie	9.94E-4	0.049251	-0.48427	-0.375721	-0.081177	-0.042162	-0.538365	0.147614	-0.197005	-0.198201	0.526736	0.364904	0.094952
Lgals3	0.232163	-2.142768	-0.069612	-0.68292	-0.596838	-0.195908	-0.729237	0.585353	1.498996	0.473155	0.531078	0.531478	-0.680065

Cluster 1 Cluster 2 Cluster 3 Cluster 4

Gene names	IO_set1_P7	IO_set3_P7	IO_set2_P7	IO_set1_P14	IO_set3_P14	IO_set0_P14	IO_set2_P14	IO_set0_P21	IO_set2_P21	IO_set1_P21	IO_set3_P21	IO_set1_Adult	IO_set0_Adult	IO_set3_Adult
Gab2	0.010575	-0.005042	-0.070922	-0.405716	-0.350425	-0.305311	-0.302153	-0.369353	-0.341511	-0.030603	-0.245317	-0.241264	-0.666549	-0.314897
Cd24a	-0.136226	0.0	-0.030275	-0.86864	-0.947763	-0.719058	-0.198635	-0.207289	-0.464308	-0.452089	-0.772408	-1.104812	-1.283712	-1.068015
Igsf3	0.104878	0.0	-0.031614	-0.752632	-0.836525	-0.844952	-0.838417	-1.296421	-1.381555	-1.007837	-1.240782	-1.454075	-1.691906	-1.36259
Ctxn1	0.066304	0.0	-0.075361	-1.033384	-1.466131	-1.061966	-0.830268	-1.318425	-1.571255	-1.28993	-1.621783	-1.596852	-1.627915	-1.360138
Panx1	-8.87E-4	0.0	0.207782	-0.762615	-0.746757	-0.666459	-0.542168	-1.0193	-1.097973	-0.98304	-1.39717	-1.830467	-2.002924	-1.596826
Tspan6	0.079451	0.096752	0.0	-0.888287	-0.797278	-1.178981	-0.771202	-1.546246	-1.623755	-1.636619	-1.598267	-2.028915	-2.66685	-1.997605
Tmeff1	-0.098064	0.047509	0.0	-0.249844	-0.174996	-0.159152	-0.238334	-0.290166	-0.307463	-0.279019	-0.2564	-0.884042	-1.46767	-0.769449
Scn3b	0.10735	-0.043372	0.200874	-1.473583	-1.342169	-1.45068	-1.500848	-1.792055	-1.671153	-1.876608	-1.886082	-1.900183	-2.251991	-1.756358
Odz3 = Tenm2	0.210801	0.0	0.212777	-0.186958	-0.207631	-0.657311	-0.446432	-0.976965	-0.862289	-0.761225	-0.681525	-1.151969	-1.197897	-1.2478
Plp2	0.325995	0.366693	0.434718	-0.261342	-0.176246	-0.977392	-0.197849	-1.222738	-0.765741	-0.883737	-0.976513	-1.213496	-1.932179	-1.227776
Stx1a	0.078715	0.161652	0.181515	-1.310958	-1.440299	-1.704537	-1.445265	-2.307524	-2.10291	-2.019932	-2.137699	-2.556893	-2.466026	-2.507397
F2r	0.070457	0.343835	0.126325	-0.428119	-0.185438	-0.871941	-0.487952	-1.016235	-0.651554	-0.540841	-0.521303	-0.628698	-1.09925	-0.826647
Ly6h	0.208961	0.442316	0.051762	-1.140048	-1.394016	-1.583633	-1.57791	-1.827547	-1.801052	-1.61396	-1.962985	-1.65874	-2.014775	-1.756271
Lrfn5	0.130749	0.130743	0.001171	-0.685855	-0.379597	-0.605596	-0.596257	-0.735092	-0.878757	-0.565847	-0.701199	-0.786146	-1.291711	-0.730604
Olfm2	0.070071	0.112992	0.003116	-0.605419	-0.434253	-0.313252	-0.389783	-0.452237	-0.663698	-0.465108	-0.587102	-1.034803	-1.328632	-0.97406
Cklf	0.141099	0.433211	0.412183	-0.016461	-0.023945	-0.38532	0.0	-0.153476	-0.463378	-0.271896	-0.609167	-0.535012	-0.716922	-0.425463
Stbd1	0.298385	0.500144	0.048013	-0.619841	-0.780067	-1.492175	-1.144631	-0.687489	-0.811137	-0.306237	-0.692115	-1.498192	-1.338952	-1.393504
Rtn4rl2	0.141499	0.524468	0.60945	-0.817595	-0.907413	-2.106579	-0.791258	-1.800316	-1.608275	-1.150343	-1.408937	-2.320588	-2.954928	-1.946524
Slc1a4	0.752885			0.087447		-0.226506	0.343593	-0.076148		0.0	-0.117392	-0.398881	-0.592283	-0.184647
Cyb561d2	0.189245	0.400559	0.234221	-0.111073	-0.167696	-0.434045	-0.202039	-0.201543	-0.316717	-0.163003	-0.348675	-0.691091	-1.202495	-0.582659
Crlf2	0.0	1.025951	0.521209	-0.581684	-0.396159	-0.765575	-0.546228	-1.217565	-1.04879	-0.479666	-0.710442	-1.75489	-2.100307	-1.658798
Cgref1	0.265444	0.408886	0.324805	-0.640487	-0.751473	-0.744628	-0.725945	-1.037028	-1.154431	-0.727163	-1.018878	-1.587523	-1.53834	-1.430446
Gpr125	0.205967	0.348962	0.329819	0.008645	-0.032228	-0.011679	0.142044	-0.212247	-0.176627	-0.04973	-0.399736	-0.604126	-0.844898	-0.608792
Znrf2	0.30188	0.246553	0.183927	-0.089468	0.0	-0.347844	-0.113153	-0.549415	-0.466082	-0.231368	-0.350958	-0.674869	-1.072102	-0.594911
2200002K05Rik = Vstm5	0.268738	0.197711	0.217064	-0.048026	-0.160754	-0.207418	-0.019274	-0.048385	0.009376	-0.025253	-0.080699	-0.651528	-0.72404	-0.045365
Cdh9	0.247381	0.276775	0.050746	-0.507651	-0.468973	-0.347373	-0.597068	-0.332868	-0.460444	-0.217811	-0.341706	-0.287621	-0.831385	-0.21255
Scarb1	0.402081	0.151896	0.280933	-0.467136	-0.428497	-0.619148	-0.195913	-0.746132	-0.796649	-0.549139	-0.794502	-1.473269	-1.557993	-1.376694
Dner	0.268522	0.158265	0.322719	-0.630073	-0.461582	-0.496344	-0.478225	-0.4541	-0.686681	-0.525293	-0.664437	-0.846859	-1.208633	-0.969219
Efna3	0.188137	0.196769	0.109059	-0.837137	-0.778442	-0.683032	-0.445693	-0.783973	-1.018769	-0.617961	-0.692031	-0.699743	-1.025715	-0.677402
Kit	0.298512	0.051882	0.231545	-0.46969	-0.657882	-0.392576	-0.468608	-0.81007	-0.365853	-0.450457	-0.599731	-0.62841	-0.990202	-0.62835
Grin3a	0.666346	0.28194	0.266953	-0.054039	-0.189332	-0.037987	-0.266654	-0.458978	-0.521021	-0.163147	-0.518194	-0.458989	-0.768974	-0.399553
Cacna1g	0.558328	0.44057	0.318339	0.418323	0.080563	-0.294885	0.0	-0.994743	-0.322508	-0.338253	-0.283076	-0.64067	-0.608268	-0.381382
Fam189a1	0.424367	0.440104	0.08726	-0.105965	-0.066302	-0.062961	0.0	-0.563188	-0.607547	-0.123082	-0.458664	-0.594097	-1.008378	-0.567322
Igf1	0.97547	1.059695	0.349754	-0.289491	-0.315387	-0.530522	-0.158706	-0.711517	-0.939443	-0.523829	-0.670232	-1.106609	-1.561918	-1.080919
Cbln4	0.785279	0.742102		-0.568204	-0.503599	-0.306573	-0.531762	-0.598402	-0.910646	-0.551339	-0.542956	-0.828536	-1.216325	-0.758856
Pvrl2	0.450786	0.47235	0.269564	-0.471605	-0.864315	-0.979573	-0.506452	-1.426011	-0.594251	-0.968819	-1.26155	-2.009883	-1.980445	-1.95923
Epha4	0.455234	0.312389	0.270276	0.0	0.097421	-0.252931	-0.152408	-0.421742	-0.372477	-0.185034	-0.393818	-0.698762	-1.134233	-0.75132
Nell1	0.512354	0.45806	0.349812	-0.111024	-0.196973	-0.335809	-0.451793	-0.758759	-0.703573	-0.253621	-0.479613	-0.657596	-1.115913	-0.505933
Gng4	0.402782	0.355595	0.552772	-0.518772	-0.79117	-0.729775	-0.505725	-1.357383	-1.098286	-1.07877	-1.24654	-1.779711	-2.113297	-1.520835
Fam20c	0.203084	0.309255	0.463697	-0.058193	-0.122025	-0.182584	-0.053242	-0.259816	-0.111154	-0.172325	-0.384347	-0.493983	-0.668068	-0.387467
Gabra5	0.735033	0.700936	0.851905	-0.324586	-0.372491	-0.361022	-0.603835	-0.747391	-0.893778	-0.616107	-0.828377	-0.556952	-0.645239	-0.301962
Rasgrp2	0.533492	0.624471	0.869657	-0.279122	-0.146289	-0.46619	-0.190907	-0.838843	-0.542	-0.771309	-0.906956	-0.085215	-0.515133	-0.321836
Scn3a	0.314759	0.090447	0.125714	-0.927649	-0.958301	-0.891207	-0.903196	-1.713993	-1.321355	-1.401077	-1.581162	-1.603368	-1.590952	-1.281763
Lphn2 = Adgrl2	0.192325	0.067671	0.348205	-0.662321	-0.891914	-1.019918	-0.420375	-1.206555	-0.938744	-1.046585	-1.293512	-1.299804	-1.223788	-1.102757
Vstm2l	0.124914	0.787247	0.548537	-0.516699	-0.800689	-0.52043	-0.207434	-0.986929	-0.461175	-0.922576	-0.897251	-0.616828	-0.887782	-0.715783
Rgs19	0.848152	1.160649	0.93292	-0.006091	0.030411	-0.113077	0.0	-0.325616	-0.137942	-0.31951	-0.505097	-0.534968	-0.717348	-2.068851
H2-Aa	0.415785		0.161235	-0.490976	0.098213	-0.501784	0.115608		-0.37546	-0.703664	-0.483173	-1.829574	-1.61151	-0.986725
Ajap1	-0.040866	-0.175255	-0.20216	0.046053	-0.088596	-0.084537	0.175928	-0.324133	-0.554933	-0.251024	-0.263915	0.0	-0.698374	-0.215343
BC048546	-1.168652	0.724438	0.773765	-0.170178	-1.20022	0.092897	0.422384		-0.523523	-1.0823	0.0	-1.02961		-1.47352
Cnih3	0.336905	0.152483	0.387762	-0.164429	0.0	0.276173	0.358209	-0.220406	0.141452	0.228122	0.431044	-0.084008	-0.049751	0.376016
Gpr64	0.343804	0.314241	0.084193	0.053419	-0.157713	0.162874	-0.2669	-0.577521	-0.040846	-0.080624	0.021092	-0.474843	-0.212514	0.320951
Ecel1	0.524849	0.514022	0.286213	0.006103	-0.197063	-0.086112	0.020562	-0.300853	-0.124226	0.0	-0.167082	0.147276	-0.417156	0.323904
Btbd11	0.623055	0.430736	0.149236	0.461025	0.227034	-0.18892	-0.045323	-0.121185	-0.351086	0.076384	-0.007739	-0.099283	-0.411842	0.073819
Kcnq5	0.97759	0.816207	0.262584	0.145813	0.324828	-0.027586	0.200001	-0.571655	-0.112931	0.178611	0.0	-0.254476	-1.093877	-0.178184
Adcyap1	0.426132	0.469371	0.375988	0.196208	-0.060466	-0.077073	-0.118372	-0.241159	0.161257	0.0	0.002231	-0.19879	-0.215834	0.012202
Cacng5	0.932268	1.032738	0.727206	0.400032	0.226059	-0.245673	0.126089	-0.545754	-0.335026	-0.173928	0.0	-0.340682	-0.624919	-0.290057
Gpr26	0.391062	0.210182	0.147938	0.262019	0.221605	0.16584	0.113093	-0.344007	-0.127083	0.159191	0.0	-0.112827	-0.157368	0.078953
Gabra4	0.645926	0.54861		0.344786	0.025059	0.376272	0.108576	-0.218408	-0.010757	0.176287	-0.125992	0.076091	-0.078129	0.0
Pcdh20	0.44776	0.414975	0.326929	0.293101	0.247024	0.312605	0.303735	-0.140053	0.162369	0.335371	0.261475	-0.258437	-0.800065	-0.211278
A930038C07Rik = Ndnf	0.532848	0.241605	0.097525	0.280128	-0.14501	0.164895	0.384048	-0.165752	0.258203	0.156257	0.149138	-0.254514	-0.487959	0.0
A730017C20Rik	0.135508	0.241277	0.190242	0.282453	0.136964	0.274544	0.230706	-0.046689	0.05138	-0.086223	-0.111142	-0.603408	-0.688763	-0.162981
Casc4	0.716996	0.489977	0.548084	0.457881	-0.066678	0.0	0.633576	-0.097789	0.3899	0.39381	-0.256304	-0.553449	-0.568062	-0.55139
Atp13a2	0.178128	0.160038	0.457206	0.216029	0.060515	0.097144	0.170103	-0.111993	0.047511	0.015693	0.0	-0.794246	-0.89275	-0.569371
Qpctl	0.347214	0.293668	0.667185	0.304781	0.262659	0.165468	0.564704	-0.068757	0.174297	0.0	-0.03115	-0.364176	-0.574244	-0.335772
Rab6b	0.443057	0.164048	0.552547	0.195869	0.213863	0.08438	0.434993	0.0	0.140032	0.231225	0.147156	-0.362322	-0.478408	-0.116155
Slc24a3	0.632476	0.362774	0.517662	0.201276	-0.016877	0.396027	0.262535	-0.08518	0.0	-0.033818	-0.145281	-0.139712	-0.417607	-0.259364
Prmt8	0.708905	0.51498	0.682862	0.124854	-0.018623	0.131385	0.396614	-0.180422	-0.024247	-0.137056	-0.154702	-0.40517	-0.495767	-0.17663
Oprl1	0.484986	0.32729	0.63814	0.110091	0.103305	0.222007	0.507457	0.08002	0.0	-0.059503	-0.174866	-0.372818	-0.737365	-0.209963
Lhfpl5	0.265781	0.554782	0.553712	0.0	-0.03011	-0.067714	0.251264	-0.083458	0.129482	0.044238	0.101322	-0.17052	-0.581048	-0.177078
Gpx3	0.326176	0.408486	0.387687	-0.132153	-0.201178	0.110666	0.227361	-0.007109	0.0	0.3617	0.158469	-0.366742	-0.498927	0.093633
Cthrc1	1.215194	1.174011	1.581742	-0.146622	0.718961	0.0	-0.046192	0.600711	0.206584	0.539988	0.267665	-1.591126	-0.778864	-1.318473
Syngr3	0.497486	0.559222	0.767683	0.338015	0.510292	0.049938	0.378908	0.0	0.015215	-0.028634	-0.070027	-0.41154	-0.910565	-0.255008
Bgn	0.632977	0.922319	0.560962	0.415389	0.475707	-0.192487	0.44146	0.098479	-0.061128	0.061886	-0.204161	-1.897099	-1.758741	-1.409516
Pde2a	0.163543	0.137544	0.533446	0.10685	0.326879	0.172044	0.469712	0.392459	0.034613	-0.057155	-0.130816	-0.249605	-0.432381	-0.1217
Vstm2a	0.282391	0.0	0.609016	0.134811	0.034571	0.124919	0.503294	0.019011	0.354413	0.094362	-0.138638	-0.40107	-0.591248	-0.079931
Lypd6b	0.83424	0.891967	0.116191	0.0	0.251618	-0.940176	0.055205	-0.522605	-0.044451	-0.081867	0.167117	0.346821	-0.349269	-0.122846
E130311K13Rik	0.18373	0.728506	0.214926	0.133609	0.414441	-0.123993	-0.160615	-0.548278	-0.296318	-0.039281	-0.318991	0.0	-0.196361	-0.131226
Mboat7	0.273293	0.120527	-0.088398	0.092388	-0.120185	-0.214782	-0.064246	-0.116074	0.064802	0.086484	0.0	-0.273699	-0.422243	-0.030981
Kcnip2	0.620636	0.755251	0.412461	0.046659	-0.137503	0.0	0.132428	-0.896826	-0.095976	-0.108809	-0.288271	-0.21927	-0.470181	-0.11788
Fam174b	0.455002	0.531736	0.551604	0.021097	-0.07293	0.0	-0.071784	-0.422589	-0.387329	-0.12466	-0.520237	-0.660581	-0.843734	-0.551041
Gjd2	0.644404	0.69478	0.450246	0.077834	-0.05807	0.163361	0.0	-0.745391	-0.759369	-0.517815	-0.683619	-1.44214	-1.875502	-1.401846
Igfbp3	0.435253	0.597431	0.608815	0.106488	-0.118844	0.51202	0.214948	-0.083473	-0.5324	-0.239845	-0.598345	-1.326558	-1.535895	-1.025079
Lypd1	0.520531	0.458355	0.778253	-0.058421	-0.024249	-0.022316	0.29157	-0.266441	-0.079767	-0.039342	-0.131149	-0.119595	-0.735973	-0.290888
Ifngr2	0.345339	0.399526	0.577227	-0.406494	-0.346707	-0.207534	0.0	-0.48646	-0.486525	-0.248482	-0.580646	-1.251906	-1.580863	-0.991464
Cdh13	0.54368	0.474768	0.817683	-0.332739	-0.457546	-0.464136	-0.050829	-0.684837	-0.855739	-0.716663	-0.887292	-1.213342	-1.449638	-1.004729
Vstm2b	0.664495	0.693499	1.013308	-0.280887	0.0	-0.378434	0.060838	-0.413099	-0.392862	-0.323862	-0.451254	-0.577855	-1.053	-0.71089
Nell2	0.326118	0.088909	0.320295	-0.123465	-0.257729	-0.140539	0.043905	-0.497423	-0.359568	-0.165526	-0.524931	-0.632026	-0.834067	-0.495777
Npnt	0.740029	0.53672		-0.179001	-0.143338	-0.097564	0.004882	-0.961938	-0.909234	-1.091077	-1.027375	-2.097607	-2.096074	-1.883584
Nptx2	0.882082	0.843261	1.210713	-0.236578	-0.410623	-0.139444	0.0	-0.954851	-0.590865	-0.635055	-0.81027	-1.412556	-1.691137	-1.466872
Pcsk5	0.5213	0.426225	0.587081	0.194933	-0.035544	-0.038303	0.07653	-0.667035	-0.50522	-0.272035	-0.61998	-0.751752	-0.855447	-0.758753
Fxyd7	0.601991	0.851591	1.004092	0.0	-0.204122	-0.104083	0.298871	-0.897825	-0.975933	-0.838198	-1.27238	-1.429915	-1.611462	-1.406755
Fam3c	0.481745	0.534802		-0.027083	0.11574	0.022178		-0.231065	-0.956876	-0.266694	-0.627831	-0.935761	-1.039566	-0.776398
Lypd6	0.874913	1.028716	1.156185	-0.174506	0.011527	-0.043833	0.123337	-0.222897	-0.461917	-0.414413	-0.686598	-0.497757	-0.840441	-0.643781
Ptn	0.21067	0.25142	0.445646	0.109598	0.049093	-0.059818	0.259346	-0.308307	-0.195176	-0.356556	-0.516491	-1.935267	-1.838826	-1.692062
Lyz1	1.237145	0.414568	0.310818	-3.342646	-2.041523	-0.057846	0.868766	0.044116	-0.19166		-0.519346	-0.036465	-0.762142	-2.582202
Tmie	0.463164	0.556919	0.251429	-0.361665	-0.02229	-0.31965	-0.320956	-0.370002	0.146972	0.0	0.177423	0.25201	-0.10342	0.263352
Lgals3	0.431089	1.541873	0.748085	-1.212653	0.0	-1.01605	0.014699	-0.134891	0.602084	-0.707362	0.070472	1.152957	-0.295343	-0.720339

Cluster 1 Cluster 2 Cluster 3 Cluster 4

Gene names	IO_set0_P0	IO_set0_E17	IO_set2_E17	IO_set1_E17	IO_set1_P0	IO_set2_P0	IO_set3_E17	IO_set3_P0	IO_set1_P3	IO_set2_P3	IO_set0_P3	IO_set3_P3	IO_set0_P7
S1pr3	-0.220205	-0.009358	0.270449	0.045219	0.019615	-0.19204	0.01724	-0.257536	0.0	-0.364892	0.616249	0.487126	-0.393081
Jakmip1	0.688953	0.066801	0.063146	-0.353899	-0.288566	0.308235	-0.225401	0.314634	0.095363	-0.060675	0.314136	-0.190523	-0.243231
March11	0.185635	0.042391	0.080047	0.093245	-0.412346	0.248426	-0.744971	0.067744	0.0	-0.324834	0.038353	0.29921	-0.237658
Tmem191c	-0.258402	-1.196981	-0.408053	-0.657021	0.0	0.504742	-0.150068	0.437074	0.087117	0.46818	0.235496	0.813731	0.183944
Znrf1	0.058803	0.021404	0.0	-0.287358	0.012995	0.054396	-0.217491	0.132684	-0.007528	-0.138264	0.113621	0.092565	-0.184163
Grid1	0.595791	-0.435677	-0.064731	-0.616169	0.087916	0.313315	-0.381175	0.148545	0.17122	0.0	0.162278	0.185777	0.042983
Sema4a	-0.22785	-0.579569	-0.228017	-0.408931	-0.206135	0.197878	-0.548665	0.266973	0.159345	0.209874	0.015927	0.419596	0.0
Slc10a4	-0.30426	-0.34589	-0.192872	-0.265392	-0.069564	0.279449	-0.048894	0.0	0.204885	0.601741	-0.043029	0.131101	-0.314063
Anxa2	-0.152354	0.135391	0.02024	-0.060187	-0.307783	-0.239019	-0.060297	-0.127346	0.042113	0.410761	0.280964	0.253109	-0.017238
Gpr176	0.704471	0.016242	-0.120792	-0.447657	-0.697819	-0.044089	-0.738383	-0.212896	0.0	-0.24517	0.229675	0.157954	0.337103
Gp1bb	0.721201	-0.324878	0.026445	-0.561225	-0.58727	0.350265	-0.924392	0.065601	0.132358	-0.229459	0.0	0.237141	0.243166
Gpr45	0.48554	-0.122191	0.081686	-0.371877	-0.44828	0.319149	-0.522408	-0.014658	-0.192969	-0.478761	0.141684	0.186881	0.140189
Ctxn2	0.936939	-0.316831	-0.10573	-0.888036	-0.161331	-0.242661	-0.362198	-0.080699	-0.225213	0.0	0.468303	0.658802	0.134938
Dos	0.286821	-0.586114	-0.616607	-0.530687	-0.26462	0.023621	-0.747209	-0.12417	-0.09987	0.035805	0.0	0.597704	0.210196
Crtap	0.279755	-0.69663	-0.58858	-0.697323	-0.387869	-0.312253	-0.372428	-0.10377	-0.006811	0.326235	0.189716	0.060565	0.128422
Chid1	0.242231	-0.516799	-0.351951	-0.376495	-0.374817	-0.236676	-0.501269	-0.476713	0.055962	0.205432	-0.077099	0.027513	0.074486
Gabrg1	0.210724	-0.395563	-0.445324	-0.692164	-0.469269	-0.15297	-0.637135	-0.168175	-0.03993	0.091536	0.107934	0.049259	0.227829
Fam19a1	0.253241	-0.291736	-0.322633	-0.653982	-0.580124	-0.04454	-0.840301	-0.135261	-0.072987	-0.1167	0.006512	0.119926	0.312101
Kcnq2	0.355567	-0.324646	-0.253143	-0.731924	-0.652807	0.062885	-0.622864	-0.011027	-0.039213	-0.154826	-0.18175	0.247151	-0.126808
Emb = Pou6f1	0.448555	-0.3024	-0.238226	-0.503206	-0.039864	0.152939	-0.606058	-0.166958	-0.12706	-0.162158	0.0	0.228047	-0.009536
Evc2	0.406842	-0.768101	-0.486492	-0.706177	-0.731922	-0.292531	-0.755763	-0.506736	-0.091926	0.183931	-0.131111	-0.026192	-0.028127
Copz2	0.325626	-0.391218	-0.381458	-0.779026	-0.887842	-0.652933	-0.388485	-0.34286	-0.178173	-0.313373	0.0	-0.168764	0.067768
Gpr88	-0.191781	-0.22926	-0.629052	-0.808198	-0.646943	-0.609883	-1.009099	-0.71947	-0.541836	0.0	0.117641	-0.153156	0.441817
Htr5b	-0.7132	-1.537	-1.441055	-1.353326	-0.883359	-1.090915	-2.130979	-1.354994	-0.99985	-0.273509	0.0	-0.168251	0.692679
Kcng1	-0.707045	-1.56216	-1.886104	-1.824204	-1.87071	-1.909154	-2.211701	-1.918213	-1.223416	-1.243223	-0.753174	-0.588932	0.457554
S100a10	-0.197558	-0.23308	-0.337104	-0.202193	-0.064768	0.0	-1.20637	-0.237316	-0.322039	-0.365539	0.067123	0.102609	0.415244
Nrcam	-0.170975	-0.468941	-0.512339	-0.366514	-0.042164	-0.245967	-0.554974	-0.532096	-0.053014	0.164263	0.14507	-0.090574	0.197559
asap1	-0.110442	-0.304353	-0.545846	-0.458769	-0.284229	-0.103267	-0.997988	-0.311028	-0.151696	-0.132708	0.0	0.039877	0.232465
Lcn2	0.0	-1.762553	-1.515891	-1.554607	-0.701999	-1.150755	-0.842262	0.19389	-1.866172	-1.905914	-1.262098	-0.487018	0.532419
S100a6	-0.705534	-2.199091	-1.685279	-1.672836	-1.308905	-0.736461	-1.655607	-0.226865	-0.316315	0.0	-0.041626	-0.212697	1.136989
S100a4	-0.696693	-2.539343	-2.302221	-2.429536	-1.799532	-1.18806	-2.311942	-0.905477	-0.99295	-0.442407	0.184332	0.0	1.593069
Tnfrsf21	-0.380973	-0.441196	-0.476174	-0.543111	-0.441494	-0.17501	-0.899245	-0.352195	-0.129806	-0.117911	-0.144865	0.045262	0.0
Gm4980	-0.580136	-1.21213	-1.275729	-1.143552	-1.126786	-0.718022	-1.925966	-1.205367	-0.238603	-0.225959	-0.233605	-0.451803	0.538662
Dusp15	-0.70403	-1.283096	-0.783072	-0.972876	-0.764238	-0.239267	-0.954832	-0.261392	-0.213707	0.0	-0.107903	-0.027968	0.551806
0610007L01Rik = Tmem248	-0.50068	-0.546763	-0.504538	-0.546969	-0.284719	-0.120263	-0.774286	-0.476673	-0.088575	0.011502	-0.213872	-0.167594	0.0
Ptprn	-0.262963	-1.080142	-0.900457	-1.023924	-0.577727	-0.195297	-1.591536	-0.351685	-0.19629	-0.216083	-0.067963	-0.002719	0.251142
Tmem205	-0.842455	-1.067739	-0.849135	-0.93682	-1.232232	-0.694954	-1.481789	-0.622708	-0.353482	-0.319825	-0.48591	-0.110264	0.0
Il10rb	-0.563694	-0.648334	-0.529112	-0.582896	-0.680832	-0.299875	-0.730896	-0.22934	-0.421754	-0.184579	-0.079621	0.0	-0.053064
Ctgf	-0.301124	-1.239295	-1.436576	-1.340768	-0.69461	0.075336	-1.514871	0.416997	-0.338554	-0.313531	-0.69478	-0.425621	0.071341
Gpr123	-0.574261	-0.986317	-1.245005	-1.228606	-0.703382	-0.7101	-1.616019	-1.050628	0.459045	-0.152936	-0.226387	-0.293833	0.023034
Ppap2c	-0.255013	-0.188681	-0.294934	-0.237109	-0.428298	-0.097996	-0.480686	-0.424699	-0.100044	-0.145641	-0.073722	0.046045	0.205711
Lpl	0.0	-0.889113	-0.972834	-0.923757	-1.004864	-0.5784	-0.736638	-0.940979	-0.509893	-0.070854	-0.337732	-0.337251	0.030373
Itm2a	-0.143212	-0.856344	-0.733016	-0.842653	-1.117776	-0.337933	-0.692255	-0.422129	-0.514858	-0.121044	-0.153852	-0.297689	0.062474
Fuca2	-0.035473	-0.985341	-0.807611	-0.854744	-0.798152	-0.568092	-1.065996	-0.705747	-0.428628	-0.22633	-0.18873	-0.14048	0.005725
Zdhhc22	-0.677932	-0.957383	-1.041997	-1.047768	-0.712607	-0.591586	-1.037383	-0.702409	-0.470767	-0.283486	-0.203332	-0.251121	0.0
Tmem180	-0.65685	-0.921936	-0.8262	-0.932636	-0.599278	-0.423089	-0.759943	-0.669234	-0.329616	-0.279475	-0.185593	-0.103985	0.0
Tmem204	-0.791286	-1.030453	-0.901043	-1.020853	-0.735567	-0.371142	-1.228569	-0.629931	-0.466205	-0.342582	-0.318177	-0.515847	0.0
Ninj1	-0.653194	-1.171992	-1.184289	-1.0609	-0.769137	-0.506311	-0.992258	-0.796245	-0.477109	-0.064364	-0.08865	-0.453776	0.461871
Shisa4	-0.803502	-1.254248	-1.020713	-0.884909	-0.624944	-0.380244	-0.837957	-0.637563	-0.310974	0.0	-0.22759	-0.03185	0.284614
Tmem19	-0.479939	-0.563695	-0.633653	-0.836421	-0.476984	-0.249072	-0.697447	-0.511493	-0.323781	-0.015478	-0.107254	-0.200533	0.102105
Tm6sf1	-0.684396	-1.171498	-1.295796	-1.22219	-0.960796	-0.882507	-1.293152	-0.775673	-0.366973	-0.21162	-0.144628	-0.17443	0.042005
Ache	-0.381488	-1.135827	-1.140926	-0.947238	-0.391906	-0.247247	-1.281666	-0.60998	-0.046276	-0.097269	-0.050252	0.0	0.340473
Acsl5	-0.285813	-0.535762	-0.552753	-0.361508	-0.3996	-0.202954	-0.697172	-0.437471	-0.225307	0.036481	0.0	-0.19028	0.037742
Crtac1	-0.526651	-0.769064	-0.658892	-0.75098	-0.413547	-0.309891	-1.020601	-0.589017	-0.272675	0.252772	0.0	-0.190594	0.328646
Tgfbr2	-0.577774	-0.861363	-0.626414	-1.103298	-1.130808	-0.785103	-0.717388	-0.316981	-0.402079	0.0	-0.070631	-0.145907	0.226125
Resp18	-0.690534	-1.103792	-1.285961	-1.048778	-0.87679	-0.563316	-1.15939	-0.875164	-0.618661	-0.275622	-0.056508	-0.324791	0.143575
C1ql1	-1.097677	-1.510982	-1.587872	-1.546182	-1.360007	-0.900481	-1.669508	-1.238801	-0.41641	0.0	-0.113187	-0.185555	0.732899
C1ql1	-1.172218	-1.381275	-1.842103	-1.73949	-1.240936	-0.837858	-1.74107	-1.269405	-0.169293	0.0	-0.109563	-0.462763	0.697164
C1ql1	-0.602617	-1.353602	-1.767381	-1.825128	-1.348166	-1.302654	-2.02651	-1.238938	-0.445918	-0.002245	-0.113408	-0.567938	0.669192
C1ql1	-1.145289	-1.399986	-1.787702	-1.91365	-1.222702	-1.055617	-1.763434	-1.351597	-0.474489	-0.102671	-0.19931	-0.411743	0.745462
Cx3cl1	-0.694613	-1.201763	-1.169904	-0.992307	-0.660862	-0.656411	-1.416089	-0.892366	-0.276751	-0.011826	-0.213204	-0.142639	0.201935
Tspan12	-0.649822	-0.968795	-0.747894	-0.465275	-0.784031	-0.564176	-0.970633	-0.801487	-0.438124	0.048601	-0.161988	-0.041455	0.336201
Susd4	-0.289327	-0.790537	-0.575969	-0.774883	-0.448478	-0.317071	-1.173168	-0.52399	-0.141052	-0.202032	0.095393	-0.038024	0.362056
Kcna6	0.052781	-0.890985	-0.828543	-0.973627	-0.595046	-0.435989	-1.294959	-0.666792	-0.212564	-0.065017	-0.161341	-0.017199	0.118143
Egfl7	-0.730169	-1.150146	-0.719994	-1.279539	-0.863332	-0.438571	-1.198915	-0.49414	-0.532313	-0.711345	-0.029566	-0.190028	0.065699
Gal	-0.215249	-0.334144	-0.812206	-0.591486	-0.444437	-0.041034	-1.560029	-0.541944	-0.43314	0.058613	-0.020856	0.0	0.412433
Cartpt	-0.309979	-0.314239	-0.46229	-0.451781	-0.534326	-0.003148	-0.870584	-0.288415	-0.330771	0.038906	-0.203546	0.111159	0.405635
Cntnap2	-0.110158	-0.492203	-0.731675	-0.455472	-0.003132	-0.153677	-0.811239	-0.209606	-0.016886	0.0	0.163674	-0.026594	-0.016097
2010011I20Rik = fam210b	0.0	-0.71935	-0.157839	-0.992803	-0.386481	0.131252	-1.080614	-0.164679	0.031548	-0.451479	-0.202985	-0.381951	-0.186512
Sema4f	-0.063229	-0.001434	-0.055029	-0.144339	-0.224917	0.009984	-0.45894	-0.235776	-0.11521	-0.27343	0.00694	-0.159783	0.0
Nrsn2	-0.689904	-0.53075	-1.273213	-0.628422	-0.906047	-0.548907	-1.362483	-0.612706	-0.581845	-0.070889	0.08378	-0.062594	-0.197868
Thy1	-1.452138	-2.439976	-2.56535	-1.957687	-1.692905	-1.255287	-2.970339	-1.384837	-0.854086	-0.574871	-0.553947	-0.469536	0.123197
Adam23	-0.655016	-1.180405	-1.248768	-1.082826	-0.753056	-0.548627	-1.430379	-0.677893	-0.546039	-0.531614	-0.247274	-0.294866	0.044408
Amhr2	-2.374182	-2.269338		-1.884828	-3.503268	-2.019174	-2.005525			-2.165586	-1.719948	-1.915777	-1.864277
CxCl12	-0.953494	-1.043199	-0.76731	-0.730662	-1.687545	-0.736189	-0.669457	-0.374104	-0.875407	-0.442416	-0.409728	-0.559228	-0.068438
Slc20a1	-0.549102	-0.534395	-0.415267	-0.48595	-0.418448	-0.069485	-0.286346	-0.365293	-0.563346	-0.173293	-0.267972	-0.158012	-0.205161
Spns2	-0.595729	-0.767982	-0.657922	-0.710344	-0.627852	-0.226382	-0.51195	-0.142616	-0.434811	-0.072206	-0.214297	-0.328669	-0.011921
Sytl2	-1.371138	-1.892094	-1.438565	-1.607296	-1.432996	-0.741141	-1.433789	-0.773523	-0.948256	-0.692106	-0.777252	-0.683082	-0.267979
Fstl1	-0.890367	-0.921869	-1.109552	-0.967898	-1.00267	-0.719564	-1.05499	-0.566465	-0.672775	-0.242848	-0.337795	-0.579735	-0.094387
Adam11	-0.825205	-1.227874	-0.86154	-0.921524	-1.096867	-0.416695	-0.552097	-0.525849	-0.489931	-0.291532	-0.164247	-0.108188	-0.139206
Srgn	-1.07807	-1.228005	-1.01587	-1.508113	-1.661326	-0.593092	-0.839119	-0.475404	-0.955132	-0.411113	-0.135586	-0.475621	-0.209719
Slc4a2	-1.195251	-1.359823	-1.124222	-1.449099	-1.228954	-0.935154	-0.996214	-1.162073	-0.963472	-0.615071	-0.604966	-0.41849	-0.199526
Mrvi1	-0.846716	-0.642424	-0.928203	-0.960755	-1.262274	-1.367703	-0.926175	-0.035934	-0.748433	-1.235607	-0.759706	-1.018962	-0.391229
Mgp	-2.226752	-2.50569	-2.837415	-2.920168	-3.260954	-2.322209	-1.72631	1.05031	-2.116165	0.0	-0.876975	-1.541856	-0.444038
Kcnh2	-0.236763	-0.900711	-0.898282	-1.137411	-0.802902	-0.584075	-1.214635	-0.717885	-0.464451	-0.37038	-0.392737	-0.298745	-0.222396
Dnajc15	0.0	-0.541969	-0.700763	-0.696193	-0.775026	-0.667738	-0.906276	-0.781242	-0.469029		-0.202177	-0.417796	-0.106872
Tmem14a	-0.756172	-1.37888	-1.058269	-1.532001	-0.984693	-0.704171	-0.946719	-0.975739	-0.547277	-0.267612	-0.230809	-0.927677	0.0
Rell2	-0.531146	-0.913555	-1.024791	-0.942405	-0.660792	-0.325246	-0.504896	-0.621434	-0.541318	-0.183138	-0.161983	-0.189227	-6.34E-4
Pmepa1	-0.812032	-0.425343	-1.385481	-1.089412	-0.802733	-0.707318	-1.217539	-1.172328	-0.932892	-0.495304	-0.288517	-0.664539	-0.139297
Npc2	-0.893729	-0.753923	-1.209271	-0.927969	-0.969123	-0.819712	-0.807734	-1.009428	-1.021798	-0.489855	-0.409117	-0.579003	-0.058438
Atp1b1	-0.863722	-1.406587	-1.434219	-1.407716	-0.885792	-0.782219	-1.566336	-1.090972	-0.585187	-0.192716	-0.246379	-0.247674	-0.03031
Tmem184b	-0.574787	-0.711342	-0.625283	-0.870346	-0.572281	-0.240154	-0.575351	-0.347883	-0.550299	-0.384635	-0.194062	-0.231033	-0.116092
Rab7l1 = Rab29	-1.084809	-1.487784	-1.587483	-1.580514	-1.107401	-1.039981	-1.188965	-0.981361	-1.018343	-0.923653	-0.449954	-0.663479	-0.076578
Smpdl3a	-0.522225	-0.530732	-0.698875	-0.434052	-0.522043	-0.385909	-0.49873	-0.529449	-0.396934	-0.020883	-0.257096	-0.093096	-0.037351
Serpinf1	-1.61394	-2.498944	-2.718329	-2.718384	-1.831021	-1.446575	-2.014817	-1.036358	-0.975086	-0.181565	-0.357024	-0.643409	0.110832
Timp2	-0.519522	-0.921181	-0.977303	-1.175621	-0.478539	-0.363751	-1.009366	-0.48085	-0.313177	-0.063478	-0.178683	-0.323943	0.0
H2-T10 /// H2-T22 /// H2-T9	-0.243711	-1.694156	-1.568825	-1.793559	-2.03816	-1.85625	-2.13539	-1.769025	-0.127679	-0.141898	0.0	0.452381	-0.477555

	Cluster 1	Cluster 2	Cluster 3	Cluster 4

Gene names	IO_set1_P7	IO_set3_P7	IO_set2_P7	IO_set1_P14	IO_set3_P14	IO_set0_P14	IO_set2_P14	IO_set0_P21	IO_set2_P21	IO_set1_P21	IO_set3_P21	IO_set1_Adult	IO_set0_Adult	IO_set3_Adult
S1pr3	0.528861	0.761124	0.430702	1.129539	0.687767	-1.032792	-0.754082	-1.300515	-0.51328	-0.383793	-0.621282	-0.763274	0.349603	0.019389
Jakmip1	0.413315	0.524912	0.070203	0.562486	0.271952	-0.46943	0.0	-0.24151	-0.260646	0.143898	-0.205761	-0.515054	-0.426142	-0.164274
March11	-0.029251	0.127844	-0.139178	0.177668	0.106715	-0.751949	-0.554371	-0.251541	-0.662504	0.064691	0.011365	-0.945452	-0.887983	-0.212866
Tmem191c	0.482151	0.795886	0.620294	0.098034	0.002109	-0.354371	0.184427	-0.522872	-0.330123	-0.377847	-0.310739	-0.148815	-0.354865	-0.125949
Znrf1	0.021046	0.168325	0.147363	0.096945	0.283234	-0.20935	0.137095	-0.336936	-0.36459	-0.241857	-0.237566	-0.839164	-1.253935	-0.834436
Grid1	0.155083	0.282187	0.193961	0.313186	0.499475	-0.102582	-0.377626	-0.458068	-1.246134	-0.123527	-0.251503	-0.612544	-0.593357	-0.678722
Sema4a	0.127278	0.28652	0.406334	0.44823	0.326924	-0.073806	0.303215	-0.287038	-0.191441	0.156174	-0.152932	-0.559829	-0.967792	-0.388764
Slc10a4	-0.131221	0.149095	0.487916	0.521756	0.484329	0.04791	0.687711	0.105372	0.012532	0.09301	-0.518017	-0.924048	-1.145201	-0.630089
Anxa2	0.173507	0.387651	0.179478	0.2753	0.096833	-0.133844	0.213306	0.0	-0.040561	0.159599	-0.216985	-0.893114	-1.23699	-0.653977
Gpr176	0.467387	0.562577	0.193	0.369789	0.552334	0.43615	0.525245	-0.111292	-0.101285	0.217564	-0.06755	-0.544316	-1.093666	-0.594706
Gp1bb	0.09005	0.524198	-0.001423	0.43001	0.520304	0.292667	0.260723	-0.895444	-0.90242	-0.730151	-0.728705	-2.052865	-2.815216	-2.282988
Gpr45	0.0	0.383454	-0.124996	0.141312	0.193513	0.156703	0.187839	-0.202765	-0.264618	0.199374	-0.150852	-0.200758	-0.502792	0.004183
Ctxn2	0.002988	0.935652	1.03727	0.455572	0.17087	0.380075	0.236092	0.432499	-0.464661	-0.070205	-0.27714	-0.759311	-0.307252	0.022129
Dos	0.228707	0.33546	0.300784	0.557869	0.237785	0.367605	0.683323	-0.056312	-0.018421	0.094508	-0.207795	-0.446129	-0.892123	-0.395878
Crtap	0.297887	0.57796	0.558258	0.286716	0.311263	0.138351	0.5192	0.051258	-0.143372	0.0	-0.31339	-0.700606	-0.804939	-0.586882
Chid1	0.138629	0.267914	0.336191	0.248328	0.207425	0.032932	0.48115	0.0	-0.053623	0.01834	-0.293219	-0.505521	-0.642692	-0.40845
Gabrg1	0.305473	0.465396	0.455669	0.117866	0.248492	0.247115	0.492667	-0.111378	-0.031536	0.0	-0.244406	-0.223091	-0.354689	0.002038
Fam19a1	0.322509	0.464129	0.339089	0.203564	0.625952	0.353819	0.126478	0.0	-0.220645	0.036883	-0.092968	-0.311887	-0.425135	0.010969
Kcnq2	0.0	0.281596	0.155118	0.204909	0.367799	-0.072403	0.203274	0.031342	-0.285558	0.23398	0.131811	0.071027	-0.135516	0.162272
Emb = Pou6f1	0.212348	0.171073	0.437142	0.378272	0.174292	0.11007	0.110828	-0.083548	-0.493743	0.17697	-0.166607	0.038617	-0.181106	0.045821
Evc2	0.083394	0.144428	0.183833	0.362134	0.0	-0.024567	0.18408	-0.386039	0.16286	0.231023	0.219683	0.497693	0.266193	0.38258
Copz2	0.08268	0.296572	0.111379	0.053894	-0.162218	-0.289923	0.129852	0.366859	0.118972	0.122213	-0.157453	0.116708	0.00297	0.060865
Gpr88	0.179376	-0.196268	-0.880759	0.236767	0.027788	0.517894	0.28832	0.035823	0.764082	0.592458	0.676409	-0.385352	0.181216	0.584462
Htr5b	0.103922	-0.010117	-0.592272	0.762978	0.969651	1.24606	1.285921	0.41402	1.434454	1.520796	1.439314	0.676847	0.790734	1.692324
Kcng1	0.074807	0.096981	-1.264144	0.936545	0.802232	0.815096	0.76074	0.0	0.914643	0.922687	1.238844	0.71606	0.365996	1.063367
S100a10	0.253271	0.058888	-0.304427	0.323953	0.544761	0.440004	0.297462	0.430298	-0.078167	0.788843	0.19519	-0.163629	-1.317624	0.581982
Nrcam	0.278077	-0.090954	-0.238278	0.420216	0.127344	0.231147	0.240052	0.283175	0.0	0.713822	0.150173	0.190424	-0.284077	0.272577
asap1	0.312738	0.085685	-0.163423	0.613956	0.302257	0.379198	0.291679	0.48885	0.305442	0.534155	0.382009	-0.067514	-0.099946	0.178521
Lcn2	-0.056805	0.005445	-1.838709	0.40987	0.713177	0.834577	0.823231	0.642151	0.42647	1.368606	0.787587	0.792019	-0.986031	0.00928
S100a6	-0.200722	0.245255	-0.335936	1.200183	1.455997	1.117287	1.312908	1.423697	1.141044	1.182021	1.122446	0.819356	0.138726	1.026661
S100a4	-0.323029	0.288374	-0.242852	0.967415	0.945102	1.185612	1.128952	1.05321	0.219906	0.275794	0.516561	0.21735	-0.328009	0.091388
Tnfrsf21	0.284097	0.035222	-0.02094	0.501917	0.636529	0.448133	0.623921	0.416714	0.152046	0.484899	0.235129	0.024594	-0.702738	0.24133
Gm4980	0.657066	0.717943	0.181784	1.696698	1.619457	1.421511	1.609682	0.568118	0.396411	1.080208	0.744532	0.0	-0.702764	0.314308
Dusp15	0.677258	0.75098	0.735549	1.530893	1.57742	1.169297	1.568392	1.081199	0.634597	1.034024	0.930869	-0.092581	-0.260181	0.241983
0610007L01Rik = Tmem248	0.049571	0.186974	0.009005	0.58898	0.447205	0.533358	0.527148	0.41247	0.425064	0.41231	0.33025	-0.032874	-0.278289	0.154399
Ptprn	0.234326	0.280305	-0.123887	0.689346	0.740152	0.666658	0.442993	0.704314	0.248578	1.015064	0.720122	0.686903	0.0	0.480132
Tmem205	0.097461	0.106587	0.081637	0.753763	0.756804	0.317024	0.571167	0.491952	0.864304	0.880154	0.713759	0.238444	-0.360635	0.231695
Il10rb	0.084729	0.269266	0.136438	0.591985	0.586656	0.205039	0.549547	0.355817	0.38371	0.635661	0.476457	0.144241	-0.147018	0.32205
Ctgf	-0.219445	0.423142	-0.185699	0.433181	0.764754	1.323698	0.936506	1.224283	0.698329	0.850591	0.249187	-0.003481	0.0	0.134361
Gpr123	0.198515	0.114955	0.158277	0.462678	0.494734	0.410167	0.634459	0.320771	0.48155	0.514039	0.237352	-0.024994	-0.27649	0.0
Ppap2c	0.125699	0.352252	0.37751	0.516575	1.05861	0.586157	0.960029	0.689011	0.469369	0.300196	0.547041	-0.188642	-0.203729	0.0
Lpl	0.06057	0.0135	0.183226	0.553813	1.147921	0.417503	1.196701	0.272957	1.001455	0.453883	0.15367	-0.220672	-0.041231	0.080292
Itm2a	0.190968	0.390513	0.332682	0.678409	0.59439	0.620984	1.083079	0.82681	0.513204	0.688865	0.49752	0.0	-0.295628	0.392717
Fuca2	0.0	0.125285	0.18457	0.542896	0.559061	0.384716	0.669649	0.432985	0.307883	0.566996	0.350599	0.009994	-0.04114	0.20558
Zdhhc22	0.315934	0.4452	0.511598	0.885186	0.95375	0.858317	1.092548	0.458347	0.790057	0.752372	0.795163	0.151142	-0.254928	0.160563
Tmem180	0.340848	0.455302	0.395428	0.975109	1.04642	0.615547	1.153861	0.698084	0.828412	0.910251	0.815503	0.116088	-0.308066	0.238545
Tmem204	0.123224	0.254135	0.189185	1.255497	1.223662	1.206017	1.61029	1.075858	1.273644	0.96761	1.004532	0.002725	-0.041775	0.167833
Ninj1	0.648115	0.546016	0.740411	1.654346	1.435564	1.478398	1.560063	0.914017	0.943706	0.801219	0.656369	0.0	-0.135267	0.133432
Shisa4	0.445947	0.495292	0.826545	1.618273	1.867748	1.272965	2.017575	1.39159	1.618819	1.395391	1.278685	-0.080168	-0.12881	0.07906
Tmem19	0.30073	0.329345	0.459282	0.950183	0.991877	0.98552	1.20009	0.788055	1.020155	0.782288	0.765797	0.0	-0.386468	0.187869
Tm6sf1	0.335005	0.446114	0.276629	0.734752	0.909173	0.535089	0.93541	0.316193	0.585855	0.76162	0.696908	0.0	-0.40623	0.294352
Ache	0.410028	0.386966	0.39237	0.664109	0.557849	0.511014	0.958719	0.374489	0.581815	0.677199	0.606948	-0.07373	-0.312762	0.35182
Acsl5	0.047136	-0.037257	0.075157	0.104404	0.219485	0.105086	0.201324	0.139119	0.089084	0.26728	0.048369	-0.091477	-0.502028	0.035438
Crtac1	0.289122	0.327396	0.554056	0.590592	0.692779	0.456637	0.820601	0.633066	0.634346	0.482652	0.254539	-0.086765	-0.234137	-0.045365
Tgfbr2	-0.040164	0.125175	0.286479	0.935789	1.052914	0.29693	1.256761	0.542844	0.655925	0.794896	0.870045	0.145648	-0.132289	0.042845
Resp18	0.068573	-0.018682	0.363517	0.361919	0.439305	0.304819	0.573061	0.471027	0.314186	0.694172	0.215222	0.162697	0.0	0.061749
C1ql1	0.327983	0.290679	0.061542	0.515676	0.561755	0.678034	0.955164	0.171316	0.324112	0.602646	0.507581	-0.355227	-0.067353	0.195663
C1ql1	0.5656	0.468647	0.183975	0.900009	0.668206	0.702184	1.080127	0.086956	0.969136	0.585414	0.626049	-0.513213	-0.045474	0.366073
C1ql1	0.349386	0.496714	0.117147	0.831149	0.673397	0.675109	0.884977	0.006442	0.447342	0.555431	0.321495	-0.222173	0.0	0.114146
C1ql1	0.391269	0.34488	0.477757	0.9583	0.71765	0.843994	1.01099	0.021966	1.030126	0.632684	0.452847	-0.271553	0.0	0.720311
Cx3cl1	0.523082	0.095274	0.289703	0.434316	0.350387	0.555552	0.548367	0.238143	0.435745	0.553627	0.371845	0.163948	-0.356774	0.0
Tspan12	0.441762	0.200762	0.38779	0.26024	0.28539	0.563526	0.712891	0.42882	0.605634	0.532319	0.239193	-0.096629	-0.339159	0.0
Susd4	0.119747	0.131838	0.094214	0.244136	0.742784	0.0	0.30969	-0.128166	0.119207	0.466606	0.319899	0.028348	-0.403445	0.213353
Kcna6	0.231164	0.213886	0.176793	0.30573	0.288674	0.088562	0.128824	0.184643	0.0	0.41783	0.286234	-0.007264	-0.226455	0.178683
Egfl7	0.083645	0.520013	0.246332	0.530568	0.728358	0.071047	0.339355	0.0	0.245691	0.683202	0.539311	0.467046	-0.354489	0.439946
Gal	0.017553	0.053524	-0.165049	0.188874	0.058487	0.132582	0.00867	0.191628	-0.020229	0.340076	0.232424	0.64179	-0.167844	0.555859
Cartpt	0.240234	0.282222	0.0	0.129327	-0.27627	-0.223031	0.044448	0.102167	0.577326	0.463389	0.614288	0.200845	-0.007064	0.433513
Cntnap2	0.434394	-0.03188	0.019859	0.301015	0.189749	0.354689	0.189155	0.275414	-0.062517	0.3686	0.04205	0.318032	0.011395	0.368639
2010011I20Rik = fam210b	0.24954	-0.01751	0.361334	0.65139	0.681245	0.304964	0.478883	0.500395	0.874121	0.579842	0.669822	-0.092201	-0.146813	0.219166
Sema4f	0.019081	-0.068358	-0.062857	1.033986	0.957647	0.734927	0.809304	0.828736	0.977706	1.062803	0.951923	0.468737	-0.073584	0.615183
Nrsn2	0.0	0.243817	-0.095676	0.634094	0.522603	0.560495	0.76457	0.629784	0.901359	1.000034	0.784842	0.307828	0.367818	0.480297
Thy1	0.0	0.181003	-0.309781	0.780025	0.823373	0.948456	0.930113	0.76064	0.921719	0.91546	0.832412	0.560888	1.135449	0.76161
Adam23	0.157289	0.0	-0.229544	1.342153	1.336233	1.379107	1.42052	1.33873	1.12559	1.397635	1.188957	0.666153	0.345821	0.673684
Amhr2	-1.25668	0.414066	-0.132605	2.256313	1.92139	1.505304	1.94067	1.077218	1.400907	1.672926	1.599538	0.132605	0.805657	0.949417
CxCl12	0.388762	0.191721	0.0	1.184124	1.239805	0.875594	1.289738	1.112531	0.470562	0.963166	1.218589	0.408723	0.162822	0.353002
Slc20a1	0.015194	0.0	0.221121	1.452666	1.482629	1.339204	1.643497	1.516849	1.626468	1.529885	1.478489	0.92632	0.919181	1.256732
Spns2	0.0	0.209183	0.47832	1.206908	1.241946	0.866277	1.298942	1.125446	0.905762	0.954869	0.783856	0.404532	0.408556	0.630717
Sytl2	0.0	0.160821	0.162508	1.565454	1.722351	1.323253	1.667382	1.259471	1.634456	1.634717	1.436159	0.955546	0.555943	1.16418
Fstl1	0.0	0.113164	0.077102	0.971802	1.012393	1.025849	1.230167	1.210405	0.681583	1.011627	0.612306	0.238533	0.395968	0.368553
Adam11	0.0	0.217984	0.04003	0.836806	0.93904	0.5665	0.86636	0.719156	0.598847	0.959864	0.741615	0.239493	0.070485	0.173043
Srgn	0.087646	0.211179	0.0	0.808531	0.915455	0.373945	1.200705	0.764905	1.002438	1.13973	0.834276	0.648755	0.240245	0.810479
Slc4a2	0.0	0.055686	0.253403	1.308021	1.482358	1.249266	1.666112	1.485373	1.821631	1.556244	1.755083	0.669231	0.698317	0.806605
Mrvi1	0.0	0.401447	0.104953	1.540925	1.401039	1.978129	1.400181	1.263219	1.478754	2.345383	0.747176	1.111396	1.035955	1.16113
Mgp	-0.153565	0.677699	-0.105632	2.251028	2.051269	2.169847	2.340515	2.710426	2.38839	2.289511	2.028365	1.404268	1.538893	1.927239
Kcnh2	0.0	0.103116	0.026495	0.868151	0.764955	0.747471	1.008248	1.182717	0.77245	0.982205	0.841968	0.713596	0.491368	0.893066
Dnajc15			0.076799	0.635083	0.53477	0.611745	0.781619	0.803593		0.74637	0.547468	0.458515	0.302101	0.701149
Tmem14a	-0.443164	0.082766	0.026459	0.889699	0.872173	0.843731	1.065351	0.928464	0.681176	0.613421	0.092411	0.875831	0.5161	1.107705
Rell2	0.0	0.338139	0.326872	0.575089	0.657578	0.38199	0.74982	0.674834	0.678926	0.485729	0.250138	0.197025	0.119101	0.882332
Pmepa1	0.064023	0.175774	0.493742	1.188099	1.169922	1.357152	1.343901	0.981333	0.998507	0.928536	0.90741	0.105722	0.0	0.282399
Npc2	0.0	0.1443	0.32505	1.115331	1.047731	1.121437	1.375385	1.294105	1.362203	1.186248	0.967629	0.067797	5.97E-4	0.277786
Atp1b1	0.0	0.052227	0.326509	0.804313	0.657465	0.796831	0.909355	0.909353	0.881489	0.839868	0.762826	0.232429	0.00876	0.468061
Tmem184b	0.0	0.134435	0.176016	0.617868	0.614349	0.505017	0.905988	0.615488	0.701562	0.849432	0.484259	0.328769	0.032662	0.529578
Rab7l1 = Rab29	0.175037	0.0	0.638453	0.901872	0.75817	0.80989	1.108643	1.024219	1.174653	1.221741	0.997414	0.457806	0.17131	0.57576
Smpdl3a	0.0	0.089661	0.308542	0.538333	0.615188	0.561915	0.946059	0.682532	0.909091	0.683307	0.580463	0.10963	0.028916	0.300639
Serpinf1	0.0	0.315152	0.332451	1.05314	1.0832	1.049421	1.535975	1.351994	1.113986	0.911908	0.829876	0.413019	-0.04967	0.285434
Timp2	0.091469	0.070128	0.223665	0.238766	0.122315	0.14767	0.431923	0.177644	0.40409	0.231771	0.258085	0.219372	-0.172911	0.405892
H2-T10 /// H2-T22 /// H2-T9	0.468634	-0.004167	-0.354596	0.885425	0.747622	0.107382	1.082335	1.653953	2.023798	1.001319	2.14739	0.992173	0.656259	1.99609
Ier3	-0.034526	0.448605	-0.088307	0.599779	0.78363	0.563867	0.50863	0.780914	0.478013	0.773309	0.630872	0.561383	0.221451	0.767513
Popdc3	-0.161745	-0.344411	-0.188733	0.538979	0.314448	0.548583	0.966974	1.026782	1.003781	1.042033	0.869685	0.400516	0.34323	0.629582
Pex5l	0.063615	0.0	-0.168998	2.083772	1.840867	1.805241	2.161207	2.509368	2.816101	2.548937	2.6641	2.442917	2.283643	2.781434

Cluster 1 Cluster 2 Cluster 3 Cluster 4

Gene names	IO_set0_P0	IO_set0_E17	IO_set2_E17	IO_set1_E17	IO_set1_P0	IO_set2_P0	IO_set3_E17	IO_set3_P0	IO_set1_P3	IO_set2_P3	IO_set0_P3	IO_set3_P3	IO_set0_P7
Ier3	0.118679	-0.423645	-0.443509	-0.545562	-1.170123	-0.212759	-0.959849	-0.325271	-0.579129	-0.382497	-0.279298	0.0	-0.403861
Popdc3	-0.323753	-0.902387	-0.904696	-0.947365	-1.081207	-0.600104	-0.717506	-0.394304	-0.399836	-0.217636	0.190492	0.0	0.066578
Pex5l	-1.112973	-1.734451	-1.786795	-1.58091	-0.798803	-0.741817	-1.806448	-1.332269	-0.773188	-0.441205	-0.445035	-0.549842	0.133601
ccl5		-1.515684	-2.056974		-0.891122		-3.734718	-3.139697	-1.770709	0.010694	-1.397327	-1.992794	-0.010694
Plxdc1	-1.831678	-2.54991	-2.414274	-2.654814	-2.251602	-2.071759	-2.4199	-2.111113	-1.163142	-0.847423	-0.846754	-1.057378	0.0
Alox5ap	-0.814045	-0.896326	-1.562699	-1.348699	-1.046762	-1.250166	-1.533895	-0.742367	-0.558476	-0.584374	-0.259921	-0.421273	0.0
Pcolce	-0.868993	-1.049832	-1.186942	-1.361083	-0.876871	-0.41894	-1.361413	-0.896728	-0.832377	-0.659859	-0.539381	-0.669873	0.0
Laptm4b	-0.386756	-1.178251	-1.299466	-1.206771	-1.494139	-1.070699	-1.509948	-1.247336	-0.55344	-0.407983	-0.398905	-0.537003	-0.087888
Mfsd6	-0.38686	-0.745611	-0.994931	-0.815246	-0.481249	-0.421863	-1.057917	-0.648145	-0.264022	-0.134214	-0.135109	-0.111203	-0.001099
Nat8l	-1.34308	-1.797172	-1.712126	-1.506589	-1.468651	-0.996446	-1.64631	-1.54468	-0.861278	-0.921168	-0.911857	-1.086976	-0.028868
Lgi2	-0.769575	-1.285162	-1.246996	-1.157696	-0.804139	-0.62507	-1.550238	-0.914265	-0.478992	-0.035351	-0.295301	-0.391556	-0.019272
Clu	-1.065351	-2.636216	-2.611449	-2.41274	-1.947365	-1.914312	-2.633126	-2.064525	-1.149651	-0.801948	-0.565991	-0.871973	-0.102533
Fxyd1	-0.792012	-2.416814	-1.959064	-1.711008	-1.298272	-0.996962	-2.245927	-0.902004	-1.037768	-0.949966	-0.6195	-0.41256	0.095956
Dnaja4	-0.030196	-0.806546	-0.925792	-1.2569	-1.078231	-0.559658	-1.248051	-0.802642	-0.617734	-0.788618	-0.21918	-0.30863	1.0E-6
Ifi27l1 = Ifi27	-0.272841	-1.535101	-1.337181	-1.901185	-1.527635	-1.06578	-1.814201	-0.906585	-0.54618	-0.425047	-0.214466	-0.30229	0.0
Cd151	-0.389245	-0.378363	-0.286126	-0.376691	-0.549559	-0.246345	-0.530405	-0.392059	-0.413246	-0.305998	0.0	-0.200669	0.135117
Tnfrsf11b	-0.644155	-0.736015	-1.46746	-0.61878	-0.753234	-0.607239	-1.135367	-0.352728	-0.918711	-0.643955	-0.064571	-0.223535	0.178253
Crh	0.009357	-0.744433	-1.98886	-1.097607	-0.818558	-0.603641	-2.132623	-0.248503	-1.600988	-0.258529	-0.149307	-0.363389	0.283073
B2m	-0.937596	-1.50166	-0.970564	-1.367563	-1.349725	-1.379192	-1.23648	-1.158566	-0.633433	0.041416	0.0	-0.422094	0.129007
Cxcr7	-1.620665	-0.693982	0.966447	-0.499	-2.431759	-2.228992	0.962538	-1.304301	-0.30796	-0.146076	-1.005451	0.0	-0.2679
Tgfbi	-1.142873	-1.555208	-0.868514	-1.507381	-1.205768	-1.246064	0.70111	-0.24375	-1.05537	-0.341262	-0.632291	-0.517055	-0.18828
C3	-4.710883	-1.203662	-0.904188	-4.04291	-3.901676	-3.090154	-2.504461	-2.92112	-2.880585	-4.064432	-0.252188	-3.054382	1.732373
Prss23	-0.429013	-0.398903	-0.248236	-0.774128	-0.447549	0.0	0.067001	0.036565	-0.47883	-0.036467	-0.008409	-0.425224	-0.278932
Arhgap15	-0.740819	-1.720133	-1.070561	-0.409262	-1.608271	-0.055794	-0.707761	-0.503395	-0.774909	-0.393158	0.378657	0.103562	0.473355
Rnaset2b = Rnaset2b+	0.116126	-0.175545	-1.689304	-2.675248	-1.121659	-0.534992	-1.794493	-0.597256	0.001103	-1.375008	0.563274	0.290411	0.746397
Vasn	-0.380524	-0.580707	-0.686608	-0.605007	-0.521202	-0.130337	-0.569034	-0.326571	0.0	0.439578	-0.031005	-0.173916	0.122044
Tspan31	-0.934258	-0.868031	-0.599027	-0.773395	-0.909428	-0.077176	-0.332246	-0.173313	0.019431	0.32093	-0.540095	-0.369576	-0.205523
Cyb561	0.081248	-0.732601	-0.46566	-0.570539	-0.523962	-0.308682	-0.381952	-0.764635	-0.09472	0.0	-0.212421	-0.082252	-0.210404
Tmem179	-0.37759	-0.762425	-0.624412	-0.947869	-0.328113	-0.07347	-0.678833	-0.445134	-0.125958	0.083369	-0.134858	-0.15728	-0.007512
Tmed10	-0.317131	-0.401747	-0.501146	-0.536531	-0.342178	-0.129318	-0.297073	-0.302003	-0.217087	0.115686	-0.00607	-0.10022	0.0
Cd164l2	-0.883584	-1.439596	-1.36053	-1.036248	-0.91295	-0.408252	-1.137165	-0.742389	0.0	0.413385	-0.283964	0.101762	-0.132773
Vegfb	-0.159135	-0.424803	-0.237718	-0.417573	-0.365861	-0.137369	-0.817761	-0.219535	-0.024759	0.127965	-0.014851	0.089954	0.0
Cd302	-0.480391	-0.915121	-1.584792	-1.541342	-1.334794	-1.182848	-1.576807	-1.265802	-0.622986	-0.312846	0.017363	-0.347433	-0.019068
Ptplad2 = Hacd4	-0.701442	-0.930634	-0.616689	-1.080276	-0.960503	-0.624848	-0.076535	-0.233923	0.0	0.330411	-0.05081		0.543787
Abcg2	-0.276183	-0.342186	-0.201276	-0.380529	-0.363748	-0.080027	-0.384027	-0.08239	-0.09429	0.15906	0.045936	-0.024074	0.032395
Rhbdd2	-0.17882	-0.699304	-0.745942	-0.476709	-0.134083	0.212726	-0.786426	-0.257796	-0.180451	0.031504	0.045863	-0.2171	-0.162058
1810041L15Rik	-0.406537	-0.51605	-0.67357	-0.752189	-0.632906	-0.196717	-1.037173	-0.73025	-0.18273	-0.323737	0.0	0.25963	0.270894
Bai1	-0.10389	-0.44773	-0.228024	-0.231441	-0.472364	0.0	-0.790385	-0.312054	0.094728	-0.110043	0.122932	-0.120902	0.107127
Tmem42	-0.179065	-0.371964	-0.22999	-0.47539	-0.551323	0.076362	-0.441936	-0.312396	-0.237093	0.0	0.208608	-0.071113	-0.109838
Slc22a23	-0.203836	-0.354727	-0.576142	-0.420071	-0.236353	-0.101811	-0.446474	-0.323703	-0.169517	0.113384	0.0	-0.199739	0.14232
Mmp15	-0.172966	-0.360918	-0.277898	-0.452183	-0.386545	-0.00859	-0.117758	-0.658608	-0.041491	0.357197	0.0	-0.081331	0.427051
Gng5	0.247587	-0.320037	-0.308852	-0.313705	-0.60623	-0.364953	-0.42528	-0.448415	-0.173451	0.0	0.067674	-0.115638	0.197106
Slc25a1	-0.264097	-0.153412	-0.126945	-0.317269	-0.175466	0.108604	0.046977	-0.169252	-0.173612	0.098109	-0.154176	0.0	-0.19374
Ifitm1	-0.77449	-0.72267	-0.640291	-0.929873	-0.861611	-0.582248	0.0	0.616515	-0.876118	-0.166641	-0.459718	-0.146886	0.192024
Tmem179b	-0.571604	-0.682719	-0.16239	-0.513049	-0.365215	-0.11275	-0.147417	-0.150587	-0.603619	-0.20522	0.0	0.050242	-0.100572
Ctla2a /// Ctla2b	-0.087132	-0.53982	-0.45884	-2.001866	-0.890621	-0.595327	-0.598665	0.0	-0.465998	-0.632324	0.157798	-0.323827	0.372818
Ctla2a	0.0	-0.159642	-0.635988	-0.468762	-0.229957	-0.056006	-0.35708	-0.011884	-0.34259	-0.269717	0.23547	-0.088869	0.336879
Tctn2	-0.495435	-0.222546	-0.340252	-0.829005	-0.594072	-0.081493	0.167437	-0.288646	-0.315957	0.047666	0.198682	-0.164797	0.035529
Masp1	-0.114077	-0.048059	0.088842	-0.075284	-0.225609	-3.65E-4	0.139329	-0.091339	0.0	0.171306	0.0686	0.102681	-0.106486
Oscp1	-0.175438	-0.293531	-0.191147	-0.275059	-0.137985	0.251641	0.21722	0.138732	0.0	0.430496	0.219723	0.316444	-0.02817
Armcx2	-0.166383	-0.076544	-0.220481	-0.246509	0.129507	0.400382	-0.253342	-0.117664	0.251223	0.221806	0.004583	0.05383	0.001225
Adcy2	-0.20715	-1.705927	-0.89317	-0.649415	-0.5693	0.0	-1.507313	-0.601828	-14.932629	-12.595935	0.3795	-0.805448	0.340016
Dirc2	0.334811	-0.404993	-0.245677	-0.360438			-0.424029				-0.060281	0.122343	
Mbl2											0.354807		-1.251574
Leprot	0.452592	0.157878	0.169593	-0.358327	-0.487659	-0.098352	-0.146473	-0.001834	-0.040534	-0.201318	0.04679	0.0	-0.029865
Gpr137b-ps	0.456828	0.0	-0.056625	-0.469688	-0.447936	0.040616	-0.527721	0.023161	-0.332687	-0.320746	-0.005059	0.077786	-0.174999
Lemd1	0.154528	0.388344	0.694314	0.114519	-0.05539	0.557691	0.18176	0.115095	-0.695019	-0.324796	-0.006341	0.109841	-0.365695
Fgl2	0.125273	0.413467	0.360116	0.060602	-0.004572	0.241694	0.0	0.102652	-0.484503	-0.212508	-0.375033	-0.350215	-0.389413
tex2 = Tex21	-1.57418	0.601072		0.55875	0.734197		-2.086328	-1.864232	-0.929245	1.080694	0.727674	0.117754	-0.178422

Cluster 1 Cluster 2 Cluster 3 Cluster 4

Gene names	IO_set1_P7	IO_set3_P7	IO_set2_P7	IO_set1_P14	IO_set3_P14	IO_set0_P14	IO_set2_P14	IO_set0_P21	IO_set2_P21	IO_set1_P21	IO_set3_P21	IO_set1_Adult	IO_set0_Adult	IO_set3_Adult
ccl5	-0.493998	-0.278	-1.312426	1.390199	0.635222	0.904961	1.500426	2.113558	3.824328	3.288309	3.853516	1.334826	1.341806	1.538337
Plxdc1	0.137052	-0.080604	0.287865	0.922203	0.742005	0.860195	1.143615	0.801949	0.858907	0.629795	0.775416	0.568732	0.529105	0.78782
Alox5ap	0.124196	-0.103515	0.091158	1.625909	1.159519	0.780099	1.309017	1.042335	1.486704	1.383579	1.169775	1.038835	1.035202	1.38218
Pcolce	0.008956	-0.024626	0.14197	0.820579	0.820506	0.843428	0.895153	1.922282	1.749481	1.410466	1.264183	2.259448	2.117672	2.290297
Laptm4b	0.0	0.116581	0.136138	0.794664	0.893738	1.046925	1.029283	1.261255	0.97689	1.153832	1.040673	0.882832	0.53821	0.940516
Mfsd6	0.078764	0.0	0.018527	1.152535	0.923195	1.053412	0.96119	1.229263	1.310319	1.329113	1.25193	0.876746	0.79905	1.145264
Nat8l	0.012186	0.0	0.155193	1.776651	1.447666	1.710847	2.002154	2.173999	1.991413	2.117534	1.796849	1.720931	1.353061	1.727996
Lgi2	0.103697	0.0	0.395072	0.959893	0.811945	1.054188	1.400686	1.052029	1.235879	1.331695	1.190944	0.987976	0.67394	1.218681
Clu	0.0	0.242591	0.203479	0.583655	0.432735	0.569662	0.816734	0.617681	1.047341	0.910673	0.552518	0.454611	0.366212	0.644232
Fxyd1	-0.161268	0.271834	0.0	1.68509	1.468492	1.507434	1.836042	1.845214	1.539235	1.889927	1.76523	1.609144	1.788326	1.618428
Dnaja4	-0.068203	0.266084	0.0	1.39017	1.440501	1.573364	1.51015	1.879554	1.712315	1.92995	1.682033	1.786204	1.476433	1.846823
Ifi27l1 = Ifi27	-0.084734	0.348602	0.447549	1.171207	1.07171	1.007737	1.137611	2.033959	1.634942	1.941945	1.694476	1.847145	1.63393	2.203987
Cd151	-0.079503	0.048094	-0.076262	0.484843	0.436226	0.765674	0.703023	0.953511	0.797983	0.964608	0.692206	0.501082	0.353777	0.629473
Tnfrsf11b	-0.060116	0.094056	0.0	0.041248	0.644716	0.771579	0.87955	0.343912	0.836496	0.352419	0.532573	0.565432	0.364082	0.885119
Crh	-0.015218	0.807745	0.0	1.040454	1.807591	1.387353	2.115256	1.286644	2.037883	1.610579	1.936453	-0.112297	1.049229	1.487614
B2m	-0.386275	0.094692	0.511118	0.057788	0.195684	-0.114477	0.814836	0.612322	1.007973	0.886491	0.601803	0.153892	-0.049158	0.27058
Cxcr7	-0.068947	-0.124531	-0.161765	2.155779	2.114447	0.154512	1.018964	0.761261	1.16995	1.138214	0.302505	0.715348	1.243801	1.487081
Tgfbi	0.0	0.258562	-0.20437	0.938089	0.884565	1.022341	0.827605	0.874419	1.14981	1.09539	0.94303	1.328819	0.712287	1.058098
C3	0.0	0.960723	-1.1506	2.136399	1.824802	1.834913	1.873614	3.496104	3.323985	3.724518	3.293704	4.530775	5.151822	4.962329
Prss23	-0.383304	-0.132337	-0.061959	0.144598	0.287828	0.682979	0.668358	0.701524	0.764754	0.611212	0.497716	0.035606	0.050943	0.300296
Arhgap15	0.0	-0.625197	0.101849	0.198823	0.140522	0.405943	0.160264	0.651815	0.690745	-0.179011	0.792605	-0.020743	1.233703	1.820264
Rnaset2b = Rnaset2b+	0.0	-0.013456	-2.346059	0.022633	-0.02217	0.095442	-1.279799	1.510586	0.594095	0.909796	0.542119	-0.701365	0.64686	1.115961
Vasn	0.10058	0.20489	0.590261	0.08785	0.398066	0.437956	1.105073	0.521763	0.984966	0.378069	0.20625	-0.021422	-0.133001	-0.053407
Tspan31	0.106346	0.0	0.594152	0.123499	0.577911	0.698926	1.08027	0.681132	0.891263	0.488939	0.377173	-0.216994	-0.354407	0.272817
Cyb561	0.001943	0.214171	0.295932	0.369874	0.384797	0.004451	0.67483	0.210921	0.539552	0.624874	0.536623	-0.023664	-0.383812	0.368291
Tmem179	0.079523	0.2961	0.454922	0.581393	0.654159	0.363498	0.723864	0.22885	0.43552	0.452703	0.349482	0.0	-0.485706	0.164505
Tmed10	0.069935	0.138982	0.336419	0.340111	0.433155	0.327116	0.64497	0.415308	0.497822	0.334112	0.260935	-0.091576	-0.326962	0.159663
Cd164l2	0.048044	0.209306	0.594174	0.525095	0.433176	0.245896	0.62203	0.091213	0.675826	0.346999	0.796978	-0.470528	-0.038612	-0.106046
Vegfb	0.183161	0.291708	0.578036	0.223536	0.35526	-0.087339	0.398002	-0.105952	0.5587	0.407543	0.420773	0.076622	-0.27059	0.336509
Cd302	0.006359	0.465201	0.279166	0.042846	0.18586	0.410981	0.496629	0.210627	0.446626	0.151312	0.146599	0.0	-0.053063	0.450263
Ptplad2 = Hacd4	0.487752	0.860086	0.613375		0.672823	0.584683	0.934434	-0.144723	0.751688	0.586573	0.523965	-0.249572	-0.23347	0.268801
Abcg2	0.090616	0.319956	0.129925	0.0	0.227387	0.32697	0.327057	0.478461	0.312768	0.335277	0.075971	-0.372967	-0.720688	-0.144013
Rhbdd2	0.095476	0.490714	0.346975	0.160106	0.026942	0.247097	0.694519	0.050305	0.396167	0.161797	0.0	-0.356531	-0.500646	-0.251735
1810041L15Rik	0.394082	0.363285	0.13029	1.027026	0.955385	0.8124	0.780485	0.283274	0.410356	0.430315	0.448103	-0.986432	-0.9941	-0.558826
Bai1	0.390491	0.304772	0.183984	0.4916	0.462225	0.372512	0.380459	0.265757	-0.020905	0.638908	0.189926	-0.187801	-0.473042	-0.385225
Tmem42	0.349418	0.167826	0.085452	0.342315	0.451655	0.115296	0.558879	0.17595	0.314446	0.526045	0.200331	-0.055008	-0.55627	-0.00992
Slc22a23	0.320019	0.270742	0.55832	0.984524	0.899848	0.840051	1.04896	0.500026	0.405954	0.345884	0.183851	-0.850195	-1.148982	-0.744958
Mmp15	0.569059	0.226219	0.666495	0.632568	0.650376	0.5001	1.02801	0.614985	0.446003	0.658432	0.411131	-0.337763	-0.659296	-0.123026
Gng5	0.125693	0.231241	0.205567	0.30886	0.34664	0.318701	0.585281	0.256965	0.334128	0.350826	-0.026605	-0.410703	-0.650619	-0.297034
Slc25a1	-0.041112	0.081339	0.168723	0.941708	1.002997	0.716488	1.142804	0.898996	0.87768	0.742209	0.621462	-0.523238	-0.684247	-0.120857
Ifitm1	0.030505	0.830021	0.264795	0.47587	0.324449	0.462695	0.803215	1.367221	0.526219	0.381201	0.477498	-0.859847	-0.731256	-0.567156
Tmem179b	0.199545	0.499115	0.391885	0.884307	1.090893	0.50517	1.212602	0.52945	0.818247	0.746773	0.557932	-0.172389	-0.452862	0.011189
Ctla2a /// Ctla2b	0.364406	0.610526	0.814604	1.064468	1.292354	1.340192	1.357614	1.097148	0.985885	1.287019	0.69318	-0.645405	-0.246939	-0.359117
Ctla2a	0.440652	0.783963	0.699787	1.447906	1.489895	1.461525	1.75617	1.206063	0.853168	1.242849	0.472294	-0.53993	-0.567499	-0.177571
Tctn2	0.076394	0.163919	0.347884	0.055057	0.293977	-0.017676	0.300517	-0.242739	0.047061	0.088323	0.215766	-0.436225	-0.886137	0.0
Masp1	-0.060709	0.01694	0.226862	-0.088722	-0.20953	0.249375	0.010121	0.47911	0.580057	0.627666	0.250273	-0.606041	-0.989067	-0.624908
Oscp1	0.05409	-0.0906	0.383629	0.213264	0.178235	0.184793	0.304958	0.239126	-0.083641	-0.159014	-0.195161	-0.16567	-0.443087	-0.180733
Armcx2	-0.069813	-0.196303	0.222321	0.189616	-0.022591	-0.232299	0.058854	0.064919	0.0	0.168449	-0.006968	-0.3955	-0.54386	0.120182
Adcy2	0.374693	0.348112	0.182859	0.495148	0.234162	0.133395	0.056547	0.079912	0.011554	0.192493	0.007677	-0.454405	-1.30862	-0.047258
Dirc2		0.280393		0.36365			0.532574	0.196524	0.26342	0.303483	0.0	-0.106776	-0.365199	-0.188811
Mbl2	-0.354807			1.15525										
Leprot	-0.037018	0.145024	-0.032917	0.684782	0.709849	0.653744	0.608273	0.726521	0.477719	0.598589	0.4381	-0.348765	-0.603208	-0.083911
Gpr137b-ps	-7.39E-4	0.259585	-0.333957	0.459685	0.384509	0.235131	0.416769	0.053077	0.306476	0.332103	0.02433	-0.305495	-0.509149	-0.250993
Lemd1	-0.231765	-0.045659	-0.249346	-0.009912	0.266165	-0.592682	0.133781	-0.357978	0.007856	0.370142	0.015584	-0.028381	-0.165802	0.0
Fgl2	-0.418633	-0.040182	-0.719798	-0.288324	-0.627593	-0.255384	0.015395	0.523461	0.160934	0.421828	0.039517	-0.045445	0.102208	0.561878
tex2 = Tex21	-0.349058	1.060682	-0.928384	-0.470793		-1.073145	0.600881	1.003871	-2.001997	0.921037	-0.117754	-0.548769	0.376873	1.466673

Data S3. (separate excel file)
CRISPR-Cas9 Offtargets.

Target		Sequence-PAM (Mismatch)	MIT / CFD Offtarget Score	Chromosome (Strand)	Start	End	Locus Description	Mutated Off-target / Sequenced Off-target
C1ql1	C1ql1 KO g1	CAGCATCACCACGCCCGCGG-CGG	-	chr11 (+)	102837281	102837304	exon1:C1ql1	-
	Offtarget1	ATGCATCACCACGCCCACTG-GGG	0,202836707746 / 0,45252525242	chr15 (+)	34245616	34245638	intron:Laptm4b	**0/14**
	Offtarget2	CAGCATCAGCACACCCACAG-GGG	0,0410278712971 / 0,380952380603	chr6 (+)	145361143	145361165	intron:Lmntd1	**0/12**
	Offtarget3	CAGCATCAACATGCCAGTGG-GGG	0,0144992773446 / 0,296703296465	chr3 (+)	84253934	84253956	intergenic:Trim2-4930565D16Rik	**0/13**
Lgi2	Lgi2 KO g3	CCCGGCATGGCGCTATGGAG-AGG	-	chr5 (+)	52723430	52723453	exon1:Lgi2	-
	Offtarget1	TCTGGCATGGAGCTGTGGAG-AGG	0,220450566456 / 0,33515625	chr10 (+)	18532463	18532485	intron:Arfgef3	**0/11**
	Offtarget2	CCAGGGATGGAACTATGGAG-GGG	0,233048279684 / 0,303333333342	chr4 (+)	136804762	136804784	intergenic:Zbtb40-Gm13001	**0/12**
	Offtarget3	CTCAGCATGGCACTATGGGG-TGG	0,245385 / 0,286363636233	chr18 (+)	68836308	68836330	intergenic:Mc2r-Mir6356	**0/11**
Crtac1	Crtac1 KO g2	ACTTCGAGATCGTTGTGGCG-GGG	-	chr19 (+)	42402378	42402401	exon2:Crtac1	-
	Offtarget1	ACTTCGGGATCATTGTGGAA-TGG	0,0663496967421 / 0,264705882545	chr15 (-)	71120688	71120710	intergenic:Gm19782-Fam135b	**0 / 13**
	Offtarget2	ACTTAGAAAACTTTGTGGCG-TGG	0,618499137931 / 0,188383045542	chr13 (-)	110848035	110848057	intergenic:Gm33045-4930526H09Rik	**0 / 13**
	Offtarget3	GCTTCGAGATAGGTATGGCG-GGG	0,0865257294304 / 0,184143222434	chr6 (+)	126630226	126630248	intergenic:Kcna1-Kcna6	**0 / 12**
Cbln1	Cbln1 KO g1	CTTCGGGCACACGGCACGCG-GGG	-	chr8 (+)	88199028	88199051	exon1:Cbln1	-
	Offtarget1	CTTCAGGCACACAGCATGCT-TGG	0,09837394875 / 0,261333333599	chr7 (-)	57291795	57291817	intron:Gabrb3	**1/19** *(shift near the NGG cutting site)*
	Offtarget2	CTTGGGGCACACAGCACACT-GGG	0,050081283 / 0,223668638935	chr6 (+)	94236515	94236537	intergenic:4930511A08Rik-Magi1	**1/10** *(point mutation at the NGG cutting site)*
	Offtarget3	CTTCAGGGAAACGGCACGAG-GGG	0,436090585443 / 0,206938775922	chr4 (+)	143474453	143474475	intergenic:Pramel24-Pramel25	**0/14**
	Cbln1 KO g2	GGACGAAGTTGGACCGCCGG-CGG	-	chr8 (+)	88196721	88196744	exon3:Cbln1	-
	Offtarget1	GGACCCAGATGGACCGCCAG-GGG	0,175030472706 / 0,23688046681	chr15 (+)	69421498	69421520	intergenic:4930504C09Rik-Gm19782	**1/11** *(point mutation at the NGG cutting site)*
	Offtarget2	GGATGGAGTTGGACAGCCAG-GGG	0,080867325 / 0,0907029476825	chr3 (+)	104231121	104231143	intergenic:Magi3-Lrig2	**2/19** *(point mutations near the NGG cutting site)*
	Offtarget3	GGATGCAGATGGACAGCCGG-AGG	0,141738197289 / 0,0750360750707	chr2 (-)	135253280	135253302	intron:Plcb1	**0/18**

Data S4. (separate excel file)
Gene clustering - Log2 of DEGs from IONs and GCs in Brainstem extracts.

Cluster 1 Cluster 2 Cluster 3 Cluster 4 Green = DEGS in GCs Pink = DEGs in IONs

GENE NAME	IO_set0_E17	IO_set1_E17	IO_set2_E17	IO_set1_P0	IO_set2_P0	IO_set3_E17	IO_set3_P0	IO_set0_P0	IO_set0_P3	IO_set1_P3	IO_set3_P3	IO_set2_P3	IO_set1_P7
Scn3b	0.165993	0.170555	0.18459	0.208382	0.361136	0.301647	0.079724	0.0	0.052628	0.06144	0.187988	0.366871	0.10735
Rnf19b	0.252408	0.100207	0.159279	0.278993	0.536329	0.138682	0.143025	0.183752	0.262022	0.079224	0.245128	0.482153	-0.015456
Stx1a	-0.06719	-0.156259	0.130424	0.073241	0.334397	0.703108	0.404186	0.068497	0.247895	0.19999	0.367743	0.390989	0.078715
Plp2	-0.209458	0.151407	0.428512	-0.008251	0.660579	0.900368	0.621684	0.0	0.541316	0.50168	0.707821	0.957363	0.325995
Odz3 = Tenm2	-0.021997	0.004526	0.041475	0.259068	0.170683	0.441074	0.425712	6.34E-4	0.132381	0.308138	0.096912	0.146007	0.210801
Pard6b	0.162605	-0.240002	0.310018	0.274192	0.611223	0.409662	0.336853	-0.024927	0.199974	-0.020348	0.17633	0.030295	0.0
Stbd1	0.379089	0.0	0.302959	-0.210472	0.096762	0.234609	-0.322194	0.134034	0.449121	0.21064	0.477271	0.559259	0.298385
Sdc1	0.585526	0.0	0.645885	-0.262986	0.371957	-0.091079	0.049317	0.105977	0.346516	0.267754	0.271109	0.572056	0.096534
Olfm2	0.021431	0.069425	0.072561	0.0	0.30108	-0.255308	0.019119	0.091468	0.212714	0.154308	0.158538	0.436974	0.070071
Lrfn5	-0.016571	0.07959	0.133241	0.0	0.440817	-0.27004	0.129534	0.030265	0.185345	0.503601	0.325557	0.531905	0.130749
Gm5868	0.356433	0.850318	1.003332	0.376686	0.0	0.542823	-0.129694	0.102101	0.122304	0.14808	1.087293	0.235587	-0.309997
Tspan6	0.330151	-0.160426	0.348348	0.156065	0.325822	0.22583	0.189799	0.309798	0.389928	0.178626	0.41479	0.223423	0.079451
Tnfsf9	1.275053	0.464042	0.701353	-0.166209	0.309812	0.756782	0.319573	0.355301	0.466497	0.42295	0.707561	0.174492	-0.027439
Tmeff1	0.306484	0.209376	0.336957	0.185339	0.50836	-0.150953	0.228113	0.173216	0.363654	0.153656	0.172619	0.258309	-0.098064
Spint2	0.053155	0.151204	0.369104	0.547735	1.052587	0.064755	0.681611	0.435473	0.320289	0.84128	0.566946	0.727284	0.0
F2r	0.296837	0.453937	0.614295	0.300642	0.601352	-0.136195	0.412531	0.179265	0.261778	0.329818	0.530993	0.0	0.070457
Lin7c	0.663809	0.706492	0.697684	0.687615	0.855189	0.356668	0.606745	0.750976	0.603059	0.58684	0.65033	0.826883	0.058325
Igsf3	0.356546	0.353334	0.207111	0.397463	0.509711	0.097608	0.053997	0.869601	0.044834	0.200965	0.197915	0.114834	0.104878
Cnr1	0.352875	0.253146	0.314194	0.084584	0.294421	0.163872	0.058427	0.621785	-0.007026	0.086587	0.060118	0.174894	0.143725
Panx1	0.610638	0.5498	0.567565	0.600357	0.72837	0.64155	0.495855	0.452487	0.352526	0.359895	0.299578	0.618729	-8.87E-4
Gprin1	0.66109	0.425813	0.510289	0.479175	0.726538	0.244881	0.341957	1.095209	0.346632	0.526452	0.3613	0.564471	-0.078588
Ctxn1	0.549028	0.212863	0.370476	0.20735	0.667406	0.297552	0.397031	0.873983	0.21583	0.213201	0.240037	0.301283	0.066304
Cd24a	2.716735	2.154336	2.640181	1.519319	1.66414	2.092454	1.586591	1.701702	0.762832	1.238282	1.140296	1.095322	-0.136226
Crlf1	0.696093	0.880074	0.918576	0.570335	0.780398	0.618609	0.423472	1.212339	0.467647	0.305455	0.736158	0.0	0.057754
Gab2	0.078639	0.052724	0.0	0.144675	0.376053	0.19922	0.140326	0.059977	0.047363	0.082312	0.185987	0.08939	0.010575
Slc1a4	0.327093		0.36426										0.752885
Rtn4rl2	-0.090899	0.0	0.10845	0.370699	0.708185	0.194508	-0.094048	0.182972	0.450011	0.112699	0.333701	0.679235	0.141499
Rtn4r	-0.11968	0.125084	0.0	0.24264	0.490303	-0.03511	0.252066	0.197507	0.371034	0.242228	0.380694	0.4708	0.112334
Cbln1	-0.006161	0.062753	0.0	0.070798	0.484445	-0.021695	-0.05867	0.192354	0.238054	0.051469	0.293966	0.302224	0.299502
Vstm2l	0.352965	-0.120579	-0.016564	0.446693	0.02304	0.192787	0.085013	0.466809	0.638176	0.0	0.362475	0.252381	0.124914
Lphn2 = Adgrl2	0.214653	0.170457	-0.090856	0.131346	0.341984	0.120194	0.016006	0.864288	0.276428	0.0	0.321625	0.534193	0.192325
Igfbp5	0.106636	0.17276	9.47E-4	0.084163	0.042607	-0.180438	0.0	0.614976	0.24306	0.117417	0.181826	0.316296	0.183751
Gpr125	0.138074	0.0	0.057998	-0.039581	0.078575	-0.022329	-0.107438	0.626461	0.12802	0.040047	0.227394	0.278632	0.205967
Fxyd7	-0.169074	-0.026421	-0.090346	0.091139	0.466069	-0.418402	0.072036	0.714716	0.535179	0.421895	0.639159	0.706497	0.601991
Fam174b	0.110686	-0.192831	0.019835	-0.16374	0.020989	-0.1672	-0.13041	0.556631	0.228477	0.063932	0.212647	0.206955	0.455002
Twsg1	0.09705	-0.142067	0.146572	0.109052	0.278617	-0.016291	0.201253	-0.098832	0.291645	0.043879	0.18525	0.348031	0.298743
Pvrl2	0.047416	-0.122665	0.0	0.078121	0.350858	-0.178535	0.246439	0.163264	0.208875	0.413737	0.57268	0.232781	0.450786
Scn3a	0.041004	0.0	-0.080498	0.307952	0.500642	-0.033151	0.282228	0.212725	0.248994	0.070642	0.279352	0.264901	0.314759
Znrf2	0.36401	-0.224997	0.067122	0.130959	0.304257	-0.199486	0.14176	0.251711	0.350878	0.173827	0.256614	0.069488	0.30188
2200002K05Rik = Vstm5	0.212025	-0.032208	0.0	-0.04876	0.360366	-0.370194	0.073293	0.240035	0.346379	0.229519	0.416351	0.290957	0.268738
Ly6h	-0.050552	0.156216	0.157624	0.305082	0.34385	-0.475556	0.17268	0.804862	0.390687	0.271804	0.45629	0.0	0.208961
Gpr25	0.196014	-0.097771	0.210166	-0.25694	0.656983	-0.790644	0.157469	0.935856	0.135817	0.326439	0.51173	0.167861	0.421644
Cyb561d2	0.120913	0.005084	0.24961	-0.055947	0.249291	0.068493	-0.005084	0.70434	0.330405	0.2353	0.433882		0.189245
Crlf2	-0.15971	0.03526	0.210047	0.190028	0.449726	-0.453767	0.154114	1.006147	0.276239	0.356735	0.680966	0.444709	0.0
Cgref1	0.072686	0.004673	0.0	0.290611	0.405772	-0.124457	-0.038267	0.903276	0.335101	0.295103	0.334511	0.307198	0.265444
Cklf	-0.129092	-0.183031	0.410007	-0.17065	0.628741	0.351823	0.529604	0.948946	0.504912	0.124428	0.64876	0.086617	0.141099
Rgs19	-0.096086	0.246082	-0.308871	0.482118	0.688021	0.442366	0.451245	-0.009332	0.487354	-0.037277	0.81171	0.315552	0.848152
Trhde	0.192817	-0.317876	-0.146084	0.274492	-0.069845	-0.138644	0.155588	0.254402	0.557058	0.174239	0.449121	0.0	0.520184
Ntf3	0.363338	0.291738	-0.02597	0.0	0.335857	-0.273586	0.284363	0.487019	1.019198	0.286415	0.920095	0.402938	0.797636
Epha4	-0.062279	0.078342	-0.055743	-0.07186	0.083782	-0.187004	0.189974	0.096965	0.269196	0.151255	0.215969	0.0733	0.455234
Vstm2b	0.127512	-0.286633	-0.038818	-0.220877	0.234172	-0.532826	0.123972	0.528352	0.798694	0.437798	0.656597	1.028945	0.664495
Pcsk5	-0.380267	-0.261381	-0.263812	0.0	0.221403	-0.081611	0.231241	0.015086	0.240763	0.23251	0.28893	0.488029	0.5213
Nptx2	-0.031532	0.217161	-0.230539	0.345882	0.837419	-0.097613	0.223996	0.527705	0.626304	0.597521	0.406169	1.026229	0.882082
Ptn	-0.084039	-0.11493	-0.167705	4.91E-4	0.209959	-0.325513	-0.034864	0.060163	0.267343	0.0	0.245965	0.203754	0.21067
Lypd6	-0.005149	-0.250368	-0.628466	0.005149		-0.774118	0.220551	0.911212	0.840221	0.544174	0.480462	0.820846	0.874913
Fam3c	-0.162969	-0.153882	-0.022178	0.070605	0.273073	-0.41856	0.13619	0.59615	0.352591	0.143093	0.488349		0.481745
slc30a10	0.0	-0.389859	-0.034069	-0.003287	0.475957	0.307819	0.408061	0.139206	0.572137	0.514833	0.91211	0.879227	0.922356
Rasgrp2	-0.112443	0.057639	-0.202712	0.211769	0.498138	0.0	0.157627	0.241208	0.616513	0.424298	0.700511	0.753561	0.533492
Lypd1	-0.103629	0.045963	0.0	0.053093	0.363859	-0.185407	0.084545	-0.01507	0.307131	0.285259	0.25528	0.55109	0.520531
Ifngr2	-0.140772	0.030402	0.069625	-0.084184	0.398018	-0.494021	0.175353	0.103135	0.286232	0.172346	0.567539	0.5666	0.345339
Cdh13	-0.11245	0.140035	0.0	0.213677	0.670938	-0.202744	0.304376	0.188579	0.408451	0.601866	0.612764	0.772026	0.54368
Lyz1	0.187548	-1.017438	-1.249513	-1.016099	0.093609	-1.169859	0.119339	-0.510591	1.199567	0.036465	0.199953	0.272242	1.237145
Scarb1	-0.011232	0.112714	0.0	0.212177	0.450382	-0.345668	0.227153	0.08502	0.298782	0.318979	0.275253	0.493783	0.402081
Ntm	0.0	0.07826	-0.016741	0.122531	0.383782	-0.291861	0.087473	0.258538	0.459712	0.336445	0.308812	0.594477	0.432685
Nell2	0.032137	-0.003263	-0.155087	0.103183	0.191567	-0.29917	0.019587	0.0	0.230879	0.107673	0.166078	0.508592	0.326118
Dner	-0.036825	0.07996	0.031103	0.071388	0.255596	-0.134115	0.0	0.220528	0.304868	0.236298	0.380073	0.575137	0.268522
Syt9	0.044738	-0.1291	-0.015912	0.130313	0.40382	0.0	0.043379	0.352841	0.54296	0.410028	0.245045	0.447745	0.484958
Npnt	0.021994	-0.004882	-0.284162	0.324995	0.412339	-0.109943	0.046102	0.259155	0.624633	0.350818	0.407405	0.653546	0.740029
Cbln4	0.102615	0.010121	-0.010121	0.257736	0.273276	-0.328349	0.178245	0.280756	0.690521	0.259617	0.614904	0.663594	0.785279
Kit	0.214192	0.190235	0.009747	0.216628	0.124049	-0.131796	-0.166331	0.234389	0.297689	0.0	0.193615	0.224249	0.298512
Grin3a	0.35133	0.082554	-0.145524	0.354986	0.243194	-0.171661	0.0	0.939478	0.377522	0.371639	0.443908	0.374303	0.666346
Kcnd2	0.0	-0.047858	-0.07267	0.200546	0.362094	-0.268254	0.238632	0.753838	0.411039	0.435268	0.542738	0.57191	0.538955
Gng4	0.0	0.023882	-0.038547	0.188789	0.552261	-0.152086	0.083259	0.797693	0.230334	0.236211	0.547629	0.652484	0.402782
Fam20c	0.007627	-0.035296	0.078205	0.065716	0.278246	-0.145532	0.0	0.638768	0.121609	0.12474	0.32845	0.396629	0.203084
Gabra5	0.0	0.140586	-0.046428	0.45538	0.595619	-0.218756	0.353733	1.026639	0.647977	0.749219	0.909534	0.986917	0.735033
Kcnip2	-0.033155	-0.27442	-0.11661	-0.140949	0.389205	-0.519963	0.006743	0.781161	0.454107	0.332319	0.652397	0.498385	0.620636
Gjd2	-0.12542	-0.121811	-0.173503	0.007719	0.184808	-0.779062	-0.018776	0.912541	0.429673	0.144333	0.449448	0.290156	0.644404
Igf1	0.161332	-0.137824	0.0	0.235541	0.49566	-0.554325	0.474861	1.112065	0.915312	0.629636	0.767623	1.043793	0.97547
Fam189a1	0.163084	-0.28537	0.068505	-0.017333	0.278141	-0.530516	0.026288	1.008542	0.298143	0.314349	0.274769	0.075305	0.424367
Nell1	-0.032455	0.0	0.121502	0.091093	0.322704	-0.540322	0.197767	0.154284	0.490266	0.530599	0.527643	0.379037	0.512354
6430571L13Rik	-0.051043	-0.062061	0.0	0.026536	0.472135	-0.586835	0.108389	0.35423	0.360247	0.423153	0.371257	0.204609	0.400689
Cacna1g	-0.093135	-0.082489	-0.004985	-0.113154	0.50553	-0.135681	0.290232	0.216308	0.261972	0.320162	0.537348	0.309417	0.558328
Ramp3	0.047765	0.0	-0.051045	0.101101	0.616169	-0.912971	0.069931	0.209826	0.348772	0.115043	0.405973	0.346026	0.293288
Efna3	0.0	0.076671	0.070134	-0.079073	0.260503	-0.161968	0.035703	0.069571	0.235285	0.241076	0.357598	0.414089	0.188137
Cbln1	0.082111	0.078921	0.053232	0.0	0.347042	-0.289319	-0.052644	0.702833	0.218312	0.013318	0.433805	0.086546	0.23756
Cbln1	0.076315	-0.025383	0.0	0.115098	0.523338	-0.132356	0.007449	0.326493	0.29444	0.252188	0.482013	0.401161	0.353244
Cbln1	0.01119	0.043713	0.050916	0.011812	0.412361	-0.263786	-0.017725	0.202993	0.270868	0.071119	0.359844	0.379333	0.276688
Cdh9	0.0	0.146662	-0.046874	0.364744	0.524751	-0.347127	0.292253	0.167878	0.459662	0.113902	0.424271	0.19519	0.247381
H2-Aa	-2.953262	0.015134	0.333792	0.046823	0.217004	0.329854	0.0	-0.969329	0.354518	-2.120732	1.546601	-1.238595	0.415785
Ajap1	0.430722	0.146233	0.142288	0.934175	0.829758	-0.438697	0.633177	0.639477	0.829187	-0.376392	0.610994	0.19499	-0.040866
Vps37b	-0.400602	-0.098467	0.100894	-0.025454	0.25407	0.088409	-0.104652	-0.449406	-0.212665	0.015428	0.0	0.18455	0.316144
Tmem191c	-1.196981	-0.657021	-0.408053	0.0	0.504742	-0.150068	0.437074	-0.258402	0.235496	0.087117	0.813731	0.46818	0.482151
Sema4a	-0.579569	-0.408931	-0.228017	-0.206135	0.197878	-0.548665	0.266973	-0.22785	0.015927	0.159345	0.419596	0.209874	0.127278
Oscp1	-0.293531	-0.275059	-0.191147	-0.137985	0.251641	0.21722	0.138732	-0.175438	0.219723	0.0	0.316444	0.430496	0.05409
Znrf1	0.021404	-0.287358	0.0	0.012995	0.054396	-0.217491	0.132684	0.058803	0.113621	-0.007528	0.092565	-0.138264	0.021046
Grid1	-0.435677	-0.616169	-0.064731	0.087916	0.313315	-0.381175	0.148545	0.595791	0.162278	0.17122	0.185777	0.0	0.155083
Igfbp3	-0.053448	-0.337702	-0.261255	0.0	0.334814	-0.50659	0.505486	0.622488	0.435217	-0.139803	0.281205	0.130585	0.435253

Cluster 1 | Cluster 2 | Cluster 3 | Cluster 4 | Green = DEGS in GCs | Pink = DEGs in IONs

GENE NAME	IO_set2_P7	IO_set0_P7	IO_set3_P7	IO_set0_P14	IO_set2_P14	IO_set1_P14	IO_set3_P14	IO_set0_P21	IO_set1_P21	IO_set2_P21	IO_set3_P21	IO_set0_Adult	IO_set3_Adult	IO_set1_Adult
Scn3b	0.200874	-0.047672	-0.043372	-1.45068	-1.500848	-1.473583	-1.342169	-1.792055	-1.876608	-1.671153	-1.886082	-2.251991	-1.756358	-1.900183
Rnf19b	0.267399	0.0	-0.036291	-0.489954	-0.020326	-0.406683	-0.327674	-0.460375	-0.517066	-0.512766	-0.625689	-1.1148	-0.772933	-0.867169
Stx1a	0.181515	0.0	0.161652	-1.704537	-1.445265	-1.310958	-1.440299	-2.307524	-2.019932	-2.10291	-2.137699	-2.466026	-2.507397	-2.556893
Plp2	0.434718	0.394934	0.366693	-0.977392	-0.197849	-0.261342	-0.176246	-1.222738	-0.883737	-0.765741	-0.976513	-1.932179	-1.227776	-1.213496
Odz3 = Tenm2	0.212777	-0.270514	0.0	-0.657311	-0.446432	-0.186958	-0.207631	-0.976965	-0.761225	-0.862289	-0.681525	-1.197897	-1.2478	-1.151969
Pard6b	0.069223	-0.170713	0.138345	-0.224515	0.02337	-0.119558	0.207982	-0.322625	-0.429236	-0.46501	-0.406702	-1.029101	-0.372414	-0.725874
Stbd1	0.048013	0.100766	0.500144	-1.492175	-1.144631	-0.619841	-0.780067	-0.687489	-0.306237	-0.811137	-0.692115	-1.338952	-1.393504	-1.498192
Sdc1	0.109675	0.029783	0.138334	-1.302862	-1.078333	-1.006306	-0.915412	-1.422678	-1.166201	-1.445096	-1.522122	-2.782237	-2.01784	-1.839371
Olfm2	0.003116	-0.031977	0.112992	-0.313252	-0.389783	-0.605419	-0.434253	-0.452237	-0.465108	-0.663698	-0.587102	-1.328632	-0.97406	-1.034803
Lrfn5	0.001171	0.008128	0.130743	-0.605596	-0.596257	-0.685855	-0.379597	-0.735092	-0.565847	-0.878757	-0.701199	-1.291711	-0.730604	-0.786146
Gm5868	0.419939	0.296339	0.82684	-2.088136	-1.038916	-2.462175	-1.836804	-2.361865	-0.768027	-2.394394	-1.123052	-3.245762	-3.720732	-3.282955
Tspan6	0.0	-0.072404	0.096752	-1.178981	-0.771202	-0.888287	-0.797278	-1.546246	-1.636619	-1.623755	-1.598267	-2.66685	-1.997605	-2.028915
Tnfsf9	0.017944	0.0	0.231327	-1.156493	-0.552078	-1.129089	-0.720822	-0.649465	-0.836156	-0.589247	-0.662171	-1.821837	-1.344477	-0.837864
Tmeff1	0.0	0.005515	0.047509	-0.159152	-0.238334	-0.249844	-0.174996	-0.290166	-0.279019	-0.307463	-0.2564	-1.46767	-0.769449	-0.884042
Spint2	-0.033834	-0.02744	0.23641	-1.120515	-1.272758	-0.92092	-1.036627	-1.171546	-1.171142	-0.967438	-1.044936	-1.357971	-1.218844	-1.222115
F2r	0.126325	-0.147956	0.343835	-0.871941	-0.487952	-0.428119	-0.185438	-1.016235	-0.540841	-0.651554	-0.521303	-1.09925	-0.826647	-0.628698
Lin7c	-0.169037	0.0	-0.101159	-0.869127	-0.949517	-0.886538	-0.910358	-1.063317	-0.80188	-1.035855	-1.020336	-1.465764	-0.996789	-0.951751
Igsf3	-0.031614	-0.199767	0.0	-0.844952	-0.838417	-0.752632	-0.836525	-1.296421	-1.007837	-1.381555	-1.240782	-1.691906	-1.36259	-1.454075
Cnr1	-0.007863	0.0	0.028125	-0.139253	-0.032581	-0.390222	-0.411588	-0.451338	-0.357718	-0.075197	-0.410143	-0.753571	-0.308468	-0.540241
Panx1	0.207782	-0.024562	0.0	-0.666459	-0.542168	-0.762615	-0.746757	-1.0193	-0.98304	-1.097973	-1.39717	-2.002924	-1.596826	-1.830467
Gprin1	0.0	-0.052604	0.012271	-1.394436	-1.519332	-1.479881	-1.623662	-1.654084	-1.757866	-1.905612	-1.999496	-2.097586	-1.734139	-1.82838
Ctxn1	-0.075361	-0.144629	0.0	-1.061966	-0.830268	-1.033384	-1.466131	-1.318425	-1.28993	-1.571255	-1.621783	-1.627915	-1.360138	-1.596852
Cd24a	-0.030275	0.047989	0.0	-0.719058	-0.198635	-0.86864	-0.947763	-0.207289	-0.452089	-0.464308	-0.772408	-1.283712	-1.068015	-1.104812
Crlf1	-0.317271	-0.526764	-0.066545	0.128599	-0.766782	-0.071066	-0.851202	-2.726167	-1.436617	-2.117685	-1.540711	-2.571766	-2.423476	-1.581863
Gab2	-0.070922	0.016495	-0.005042	-0.305311	-0.302153	-0.405716	-0.350425	-0.369353	-0.030603	-0.341511	-0.245317	-0.666549	-0.314897	-0.241264
Slc1a4		0.555869		-0.226506	0.343593	0.087447		-0.076148	0.0		-0.117392	-0.592283	-0.184647	-0.398881
Rtn4rl2	0.60945	0.304818	0.524468	-2.106579	-0.791258	-0.817595	-0.907413	-1.800316	-1.150343	-1.608275	-1.408937	-2.954928	-1.946524	-2.320588
Rtn4r	0.651463	0.275688	0.332623	-1.04438	-0.402021	-0.842799	-0.727782	-0.991377	-1.368503	-1.209899	-1.399036	-2.091295	-1.638503	-1.863419
Cbln1	0.400692	0.388263	0.07806	-0.575043	0.14678	-0.348154	-0.716529	-0.395858	-0.402264	-0.459004	-0.413609	-0.709266	-0.446639	-0.470578
Vstm2l	0.548537	0.104553	0.787247	-0.52043	-0.207434	-0.516699	-0.800689	-0.986929	-0.922576	-0.461175	-0.897251	-0.887782	-0.715783	-0.616828
Lphn2 = Adgrl2	0.348205	-0.089007	0.067671	-1.019918	-0.420375	-0.662321	-0.891914	-1.206555	-1.046585	-0.938744	-1.293512	-1.223788	-1.102757	-1.299804
Igfbp5	0.174935	-0.20971	0.187958	-0.62072	-0.501781	-0.467529	-0.228777	-0.849245	-0.879276	-1.329663	-0.828612	-1.45345	-1.01973	-1.12077
Gpr125	0.329819	-0.009742	0.348962	-0.011679	0.142044	0.008645	-0.032228	-0.212247	-0.04973	-0.176627	-0.399736	-0.844898	-0.608792	-0.604126
Fxyd7	1.004092	0.629534	0.851591	-0.104083	0.298871	0.0	-0.204122	-0.897825	-0.838198	-0.975933	-1.27238	-1.611462	-1.406755	-1.429915
Fam174b	0.551604	0.302331	0.531736	0.0	-0.071784	0.021097	-0.07293	-0.422589	-0.12466	-0.387329	-0.520237	-0.843734	-0.551041	-0.660581
Twsg1	0.11476	0.078676	0.803535	-0.477568	0.0	-0.049239	-0.199767	-0.373654	-0.23145	-0.151109	-0.214787	-0.816589	-0.292534	-0.353221
Pvrl2	0.269564	0.011613	0.47235	-0.979573	-0.506452	-0.471605	-0.864315	-1.426011	-0.968819	-0.594251	-1.26155	-1.980445	-1.95923	-2.009883
Scn3a	0.125714	0.05956	0.090447	-0.891207	-0.903196	-0.927649	-0.958301	-1.713993	-1.401077	-1.321355	-1.581162	-1.590952	-1.281763	-1.603368
Znrf2	0.183927	-0.020005	0.246553	-0.347844	-0.113153	-0.089468	0.0	-0.549415	-0.231368	-0.466082	-0.350958	-1.072102	-0.594911	-0.674869
2200002K05Rik = Vstm5	0.217064	0.030397	0.197711	-0.207418	-0.019274	-0.048026	-0.160754	-0.048385	-0.025253	0.009376	-0.080699	-0.72404	-0.045365	-0.651528
Ly6h	0.051762	0.148684	0.442316	-1.583633	-1.57791	-1.140048	-1.394016	-1.827547	-1.61396	-1.801052	-1.962985	-2.014775	-1.756271	-1.65874
Gpr25	-0.05889	0.093665	0.48738	-0.504217	-0.33701	0.060446	0.0	-1.185994	-0.141527	-0.60212	-0.435559	-1.807589	-1.2123	-1.016772
Cyb561d2	0.234221	0.206082	0.400559	-0.434045	-0.202039	-0.111073	-0.167696	-0.201543	-0.163003	-0.316717	-0.348675	-1.202495	-0.582659	-0.691091
Crlf2	0.521209	0.183155	1.025951	-0.765575	-0.546228	-0.581684	-0.396159	-1.217565	-0.479666	-1.04879	-0.710442	-2.100307	-1.658798	-1.75489
Cgref1	0.324805	0.127263	0.408886	-0.744628	-0.725945	-0.640487	-0.751473	-1.037028	-0.727163	-1.154431	-1.018878	-1.53834	-1.430446	-1.587523
Cklf	0.412183	0.111685	0.433211	-0.38532	0.0	-0.016461	-0.023945	-0.153476	-0.271896	-0.463378	-0.609167	-0.716922	-0.425463	-0.535012
Rgs19	0.93292	0.213816	1.160649	-0.113077	0.0	-0.006091	0.030411	-0.325616	-0.31951	-0.137942	-0.505097	-0.717348	-2.068851	-0.534968
Trhde	0.301591	0.14825	0.449503	-0.212075	-0.418032	0.190453	0.045931	-0.582689	-0.423132	-0.696821	-0.721583	-1.098057	-0.995886	-0.745843
Ntf3	0.655508	0.612472	0.831872	-0.884064	-0.688705	-0.180519	-0.494831	-1.206922	-0.286131	-0.779265	-0.796681	-1.667785	-1.702417	-2.289258
Epha4	0.270276	0.1893	0.312389	-0.252931	-0.152408	0.0	0.097421	-0.421742	-0.185034	-0.372477	-0.393818	-1.134233	-0.75132	-0.698762
Vstm2b	1.013308	0.745713	0.693499	-0.378434	0.060838	-0.280887	0.0	-0.413099	-0.323862	-0.392862	-0.451254	-1.053	-0.71089	-0.577855
Pcsk5	0.587081	0.691485	0.426225	-0.038303	0.07653	0.194933	-0.035544	-0.667035	-0.272035	-0.50522	-0.61998	-0.855447	-0.758753	-0.751752
Nptx2	1.210713	0.93118	0.843261	-0.139444	0.0	-0.236578	-0.410623	-0.954851	-0.635055	-0.590865	-0.81027	-1.691137	-1.466872	-1.412556
Ptn	0.445646	0.255113	0.25142	-0.059818	0.259346	0.109598	0.049093	-0.308307	-0.356556	-0.195176	-0.516491	-1.838826	-1.692062	-1.935267
Lypd6	1.156185	0.890991	1.028716	-0.043833	0.123337	-0.174506	0.011527	-0.222897	-0.414413	-0.461917	-0.686598	-0.840441	-0.643781	-0.497757
Fam3c		0.468091	0.534802	0.022178		-0.027083	0.11574	-0.231065	-0.266694	-0.956876	-0.627831	-1.039566	-0.776398	-0.935761
slc30a10	1.16815	0.776948	0.997789	-0.370781	0.163617	-0.042396	-0.092062	-0.405752	-0.409173	-0.3613	-0.446529	-0.965208	-0.754732	-0.874353
Rasgrp2	0.869657	0.502264	0.624471	-0.46619	-0.190907	-0.279122	-0.146289	-0.838843	-0.771309	-0.542	-0.906956	-0.515133	-0.321836	-0.085215
Lypd1	0.778253	0.35718	0.458355	-0.022316	0.29157	-0.058421	-0.024249	-0.266441	-0.039342	-0.079767	-0.131149	-0.735973	-0.290888	-0.119595
Ifngr2	0.577227	0.087221	0.399526	-0.207534	0.0	-0.406494	-0.346707	-0.48646	-0.248482	-0.486525	-0.580646	-1.580863	-0.991464	-1.251906
Cdh13	0.817683	0.411431	0.474768	-0.464136	-0.050829	-0.332739	-0.457546	-0.684837	-0.716663	-0.855739	-0.887292	-1.449638	-1.004729	-1.213342
Lyz1	0.310818	0.479374	0.414568	-0.057846	0.868766	-3.342646	-2.041523	0.044116		-0.19166	-0.519346	-0.762142	-2.582202	-0.036465
Scarb1	0.280933	0.324632	0.151896	-0.619148	-0.195913	-0.467136	-0.428497	-0.746132	-0.549139	-0.796649	-0.794502	-1.557993	-1.376694	-1.473269
Ntm	0.329447	0.510996	0.172389	-0.038442	-0.219917	-0.223926	-0.32435	-0.225663	-0.1632	-0.433916	-0.479542	-0.795687	-0.370879	-0.253189
Nell2	0.320295	0.222152	0.088909	-0.140539	0.043905	-0.123465	-0.257729	-0.497423	-0.165526	-0.359568	-0.524931	-0.834067	-0.495777	-0.632026
Dner	0.322719	0.238922	0.158265	-0.496344	-0.478225	-0.630073	-0.461582	-0.4541	-0.525293	-0.686681	-0.664437	-1.208633	-0.969219	-0.846859
Syt9	0.385322	0.267999	0.319276	-0.353555	-0.121759	-0.179926	-0.143711	-0.54781	-0.206938	-0.406317	-0.403268	-0.867335	-0.416504	-0.429421
Npnt		0.512943	0.53672	-0.097564	0.004882	-0.179001	-0.143338	-0.961938	-1.091077	-0.909234	-1.027375	-2.096074	-1.883584	-2.097607
Cbln4		0.653544	0.742102	-0.306573	-0.531762	-0.568204	-0.503599	-0.598402	-0.551339	-0.910646	-0.542956	-1.216325	-0.758856	-0.828536
Kit	0.231545	0.308327	0.051882	-0.392576	-0.468608	-0.46969	-0.657882	-0.81007	-0.450457	-0.365853	-0.599731	-0.990202	-0.62835	-0.62841
Grin3a	0.266953	0.428916	0.28194	-0.037987	-0.266654	-0.054039	-0.189332	-0.458978	-0.163147	-0.521021	-0.518194	-0.768974	-0.399553	-0.458989
Kcnd2	0.521012	0.362925	0.502498	-0.122594	-0.065388	0.049624	-0.063005	-0.431687	-0.364249	-0.509935	-0.596859	-0.966908	-0.590029	-0.665976
Gng4	0.552772	0.310663	0.355595	-0.729775	-0.505725	-0.518772	-0.79117	-1.357383	-1.07877	-1.098286	-1.24654	-2.113297	-1.520835	-1.779711
Fam20c	0.463697	0.164566	0.309255	-0.182584	-0.053242	-0.058193	-0.122025	-0.259816	-0.172325	-0.111154	-0.384347	-0.668068	-0.387467	-0.493983
Gabra5	0.851905	0.785032	0.700936	-0.361022	-0.603835	-0.324586	-0.372491	-0.747391	-0.616107	-0.893778	-0.828377	-0.645239	-0.301962	-0.556952
Kcnip2	0.412461	0.765819	0.755251	0.0	0.132428	0.046659	-0.137503	-0.896826	-0.108809	-0.095976	-0.288271	-0.470181	-0.11788	-0.21927
Gjd2	0.450246	0.580751	0.69478	0.163361	0.0	0.077834	-0.05807	-0.745391	-0.517815	-0.759369	-0.683619	-1.875502	-1.401846	-1.44214
Igf1	0.349754	0.946016	1.059695	-0.530522	-0.158706	-0.289491	-0.315387	-0.711517	-0.523829	-0.939443	-0.670232	-1.561918	-1.080919	-1.106609
Fam189a1	0.08726	0.344139	0.440104	-0.062961	0.0	-0.105965	-0.066302	-0.563188	-0.123082	-0.607547	-0.458664	-1.008378	-0.567322	-0.594097
Nell1	0.349812	0.382029	0.45806	-0.335809	-0.451793	-0.111024	-0.196973	-0.758759	-0.253621	-0.703573	-0.479613	-1.115913	-0.505933	-0.657596
6430571L13Rik	0.098506	0.277903	0.128253	-0.574717	-0.202359	0.049619	-0.175431	-0.323798	-0.25323	-0.65412	-0.225247	-0.500676	-0.069727	-0.388036
Cacna1g	0.318339	0.444413	0.44057	-0.294885	0.0	0.418323	0.080563	-0.994743	-0.338253	-0.322508	-0.283076	-0.608268	-0.381382	-0.64067
Ramp3	0.028095	0.336231	0.119214	-2.26805	-1.715825	-2.014216	-2.589442	-2.748544	-1.745619	-1.566599	-1.664146	-1.898221	-1.516665	-1.287483
Efna3	0.109059	0.227387	0.196769	-0.683032	-0.445693	-0.837137	-0.778442	-0.783973	-0.617961	-1.018769	-0.692031	-1.025715	-0.677402	-0.699743
Cbln1	0.102536	0.277838	0.16821	-0.61565	-0.063904	-0.393762	-0.699599	-0.542907	-0.435832	-0.612206	-0.485908	-0.68401	-0.474866	-0.448351
Cbln1	0.183649	0.417591	0.148982	-0.472478	-0.051829	-0.183797	-0.564952	-0.380726	-0.303857	-0.183129	-0.166233	-0.725416	-0.419301	-0.644423
Cbln1	0.142229	0.32901	0.0	-0.628124	-0.161064	-0.613016	-0.695326	-0.34215	-0.355152	-0.494003	-0.312727	-0.911391	-0.467638	-0.404129
Cdh9	0.050746	0.321712	0.276775	-0.347373	-0.597068	-0.507651	-0.468973	-0.332868	-0.217811	-0.460444	-0.341706	-0.831385	-0.21255	-0.287621
H2-Aa	0.161235	1.222625		-0.501784	0.115608	-0.490976	0.098213		-0.703664	-0.37546	-0.483173	-1.61151	-0.986725	-1.829574
Ajap1	-0.20216	0.897561	-0.175255	-0.084537	0.175928	0.046053	-0.088596	-0.324133	-0.251024	-0.554933	-0.263915	-0.698374	-0.215343	0.0
Vps37b	0.400249	0.134196	0.241795	0.097916	0.434698	0.099977	0.119691	-0.341904	-0.20151	-0.289793	-0.562895	-1.49729	-1.398943	-1.335802
Tmem191c	0.620294	0.183944	0.795886	-0.354371	0.184427	0.098034	0.002109	-0.522872	-0.377847	-0.330123	-0.310739	-0.354865	-0.125949	-0.148815
Sema4a	0.406334	0.0	0.28652	-0.073806	0.303215	0.44823	0.326924	-0.287038	0.156174	-0.191441	-0.152932	-0.967792	-0.388764	-0.559829
Oscp1	0.383629	-0.02817	-0.0906	0.184793	0.304958	0.213264	0.178235	0.239126	-0.159014	-0.083641	-0.195161	-0.443087	-0.180733	-0.16567
Znrf1	0.147363	-0.184163	0.168325	-0.20935	0.137095	0.096945	0.283234	-0.336936	-0.241857	-0.36459	-0.237566	-1.253935	-0.834436	-0.839164
Grid1	0.193961	0.042983	0.282187	-0.102582	-0.377626	0.313186	0.499475	-0.458068	-0.123527	-1.246134	-0.251503	-0.593357	-0.678722	-0.612544
Igfbp3	0.608815	0.488279	0.597431	0.51202	0.214948	0.106488	-0.118844	-0.083473	-0.239845	-0.5324	-0.598345	-1.535895	-1.025079	-1.326558

Cluster 1 | Cluster 2 | Cluster 3 | Cluster 4 | Green = DEGS in GCs | Pink = DEGs in IONs

GENE NAME	IO_set0_E17	IO_set1_E17	IO_set2_E17	IO_set1_P0	IO_set2_P0	IO_set3_E17	IO_set3_P0	IO_set0_P0	IO_set0_P3	IO_set1_P3	IO_set3_P3	IO_set2_P3	IO_set1_P7
Ctxn2	-0.316831	-0.888036	-0.10573	-0.161331	-0.242661	-0.362198	-0.080699	0.936939	0.468303	-0.225213	0.658802	0.0	0.002988
Ehd1	0.0	-0.043152	0.058477	-0.155732	0.098856	-0.123087	-0.173877	0.489087	-0.078443	-0.063353	0.04491	0.152465	0.050502
Dos	-0.586114	-0.530687	-0.616607	-0.26462	0.023621	-0.747209	-0.12417	0.286821	0.0	-0.09987	0.597704	0.035805	0.228707
A730017C20Rik	-0.121487	-0.259473	-0.075654	0.003611	0.008877	-0.128203	-0.148776	-0.221782	0.039414	0.0	0.11537	0.097691	0.135508
Anxa2	0.135391	-0.060187	0.02024	-0.307783	-0.239019	-0.060297	-0.127346	-0.152354	0.280964	0.042113	0.253109	0.410761	0.173507
BC048546	1.385169	-0.797897	-0.762703	-0.578675	-0.095836	0.615953	0.059856	-0.376141	2.358805	0.54219	0.588624	0.518731	-1.168652
March11	0.042391	0.093245	0.080047	-0.412346	0.248426	-0.744971	0.067744	0.185635	0.038353	0.0	0.29921	-0.324834	-0.029251
Jakmip1	0.066801	-0.353899	0.063146	-0.288566	0.308235	-0.225401	0.314634	0.688953	0.314136	0.095363	-0.190523	-0.060675	0.413315
Gpr137b	-0.123022	-0.340599	0.286576	-0.193222	0.386515	-0.250336	0.433474	0.648157	0.159786	0.01507	0.503347	-0.041042	0.175069
Gpr45	-0.122191	-0.371877	0.081686	-0.44828	0.319149	-0.522408	-0.014658	0.48554	0.141684	-0.192969	0.186881	-0.478761	0.0
Grik2	-0.134392	-0.260761	0.02862	-0.081108	0.141516	-0.284466	-0.091934	0.561174	0.119027	0.0	0.201606	-0.248201	0.250347
Gp1bb	-0.324878	-0.561225	0.026445	-0.58727	0.350265	-0.924392	0.065601	0.721201	0.0	0.132358	0.237141	-0.229459	0.09005
S1pr3	-0.009358	0.045219	0.270449	0.019615	-0.19204	0.01724	-0.257536	-0.220205	0.616249	0.0	0.487126	-0.364892	0.528861
Tmie	0.049251	-0.375721	-0.48427	-0.081177	-0.042162	-0.538365	0.147614	9.94E-4	0.526736	-0.197005	0.364904	-0.198201	0.463164
Lypd6b	-0.231309	-0.808172	-0.095487	-0.359398	-0.178523	-0.99758	0.097177	0.733528	0.93006	-0.211209	0.566615	0.265584	0.83424
Lgals3	-2.142768	-0.68292	-0.069612	-0.596838	-0.195908	-0.729237	0.585353	0.232163	0.531078	1.498996	0.531478	0.473155	0.431089
Mboat7	-0.271187	-0.288885	-0.339728	0.24225	0.138298	-0.492362	-0.106164	0.083624	0.31023	0.242586	0.307967	0.432426	0.273293
Ipcef1	-0.275159	-0.439949	-0.405915	-0.131107		-1.384838	0.300733	1.477439	1.233677	0.377512	1.38284	0.372653	
Grm4	-0.035733	-0.637658	-0.189618	-0.70808	0.093224	-1.059784	0.005358	1.03203	0.607591	0.323673	0.38771	-0.005358	0.480697
E130311K13Rik	-0.298479	-0.470595	-0.134432	-0.513487	0.022426	-0.486098	0.10225	0.590797	0.509868	0.420185	0.460697	0.388747	0.18373
Gpr64	-0.470146	-0.34248	-0.497749	-0.080565	0.0	-0.51624	-0.294819	0.166747	0.261571	0.270273	0.242102	0.26351	0.343804
Ecel1	-0.270869	-0.286959	-0.405679	-0.194791	0.047585	-0.49095	-0.122711	0.428967	0.13272	-0.093175	0.447528	0.378876	0.524849
Kcnq5	-0.294826	-0.746632	-0.774326	-0.602927	-0.83749	-1.334076	-0.331309	0.684456	0.573374	0.394942	0.403379	0.039813	0.97759
Btbd11	-0.237537	-0.493961	-0.595211	-0.32883	0.0	-1.165141	-0.234616	0.189205	0.34345	0.262117	0.256714	0.083659	0.623055
Cacng5	-0.43085	-0.484614	-0.522141	-0.530065	0.281492	-1.057002	-0.144562	0.271697	0.70458	0.514858	0.754401	0.258295	0.932268
Adcyap1	-0.6813	-0.656161	-0.936092	-0.220733	-0.090427	-1.099183	-0.31453	0.023917	0.369732	0.242648	0.248335	0.310357	0.426132
Masp1	-0.048059	-0.075284	0.088842	-0.225609	-3.65E-4	0.139329	-0.091339	-0.114077	0.0686	0.0	0.102681	0.171306	-0.060709
Tctn2	-0.222546	-0.829005	-0.340252	-0.594072	-0.081493	0.167437	-0.288646	-0.495435	0.198682	-0.315957	-0.164797	0.047666	0.076394
Stap2	-0.747574	-0.517349	-0.332147	-1.155862	-0.47373	0.009597	-0.132729	-1.081502	-0.015821	-0.488574	0.133828	-0.80982	0.321004
Ptplad2 = Hacd4	-0.930634	-1.080276	-0.616689	-0.960503	-0.624848	-0.076535	-0.233923	-0.701442	-0.05081	0.0		0.330411	0.487752
Slc22a23	-0.354727	-0.420071	-0.576142	-0.236353	-0.101811	-0.446474	-0.323703	-0.203836	0.0	-0.169517	-0.199739	0.113384	0.320019
Mmp15	-0.360918	-0.452183	-0.277898	-0.386545	-0.00859	-0.117758	-0.658608	-0.172966	0.0	-0.041491	-0.081331	0.357197	0.569059
Tmem159	-0.652958	-0.799371	-1.177223	-0.516773	-0.283265	-1.168348	-0.572903	-0.442139	0.354916	-0.063402	0.0	-0.225776	0.822545
Crtac1	-0.769064	-0.75098	-0.658892	-0.413547	-0.309891	-1.020601	-0.589017	-0.526651	0.0	-0.272675	-0.190594	0.252772	0.289122
Sng5	-0.320037	-0.313705	-0.308852	-0.60623	-0.364953	-0.42528	-0.448415	0.247587	0.067674	-0.173451	-0.115638	0.0	0.125693
Tmem179b	-0.682719	-0.513049	-0.16239	-0.365215	-0.11275	-0.147417	-0.150587	-0.571604	0.0	-0.603619	0.050242	-0.20522	0.199545
Ppap2c	-0.188681	-0.237109	-0.294934	-0.428298	-0.097996	-0.480686	-0.424699	-0.255013	-0.073722	-0.100044	0.046045	-0.145641	0.125699
Ctla2a /// Ctla2b	-0.53982	-2.001866	-0.45884	-0.890621	-0.595327	-0.598665	0.0	-0.087132	0.157798	-0.465998	-0.323827	-0.632324	0.364406
Ctla2a	-0.159642	-0.468762	-0.635988	-0.229957	-0.056006	-0.35708	-0.011884	0.0	0.23547	-0.34259	-0.088869	-0.269717	0.440652
Tmem42	-0.371964	-0.47539	-0.22999	-0.551323	0.076362	-0.441936	-0.312396	-0.179065	0.208608	-0.237093	-0.071113	0.0	0.349418
Bai1	-0.44773	-0.231441	-0.228024	-0.472364	0.0	-0.790385	-0.312054	-0.10389	0.122932	0.094728	-0.120902	-0.110043	0.390491
1810041L15Rik	-0.51605	-0.752189	-0.67357	-0.632906	-0.196717	-1.037173	-0.73025	-0.406537	0.0	-0.18273	0.25963	-0.323737	0.394082
Rhbdd2	-0.699304	-0.476709	-0.745942	-0.134083	0.212726	-0.786426	-0.257796	-0.17882	0.045863	-0.180451	-0.2171	0.031504	0.095476
Abcg2	-0.342186	-0.380529	-0.201276	-0.363748	-0.080027	-0.384027	-0.08239	-0.276183	0.045936	-0.09429	-0.024074	0.15906	0.090616
Ifitm1	-0.72267	-0.929873	-0.640291	-0.861611	-0.582248	0.0	0.616515	-0.77449	-0.459718	-0.876118	-0.146886	-0.166641	0.030505
Gprc5c	-0.283869	-1.052315	0.0	-0.970176	-0.385985	-0.063246	0.037567	0.178236	-0.198015	-0.160201	-0.136483	-0.362175	0.257019
Cdh15	-1.519218	0.173221	-0.964433	0.118321	-1.053106	-0.235483	-0.835052	0.15286	0.668336	0.478635	-2.357896	-2.62999	0.0
Leprot	0.157878	-0.358327	0.169593	-0.487659	-0.098352	-0.146473	-0.001834	0.452592	0.04679	-0.040534	0.0	-0.201318	-0.037018
Gpr137b-ps	0.0	-0.469688	-0.056625	-0.447936	0.040616	-0.527721	0.023161	0.456828	-0.005059	-0.332687	0.077786	-0.320746	-7.39E-4
Dirc2	-0.404993	-0.360438	-0.245677			-0.424029		0.334811	-0.060281		0.122343		
Slc25a1	-0.153412	-0.317269	-0.126945	-0.175466	0.108604	0.046977	-0.169252	-0.264097	-0.154176	-0.173612	0.0	0.098109	-0.041112
Comp	-1.111412							-2.274023		-0.084675	-0.837204	-1.544039	0.096708
Cdon	0.001048	-0.219261	0.078197	-0.562028	-0.109476	-0.0687	-0.097138	-0.459403	-0.120928	-0.309904	-0.0044	-0.451591	0.122255
Rnaset2b = Rnaset2b+	-0.175545	-2.675248	-1.689304	-1.121659	-0.534992	-1.794493	-0.597256	0.116126	0.563274	0.001103	0.290411	-1.375008	0.0
S100a6	-2.199091	-1.672836	-1.685279	-1.308905	-0.736461	-1.655607	-0.226865	-0.705534	-0.041626	-0.316315	-0.212697	0.0	-0.200722
S100a4	-2.539343	-2.429536	-2.302221	-1.799532	-1.18806	-2.311942	-0.905477	-0.696693	0.184332	-0.99295	0.0	-0.442407	-0.323029
Gal	-0.334144	-0.591486	-0.812206	-0.444437	-0.041034	-1.560029	-0.541944	-0.215249	-0.020856	-0.43314	0.0	0.058613	0.017553
Ptprn	-1.080142	-1.023924	-0.900457	-0.577727	-0.195297	-1.591536	-0.351685	-0.262963	-0.067963	-0.19629	-0.002719	-0.216083	0.234326
Itgav	-0.611688	-0.750664	-1.04198	-0.46016	-0.55053	-1.592444	-0.790643	-0.31298	-0.108115	-0.444644	-0.216872	-1.132451	0.340602
Gpr22	-0.469027	-0.416583	-0.386572	-0.522639	-0.179978	-0.848749	-0.448772	-0.374052	-0.141091	-0.401381	-0.112751	-0.231939	0.130454
asap1	-0.304353	-0.458769	-0.545846	-0.284229	-0.103267	-0.997988	-0.311028	-0.110442	0.0	-0.151696	0.039877	-0.132708	0.312738
S100a10	-0.23308	-0.202193	-0.337104	-0.064768	0.0	-1.20637	-0.237316	-0.197558	0.067123	-0.322039	0.102609	-0.365539	0.253271
Lcn2	-1.762553	-1.554607	-1.515891	-0.701999	-1.150755	-0.842262	0.19389	0.0	-1.262098	-1.866172	-0.487018	-1.905914	-0.056805
Kcng1	-1.56216	-1.824204	-1.886104	-1.87071	-1.909154	-2.211701	-1.918213	-0.707045	-0.753174	-1.223416	-0.588932	-1.243223	0.074807
Htr5b	-1.537	-1.353326	-1.441055	-0.883359	-1.090915	-2.130979	-1.354994	-0.7132	0.0	-0.99985	-0.168251	-0.273509	0.103922
Gpr88	-0.22926	-0.808198	-0.629052	-0.646943	-0.609883	-1.009099	-0.71947	-0.191781	0.117641	-0.541836	-0.153156	0.0	0.179376
Sema4f	-0.001434	-0.144339	-0.055029	-0.224917	0.009984	-0.45894	-0.235776	-0.063229	0.00694	-0.11521	-0.159783	-0.27343	0.019081
Unc13c	-1.145306	-1.239007	-1.555357	-1.144212	-1.06163	-1.47449	-1.345264	-0.832233	-0.380979	-0.893659	-0.985807	-0.419716	0.0
Pcolce	-1.049832	-1.361083	-1.186942	-0.876871	-0.41894	-1.361413	-0.896728	-0.868993	-0.539381	-0.832377	-0.669873	-0.659859	0.008956
Sh3gl2	-1.013858	-0.854747	-0.966715	-0.597077	-0.466729	-0.864369	-0.746546	-0.601138	-0.287792	-0.621721	-0.377835	-0.228877	-0.005153
Rock2	-0.459814	-0.595212	-0.748955	-0.3995	-0.369262	-0.566194	-0.544744	-0.421453	-0.141259	-0.544172	-0.282848	-0.398338	0.068006
Plxdc1	-2.54991	-2.654814	-2.414274	-2.251602	-2.071759	-2.4199	-2.111113	-1.831678	-0.846754	-1.163142	-1.057378	-0.847423	0.137052
Laptm4b	-1.178251	-1.206771	-1.299466	-1.494139	-1.070699	-1.509948	-1.247336	-0.386756	-0.398905	-0.55344	-0.537003	-0.407983	0.0
Inadl	-1.65342	-1.880691	-1.798571	-1.420315	-1.292175	-1.957325	-1.191291	-1.120783	-0.417388	-1.337487	-0.781239	-1.196672	0.0
Kcnk12	-2.111605	-1.626618	-2.227046	-1.640774	-2.039626	-2.535045	-1.485993	-0.467885	-1.069814	-0.844025	-0.548558	-0.84627	0.173967
Mfsd6	-0.745611	-0.815246	-0.994931	-0.481249	-0.421863	-1.057917	-0.648145	-0.38686	-0.135109	-0.264022	-0.111203	-0.134214	0.078764
Nat8l	-1.797172	-1.506589	-1.712126	-1.468651	-0.996446	-1.64631	-1.54468	-1.34308	-0.911857	-0.861278	-1.086976	-0.921168	0.012186
Lgi2	-1.285162	-1.157696	-1.246996	-0.804139	-0.62507	-1.550238	-0.914265	-0.769575	-0.295301	-0.478992	-0.391556	-0.035351	0.103697
Alox5ap	-0.896326	-1.348699	-1.562699	-1.046762	-1.250166	-1.533895	-0.742367	-0.814045	-0.259921	-0.558476	-0.421273	-0.584374	0.124196
Gabrd	-2.385436	-2.875785	-2.442311	-2.288592	-2.482483	-2.692284	-2.705654	-1.75892	-0.237037	-0.784214	-0.538553	-1.244247	0.098177
Tmem14a	-1.37888	-1.532001	-1.058269	-0.984693	-0.704171	-0.946719	-0.975739	-0.756172	-0.230809	-0.547277	-0.927677	-0.267612	-0.443164
Il17re	-1.672168	-3.26636	-2.277001	-2.115902	-1.68712	-2.299722	-2.248252	-1.974552	-0.684391	-0.594699	-1.290785	-0.687821	-0.243145
Fstl1	-0.921869	-0.967898	-1.109552	-1.00267	-0.719564	-1.05499	-0.566465	-0.890367	-0.337795	-0.672775	-0.579735	-0.242848	0.0
Ifi27l1 = Ifi27	-1.535101	-1.901185	-1.337181	-1.527635	-1.06578	-1.814201	-0.906585	-0.272841	-0.214466	-0.54618	-0.30229	-0.425047	-0.084734
Dnaja4	-0.806546	-1.2569	-0.925792	-1.078231	-0.559658	-1.248051	-0.802642	-0.030196	-0.21918	-0.617734	-0.30863	-0.788618	-0.068203
Fxyd1	-2.416814	-1.711008	-1.959064	-1.298272	-0.996962	-2.245927	-0.902004	-0.792012	-0.6195	-1.037768	-0.41256	-0.949966	-0.161268
Cnksr2	-0.266741	-0.561474	-0.540059	-0.48945	-0.399341	-0.554998	-0.645658	0.223753	-0.328633	-0.878532	-0.356825	-0.73483	0.0
Popdc3	-0.902387	-0.947365	-0.904696	-1.081207	-0.600104	-0.717506	-0.394304	-0.323753	0.190492	-0.399836	0.0	-0.217636	-0.161745
ccl5	-1.515684		-2.056974	-0.891122		-3.734718	-3.139697		-1.397327	-1.770709	-1.992794	0.010694	-0.493998
Stxbp5	-0.468614	-0.595324	-0.627469	-0.173609	-0.119417	-0.238154	-0.199848	-0.309814	-0.080792	-0.368187	-0.133077	-0.240695	0.125059
Pex5l	-1.734451	-1.58091	-1.786795	-0.798803	-0.741817	-1.806448	-1.332269	-1.112973	-0.445035	-0.773188	-0.549842	-0.441205	0.063615
Asph	-0.714422	-0.696194	-0.72079	-0.407348	-0.36489	-1.003171	-0.436785	-0.466393	-0.148036	-0.308963	-0.213005	-0.181383	0.112012
Thy1	-2.439976	-1.957687	-2.56535	-1.692905	-1.255287	-2.970339	-1.384837	-1.452138	-0.553947	-0.854086	-0.469536	-0.574871	0.0
Adam23	-1.180405	-1.082826	-1.248768	-0.753056	-0.548627	-1.430379	-0.677893	-0.655016	-0.247274	-0.546039	-0.294866	-0.531614	0.157289
Cd151	-0.378363	-0.376691	-0.286126	-0.549559	-0.246345	-0.530405	-0.392059	-0.389245	0.0	-0.413246	-0.200669	-0.305998	-0.079503
Tnfrsf11b	-0.736015	-0.61878	-1.46746	-0.753234	-0.607239	-1.135367	-0.352728	-0.644155	-0.064571	-0.918711	-0.223535	-0.643955	-0.060116
Crtam	-0.701178	-1.331226	-1.237439	-0.835829	-0.24088	-1.315729	-0.358896	-0.129501	0.322333	-0.396409	0.0	-0.401183	-0.221468
C3	-1.203662	-4.04291	-0.904188	-3.901676	-3.090154	-2.504461	-2.92112	-4.710883	-0.252188	-2.880585	-3.054382	-4.064432	0.0
Arhgap15	-1.720133	-0.409262	-1.070561	-1.608271	-0.055794	-0.707761	-0.503395	-0.740819	0.378657	-0.774909	0.103562	-0.393158	0.0
Vasn	-0.580707	-0.605007	-0.686608	-0.521202	-0.130337	-0.569034	-0.326571	-0.380524	-0.031005	0.0	-0.173916	0.439578	0.10058

Cluster 1 | Cluster 2 | Cluster 3 | Cluster 4 | Green = DEGS in GCs | Pink = DEGs in IONs

GENE NAME	IO_set2_P7	IO_set0_P7	IO_set3_P7	IO_set0_P14	IO_set2_P14	IO_set1_P14	IO_set3_P14	IO_set0_P21	IO_set1_P21	IO_set2_P21	IO_set3_P21	IO_set0_Adult	IO_set3_Adult	IO_set1_Adult
Tspan31	0.594152	-0.205523	0.0	0.698926	1.08027	0.123499	0.577911	0.681132	0.488939	0.891263	0.377173	-0.354407	0.272817	-0.216994
Tmem204	0.189185	0.0	0.254135	1.206017	1.61029	1.255497	1.223662	1.075858	0.96761	1.273644	1.004532	-0.041775	0.167833	0.002725
Tmem180	0.395428	0.0	0.455302	0.615547	1.153861	0.975109	1.04642	0.698084	0.910251	0.828412	0.815503	-0.308066	0.238545	0.116088
Zdhhc22	0.511598	0.0	0.4452	0.858317	1.092548	0.885186	0.95375	0.458347	0.752372	0.790057	0.795163	-0.254928	0.160563	0.151142
Tmem19	0.459282	0.102105	0.329345	0.98552	1.20009	0.950183	0.991877	0.788055	0.782288	1.020155	0.765797	-0.386468	0.187869	0.0
Shisa4	0.826545	0.284614	0.495292	1.272965	2.017575	1.618273	1.867748	1.39159	1.395391	1.618819	1.278685	-0.12881	0.07906	-0.080168
Ninj1	0.740411	0.461871	0.546016	1.478398	1.560063	1.654346	1.435564	0.914017	0.801219	0.943706	0.656369	-0.135267	0.133432	0.0
Sln	0.977242	-0.629596	0.630276	1.651749	4.049346	2.742476	2.574258	1.986272	1.820032	3.360396	3.791799	-0.344323	-0.071514	0.073294
Tm6sf1	0.276629	0.042005	0.446114	0.535089	0.93541	0.734752	0.909173	0.316193	0.76162	0.585855	0.696908	-0.40623	0.294352	0.0
Ache	0.39237	0.340473	0.386966	0.511014	0.958719	0.664109	0.557849	0.374489	0.677199	0.581815	0.606948	-0.312762	0.35182	-0.07373
Elmo1	0.219078	-0.117818	0.217744	0.458841	0.878275	0.580202	0.654286	0.609593	0.591652	0.649954	0.517956	-0.315404	0.207471	0.0
Fuca2	0.18457	0.005725	0.125285	0.384716	0.669649	0.542896	0.559061	0.432985	0.566996	0.307883	0.350599	-0.04114	0.20558	0.009994
Itm2a	0.332682	0.062474	0.390513	0.620984	1.083079	0.678409	0.59439	0.82681	0.688865	0.513204	0.49752	-0.295628	0.392717	0.0
Gpr123	0.158277	0.023034	0.114955	0.410167	0.634459	0.462678	0.494734	0.320771	0.514039	0.48155	0.237352	-0.27649	0.0	-0.024994
Resp18	0.363517	0.143575	-0.018682	0.304819	0.573061	0.361919	0.439305	0.471027	0.694172	0.314186	0.215222	0.0	0.061749	0.162697
Tgfbr2	0.286479	0.226125	0.125175	0.29693	1.256761	0.935789	1.052914	0.542844	0.794896	0.655925	0.870045	-0.132289	0.042845	0.145648
Lpl	0.183226	0.030373	0.0135	0.417503	1.196701	0.553813	1.147921	0.272957	0.453883	1.001455	0.15367	-0.041231	0.080292	-0.220672
Acsl5	0.075157	0.037742	-0.037257	0.105086	0.201324	0.104404	0.219485	0.139119	0.26728	0.089084	0.048369	-0.502028	0.035438	-0.091477
Nrxn3	0.251838	-0.032335	-0.04551	0.259961	0.723029	0.326656	0.246505	0.205202	0.336106	0.256853	0.084509	-0.202887	0.207075	0.054043
Tspan12	0.38779	0.336201	0.200762	0.563526	0.712891	0.26024	0.28539	0.42882	0.532319	0.605634	0.239193	-0.339159	0.0	-0.096629
Cx3cl1	0.289703	0.201935	0.095274	0.555552	0.548367	0.434316	0.350387	0.238143	0.553627	0.435745	0.371845	-0.356774	0.0	0.163948
Chn2	0.224408	0.287955	0.0	1.746469	1.242815	1.207071	1.026124	1.200374	1.199377	1.171558	1.034523	-0.292381	0.098196	0.058161
Vegfb	0.578036	0.0	0.291708	-0.087339	0.398002	0.223536	0.35526	-0.105952	0.407543	0.5587	0.420773	-0.27059	0.336509	0.076622
Cd164l2	0.594174	-0.132773	0.209306	0.245896	0.62203	0.525095	0.433176	0.091213	0.346999	0.675826	0.796978	-0.038612	-0.106046	-0.470528
Tmem179	0.454922	-0.007512	0.2961	0.363498	0.723864	0.581393	0.654159	0.22885	0.452703	0.43552	0.349482	-0.485706	0.164505	0.0
Tmed10	0.336419	0.0	0.138982	0.327116	0.64497	0.340111	0.433155	0.415308	0.334112	0.497822	0.260935	-0.326962	0.159663	-0.091576
Cyb561	0.295932	-0.210404	0.214171	0.004451	0.67483	0.369874	0.384797	0.210921	0.624874	0.539552	0.536623	-0.383812	0.368291	-0.023664
Il16	0.123376	0.083838	0.027504	-0.332235	0.782602	0.369543	0.419876	-0.040476	0.653459	0.616713	0.193735	0.0	0.29043	0.038429
B2m	0.511118	0.129007	0.094692	-0.114477	0.814836	0.057788	0.195684	0.612322	0.886491	1.007973	0.601803	-0.049158	0.27058	0.153892
Timp2	0.223665	0.0	0.070128	0.14767	0.431923	0.238766	0.122315	0.177644	0.231771	0.40409	0.258085	-0.172911	0.405892	0.219372
Slc4a2	0.253403	-0.199526	0.055686	1.249266	1.666112	1.308021	1.482358	1.485373	1.556244	1.821631	1.755083	0.698317	0.806605	0.669231
Slc17a7	0.553547	0.0	0.234521	1.663335	2.068236	1.782668	2.376211	2.278004	1.638278	1.912831	1.84777	0.783737	1.321022	1.106577
Sytl2	0.162508	-0.267979	0.160821	1.323253	1.667382	1.565454	1.722351	1.259471	1.634717	1.634456	1.436159	0.555943	1.16418	0.955546
Spns2	0.47832	-0.011921	0.209183	0.866277	1.298942	1.206908	1.241946	1.125446	0.954869	0.905762	0.783856	0.408556	0.630717	0.404532
Slc20a1	0.221121	-0.205161	0.0	1.339204	1.643497	1.452666	1.482629	1.516849	1.529885	1.626468	1.478489	0.919181	1.256732	0.92632
Gabra6	0.83422	-1.997874	0.523985	1.652046	4.955843	2.766586	2.860714	3.265921	0.695887	4.250506	3.76761	0.304725	1.222368	1.929682
Pmepa1	0.493742	-0.139297	0.175774	1.357152	1.343901	1.188099	1.169922	0.981333	0.928536	0.998507	0.90741	0.0	0.282399	0.105722
Npc2	0.32505	-0.058438	0.1443	1.121437	1.375385	1.115331	1.047731	1.294105	1.186248	1.362203	0.967629	5.97E-4	0.277786	0.067797
Syt12	0.227472	0.0	0.087336	0.874488	1.185301	0.981474	0.896782	0.922196	0.882166	0.859318	0.705652	-0.133589	0.442415	0.237924
Serpinf1	0.332451	0.110832	0.315152	1.049421	1.535975	1.05314	1.0832	1.351994	0.911908	1.113986	0.829876	-0.04967	0.285434	0.413019
Rab7l1 = Rab29	0.638453	-0.076578	0.0	0.80989	1.108643	0.901872	0.75817	1.024219	1.221741	1.174653	0.997414	0.17131	0.57576	0.457806
Atp1b1	0.326509	-0.03031	0.052227	0.796831	0.909355	0.804313	0.657465	0.909353	0.839868	0.881489	0.762826	0.00876	0.468061	0.232429
Tmem184b	0.176016	-0.116092	0.134435	0.505017	0.905988	0.617868	0.614349	0.615488	0.849432	0.701562	0.484259	0.032662	0.529578	0.328769
Smpdl3a	0.308542	-0.037351	0.089661	0.561915	0.946059	0.538333	0.615188	0.682532	0.683307	0.909091	0.580463	0.028916	0.300639	0.10963
slc24a5	0.49355	-1.265001	0.0	1.808602	2.285768	2.150471	2.047293	2.690077	2.076069	1.873412	1.825843	0.941643	1.557391	1.14579
Amhr2	-0.132605	-1.864277	0.414066	1.505304	1.94067	2.256313	1.92139	1.077218	1.672926	1.400907	1.599538	0.805657	0.949417	0.132605
Mrvi1	0.104953	-0.391229	0.401447	1.978129	1.400181	1.540925	1.401039	1.263219	2.345383	1.478754	0.747176	1.035955	1.16113	1.111396
Tmem205	0.081637	0.0	0.106587	0.317024	0.571167	0.753763	0.756804	0.491952	0.880154	0.864304	0.713759	-0.360635	0.231695	0.238444
Il10rb	0.136438	-0.053064	0.269266	0.205039	0.549547	0.591985	0.586656	0.355817	0.635661	0.38371	0.476457	-0.147018	0.32205	0.144241
Srgn	0.0	-0.209719	0.211179	0.373945	1.200705	0.808531	0.915455	0.764905	1.13973	1.002438	0.834276	0.240245	0.810479	0.648755
Adam11	0.04003	-0.139206	0.217984	0.5665	0.86636	0.836806	0.93904	0.719156	0.959864	0.598847	0.741615	0.070485	0.173043	0.239493
CxCl12	0.0	-0.068438	0.191721	0.875594	1.289738	1.184124	1.239805	1.112531	0.963166	0.470562	1.218589	0.162822	0.353002	0.408723
2010011I20Rik = fam210b	0.361334	-0.186512	-0.01751	0.304964	0.478883	0.65139	0.681245	0.500395	0.579842	0.874121	0.669822	-0.146813	0.219166	-0.092201
Rell2	0.326872	-6.34E-4	0.338139	0.38199	0.74982	0.575089	0.657578	0.674834	0.485729	0.678926	0.250138	0.119101	0.882332	0.197025
Kcnc1	0.403045	-0.108592	0.0	1.374226	1.610031	1.453917	1.116287	1.555191	1.601399	1.467923	1.327611	1.034907	1.427463	1.238189
Kcnh2	0.026495	-0.222396	0.103116	0.747471	1.008248	0.868151	0.764955	1.182717	0.982205	0.77245	0.841968	0.491368	0.893066	0.713596
Dnajc15	0.076799	-0.106872		0.611745	0.781619	0.635083	0.53477	0.803593	0.74637		0.547468	0.302101	0.701149	0.458515
Clu	0.203479	-0.102533	0.242591	0.569662	0.816734	0.583655	0.432735	0.617681	0.910673	1.047341	0.552518	0.366212	0.644232	0.454611
Crh	0.0	0.283073	0.807745	1.387353	2.115256	1.040454	1.807591	1.286644	1.610579	2.037883	1.936453	1.049229	1.487614	-0.112297
Cd302	0.279166	-0.019068	0.465201	0.410981	0.496629	0.042846	0.18586	0.210627	0.151312	0.446626	0.146599	-0.053063	0.450263	0.0
Bmp5	0.061711	0.0	0.295931	0.468822	0.444519	0.487486	0.287112	0.702624	0.46579	0.209535	-0.056942	0.191438	0.214524	0.247423
Mgp	-0.105632	-0.444038	0.677699	2.169847	2.340515	2.251028	2.051269	2.710426	2.289511	2.38839	2.028365	1.538893	1.927239	1.404268
Ctgf	-0.185699	0.071341	0.423142	1.323698	0.936506	0.433181	0.764754	1.224283	0.850591	0.698329	0.249187	0.0	0.134361	-0.003481
Wnt7a	0.069456	0.230299	0.364102	-0.174483	0.16529	0.685214	0.351855	0.038378	0.61864	0.385631	0.825573	-0.247978	0.170389	0.0
Susd4	0.094214	0.362056	0.131838	0.0	0.30969	0.244136	0.742784	-0.128166	0.466606	0.119207	0.319899	-0.403445	0.213353	0.028348
Kcna6	0.176793	0.118143	0.213886	0.088562	0.128824	0.30573	0.288674	0.184643	0.41783	0.0	0.286234	-0.226455	0.178683	-0.007264
Egfl7	0.246332	0.065699	0.520013	0.071047	0.339355	0.530568	0.728358	0.0	0.683202	0.245691	0.539311	-0.354489	0.439946	0.467046
Diras2	0.187757	0.381449	0.303676	0.137524	0.391325	0.153506	-0.032621	0.149505	0.228601	0.286797	0.0	-0.061191	0.235991	0.204288
Cartpt	0.0	0.405635	0.282222	-0.223031	0.044448	0.129327	-0.27627	0.102167	0.463389	0.577326	0.614288	-0.007064	0.433513	0.200845
Nrcam	-0.238278	0.197559	-0.090954	0.231147	0.240052	0.420216	0.127344	0.283175	0.713822	0.0	0.150173	-0.284077	0.272577	0.190424
Cntnap2	0.019859	-0.016097	-0.03188	0.354689	0.189155	0.301015	0.189749	0.275414	0.3686	-0.062517	0.04205	0.011395	0.368639	0.318032
Tnfrsf21	-0.02094	0.0	0.035222	0.448133	0.623921	0.501917	0.636529	0.416714	0.484899	0.152046	0.235129	-0.702738	0.24133	0.024594
Gm4980	0.181784	0.538662	0.717943	1.421511	1.609682	1.696698	1.619457	0.568118	1.080208	0.396411	0.744532	-0.702764	0.314308	0.0
Dusp15	0.735549	0.551806	0.75098	1.169297	1.568392	1.530893	1.57742	1.081199	1.034024	0.634597	0.930869	-0.260181	0.241983	-0.092581
0610007L01Rik = Tmem248	0.009005	0.0	0.186974	0.533358	0.527148	0.58898	0.447205	0.41247	0.41231	0.425064	0.33025	-0.278289	0.154399	-0.032874
Clec10a	-0.451323	0.011676	1.176108	1.35783	1.751736	1.990494	1.281153	-0.157876	1.986255	1.743934	0.759307	-1.86725	0.0	0.495224
C1ql1	0.477757	0.745462	0.34488	0.843994	1.01099	0.9583	0.71765	0.021966	0.632684	1.030126	0.452847	0.0	0.720311	-0.271553
C1ql1	0.117147	0.669192	0.496714	0.675109	0.884977	0.831149	0.673397	0.006442	0.555431	0.447342	0.321495	0.0	0.114146	-0.222173
C1ql1	0.183975	0.697164	0.468647	0.702184	1.080127	0.900009	0.668206	0.086956	0.585414	0.969136	0.626049	-0.045474	0.366073	-0.513213
C1ql1	0.061542	0.732899	0.290679	0.678034	0.955164	0.515676	0.561755	0.171316	0.602646	0.324112	0.507581	-0.067353	0.195663	-0.355227
Dock4	0.0	-0.235626	0.042511	0.359779	0.616805	0.809936	0.598976	0.175572	0.461013	0.165612	5.86E-4	-0.137166	-0.060175	0.046486
Cbln3	0.88665	-0.019994	0.187506	0.767615	3.071064	1.378177	1.572928	1.268808	0.663178	1.982802	2.128478	-0.850562	-0.225252	0.868402
Boc	0.263962	0.020348	0.0	0.275878	0.249223	0.576135	0.137515	0.069998	0.460654	0.240184	0.140444	-0.432364	-0.125415	0.679753
Rnaset2a	0.412116	0.211225	0.054392	0.723316	0.932798	0.496711	0.454832	0.393208	0.060542	0.291848	0.0	-0.028246	-0.08619	0.097891
Vstm2a	0.609016	0.287432	0.0	0.124919	0.503294	0.134811	0.034571	0.019011	0.094362	0.354413	-0.138638	-0.591248	-0.079931	-0.40107
Pde2a	0.533446	0.20406	0.137544	0.172044	0.469712	0.10685	0.326879	0.392459	-0.057155	0.034613	-0.130816	-0.432381	-0.1217	-0.249605
Dgcr2	0.047797	0.080419	0.0	0.263555	0.308772	0.109417	0.129507	0.222525	0.228812	0.004567	0.06818	-0.699365	-0.31412	-0.334301
Cnih3	0.387762	0.411818	0.152483	0.276173	0.358209	-0.164429	0.0	-0.220406	0.228122	0.141452	0.431044	-0.049751	0.376016	-0.084008
Armcx2	0.222321	0.001225	-0.196303	-0.232299	0.058854	0.189616	-0.022591	0.064919	0.168449	0.0	-0.006968	-0.54386	0.120182	-0.3955
Kcnq2	0.155118	-0.126808	0.281596	-0.072403	0.203274	0.204909	0.367799	0.031342	0.23398	-0.285558	0.131811	-0.135516	0.162272	0.071027
Emb = Pou6f1	0.437142	-0.009536	0.171073	0.11007	0.110828	0.378272	0.174292	-0.083548	0.17697	-0.493743	-0.166607	-0.181106	0.045821	0.038617
Evc2	0.183833	-0.028127	0.144428	-0.024567	0.18408	0.362134	0.0	-0.386039	0.231023	0.16286	0.219683	0.266193	0.38258	0.497693
Tspan9	0.330316	0.312152	0.404365	0.337016	0.581121	0.248217	0.305947	0.330589	0.553419	-0.180923	0.024315	-0.995985	-0.641959	-0.68562
Pcdh20	0.326929	0.357278	0.414975	0.312605	0.303735	0.293101	0.247024	-0.140053	0.335371	0.162369	0.261475	-0.800065	-0.211278	-0.258437
Rab6b	0.552547	-0.037064	0.164048	0.08438	0.434993	0.195869	0.213863	0.0	0.231225	0.140032	0.147156	-0.478408	-0.116155	-0.362322
Qpctl	0.667185	0.105465	0.293668	0.165468	0.564704	0.304781	0.262659	-0.068757	0.0	0.174297	-0.03115	-0.574244	-0.335772	-0.364176
Atp13a2	0.457206	0.058965	0.160038	0.097144	0.170103	0.216029	0.060515	-0.111993	0.015693	0.047511	0.0	-0.89275	-0.569371	-0.794246
Casc4	0.548084	0.340205	0.489977	0.0	0.633576	0.457881	-0.066678	-0.097789	0.39381	0.3899	-0.256304	-0.568062	-0.55139	-0.553449
Syngr3	0.767683	0.358283	0.559222	0.049938	0.378908	0.338015	0.510292	0.0	-0.028634	0.015215	-0.070027	-0.910565	-0.255008	-0.41154
Crtap	0.558258	0.128422	0.57796	0.138351	0.5192	0.286716	0.311263	0.051258	0.0	-0.143372	-0.31339	-0.804939	-0.586882	-0.700606

Cluster 1 | Cluster 2 | Cluster 3 | Cluster 4 — Green = DEGS in GCs — Pink = DEGs in IONs

GENE NAME	IO_set0_E17	IO_set1_E17	IO_set2_E17	IO_set1_P0	IO_set2_P0	IO_set3_E17	IO_set3_P0	IO_set0_P0	IO_set0_P3	IO_set1_P3	IO_set3_P3	IO_set2_P3	IO_set1_P7
Chid1	-0.516799	-0.376495	-0.351951	-0.374817	-0.236676	-0.501269	-0.476713	0.242231	-0.077099	0.055962	0.027513	0.205432	0.138629
Gabrg1	-0.395563	-0.692164	-0.445324	-0.469269	-0.15297	-0.637135	-0.168175	0.210724	0.107934	-0.03993	0.049259	0.091536	0.305473
Dlgap1	-0.567314	-0.287916	-0.801308	-0.23461	-0.20774	-0.876961	-0.427001	0.277014	0.008107	0.0	-0.004038	0.183258	0.359268
Slc24a3	-0.294264	-0.258256	-0.40547	-0.033682	0.107154	-0.673097	-0.22857	0.157739	0.480107	0.255034	0.253744	0.443734	0.632476
Prmt8	-0.124695	-0.211223	-0.25391	0.0	0.116821	-0.197925	-0.138947	0.161424	0.482314	0.104901	0.303704	0.361848	0.708905
Oprl1	-0.024403	0.032814	-0.186769	-0.295129	-0.161132	-0.021796	-0.428085	-0.065715	0.247705	-0.150637	0.261809	0.320477	0.484986
Olfm3	-0.25892	-0.217906	-0.334017	-0.267654	-0.0527	-0.485853	-0.255698	0.0	0.32133	0.21652	0.192531	0.394289	0.611514
Cthrc1	-0.614154	-0.896601	-0.436676	-0.639866	-0.772217	-1.286512	-0.032791	-0.09027	0.622139	0.384426	0.028571	0.491193	1.215194
Bgn	-0.937092	-0.973624	-1.110791	-1.201534	-0.741555	-0.834594	0.24411	-0.483998	0.184672	0.0	0.204896	0.240265	0.632977
Lhfpl5	-0.813097	-0.43784	-0.428454	-0.272106	-0.138443	-0.476009	-0.23199	0.26711	0.00539	0.226227	0.31332	0.562908	0.265781
Gpx3	-0.531873	-0.32888	-0.412441	-0.329014	-0.153306	-0.744461	-0.403172	-0.022656	0.209369	0.0607	0.235678	0.368932	0.326176
Ap2a2	-0.30692	-0.101671	-0.199081	0.034487	0.127876	-0.233194	-0.132474	0.039979	0.147523	0.058876	0.218623	0.447536	0.317153
Gpr26	-0.473666	-0.581519	-0.634015	-0.6853	-0.299368	-0.782032	-0.644628	0.226216	0.079488	-0.433287	0.043992	-0.326119	0.391062
Gabra4	-0.293616	-0.504911	-0.422053	-0.341633	-0.114319	-1.06839	-0.523509	0.686175	0.416075	-0.079108	0.341514		0.645926
Gpr176	0.016242	-0.447657	-0.120792	-0.697819	-0.044089	-0.738383	-0.212896	0.704471	0.229675	0.0	0.157954	-0.24517	0.467387
Fam19a1	-0.291736	-0.653982	-0.322633	-0.580124	-0.04454	-0.840301	-0.135261	0.253241	0.006512	-0.072987	0.119926	-0.1167	0.322509
Cadps2	-0.367695	-1.521262	-0.16038	-0.456016	-0.837782	-1.231625	-0.486186	-0.056225	0.266945	0.098522	0.028678	-0.33684	0.385963
A930038C07Rik = Ndnf	-0.161709	-0.279413	-0.666266	-0.13888	-0.067602	-0.758576	-0.55846	-0.024445	0.187761	-0.222243	0.177278	0.080744	0.532848
Adcy2	-1.705927	-0.649415	-0.89317	-0.5693	0.0	-1.507313	-0.601828	-0.20715	0.3795	-14.932629	-0.805448	-12.595935	0.374693
Dlg4	-0.302189	-0.318347	-0.429518	-0.169043	-0.233447	-0.631153	-0.568706	0.340987	0.050617	-0.205851	-0.236545	0.085047	0.140335
Copz2	-0.391218	-0.779026	-0.381458	-0.887842	-0.652933	-0.388485	-0.34286	0.325626	0.0	-0.178173	-0.168764	-0.313373	0.08268
tex2 = Tex21	0.601072	0.55875		0.734197		-2.086328	-1.864232	-1.57418	0.727674	-0.929245	0.117754	1.080694	-0.349058
Lemd1	0.388344	0.114519	0.694314	-0.05539	0.557691	0.18176	0.115095	0.154528	-0.006341	-0.695019	0.109841	-0.324796	-0.231765
Jup	0.0	-0.312622	0.047813	-0.218677	0.046667	-0.26678	-0.15633	0.338576	-0.497966	-0.233896	-0.27933	-0.44951	-0.421053
Fzd7	0.230105	-0.11445	0.08991	-0.215472	-0.031567	-0.229458	-0.07909	0.333339	-0.186229	-0.129519	0.0	0.016018	-0.077751
Fgl2	0.413467	0.060602	0.360116	-0.004572	0.241694	0.0	0.102652	0.125273	-0.375033	-0.484503	-0.350215	-0.212508	-0.418633
Tgfbi	-1.555208	-1.507381	-0.868514	-1.205768	-1.246064	0.70111	-0.24375	-1.142873	-0.632291	-1.05537	-0.517055	-0.341262	0.0
Cxcr7	-0.693982	-0.499	0.966447	-2.431759	-2.228992	0.962538	-1.304301	-1.620665	-1.005451	-0.30796	0.0	-0.146076	-0.068947
Prss23	-0.398903	-0.774128	-0.248236	-0.447549	0.0	0.067001	0.036565	-0.429013	-0.008409	-0.47883	-0.425224	-0.036467	-0.383304
Mbl2									0.354807				-0.354807
Nrsn2	-0.53075	-0.628422	-1.273213	-0.906047	-0.548907	-1.362483	-0.612706	-0.689904	0.08378	-0.581845	-0.062594	-0.070889	0.0
H2-T10 /// H2-T22 /// H2-T9	-1.694156	-1.793559	-1.568825	-2.03816	-1.85625	-2.13539	-1.769025	-0.243711	0.0	-0.127679	0.452381	-0.141898	0.468634
Ier3	-0.423645	-0.545562	-0.443509	-1.170123	-0.212759	-0.959849	-0.325271	0.118679	-0.279298	-0.579129	0.0	-0.382497	-0.034526
Aqp6	-0.055663	-0.068279	-0.001249	-0.636723	-0.293009	-0.141331	-0.867377	-0.292469	-0.239238	-0.037365	0.459217	0.0	-0.2806

GENE NAME	IO_set2_P7	IO_set0_P7	IO_set3_P7	IO_set0_P14	IO_set2_P14	IO_set1_P14	IO_set3_P14	IO_set0_P21	IO_set1_P21	IO_set2_P21	IO_set3_P21	IO_set0_Adul	IO_set3_Adul	IO_set1_Adult
Chid1	0.336191	0.074486	0.267914	0.032932	0.48115	0.248328	0.207425	0.0	0.01834	-0.053623	-0.293219	-0.642692	-0.40845	-0.505521
Gabrg1	0.455669	0.227829	0.465396	0.247115	0.492667	0.117866	0.248492	-0.111378	0.0	-0.031536	-0.244406	-0.354689	0.002038	-0.223091
Dlgap1	0.298919	0.212492	0.296936	0.255491	0.417806	0.224298	0.210858	0.113289	-0.012498	-0.056081	-0.193427	-0.24737	-0.192832	0.06397
Slc24a3	0.517662	0.646227	0.362774	0.396027	0.262535	0.201276	-0.016877	-0.08518	-0.033818	0.0	-0.145281	-0.417607	-0.259364	-0.139712
Prmt8	0.682862	0.70211	0.51498	0.131385	0.396614	0.124854	-0.018623	-0.180422	-0.137056	-0.024247	-0.154702	-0.495767	-0.17663	-0.40517
Oprl1	0.63814	0.384499	0.32729	0.222007	0.507457	0.110091	0.103305	0.08002	-0.059503	0.0	-0.174866	-0.737365	-0.209963	-0.372818
Olfm3	0.581519	0.466169	0.471688	0.291435	0.195476	-0.040516	0.061824	0.098017	0.031228	-0.179642	-0.014987	-0.847158	-0.445077	-0.417012
Cthrc1	1.581742	0.729759	1.174011	0.0	-0.046192	-0.146622	0.718961	0.600711	0.539988	0.206584	0.267665	-0.778864	-1.318473	-1.591126
Bgn	0.560962	0.519255	0.922319	-0.192487	0.44146	0.415389	0.475707	0.098479	0.061886	-0.061128	-0.204161	-1.758741	-1.409516	-1.897099
Lhfpl5	0.553712	0.295318	0.554782	-0.067714	0.251264	0.0	-0.03011	-0.083458	0.044238	0.129482	0.101322	-0.581048	-0.177078	-0.17052
Gpx3	0.387687	0.340972	0.408486	0.110666	0.227361	-0.132153	-0.201178	-0.007109	0.3617	0.0	0.158469	-0.498927	0.093633	-0.366742
Ap2a2	0.23401	0.20975	0.289262	0.001571	-0.089739	-0.275678	-0.122263	-0.071448	0.03262	0.0	-0.072145	-0.792426	-0.446608	-0.38911
Gpr26	0.147938	0.188969	0.210182	0.16584	0.113093	0.262019	0.221605	-0.344007	0.159191	-0.127083	0.0	-0.157368	0.078953	-0.112827
Gabra4		0.624057	0.54861	0.376272	0.108576	0.344786	0.025059	-0.218408	0.176287	-0.010757	-0.125992	-0.078129	0.0	0.076091
Gpr176	0.193	0.337103	0.562577	0.43615	0.525245	0.369789	0.552334	-0.111292	0.217564	-0.101285	-0.06755	-1.093666	-0.594706	-0.544316
Fam19a1	0.339089	0.312101	0.464129	0.353819	0.126478	0.203564	0.625952	0.0	0.036883	-0.220645	-0.092968	-0.425135	0.010969	-0.311887
Cadps2	-0.040073	0.386587	0.148047	0.284592	0.0598	0.301203	-0.062358	0.0	0.273364	-0.273066	0.131433	-0.629857	0.281308	0.12321
A930038C07Rik = Ndnf	0.097525	0.502605	0.241605	0.164895	0.384048	0.280128	-0.14501	-0.165752	0.156257	0.258203	0.149138	-0.487959	0.0	-0.254514
Adcy2	0.182859	0.340016	0.348112	0.133395	0.056547	0.495148	0.234162	0.079912	0.192493	0.011554	0.007677	-1.30862	-0.047258	-0.454405
Dlg4	0.130292	0.072734	0.028514	0.11603	0.309024	0.032322	-0.13117	0.162903	0.0	0.320926	-0.241246	-0.154778	0.038656	-0.103609
Copz2	0.111379	0.067768	0.296572	-0.289923	0.129852	0.053894	-0.162218	0.366859	0.122213	0.118972	-0.157453	0.00297	0.060865	0.116708
tex2 = Tex21	-0.928384	-0.178422	1.060682	-1.073145	0.600881	-0.470793		1.003871	0.921037	-2.001997	-0.117754	0.376873	1.466673	-0.548769
Lemd1	-0.249346	-0.365695	-0.045659	-0.592682	0.133781	-0.009912	0.266165	-0.357978	0.370142	0.007856	0.015584	-0.165802	0.0	-0.028381
Jup	-0.552131	-0.542592	-0.240892	0.10513	0.17306	0.228924	0.190512	0.493445	0.653645	0.293648	0.526782	-0.12815	0.152753	0.209513
Fzd7	-0.312055	-0.382137	0.103894	-0.185057	-0.137106	0.232327	-0.356681	0.22336	0.375699	0.374525	0.293188	0.052881	0.651403	0.492487
Fgl2	-0.719798	-0.389413	-0.040182	-0.255384	0.015395	-0.288324	-0.627593	0.523461	0.421828	0.160934	0.039517	0.102208	0.561878	-0.045445
Tgfbi	-0.20437	-0.18828	0.258562	1.022341	0.827605	0.938089	0.884565	0.874419	1.09539	1.14981	0.94303	0.712287	1.058098	1.328819
Cxcr7	-0.161765	-0.2679	-0.124531	0.154512	1.018964	2.155779	2.114447	0.761261	1.138214	1.16995	0.302505	1.243801	1.487081	0.715348
Prss23	-0.061959	-0.278932	-0.132337	0.682979	0.668358	0.144598	0.287828	0.701524	0.611212	0.764754	0.497716	0.050943	0.300296	0.035606
Mbl2		-1.251574				1.15525								
Nrsn2	-0.095676	-0.197868	0.243817	0.560495	0.76457	0.634094	0.522603	0.629784	1.000034	0.901359	0.784842	0.367818	0.480297	0.307828
H2-T10 /// H2-T22 /// H2-T9	-0.354596	-0.477555	-0.004167	0.107382	1.082335	0.885425	0.747622	1.653953	1.001319	2.023798	2.14739	0.656259	1.99609	0.992173
Ier3	-0.088307	-0.403861	0.448605	0.563867	0.50863	0.599779	0.78363	0.780914	0.773309	0.478013	0.630872	0.221451	0.767513	0.561383
Aqp6	0.154791	-0.517499	-0.036242	1.673211	1.872083	2.266429	2.022012	2.288293	4.164559	2.706032	3.515183	0.790196	1.391781	0.296958

Part II. Does postnatal neuronal activity control synapse molecular specification?

1. Introduction

Molecular and activity-dependent mechanisms have been both proposed to determine the specificity of neuronal networks. However, the question of their relative contribution remains misunderstood. Our latest results in addition to many others support the existence of a "chemoaffinity code" that precisely regulates neurons connectivity (Zipursky and Sanes 2010). We have identified a combination of presynaptic secreted molecules, from different CAM families, underlying the identity of the CF/PC synapse. Nevertheless, contrary to Roger Sperry's hypothesis which postulated that these "specific molecular markers" are generated during cell differentiation (Sperry 1963), our results show that the synaptogenic combination is not pre-established, appears during postnatal brain development and is regulated in a synapse-specific manner. Indeed, GCs acquire their molecular code in one step, while IONs go through a multi-step acquisition of their neuronal identity. Thus, one remaining question is what regulates the multi-step acquisition of the molecular identity of CF/PC synapse?

Neuronal activity has been shown not only to mediate transcriptional program transition in early postnatal neurons, but also to control the differential expression of genes depending on the activity pattern (Tyssowski et al. 2018; Stroud et al. 2020). The expression of a specific C1Q-related protein in each input, C1QL1 at CF and CBLN1 at PF, regulates their proper connectivity on PC (Matsuda et al. 2010a; Kakegawa et al. 2015; Sigoillot et al. 2015). In hippocampal culture, the expression of *C1ql* genes was previously demonstrated to increase after TTX application (Martinelli et al. 2016). In the cerebellum, CBLN1 exocytosis from lysosomes at PF inputs was shown to be regulated by activity in a Ca^{2+}-dependent manner (Ibata et al. 2019). Moreover, chronic blocking of electrical activity in the cerebellar cortex by TTX injection results in the loss of CF innervation and the increase of dendritic spines receiving PFs on PC (Bravin et al. 1999; Andjus et al. 2003; Cesa et al. 2007; Cesa et al. 2011). Experiments using genetically modified mice have shown that blocking neurotransmission in GCs (White and Sillitoe 2017) or in Basket and Stellate cells (Fritschy 2006) do not lead to the loss of PC innervation by CFs, as well as inhibiting PC neuronal activity (Lorenzetto et al. 2009). These

studies suggest that the activity of the CF could itself be necessary for the establishment and maintenance of its innervation with the PC. However, this has never been demonstrated. Therefore, because the synaptic territory of PC excitatory afferents (proximal for the CF and distal for the PFs) is actively maintained, we hypothesize that activity-dependent neuron-specific mechanisms could control the specification of the molecular identity of synapses. Neuronal activity could regulate the specific molecular combination that instructs neurons specific connectivity in two different ways: either by modulating the released of these secreted molecules at CF and/or by modulating the expression of these synaptogenic genes. Consequently, to decipher the mechanisms involved here, I started with two different approaches to specifically inhibit CF activity during postnatal development. The first was to inhibit all calcium-dependent exocytosis from the CF, thereby preventing the potential release of secreted synaptogenic molecules. The second approach was to specifically inhibit action potential generation in IONs, resulting in changes in gene transcription, but could also affect calcium-dependent exocytosis in the CF.

2. Modulation of calcium-dependent release in climbing fibers

To selectively block calcium-dependent exocytosis in CF, I used the *clostridial botulinum* neurotoxin serotype B-light chain (BoNT/B). BoNT/B cleaves the SNARE (soluble NSF-attachment protein receptor) proteins: VAMP1, VAMP2, VAMP3 (Schiavo et al. 1992; Humeau et al. 2000). VAMP1 and VAMP2 participate in neurotransmitter release, while VAMP2 and VAMP3 regulate the exocytosis of secretory granules that contain secreted proteins. An iBot mouse expressing BoNT/B in a cre-dependent manner was previously generated in which a floxed-STOP cassette was inserted upstream of the *BoNT/B* gene and the ires-EGFP **(Figure 28A)** (Slezak et al. 2012). I crossed this mouse line with a transgenic line expressing the CRE recombinase under the *C1ql1* promoter to enable recombination and expression of BoNT/B in IONs (*C1ql1*^{Cre} mouse; Moghimyfiroozabad et al., in preparation) **(Figure 28A)**. In the *C1ql1*^{Cre} mouse, the CRE is also expressed in the EGL since *C1ql1* is transiently expressed in GC precursors (Sigoillot et al. 2015), implying that, in addition to IONs, GCs also express the BoNT/B. Immunofluorescence staining against the EGFP, which is co-expressed with the toxin upon recombination, was performed on cerebellar sections from P21 mice. No EGFP signal was observed in IONs in the brainstem and neither in the cerebellum **(Figure 28A)**. Nevertheless, these animals exhibit an important motor phenotype similar to ataxia, such as gait and balance difficulties compared to their littermates. Since the cerebellum

is involved in motor coordination, this may indicate that BoNT/B recombination has occurred successfully in the olivo-cerebellar system, but that the ires does not allow expression of GFP at a level sufficient for detection with standard immunofluorescence and spinning disk confocal microscope. Moreover, despite the absence of GFP positive CFs, immunohistochemical staining against VGLUT2, which is a specific marker of CF/PC presynaptic vesicles, showed fewer and bigger CF presynaptic boutons in the ML compare to control mouse **(Figure 28A)**. PF inputs are important for the proper formation of PC dendritic tree (Baptista Mary E.Hatten et al., 1994). A recent study demonstrated a reduced ML thickness when tetanus toxin light chain, which also cleaves VAMP1, 2 and 3, is expressed in PFs (Park et al. 2019). Here, the ML thickness was smaller in mice with BoNT/B expression compared to controls supporting the idea that PFs could also express the BoNT/B and affect PC development and maturation.

To perform ION-specific expression of BoNT/B, we used an intersectional strategy with the iBot mouse and injections of viral particles driving the expression of the CRE recombinase under the CamKII promoter specific to IONs and not GCs **(Figure 28B)**. The virus was injected at P0 to inhibit specifically ION activity during early development prior to the specification of PC inputs. Immunofluorescence labeling of parasagittal cerebellar sections was done 2 weeks later at P14, a stage when CF molecular and territory specification occurs (Paul et al. 2023). Again, EGFP signal was not found in the IONs and in the CFs in the cerebellum **(Figure 28B)**. Because P0 injections of this virus serotype (AAVretro) combine with the CamKII promoter mostly target the same lobules of the cerebellum, especially lobules VI, VIII and IX, images were taken in these regions. Even though GFP was not visible, less CF presynaptic boutons were observed **(Figure 28B)**.

Therefore, to visualize CFs expression, I decided to co-inject at P0 the CamKII CRE virus allowing the recombination of the BoNT/B, with a CamKII GFP virus whose backbone is similar and had been previously characterized *in vivo*. This time, immunofluorescence labeling of parasagittal cerebellar sections was done at P10. As expected, transduced GFP (GFP+) expressing CFs were visible. In the control condition, GFP+ CFs are mainly found around the PC soma, which is quite normal given that CFs start translocating around P9. However, in the BoNT/B condition, more CFs appear to have translocated **(Figure 28C)**. At this stage, VGLUT2 is also expressed in PF terminals but can be differentiated from CF terminals as their puncta are smaller and higher in the ML. In addition to the early translocation of CFs expressing BoNT/B, CF presynaptic boutons on PC soma seems to be more numerous, compare to the control mouse **(Figure 28C)**.

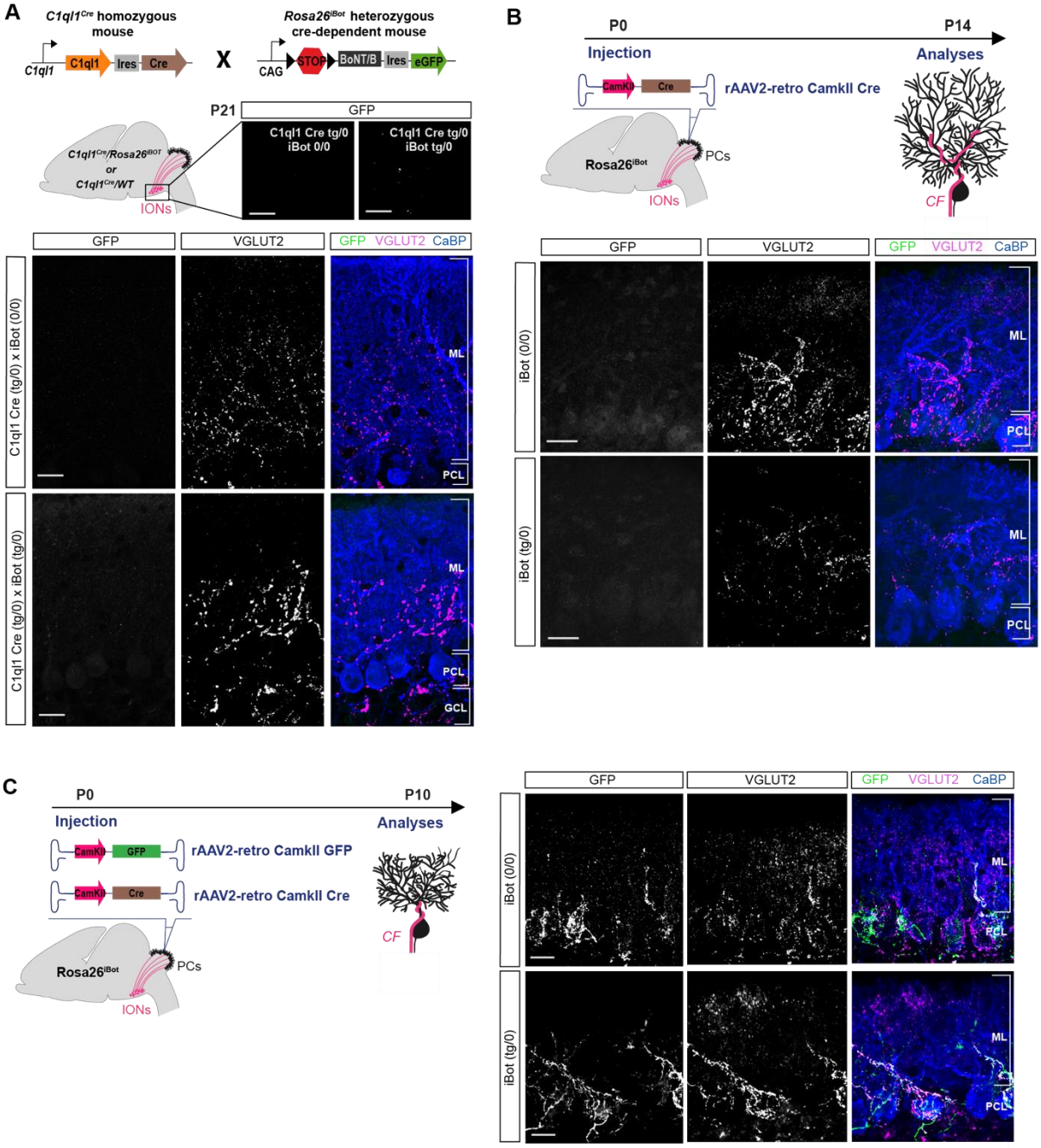

Figure 28. Experimental tests to specifically modulate climbing fiber activity-dependent release.

(A) Top: Breeding strategy between the iBot mouse expressing the BoNT/B in a Cre-dependent manner with the C1ql1^{Cre} line expressing the CRE under C1ql1 promoter in IONs and GC precursors. Analyses were performed at P21 in parasagittal cerebellar sections from C1ql1^{Cre} Rosa26^{iBot} or C1ql1^{Cre} WT mouse from the same litter. Scale bars: 125 µm. Bottom: Confocal images of cerebellar sections immunostained for GFP (green), CF presynaptic boutons (VGLUT2, magenta) and PC (Calbindin, blue). (B) Top: Schematic illustration of the strategy to specifically express BoTN/B in IONs during postnatal development. P0 stereotaxic injection of retrograde rAAVs expressing the CRE, under the CamKII promoter, were performed in the cerebellum of Cre-dependent iBot mice. Analyses were performed at P14 in parasagittal cerebellar sections from Rosa26^{iBot} or WT injected mice from the same litter. Bottom: GFP

(green), CF presynaptic boutons (VGLUT2, magenta) and PC (Calbindin, blue) were immunostained. (C) Left: Schematic illustration of the strategy to specifically express BoTN/B in IONs and to visualize infected BoTN/B CFs. P0 stereotaxic co-injection of retrograde rAAVs expressing the CRE and rAAVs expressing the GFP both under the CamKII promoter, were performed in the cerebellum of Cre-dependent iBot mice. Analyses were performed at P9 in parasagittal cerebellar sections from Rosa26^{iBot} or WT injected mice from the same litter. Right: GFP (green), CF presynaptic boutons (VGLUT2, magenta) and PC (Calbindin, blue) were immunostained. For all the panels, scale bars: 20 µm.

3. Modulation of the activity of inferior olivary neurons

The second approach was to determine if ION neuronal activity could regulate the expression of the specific molecular combination that instructs CF connectivity, since an increasing number of synaptogenic genes have been identified to be regulated by neuronal activity (Yap and Greenberg 2018). We decided first to use a chemogenetic tool and specifically express the modified inhibitory human muscarinic receptor 4 (hM4Di) in IONs. This receptor is a Gi-coupled DREADD (Designer Receptors Exclusively Activated by Designer Drug) and can be activated by clozapine-N-oxide (CNO) leading to Gi signaling activation and thus to the inhibition of neuronal excitability (Wess et al. 2013). We crossed the hM4di Cre-dependent mouse line with the *C1ql1^{Cre}* mouse to express the Gi-DREADD in IONs. Immunofluorescence labeling of parasagittal cerebellar sections was done between P35-P40. The recombined mCitrine reporter was expressed in the IO and in GCs, and in the ML which might correspond to CFs and PFs **(Figure 29A)**. Surprisingly, we noticed that, when a *C1ql1^{Cre}* female mouse is crossed with a hM4Di male, recombination appears to occur in Bergmann glia, which is not observed in the opposite mating, suggesting a maternal imprinting of the CRE transgene (Chaillet 1994; Luo et al. 2020).

DREADDs have always been the subject of debate about the mechanisms by which they inhibit neuronal activity with some studies arguing that hM4Di does not affect action potential but neurotransmission (Wiegert et al. 2017). Thus, because of their indirect effect, we decided to switch to a more direct way to inhibit ION activity, by reducing action potential initiation using expression of the inward-rectifying potassium channel Kir2.1. Injection of a retrograde AAV driving the expression of the Kir2.1 in a Cre-dependent manner under the hSyn promoter was performed in the *C1ql1^{Cre}* mouse at P0. This promoter is not specific to IONs and could also drive expression in GCs. Nevertheless, at P0 there are no GCs, thus the Kir2.1 construct from retrograde AAV cannot be expressed in GCs. As expected, no GFP staining was observed in

GCs **(Figure 29B)**. The effects of activity blocking on IONs were quantified 2 weeks later at the morphological level using VGLUT2 immunostaining of transduced CFs that are GFP+ and calbindin for PCs. Quantification of CF extension, presynaptic boutons size and density was performed **(Figure 29B)**. No difference in the volume of the VGLUT2 clusters was observed in Kir2.1 mouse when compared to the control mouse in which a non-functional Kir2.1 mutant was injected. A small but significant change in GFP^+ CF extension was detected (9% decrease) accompanied by a 33% decrease of the number of VGLUT2 clusters. These results suggest that CF neuronal activity is important for its proper connectivity on PC.

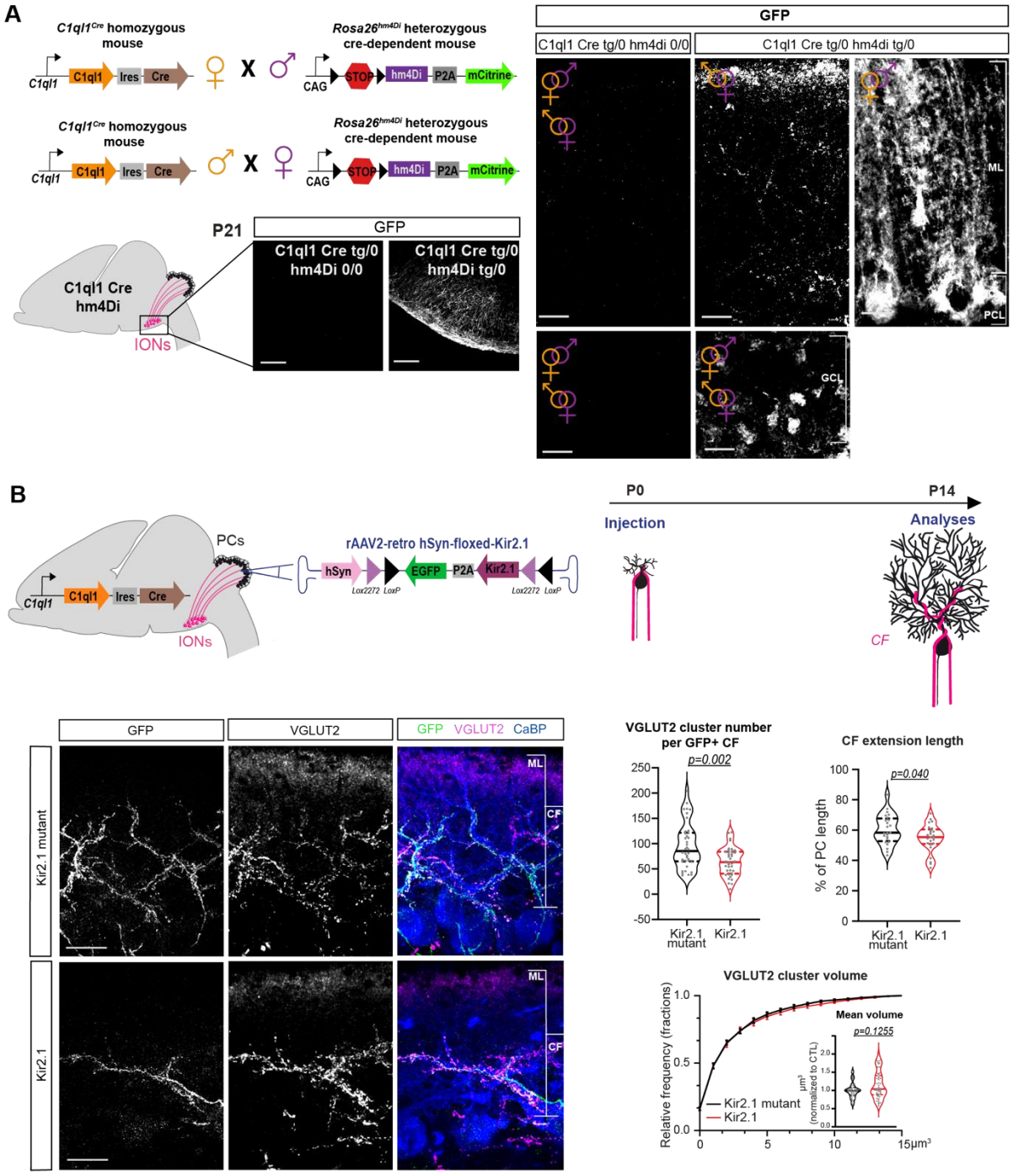

Figure 29. Experimental tests to specifically modulate climbing fiber activity.

(A) Left: Strategy of mating between the hM4Di mouse expressing the Gi-DREADD in Cre-dependent manner with the C1ql1^{Cre} line expressing the CRE. The two directions of crossbreeding were compared with: either a male C1ql1^{Cre} mouse crossed with a female hM4Di or female C1ql1^{Cre} mouse crossed with a male hM4Di. Analyses were performed at P21 in parasagittal cerebellar sections from hM4Di or WT from the same litter. Scale bars: 125 µm. Right: GFP (green), CF presynaptic boutons (VGLUT2, magenta) and PC (Calbindin, blue) were immunostained. Scale bars, 20 µm for the top panel and 12 µm for the bottom panel. (B) Top: Schematic illustration of the strategy to specifically express the Kir2.1 channel in IONs. P0 stereotaxic injections of retrograde rAAVs expressing the floxed Kir2.1 or Kir2.1 mutant

under the hSyn promoter, were performed in the cerebellum of C1ql1^{Cre} mice. Analyses were performed at P14 in parasagittal cerebellar sections. Bottom left: GFP (green), CF presynaptic boutons (VGLUT2, magenta) and PC (Calbindin, blue) were immunostained. Scale bars, 20 µm. Bottom right: GFP^{+} CF connectivity was assessed measuring the percentage of CF extension length on PC dendrite, VGLUT2 cluster number and volume. Data are presented as violin plot with the median and quartiles. n ≥ 24 images per condition, 10-13 animals per condition; 3 independent experiments. Statistics: unpaired Student's test for CF extension and Mann-Whitney test for VGLUT2 cluster number and volume.

4. Discussion and perspectives

After demonstrating that the proper formation of CF/PC synapses rely on a stepwise acquisition of the specific expression of a combination of secreted molecules by CFs (Paul et al. 2023), the last aim of my PhD was to test that ION activity itself regulates this molecular specification. Thus, I tried to specifically inhibit CF activity during cerebellar development using two different strategies since neuronal activity could regulate the specific molecular combination either by modulating the release of these secreted molecules and/or by modulating their expression.

For the first strategy, I combined mouse genetics and viral injection approaches to enable the blocking of calcium-dependent exocytosis in CF. Bigger and fewer CF presynaptic boutons were observed in BoTN/B condition suggesting that the blocking of calcium-dependent exocytosis in CF perturbs CF synapse formation. Moreover, co-injection with a reporter GFP virus revealed the premature translocation of more GFP^{+} CFs expressing the BoTN/B compare to the control.

Since the co-injected GFP expressing virus was not Cre-dependent, it is difficult to say whether or not GFP^{+}CFs also express the BoTN/B. Between P3 to P7, an intense competition occurs between multiple CFs and enables the strengthening of one single CF for each PC, which will translocate around P9. Thus, we could argue that GFP^{+} CFs that do not express the BoTN/B are favored and thus translocate more rapidly. More experiments are needed here with a Cre-dependent GFP expressing virus construction. Interestingly, we have just demonstrated that in *Cbln1* specific KO in IONs, CFs translocate earlier (Paul et al. 2023). CBLN1 secretion was already shown to be dependent on neuronal activity in GCs but insensitive to tetanus neurotoxin, which cleaves the VAMP1,2 and 3 as the BoTN/B, since CBLN1 is secreted by lysosomes (Ibata et al. 2019). This similar phenotype between *Cbln1* KO and the expression of

the BoTN/B in IONs could be explained either by a different mechanism of CBLN1 secretion at the CF compare to the PF, or by the blockade of the secretion of other molecules among the molecular combination of synaptogenic genes previously identified.

The second strategy was based on a viral approach to deliver an inward-rectifying potassium channel Kir2.1 in IONs to enable the reduction of their action potentials. A 33% decrease of CF/PC synapses were observed, suggesting that CF neuronal activity is important for its proper connectivity on PC. smFISH experiments are in progress in Kir2.1 injected mice to quantify the expression level *in vivo* of the different genes involved in the CF/PC molecular code. Finally, contrary to the original experiment of Bravin et al. where CFs are lost after TTX infusion in the adult cerebellum, we do not see the total regression of the CFs. One possibility is that the level of inhibition of CF activity is not enough or because the loss of CF is due to the inhibition of the activity of multiple cerebellar neurons. A computer simulation of the inhibition of IONs activity expressing Kir2.1 is in progress, in collaboration with the laboratory of Vincent Hakim at the Ecole Normale Supérieure, Paris.

DISCUSSION

“The important thing is to never stop questioning”

— Albert Einstein

1. Summary of the main results

Specific neuronal wiring is thought to be regulated by molecular recognition cues. However, it remains to be determined how and to what extent a combination of proteins instructs the formation of a specific type of synapse on a specific subcellular domain. Using the cerebellar PCs and the specific innervation by their two excitatory afferents as a model, we demonstrated the existence of a combination of membrane and secreted proteins underlying the specificity of CF/PC synapse. These molecules belong to different families, some of which have already been shown to be synaptogenic in other regions of the CNS. The secreted C1QL1, LGI2 and CRTAC1 control CF/PC synapse formation and stabilization, while the membrane NRCAM inhibits it, suggesting a very fine balance between promoting and inhibiting CF/PC synaptogenesis. In addition to their role in regulating synapse formation, some of these molecules such as NRCAM mediate axon morphogenesis. The triple KO of *C1ql1, Lgi2,* and *Crtac1* reveals that these molecular pathways are not redundant and might work in parallel, since the magnitude of the effect is similar to the sum of the individual effect. Thus, C1QL1, CRTAC1 and LGI2 constitute a secreted combinatorial code promoting the formation and the identity of CF/PC synapses.

Interestingly, at early stages of the development, PC inputs rely initially on the same signaling pathway, *via* CBLN1 expression, for CF and PF proper connectivity on PC. It also prevents the winning CF to translocate too early and regulates CF morphology. Then, as the circuit matures, the molecular identity of CFs evolves, while PF synapse still rely on the initial combination of molecules. This observation highlights the existence of different and input-specific rules to generate the molecular synaptic diversity required for the formation of neural networks.

We postulate that neuronal activity could trigger this molecular specification since IONs start receiving synapses during the second postnatal week of development and undergo a significant increase in CF-evoked EPSC (Bourrat and Sotelo 1983; Hashimoto and Kano 2003). Inhibition of IONs activity during postnatal development leads to a decrease in CF/PC number similar to what is observed in *C1ql1, Crtac1* or *Lgi2* LOF. More experiments are in progress to determine whether ION activity blockade during the early postnatal development could prevent the molecular switch that occurred at the mRNA levels in IONs.

2. How to generate synapse molecular diversity and identity?

In his original paper from 1963, Roger Sperry wrote "*The chemoaffinity interpretation also met objections on the grounds that there are not enough distinct chemical labels available in the embryo*''. At that time, Sperry was already raising the question as to how so many different types and identities of synapses can be generated with a limited number of genes. In the human brain, 10^{14} synapses were estimated for only 2.5 x 10^4 genes (Scale of the Human Brain 2015; Willyard 2018). It seems that evolution has generated several mechanisms in parallel to produce the synaptic molecular diversity required for the formation and the sophistication of the neuronal architecture. Using endogenous labeling of PSD95 and SAP102, Zhu and colleagues demonstrated that synapse diversity can already be observed with only two postsynaptic proteins from their differential distribution with some synapses containing either SAP102 or PSD95, or both (Zhu et al. 2018). Thus, Grant postulated that if the combination of proteins could generate synapses containing either or both proteins, the number of synapse types could be estimated by the following mathematical function: $Synapse_{types} = 2^{n-1}$ (n, protein number) (Grant 2019). Hence, by increasing the number of CAMs available, the number of synapse types increases exponentially. Indeed, with only 50 different proteins, which corresponds to less than 5% of the synaptome, 10^{14} synapse types can be generated, demonstrating that the combinatorial action of proteins can generate a very large diversity of synapses.

The differential splicing and post-translational modifications of NRXNs, which can potentially produce thousands of different proteins, is the most extensive evidence for the generation of molecular synapse diversity. The first evidence of such a mechanism was identified for a *Drosophila* axon guidance receptor, DSCAM, with up to ~38,000 different isoforms (Schmucker et al. 2000; Wang et al. 2002; Zhan et al. 2004; Wojtowicz et al. 2007). In mammals, NRXN are encoded by three homologous genes *Nrxn1*, *Nrxn2* and *Nrxn3*. Each *Nrxn* gene contains two promoters that produce a long *α-Nrxn* and a shorter *β-Nrxn* isoform. The *Nrxn1* gene contains a third promoter and generates a very short γ-isoform. *Nrxn* transcripts have up to 6 canonical alternative splice sites, thus generating more than 3,000 protein-coding mRNAs (Baudouin and Scheiffele 2010; Südhof 2017; Gomez et al. 2021). NRXNs were thought to regulate neuron specific connectivity, *via* the specific expression of *Nrxn* isoform repertoires. For instance, in the hippocampus, excitatory and inhibitory neurons expressed

Nrx1-2-3 transcripts but differentially experienced cell type-specific alternative splicing (Nguyen et al. 2016). NRXNs are known to regulate synapse assembling and remodeling. In heterologous synapse formation assays, NRXN mediates the clustering of NLGNs enabling the recruitment of NMDA-R and scaffolding proteins (Scheiffele et al. 2000; Graf et al. 2004; Chih et al. 2006). There is still little evidence suggesting that they act directly as determinants of partners specific connectivity *per se*. Nevertheless, a growing body of literature has shown that NRXNs can instruct synapse-specific properties and thus identity, by recruiting key elements of the synapse machinery (Südhof 2017; Gomez et al. 2021). NRXN isoforms interact with different ligands such as NLGNs, LRRTMs and the CBLN-GluD complex (Baudouin and Scheiffele 2010; Südhof 2017; Gomez et al. 2021). Only NRXN1 and NRXN3 containing an insert at splice site 4 ($SS4^+$) bind to the secreted CBLN1 and CBLN2, and to the postsynaptic GluD1 and GluD2 receptors **(Figure 30)** (Chih et al. 2006; Joo et al. 2011). Interestingly, in hippocampal CA1-subiculum synapses, the alternative splicing of the presynaptic *Nrxn1* and *Nrxn3* at SS4 differentially controls the postsynaptic receptor composition (Aoto et al. 2013; Dai et al. 2019; Dai et al. 2021). Presynaptic NRXN1-$SS4^+$ trans-synaptically enhances NMDAR EPSCs without affecting AMPA responses, whereas NRXN3-$SS4^+$ suppresses AMPAR EPSCs without affecting NMDA responses (Dai et al. 2019). Specifically, NRXN-$SS4^+$– CBLN2 and NRXN3-$SS4^+$ – CBLN2 complexes control the levels of NMDA and AMPA receptors by activating GluD1 differential signaling **(Figure 30)** (Dai et al. 2021).

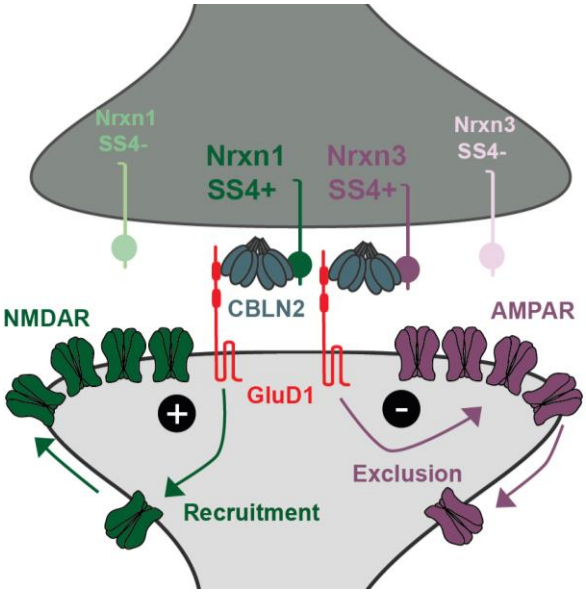

Figure 30. NRXN1-SS4+ and NRXN3-SS4+ enhance NMDAR levels and suppress AMPAR levels respectively, by activating GluD1 *via* CBLN2 at hippocampal synapses.

Another way to overcome this limited repertoire of CAMs is to form multimeric complexes of molecules from various families involved in different signaling pathways **(Figure 31)**. Proteomics studies at single-synapse type highlighted this degree of complexity in the protein composition at the pre- and the postsynaptic site (Selimi et al. 2009; Apóstolo et al. 2020). In the cerebellum, 65 proteins have been identified at the PSD of PF/PC, some of which are involved in cell adhesion (Selimi et al. 2009). More recently, in the hippocampus, at the level of the MF/CA3 synapse, a large repertoire of 77 proteins was identified, in which the main CAM families are represented such as IgSF, fibronectin type III (FN3) and the LRR family (Apóstolo et al. 2020).

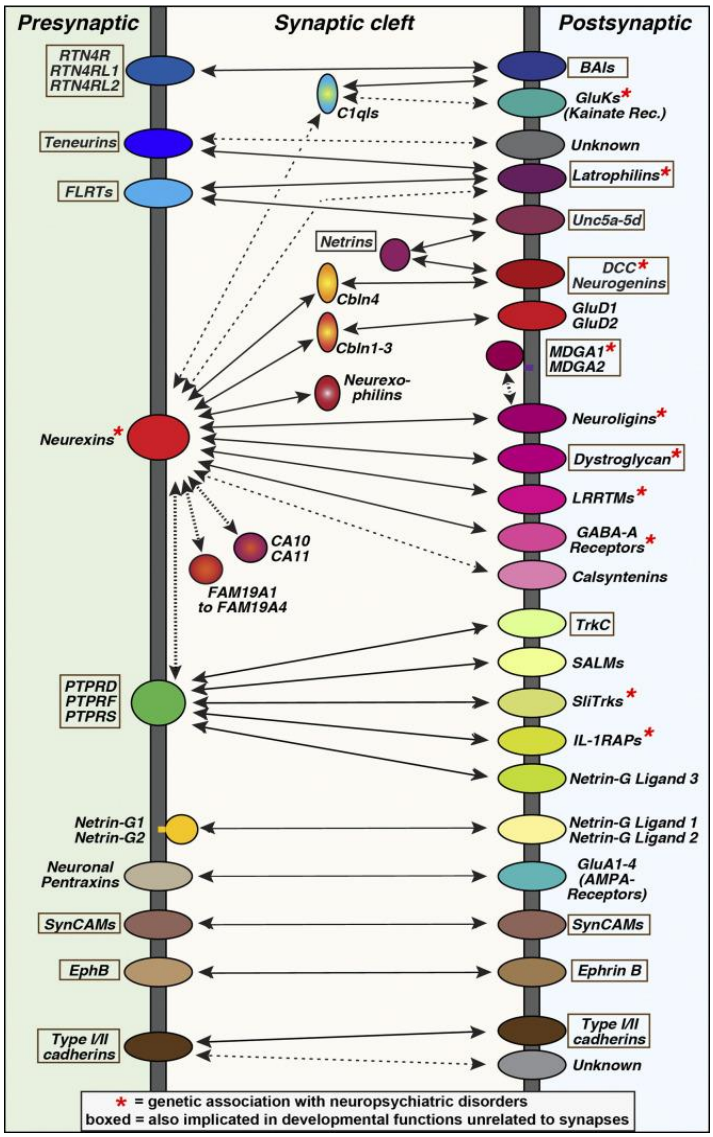

Figure 31. Schematic diagram of CAMs interactions network known to regulate the establishment and specification of synapses.

Lines and arrows indicate interactions, with cis-interactions shown as dotted lines and less validated trans-interactions shown as dashed lines. From Südhof 2021.

Supporting this hypothesis of a combined action of molecules from several CAM families, our study revealed the existence at CF/PC synapses of 3 different proteins belonging to 3 different CAM families: C1QL1 from the C1Q family, LGI2 from the LRR family and CRTAC1 from the β-propeller family **(Figure 32)**. Double and triple LOF of *C1ql1*, *Crtac1* and *Lgi2* indicate that these 3 different CAMs have non-redundant functions since they have an additive phenotype on the number of CF/PC synapses, in accordance with the fact that they are involved in different signaling pathways. C1QL1 interacts with BAI3 (Bolliger et al. 2011; Kakegawa et al. 2015; Sigoillot et al. 2015), LGI2 with the ADAM receptors (Seppälä et al. 2011) most likely with the ADAM 11 at the pre- and the ADAM23 at the postsynaptic part as suggested by our smFISH data, and CRTAC1 with RTN4R (Sato et al. 2011). Our results suggest that these three different signaling pathways seem to promote the formation and/or stabilization of CF/PC synapses. Nevertheless, they could lead to the same phenotype but act in a slightly different way. For instance, LGI1, which is the homolog of LGI2, recruits AMPAR at the postsynaptic part *via* the ADAM receptors (Petit-Pedrol et al. 2018), while C1QL1-BAI3 interaction activates Rac1 signaling (Duman et al. 2016), and CRTAC1-RTN4R prevents RhoA activation and thus promote the formation and growth of synapses and spines (Kawakami et al. 2018). Similarly, three LRR proteins from different families at Schaffer collaterals/CA1 pyramidal neurons, were also shown to play different functions (Schroeder et al. 2018).

Finally, our study revealed a new potential mechanism to generate this molecular diversity. Indeed, beyond the traditional trans-synaptic interactions between CAMs, secreted molecules could play a key role in increasing the molecular complexity and regulation at the synapse. In addition to interacting with their respective receptors, they can also bind to other receptors and modulate their functions by competing with other ligands. Similarly to BAI3, CRTAC1 and LGI1 (LGI2 ortholog) interaction with RNT4R prevent its binding with its endogenous ligand NOGO. This inhibitory action could promote synapse formation **(Figure 32)** (Thomas et al. 2010; Sato et al. 2011; Wang et al. 2021). Indeed, RTN4R-NOGO is known to decrease synapse stability (Wills et al. 2012). In PC *Nogo-A* LOF, both the numbers of CF/PC and PF/PC synapses are increased suggesting that the NOGO ligand inhibits synapse formation at both PC inputs (Petrinovic et al. 2013). However, overexpression of NOGO-A in PCs results in a different phenotype depending on the afferent type (Petrinovic et al. 2013). A decrease in the number of PF/PC synapses is observed, while CF/PC synapses number are not changed. One possible explanation for that, is that RTN4R receptors were occupied by the secreted molecules

C1QL1, CRTAC1 and LGI2 at the CF/PC synapses, contrary to PF/PC synapses. Thus, the overexpression of NOGO in PC would only affect PF/PC synapse.

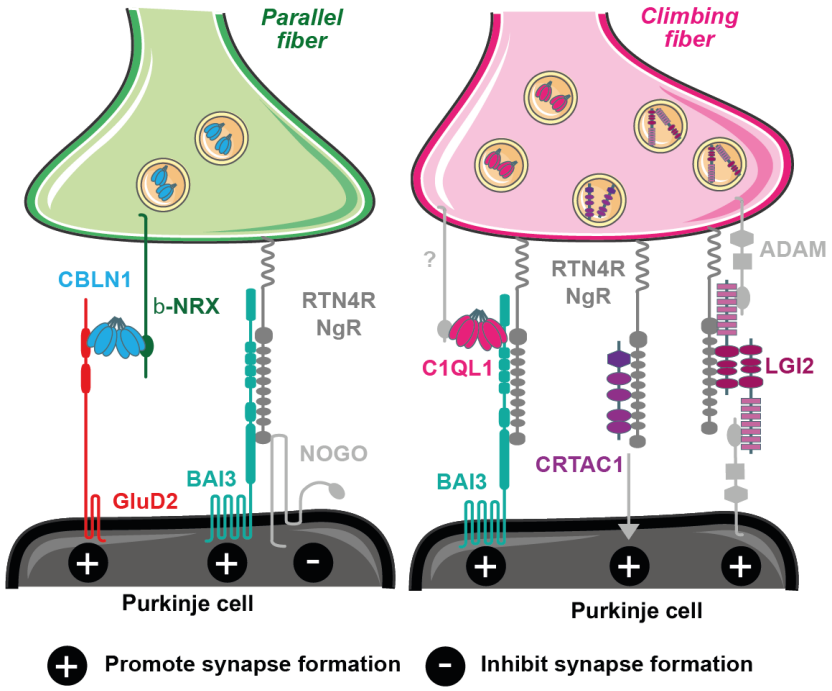

Figure 32. Model of the molecular composition at climbing fiber/Purkinje cell and parallel fiber/Purkinje cell synapses.

3. Synapse identity is not fixed during the development

Roger Sperry's hypothesis postulated that the "specific molecular markers" underlying synapse specificity are generated at the time of neuronal differentiation (Sperry 1963). In other words, the synaptic molecular combination is established early and fixed throughout life, and would be sufficient to form stereotyped neuronal wiring patterns. However, our data revealed that during postnatal development, the synaptic molecular combination is acquired gradually, in a neuron specific manner. Indeed, at the beginning, CF/PC and PF/PC synapses express a common molecular combination, instructing CF and PF targeting to PC (**Figure 33)**. Then, as the cerebellum develops, CF synaptic molecular composition changes contrary to PF/PC synapses, most likely to instruct subcellular targeting on PC, by the addition of C1QL1, CRTAC1 and LGI2 (**Figure 33)**. This addition will expand a neuron's wiring gene repertoire to diversify the initial set of CAMs per synapse-type. We therefore hypothesized that since CF/PC and PF/PC synapses exhibit the same combination of receptors at early stage, one way

to specify CF synapse identity from PF synapse identity, to instruct subcellular targeting on PC, is to add these secreted molecules.

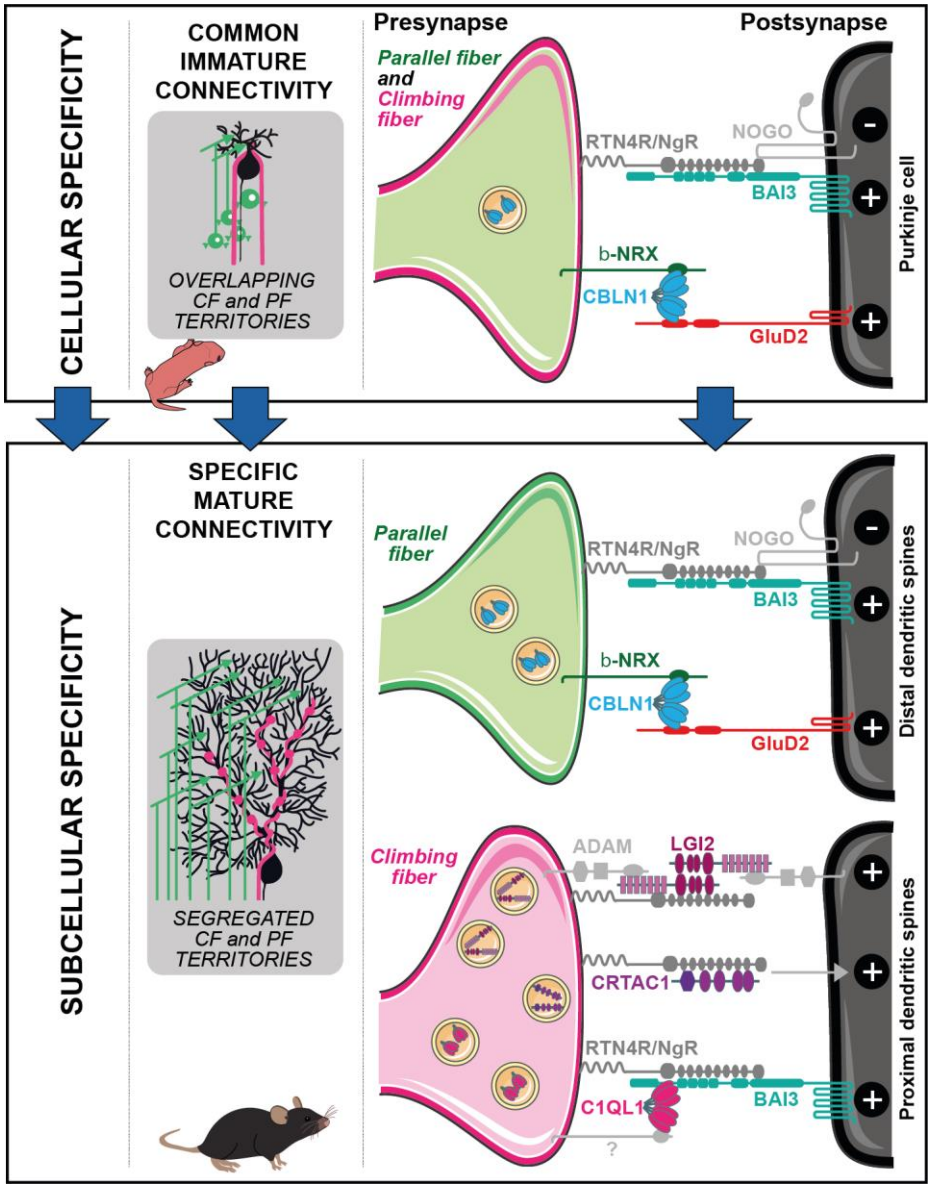

Figure 33. Model of the molecular specification at climbing fiber/Purkinje cell and parallel fiber/Purkinje cell synapses during postnatal development.
At early stages, CF/PC and PF/PC synapses exhibit the same combination of molecules. At later stages, the secreted proteins C1QL1, CRTAC1 and LGI2 specifically at CF/PC synapses may exclude GluRδ2 from CF/PC synapses.

In adult, GLURδ2 is no more localized at the CF/PC synapses and is restricted to PF/PC synapse, contrary to BAI3 and RTN4R (Landsend et al. 1997). Thus, one remaining question that we want to address is the exclusion of GluRδ2 at CF/PC synapse. In addition, blockade of the cerebellum activity by TTX infusion or IO lesions in adult leading to CFs re-sprouting,

demonstrated the appearance of GluRδ2 at CF/PC synapses and then its removal once the CF matures (Landsend et al. 1997; Zhao et al. 1998; Cesa et al. 2003). One hypothesis for its exclusion is the decrease of *Cbln1* expression as IONs mature leading to the non-clustering of GluRδ2 in favor of PF/PC synapses. Nevertheless, would this decrease be enough to exclude GluRδ2 at CF/PC synapses? One potential explanation is its endocytosis *via* intracellular signaling when not stabilized by CBLN1. Another hypothesis is that the expression of secreted molecules such C1QL1, LGI2 and CRTAC1 might exclude GluRδ2 at CF/PC synapses by steric hindrance. Crystal structure revealed that C1QL1 organizes in big complex with each trimer structure assembled into high-order oligomers (Ressl et al. 2015). To test this hypothesis, *in vitro* experiments are in progress where C1QL1 and/or LGI2, CRTAC1 are expressed in GCs followed by immunohistochemical staining of GluRδ2 to assess its exclusion or not from PC spines.

4. CBLN1 instructs partners selectivity

In our study, CBLN1 was shown to control CF morphogenesis. In *Cbln1* LOF, CF branching is increased and CF extension is decreased. Similarly, a recent study also identified that CBLN1 regulates axon growth and guidance in dorsal commissural neurons and in cerebellar GCs *in vitro* (Han et al. 2022).

In addition to that, our results on *Cbln1* KO in IONs showed an early translocation of CF at P7 and a decrease of the number of CF/PC synapses on PC somata compared to control. A question naturally arises: what is the exact role of Cbln1? Is it involved in the formation of synapses or rather in their stabilization? Synapse formation involves the initiation of the contact between the two partners, the assembly of its pre- and postsynaptic specializations and the appearance of its specific properties. For years, there has been a debate about the formation *vs* stabilization of synapses. Some argue that formation and stabilization occur concomitantly enabling the maintenance of the newly formed synapse, while for others, formation and stabilization are two successive steps.

This question is not new and dates back to the discovery of PC free spine in both *GluRδ2* KO and *Cbln1* KO mouse (Kurihara et al. 1997; Hirai et al. 2005). Some scientists argue that CBLN1 does not contribute to synapse formation but to synapse stabilization since “these presynaptic specializations are subsequently disassembled” (Seigneur and Südhof 2018; Südhof 2018), while others postulate that PC spines are formed prior to PF contact and that CBLN1 induces presynaptic structural changes and differentiation of mature synapses (Ito-

Ishida et al. 2012). The explanation of these "naked" spines as well as the exact role of CBLN1 is still very controversial. One argument in favor of synapse stabilization is that these free spines are located at the distal dendrites of the PC and not at the proximal dendrites. Kurihara and colleagues examined PF/PC synapses in developing *GluRδ2* mutant mouse using electron microscopy. They did not find any deficits at P7 but at P14, *GluRδ2* mutant mouse began to display impairment in PF/PC connections (Kurihara et al. 1997). They suggested a failed stabilization of synaptic contact with PFs. However, there are some limitations to this study. First, an older study demonstrate the existence of naked spines in wild-type mouse at very early stage such as P7 (Larramendi 1969). Second, at P7 there are very few PF/PC contacts, it is only during the second postnatal week that PF synapses are mainly formed. Since the number of PF/PC contact quantified is very low by Kurihara and colleagues, impairment might not be easy to observe at very early stage. Third, it is accepted that PC spines are known to develop independently of presynaptic terminals in a cell-autonomous manner, this model is known as the "Sotelo model" (Sotelo 1978; Sotelo 1990). This hypothesis of PC spinogenesis was generated based on the observation of hypo-granular cerebellar mouse model, where PC dendritic arborization is impaired but still exhibit "naked spines" without presynaptic structures (Caviness et al. 1972; Hirano and Dembitzer 1973; Rakic and Sidman 1973; Sotelo 1975). Thus, taken together, these studies indicated that PC spines are formed before the contact with PFs.

Ito-Ishida and colleagues tackled this question of whether or not CBLN1 induces synapse formation. For that, they performed live-imaging on cerebellar slice cultures at P8 of *GluRδ2* KO mouse, they labelled specifically PFs and PCs, and observed sequential events of synaptogenesis. Time-lapse images at 6-8 days *in vitro* (DIV), where recombinant WT CBLN1 was added to the organotypic culture, showed the formation of protrusions at PF that subsequently developed into axonal boutons which often encapsulate PC spines (Ito-Ishida et al. 2012). This encapsulation of PC spines by PF protrusions is accompanied with synaptic vesicles accumulation. This observation was confirmed *in vivo* by electron microscopy in cerebellum at early stages and appeared to be dependent on NRXN-CBLN1-GluRδ2 interaction. Thus, Ito-Ishida and Yusaki postulated a "bidirectional interaction model of CBLN1" which occurs in different steps **(Figure 34)**: (1) PC spines are formed in a cell-autonomous manner, independently of PF inputs ("Sotelo model"); (2) PF and PC first contact allow the interaction of CBLN1-GluRδ2 which triggers accumulation of NRXN, GluRδ2 and synaptic vesicles at the future presynaptic sites; (3) NRXN-CBLN1 interactions activate cytoskeleton rearrangement leading to PF protrusions that encapsulate PC spines; (4) this transient PC spines encapsulation increase the interaction between NRXN-CBLN1-GluRδ2

promoting a stronger contact with PF-PC as a positive feed-back, but would also decrease diffusion of glutamate into the synaptic cleft; (5) then the PF protrusions retracts (Ito-Ishida et al. 2014).

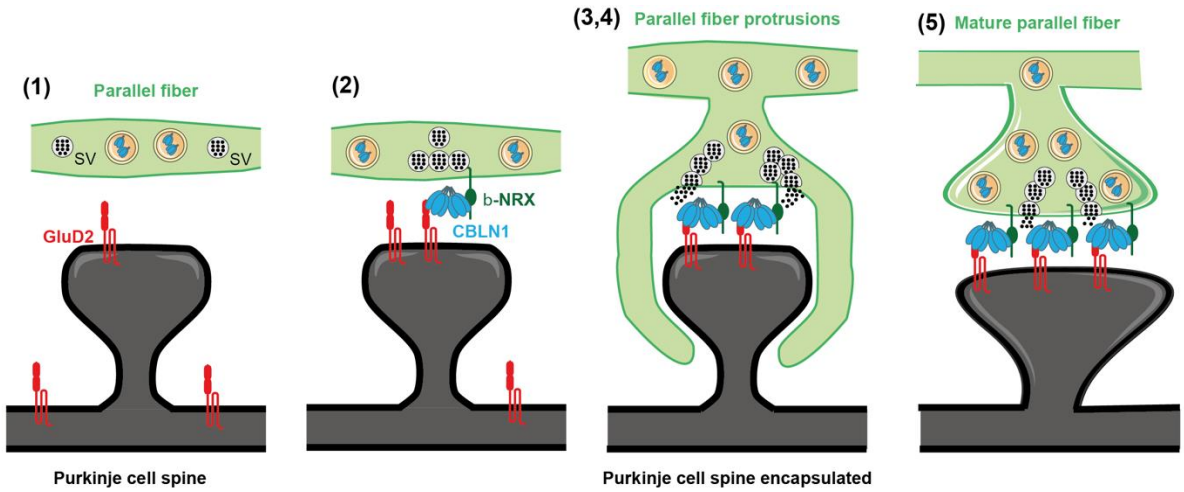

Figure 34. CBLN1 induces structural changes at parallel fiber/Purkinje cell synapses during their formation: the "bidirectional interaction model of CBLN1".
(1) PC spines are formed independently of PF inputs through an intrinsic program. (2) PFs and PCs initiate their first contact triggering the interaction between CBLN1 and GluRδ2 and the recruitment of synaptic vesicles (SV) and GluRδ2. (3,4) This transsynaptic interaction promotes actin cytoskeleton remodeling leading to the formation of PF axon protrusions that encapsulates PC spines. (5) As PF/PC synapse mature, PF protrusions disappear. Adapted from Ito-Ishida et al., 2014.

The fact that PC spines are formed before PF contact and that CBLN1 might induce presynaptic structural changes by the accumulation of NRXN at the presynaptic part and of GluRδ2 at the postsynaptic part may seem counterintuitive at first sight. Indeed, synapse formation has been extensively studied and described in the cortex and in the hippocampus where the interactions between axons and dendrites are essential for spine formation, which does not seem to be the case for PC and its excitatory afferents. Thus, in view of this model, one could wonder if such a mechanism could be similar at the CF. First, the spines of the PCs would be formed and freely accessible. Then, CBLN1 would allow PC recognition at PF and CF inputs, attachment and presynaptic differentiation as well as clustering of the receptors at the postsynaptic compartment. Only live-imaging on explant co-culture of cerebellum and brainstem could decipher the precise role of CBLN1 as well as the other secreted molecules.

5. What mechanism controls the acquisition of the specific expression repertoire of wiring genes for each neuron type?

Over the past few decades, it has been accepted that activity-independent and activity-dependent mechanisms control neuronal wiring specificity. The activity-independent process occurs during early development and is thought to be hardwired by the genetic program, whereas the activity-dependent program combines neuronal spontaneous activity and sensory-driven experience. However, this dichotomy appears to be disappearing, with some evidence showing that neuronal activity can regulate the synaptic molecular repertoire. For instance, neuronal activity can modulate the alternative splicing of CAMs such as *Nrxn* (Rozic-Kotliroff and Zisapel 2007; Iijima et al. 2011). It can also induce differential gene expression, instructing neuron specific targeting. A study in the mouse olfactory system demonstrated the instructive role of neuronal activity in the precise wiring of OSNs during development (Nakashima et al. 2019). Using calcium imaging, they identified three subclasses of OSNs characterized by different patterns of spontaneous activity (i.e., tonic, short burst, prolonged burst firing) and by three different CAMs involved in the appropriate targeting. They showed that these activity patterns are not spatially organized but correlated with the ORs expression. Indeed, the switch from one OR type to another one leads to a switch in the spontaneous firing pattern. Furthermore, prolonged burst using optogenetic experiment leads to the expression of the wrong OR and thus to an inappropriate targeting (Nakashima et al. 2019). However, there is still not clear evidence linking neuronal activity and synaptic molecular combination underlying subcellular specificity.

Tyssowski and colleagues demonstrated, first in cultured cortical neurons and then *in vivo* in the visual cortex, that different patterns of neuronal activity (sustained, intermediate and brief visual stimulation) induce the expression of different sets of genes (Tyssowski et al. 2018). Sustained activity induced the generation of three temporal and mechanistically distinct waves of genes expression, whereas brief activity induces only the first wave. It is now established that a certain number of genes respond to neuronal activity with the activation of a first set of genes, called immediate early genes (IEGs) such as *Fos, Egr1* and *Npas4* (Yap and Greenberg 2018). IEGs are not neuron type specific, but their targets are and correspond to the second round of gene activation upon neuronal activity, called the late response genes (LRGs). Among LRGs, some of them were shown to be directly involved in circuit wiring formation (Yap and

Greenberg 2018). Interestingly, the complex FOS-JUN (i.e. IEGs) appears to occupy cell-type specific binding sites in the nucleus (Malik et al. 2014; Yap and Greenberg 2018). Recent work from Michael Greenberg's lab showed an activity-mediated transition in the transcriptional program in early postnatal neurons (Stroud et al. 2020). This developmental transition appears to regulate the formation of cell-type-specific neuronal enhancers that could thus regulate cell-type specificity. In favor of this idea, we demonstrated that acquisition of the adult-specific surfaceome of GCs and IONs follows different time courses during postnatal development. GCs acquire their adult identity in one step during their differentiation, while the IONs surfaceome changes progressively to acquire the adult combination. Interestingly, the BacTRAP analysis performed on IONs and GCs reveals that GCs express a larger number of specific nuclear proteins, including transcription factors and chromatin modifying enzymes (Veleanu, Urrieta-Chávez, Sigoillot, et al. 2022). Thus, we can wonder whether IEGs might activate a different set of LRGs in GCs and IONs, resulting in the differential expression of synaptic molecules at CF/PC and PF/PC synapses. To test the hypothesis that the increase of neuronal activity in IONs trigger the expression of C1QL1, LGI2 and CRTAC1 at CF/PC synapses, I performed experiments to selectively inhibit IONs activity by expressing the inward-rectifying potassium channel Kir2.1. The effects of activity blocking on IONs showed a decrease of the number of CF/PC synapses, similar to the phenotype observed when C1QL1, LGI2 or CRTAC1 are removed from the CF. Experiments in cortical cultures expressing Kir2.1 demonstrate, as expected, a decrease in *cFos* mRNA in Kir2.1 condition, accompanied by a decrease in *C1ql1* and *Lgi2* mRNA whereas *Cbln1*, *Nrcam* and *Crtac1* mRNA levels do not change compared to the Kir2.1 mutant condition **(Figure 35)**. *In vivo* smFISH experiments are in progress on brainstem sections, and more particularly on IO for quantification of *C1ql1* and *Lgi2* mRNA levels in Kir2.1 injected animals to confirm this observation. We hypothesize that the decrease in ION activity prevents the gene expression change characterizing CF/PC synapses.

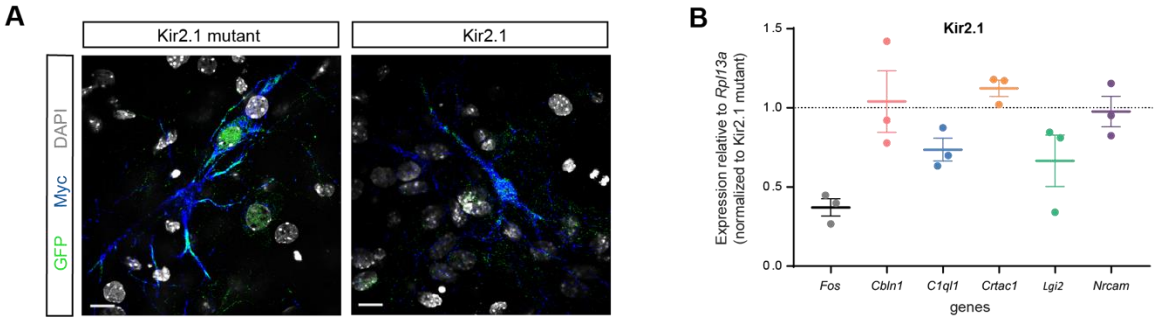

Figure 35. Expression of Kir2.1 and Kir2.1 mutant in cortical cell culture.
Cortical cell cultures were transduced at DIV3 with a retrograde AAV driving the expression of the Myc-tagged Kir2.1 or Kir2.1 mutant and the soluble eGFP under the CamKII promoter. (A) Neurons were imaged at DIV14 after immunostaining for Myc (blue) and GFP (green). Scale bars, 13 µm. (B) Cultured cortical neurons were analyzed by quantitative RT-PCR on RNA extracts. Gene expressions relative to Rpl13a were normalized to the Kir2.1 mutant.

6. How this study could contribute to understand neurodevelopmental disorders?

Disruption in neuronal connectivity and/or activity are linked to the appearance of neurodevelopmental disorders such as schizophrenia, autism spectrum disorders (ASD), intellectual disability (ID) or epileptic disorders. Alterations in molecular and cellular mechanisms have been observed in these pathologies, leading to synaptic dysfunctions, hence considered as synaptopathies. Indeed, a substantial proportion of genes coding for CAMs was shown to confer a risk of neurodevelopmental disorders. A classic example is the *Nrxn* and *Ngln* whose mutations have been identified in many ASD, ID and schizophrenic patients (Walsh et al. 2008; Südhof 2008; Sanders et al. 2015; Gomez et al. 2021; Ea et al. 2022; Fu et al. 2022). Among the identified genes coding for membrane and secreted proteins underlying the specificity of CF/PC synapse, some of them are linked to some brain disorders. NRCAM was shown to be associated with addictive behavior and autism susceptibility due to brain wiring alterations (Sakurai 2012). *Lgi* mutations, causing hyperexcitability, were reported in juvenile epilepsy (Pakozdy et al. 2015). Indeed, LGI-ADAM interaction allowing for the recruitment and clustering of AMPAR receptor, contribute to synaptic transmission (Fukata et al. 2010). BAI proteins are also linked to some psychiatric disorders such as bipolar disorders, addiction and schizophrenia (Liu et al. 2006; DeRosse et al. 2008; McCarthy et al. 2012; Lips et al. 2012; Lanoue et al. 2013; Cheng et al. 2021). Finally, recent studies reported CRTAC1 as a potential plasmatic biomarker in children for ASD, and single nucleotide polymorphisms were found in children affected by dyslexia (Doust et al. 2022; Zhang et al. 2023).

There are growing evidences to suggest the involvement of the cerebellum in many neurodevelopmental disorders. For many years, the cerebellum was only considered to contribute to motor functions (Eccles 2013). However, in the 1990s, the idea that the cerebellum is involved in more complex cognitive processes emerged after observations of cerebellar patients with various cognitive deficits (Schmahmann 1997; Buckner 2013). For example, damage to the posterior lobes results in executive function impairment, language deficits and thought dysmetria, a symptom classically present in schizophrenic patients (Schmahmann and Sherman 1998; Schmahmann 1998). Later, studies using neuronal virus tracing of cerebellum-associated regions as well as functional neuroimaging studies have demonstrated a regionalization of the cerebellum (Stoodley and Schmahmann 2009; Buckner et al. 2011; Stoodley 2012; Buckner 2013). The cerebellar anterior lobes are involved in sensorimotor functions, while different posterior cerebellar lobules and hemispheric extensions (CrusI-II) are more implicated in cognitive tasks such as language, working memory organization and emotional processing. At the cellular level, a reduction in PC density as well as GCs number were shown in postmortem ASD brain tissue (Whitney et al. 2008; Skefos et al. 2014). Additionally, our lab recently demonstrated that neonatal phencyclidine model of schizophrenia results in modified CF/PC synaptic connectivity (Veleanu, Urrieta-Chávez, Sigoillot, et al. 2022). Hence, we can wonder whether CF/PC molecular synaptic combination is affected in the context of neurodevelopmental disorders.

The current main hypothesis for the development of brain disorders is the alteration of circuit assembly leading to impairment of neuronal network activity, resulting in the apparition of behavioral symptoms. Nevertheless, we discussed earlier the potential role of neuronal activity in the regulation of CF/PC synapse molecular specification by CF activity. Interestingly, a study demonstrated a significant dysregulation of activity-dependent gene expression in schizophrenia human-induced pluripotent stem cell neurons (Roussos et al. 2016). This raises the question of whether a genetic predisposition could lead to a deficit in the regulation of activity-related genes, resulting in misexpression of CAMs at the synapse.

7. Conclusion and remarks

Brain function is based on the establishment of highly stereotyped neuronal networks through precise and diverse synaptic contacts. Understanding what controls synapse specificity and identity is thus mandatory not only to understand brain functions but also the etiology of synaptopathies such as autism spectrum disorders or schizophrenia. While Sperry postulated

the chemo-affinity hypothesis in the 1960s, implying a molecular combination for each synapse type, the existence and nature of these combinations have not been demonstrated. We have identified a unique combination of presynaptic secreted proteins for the specification of the CF/PC synapse. Surprisingly, we have also discovered that this specific code is generated, during development, in an afferent-specific manner starting from a common code. Since these synaptogenic molecules are not only expressed in the cerebellum but also in other brain regions such as the olfactory bulbs, the hippocampus and the cortex, one may wonder whether such a mechanism of input specification through molecule secretion could also exist in other circuits. Finally, we suggest that this specification of the molecular code is regulated by neuronal activity during postnatal development. Our latest results in culture seems to indicate a dysregulation of *C1ql1* and *Lgi2* expression after cortical cells activity blockade. *In vivo* experiments are in progress to confirm these observations in IONs. This work will shed light on the rules controlling the establishment of proper network connectivity and brain function and the synapse-specific mechanisms potentially involved in the etiology of neurodevelopmental disorders such as autism and schizophrenia.

To conclude, in our study and many others, synaptic specificity is investigated in the context of one neuron receiving connection from several other neurons. However, there are very few studies that focus on understanding synaptic specificity in the perspective of a neuron that must connect multiple targets. This question is relevant because one could imagine that different mechanisms could be deployed. We demonstrated that the presynaptic combination of membrane and secreted proteins instructs the specificity and identity of CF/PC synapse. If we take the example of pyramidal neurons in layer 5 of the mouse cortex, this neuron is able to project to up to 12 individual cortical targets simultaneously **(Figure 36)** (Blockus and Polleux 2021b), thus we can wonder in this context, if the postsynaptic neurons might not further instruct the cellular and/or subcellular specificity. If not, the presynaptic neurons must develop some molecular strategies to specifically localize CAMs along their axons by synapse-specific local translation (Bernard et al. 2022) or subcellular sorting for example.

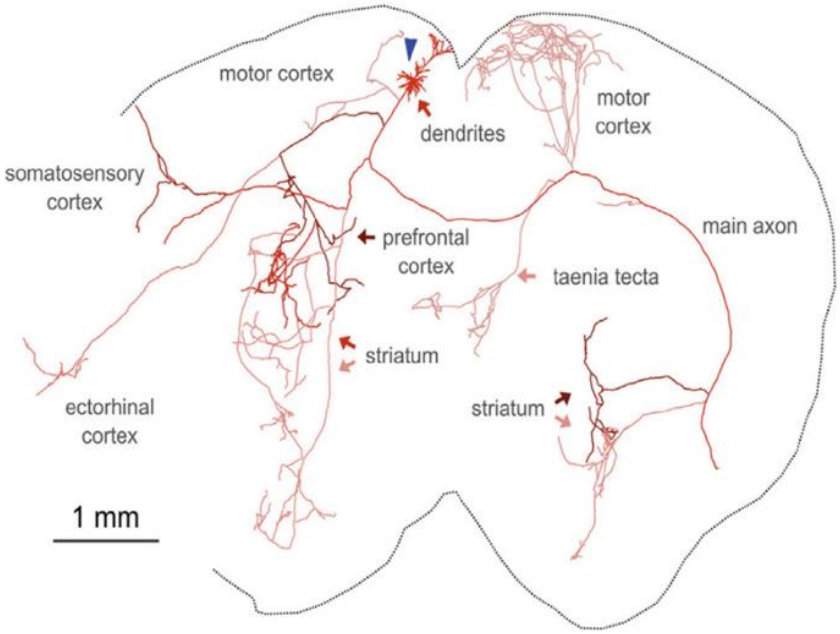

Figure 36. The complexity of the axon projections of a single layer 5 pyramidal neuron in the mouse motor cortex.

Cell body position is indicated by the blue arrow. From Blockus and Polleux 2021.

ANNEXE:

1. Modified climbing fiber/Purkinje cell synaptic connectivity in the cerebellum of the neonatal phencyclidine model of schizophrenia

Maxime Veleanu[1*], Beetsi Urrieta-Chavez[1*], Séverine M. Sigoillot[1*], Maëla Paul[1], Alessia Usardi[1], Keerthana Iyer[1], Marine Delagrange[2], Joseph P. Doyle[3], Nathaniel Heintz[3], Carine Bécamel[4], Fekrije Selimi[1].

[1]Center for Interdisciplinary Research in Biology (CIRB), College de France, CNRS, INSERM, Université PSL, Paris, France
[2]Plateforme qPCR-HD-GPC, Institut de Biologie de l'Ecole Normale Supérieure, Paris, France
[3]Laboratory of Molecular Biology, Howard Hughes Medical Institute, The Rockefeller University, New York, NY, USA
[4]Institute for Functional Genomics (IGF), University of Montpellier, CNRS, INSERM, Montpellier, France
*Equal contribution

Abstract/Summary

Environmental perturbations during the first years of life are a major factor in psychiatric diseases. Phencyclidine (PCP), a drug of abuse, has psychomimetic effects, and neonatal subchronic administration of PCP in rodents leads to long-term behavioral changes relevant for schizophrenia. The cerebellum is increasingly recognized for its role in diverse cognitive functions. However, little is known about potential cerebellar changes in models of schizophrenia. Here, we analyzed the characteristics of the cerebellum in the neonatal subchronic PCP model. We found that, while the global cerebellar cytoarchitecture and Purkinje cell spontaneous spiking properties are unchanged, climbing fiber/Purkinje cell synaptic connectivity is increased in juvenile mice. Neonatal subchronic administration of PCP is accompanied by increased cFos expression, a marker of neuronal activity, and transient modification of the neuronal surfaceome in the cerebellum. The largest change observed is the overexpression of *Ctgf*, a gene previously suggested as a biomarker for schizophrenia. This neonatal increase in *Ctgf* can be reproduced by increasing neuronal activity in the cerebellum during the second postnatal week using chemogenetics. However, it does not lead to increased climbing fiber/Purkinje cell connectivity in juvenile mice, showing the complexity of PCP action. Overall, our study shows that administration of the drug of abuse PCP during the developmental period of intense cerebellar synaptogenesis and circuit remodeling has long-term and specific effects on Purkinje cell connectivity and warrants the search for this type of synaptic changes in psychiatric diseases.

PNAS
www.pnas.org

Main Manuscript for

Transient molecular changes and lasting synaptic effects in the cerebellum of the neonatal phencyclidine mouse model of schizophrenia.

Maxime Veleanu[1], Beetsi Urrieta-Chavez[1], Séverine M. Sigoillot[1], Maëla Paul[1], Alessia Usardi[1], Keerthana Iyer[1], Marine Delagrange[2], Joseph P. Doyle[3], Nathaniel Heintz[3], Carine Bécamel[4], Fekrije Selimi[1].
[1]Center for Interdisciplinary Research in Biology (CIRB), College de France, CNRS, INSERM, Université PSL, Paris, France
[2]Plateforme qPCR-HD-GPC, Institut de Biologie de l'Ecole Normale Supérieure, Paris, France
[3]Laboratory of Molecular Biology, Howard Hughes Medical Institute, The Rockefeller University, New York, NY, USA
[4]Institute for Functional Genomics (IGF), University of Montpellier, CNRS, INSERM, Montpellier, France

*corresponding authors: Fekrije Selimi and Nathaniel Heintz.
Email: fekrije.selimi@college-de-france.fr; heintz@rockefeller.edu

Author Contributions: FS and NH designed the research; MV, BUC, SMS, MP, AU, KI, MD, JPD and FS performed and analyzed the experiments; MV, BUC, SMS, MP, AU, KI, JPD and FS prepared the figures; CB provided the first batches of PCP animals and expertise. NH provided tools, mouse lines and expertise. FS and MV wrote the paper. All authors read the manuscript.
Competing Interest Statement: The authors declare no competing interest.
Classification: Biological Sciences/ Neuroscience
Keywords: Synapse, cerebellum, development, schizophrenia, phencyclidine
This PDF file includes:

Abstract

Environmental perturbations during the first years of life are a major factor in psychiatric diseases. Phencyclidine (PCP), a drug of abuse, has psychomimetic effects, and neonatal subchronic administration of PCP in rodents leads to long-term behavioral changes relevant for schizophrenia. The cerebellum is increasingly recognized for its role in diverse cognitive functions. However, little is known about potential cerebellar changes in models of schizophrenia. Here, we analyzed the characteristics of the cerebellum in the neonatal subchronic PCP model. We found that, while the global cerebellar cytoarchitecture and Purkinje cell spontaneous spiking properties are unchanged, climbing fiber/Purkinje cell synaptic connectivity is increased in juvenile mice. The transient increase in neuronal activity induced by PCP is accompanied by transient modification of the neuronal surfaceome in the cerebellum, including increased expression of *Ctgf*, a gene previously suggested as a biomarker for schizophrenia. Transient increased neuronal activity in the cerebellum using chemogenetics also leads to *Ctgf* overexpression, but not to the increased climbing fiber/Purkinje cell connectivity. Overall, our study shows that administration of the drug of abuse PCP during the developmental period of intense synaptogenesis and circuit remodeling has long-term and specific effects on Purkinje cell connectivity, and warrants the search for this type of synaptic changes in psychiatric diseases. Furthermore, while PCP modifies the expression pattern of several genes relevant for circuit development and maturation in the cerebellum, *Ctgf* is more a marker of changes in neuronal activity rather than of synaptic changes linked to the disease.

Significance Statement

Synaptogenesis and neural network remodeling are at their maximum during the perinatal period of human brain development. Perturbations of this highly sensitive stage might underlie the etiology of neurodevelopmental disorders. Subchronic neonatal administration phencyclidine, a drug of abuse, has been used to model schizophrenia in rodents. In this model, we found specific long-term synaptic changes in cerebellar Purkinje cells and transient modification of cerebellar gene expression pattern. While transient increased neuronal activity in the cerebellum, induced using chemogenetics, reproduces some phencyclidine-induced molecular changes, it is insufficient to reproduce the long-term synaptic effects. Our results show the complex mechanism of action of phencyclidine on the development of neuronal connectivity and further highlight the potential contribution of cerebellar defects in psychiatric diseases.

Main Text

Phencyclidine (PCP), a non-competitive NMDA antagonist initially developed for its properties as an anesthetic, became a popular drug of abuse in the 1960s (1, 2). Nowadays PCP is often mixed with other drugs, in particular marijuana, and a US 2013 report estimated that PCP-related emergency department visits increased more than 400% between 2005 and 2011 (https://www.samhsa.gov/data/sites/default/files/DAWN143/DAWN143/sr143-emergency-phencyclidine-2013.htm). PCP has important psychotomimetic effects such as alterations of body image, feelings of estrangement and loneliness, and disorganization of thought. Repeated use of PCP induces persistent symptoms found in schizophrenia, including both positive (hallucinations, psychosis …), cognitive and negative (social withdrawal) effects. PCP also produces regressive symptoms in schizophrenic patients. These observations led to the NMDA hypothesis of schizophrenia and the development of animal models using both acute and chronic PCP administration to study the pathophysiology of this disease (3). Because schizophrenia is now considered a developmental disorder, neonatal administration of PCP in rodents has been tested and shown to produce a wide range of behavioral alterations in the adult, including spatial memory deficits (4, 5) and a deficit in social novelty discrimination (6–8). Some studies found defects in prepulse inhibition (PPI) of the startle response, a sensorimotor gating task used both in animal models and humans as a behavioral marker of psychiatric disorders (4, 9, 10). Interestingly, these PPI deficits last even after withdrawal which is not the case when PCP is administered in adulthood, suggesting that this aspect of the disease is better modeled by neonatal administration of PCP. Finally, PCP abuse during pregnancy has been associated with neurobehavioral defects (11) and with long-term consequences on social behavior and motor control in

children (12), further highlighting the need to understand the consequences of PCP exposure on the development of neuronal networks.

In the subchronic neonatal PCP model, the drug is administered three times during the second postnatal week in rodents (**Figure 1A**), a period of intense neuronal growth and synaptogenesis. This developmental stage is particularly sensitive to early environmental stressors associated with increased risk of developing schizophrenia in humans (13). Histopathological and genetic studies have revealed that schizophrenia is a synaptopathy. Mutations and expression changes have been found in genes coding for synaptic proteins (14–19) (meta-analysis in (20)). Postmortem studies of the cortex of patients with schizophrenia have revealed deficits in dendritic arborization, spine densities and number of parvalbumin interneurons (21–25). Similar spine and cellular deficits have been reported in the PCP neonatal model (5, 26, 27), as well as impaired function of both excitatory and inhibitory synapses (28–30). It is however still unclear whether these common alterations in schizophrenia and the neonatal PCP model are due to the direct inhibition of NMDA function or a complex interaction between perturbations of neuronal activity and genetic factors.

While initially thought to be a motor-related structure, it is now well established that the cerebellum also plays a role in cognitive processes (31, 32) such as spatial navigation (33), language (34), reward (35) and social cognition (36). In addition, while schizophrenia has been primarily thought of as a disease of the prefrontal cortex or hippocampus, the cerebellum has emerged as a potential actor in this pathology. Schizophrenic patients often present a decreased cerebellar volume (37–39), as well as neurological soft signs, a type of sensorimotor impairment that implicates the cerebellum (40). Interestingly, neurological soft signs have been correlated with a poor outcome and greater negative and cognitive symptoms (41–43). A significant correlation between negative symptoms in schizophrenia and diminished connectivity between dorsolateral prefrontal cortex and vermal posterior cerebellum was found in a study of whole-brain connectivity using resting state fMRI in schizophrenic patients (44). It is however still unknown whether synaptic deficits are present in the cerebellum of schizophrenic patients. Furthermore, interference with the glutamatergic system during development of the cerebellum may lead to long-term alterations in this structure and associated behaviors.

In this study, we combined morphological, electrophysiological and molecular approaches to study the olivocerebellar network in the PCP neonatal model. Lasting synaptic changes were detected in juvenile mice, in particular at the climbing fiber/Purkinje cell excitatory synapses which are key for cerebellar computation. PCP was also found to induce a transient misregulation of the expression pattern of genes coding for membrane and secreted proteins in the cerebellum. One of these genes, *Ctgf,* has previously been documented as a biomarker in schizophrenic patients. Our data indicate that *Ctgf* is a biomarker of increased neuronal activity rather than of synaptopathy: reproducing the transient misregulation of *Ctgf* during the second postnatal week using chemogenetics is not sufficient to recapitulate the long-term synaptic changes induced by PCP in the olivocerebellar network.

Results

Global cerebellar cytoarchitecture and spontaneous spiking properties of Purkinje cells are normal in juvenile mice treated neonatally with PCP

A decreased cerebellar volume is often found in schizophrenic patients (for review cf. (45)). Morphological analysis of the global cytoarchitecture of the cerebellum in mice treated subchronically during the second postnatal week with PCP did not reveal any change compared to the one of vehicle-treated mice at a stage when the development of the cerebellum is completed (postnatal day 30, P30; **Figure 1B**). Calbindin immunostaining of cerebellar parasagittal sections, staining the whole dendritic arborization, soma and axon of Purkinje cells (PCs), revealed the stereotypical organization of the cerebellar cortex in layers: the white matter, the internal granular layer, the monolayer of Purkinje cell somata and the molecular layer (**Figure 1B**). The molecular layer contains the dendritic tree of Purkinje cells, which receives all the excitatory inputs, from parallel fibers and climbing fibers, and the inhibitory inputs from stellate cells, also located in the molecular layer. Quantification showed no change in the surface of parasagittal vermal sections of the cerebellum or in the mean thickness of the molecular layer (**Figure 1B**). While a previous study reported a deficit in parvalbumin cells in the brain of PCP-treated rodents (5), our quantification did not reveal any change in parvalbumin expression and density of inhibitory interneurons in the cerebellum of PCP-treated mice (**Figure S1**). Altogether these quantifications support the absence of major deficits in granule cell and Purkinje cell genesis and differentiation after neonatal subchronic PCP treatment. The firing pattern of Purkinje cells is characterized by simple spikes. Granule cell inputs modulate their frequency and control the acquisition of a mature firing pattern during postnatal development (46). Spontaneous PC spiking activity was recorded in acute cerebellar slices from PCP mice and compared to controls using high resolution

microelectrode arrays (MEA) (**Figure 1C**). Spike sorting using SpyKING CIRCUS allowed estimations of the mean firing rate (representing the mean activity of each recorded neuron), the coefficient of variation (CV, measuring the mean variance of interspike intervals during the whole recording), and CV2 (measuring the variability of spiking between two adjacent interspike intervals (47). None of these parameters showed any statistically significant difference between PCP-treated versus control mice (**Figure 1C**). Altogether, these results show that neonatal PCP treatment does not affect the development of the cytoarchitecture of the cerebellar cortex and the differentiation of cerebellar Purkinje cells in a major and long-lasting manner.

Neonatal PCP treatment induces afferent-specific synaptic deficits in cerebellar Purkinje cells

Purkinje cells receive two excitatory inputs, the climbing fibers (CFs) coming from inferior olivary neurons in the brainstem and the parallel fibers (PFs) coming from the granule cells in the granular layer of the cerebellar cortex, and two inhibitory inputs coming from stellate and basket cells in the molecular layer. To analyze potential long-term synaptic deficits induced by neonatal PCP administration, we performed immunolabeling, followed by high resolution confocal microscopy and quantitative analysis, for markers specific of the presynaptic terminal of each of these afferents on cerebellar sections from P30 animals. Because of the functional topography found in the cerebellum (48), we focused our quantitative morphological analysis in lobules engaged in various functions relevant for schizophrenia: lobule VI (language tasks, working memory paradigms, and spatial navigation) and lobule VIII (sensorimotor tasks) (32).

During the second postnatal week, the CF translocates along the dendritic tree of its target Purkinje cell to form a few hundred synapses (presynaptic boutons labelled using the specific VGLUT2 marker, **Figure 2A)** along the proximal dendrites. Its final territory extends up to approximately 80% of the height of the molecular layer. In lobule VI, the extension of the CF synaptic territory was unchanged in PCP- versus vehicle-treated mice, while in lobule VIII, a small (7%) but statistically significant increase in the extension of CF synaptic territory was detected (ratio relative to PC height are presented as mean ± SEM, lobule VIII: vehicle: mean±SEM=0.725±0.012, n=14; PCP: 0.781±0.006, n=16; p=0,0006, Welch's t test; **Figure 2A**). The density of the VGLUT2 puncta was significantly increased by 33% in lobule VI (mean number per μm^3±SEM, vehicle: 0.003±0.0001, n=14, PCP: 0.004±0.0002, n=15, Welch's t-test: p=0,0039, **Figure 2A**), while it remained unchanged in lobule VIII. Our 3D quantitative analysis of VGLUT2 puncta also revealed a general 20 % decrease in the mean volume in PCP-treated mice compared to vehicle in both lobules (for lobule VI, vehicle: mean volume in μm^3±SEM= 1.796±0.124, n=14; PCP: 1.395±0.078, n=14, p=0,0114 unpaired Student's t test; for lobule VIII: vehicle: 1.429±0.097, n=13; PCP: 1.171±0.059**,** n=15, p=0.0283 unpaired Student's t test, **Figure 2A)**. Altogether these results demonstrate an overall decrease in the volume of VGLUT2 labeled presynaptic boutons and an increase in their total number. The magnitude of the increase in the number of VGLUT2 presynaptic boutons is higher in lobule VI, where it is the consequence of increased density, while the small increase in lobule VII is due to increased synaptic territory. This shows a lobule-specific effect on CF/PC synaptic connectivity. The other excitatory afferent, the parallel fibers, forms densely packed synapses with PC spines via small VGLUT1 positive presynaptic boutons **(Figure S2A)**. As a proxy for synapse density, we measured the mean intensity of VGLUT1 labeling in the molecular layer (49) and found no difference between PCP- and vehicle-treated mice **(Figure S2A)**. While alterations of glutamatergic synapses are one of the most widely highlighted physiopathological deficits in schizophrenia, there are also evidence for inhibitory deficits (50, 51). We also analyzed inhibitory synapses using GAD65 immunostaining of cerebellar sections. A similar pattern of inhibitory innervation was found in PCP-treated mice and in control animals: big boutons were observed around the soma and axon initial segment of PCs, corresponding to the basket cell innervation, and small GAD65 positive boutons were found in the molecular layer on the dendrite of PCs corresponding to synapses from stellate cells. 3D quantification did not show any change in the density or volume of inhibitory boutons in the molecular layer (**Figure S2B**)**.** Altogether, these results point to a long-term effect of the PCP neonatal treatment on one particular synapse type made on cerebellar Purkinje cells, the climbing fiber/Purkinje cell synapses, with an increased total number accompanied by a decrease in the volume of the CF presynaptic boutons.

To further analyze the long-term effect of PCP neonatal treatment on CF/PC connectivity, we performed patch-clamp recordings of PC responses to CF stimulation in lobule VI using acute cerebellar slices from P24-P28 animals. The responses to CF stimulation are characterized by a strong, all-or-none, excitatory postsynaptic current (EPSC) that is depressed by paired-pulse stimulation (52). CF responses with the characteristic paired-pulse depression were detected in PCs of both PCP- and vehicle-treated animals. Paired-pulse depression was of similar magnitude across the interstimulus intervals tested (**Figure 2B**), showing that short-term plasticity of the CF/PC synapse is not affected by PCP neonatal treatment. Interestingly, the mean values for the charge transfer, amplitude and kinetics of the CF/PC

EPSCs were not statistically different between PCP- and vehicle-treated animals (**Figure 2B and S3**), but a different distribution of the mean charge was evident. In the PCP-treated condition, the distribution spanned a larger range with a subpopulation of PCs responding with a much higher charge transfer to CF stimulation. This result, together with our morphological analysis of CF synaptic boutons, indicates that PCP exposure during the second postnatal week increases CF innervation of a subgroup of PCs, in particular in lobule VI, in juvenile animals. Thus, exposure to NMDA antagonists like PCP during the synaptogenic period of olivocerebellar network development could have a long-term effect on cerebellar computation in certain lobules that are relevant for psychiatric disorders.

Neonatal PCP induces transient misregulation of the neuronal surfaceome

Neuronal activity is well known to modulate gene expression (53) and thus an NMDA antagonist like PCP could induce changes in the expression of genes that are key for circuit development. The formation of neuronal networks relies on the proper expression of secreted and membrane proteins, constituting the neuronal surfaceome, that are cues for many developmental steps from cell migration and differentiation to synapse formation. In the olivocerebellar system, several examples of secreted and transmembrane proteins such as the C1Q related protein family or Ig molecules have been demonstrated to partially control synapse specificity and territory through specific expression in each PC afferent (54–56). Because of the long-term effect of neonatal PCP administration on the CF/PC synapse, we first aimed to identify the gene expression profile of inferior olivary neurons using the bacTRAP strategy (57). We used two mouse lines expressing the EGFP-L10a transgene under the control of two different drivers: the S100a10 and Cdk6 bacterial artificial chromosomes (BACs, **Figure 3A and Figure S4**). The S100a10 mouse line, previously described (58), drove EGFP-L10a expression in the entire inferior olive (IO), as well as in other brainstem neurons in the hypoglossal nucleus and dorsal motor nucleus of the vagus nerve. In contrast, EGFP-L10a expression using the Cdk6 BAC driver was restricted to IO neurons, but targeted only specific subnuclei, namely the medial accessory olive, the dorsal accessory olive and the dorsal part of the principal accessory olive (**Figure 3A and data not shown**). This expression pattern was consistent with data from the GENSAT database (http://www.gensat.org). We performed immunoprecipitation of GFP-tagged polysomes using both mouse lines independently to identify the genes highly expressed in IO neurons. In both cases, genes known to be expressed in IO neurons were identified such as the transcription factor FoxP2 (59) and the serotonin receptor Htr5b (https://mouse.brain-map.org/experiment/show/71247644; http://www.gensat.org/). We defined the ION dataset as the ensemble of genes in common using both bacTRAP lines. We then compared the ION dataset to the granule cell (GC) dataset identified previously (57) to identify genes that would constitute the specific “surfaceome” for each of these two glutamatergic afferents of PCs. A comparison using a five-fold change as a threshold was performed to identify genes clearly differentially expressed (DEGs) (**Figure 3B**), yielding 598 DEGs for IONs and 401 DEGs for GCs. Classification using the DAVID functional annotation clustering tool identified DEGs coding for membrane and secreted proteins in both datasets, constituting the specific surfaceome for each of the PC excitatory afferent. Of note, the IONs were more complex in the diversity of genes coding for membrane and secreted proteins than GCs (250 genes, 42% versus 74 genes, 18% respectively, **Figure 3B and dataset S1**). This might be related to their more complex morphology and the need for molecular cues to control the topographical organization of olivocerebellar connectivity.

Having identified the specific surfaceome of IONs and GCs, we analyzed the expression changes induced by PCP treatment using high throughput quantitative RT-PCR assessment of these genes in cerebellar and brainstem extracts from P11 animals, right after the last PCP injection, or from P30 animals to detect acute effects and long-lasting changes, respectively **(Figure 3C and dataset S1)**. After multiple t test comparison with a Benjamini-Hochberg False Discovery Rate (FDR) correction (60), genes changed significantly by at least 10% were only found in the cerebellum at P11 (**Figure 3C)**, indicating a direct effect of PCP treatment on gene expression patterns in this structure. With an FDR threshold set to 10%, six genes were significantly misregulated: *Ctgf*, *Gal*, *Ier3* and *Ly6h* were upregulated, while *Rab7l1* and Cdon were downregulated **(Figure 3C and S5A)**. Interestingly all four upregulated genes were originally enriched in the ION dataset compared to GCs, suggesting that PCP decreases transiently the specification of gene expression in these two PC inputs at a stage when heterosynaptic competition between the two inputs is important for proper development of PC connectivity (61). We then analyzed potential functional links in genes misregulated by PCP in the cerebellum using the string database (https://string-db.org/) that predicts protein-protein interactions, including direct (physical) and indirect (functional) association (62). For this analysis, we included 30 genes with a fold change of at least 10% in the cerebellum that reached significance in multiple t tests without correction for FDR, thus accepting a higher rate of false positive **(Figure S5B)**. Predicted interaction was found between seven genes (*Cxcl12, Cnr1, Gal, Oprl1*, *Ctgf, Rock2 and Igfbp5,* **Figure**

S5B). Interestingly, *Ctgf* codes for Connective Tissue Growth Factor (CTGF, also known as CCN2), a secreted protein implicated in extracellular matrix remodeling, cell adhesion, dendritogenesis, and the formation of the neuromuscular junction (63–66). *Ctgf* is expressed in the cerebellum and the brainstem in a pattern that follows synaptic formation and refinement in the olivocerebellar network (increase in expression from P7 to P21 in the cerebellum, and a two-fold increase from birth to P14 in the brainstem (**Figure S5C**)). The increase in *Ctgf* induced by PCP in the cerebellum results in a level of expression equivalent to the one found in the brainstem, potentially impairing the specificity of signaling in the olivocerebellar system. Thus, the misregulation of the IO-specific surfaceome by PCP in the cerebellum could interfere with normal synapse formation and maturation.

CTGF is a marker of increased neuronal activity

PCP modulates neuronal activity in the brain and previous studies have shown increased *cFos* expression, an indicator of increased neuronal activity, in the inferior olive and in cerebellar granule cells and Purkinje cells in PCP-treated rodents (67). Analysis using droplet digital PCR confirmed that *cFos* mRNA expression increases in both the cerebellum and brainstem at P11 after the last PCP injection in the subchronic neonatal PCP model (**Figure S5A**). The PCP misregulated genes could either be simply indicators of changes in the pattern of neuronal activity or directly involved in the long-lasting synaptic defects observed after PCP subchronic treatment. To test this, we focused on the increased activity in the cerebellum and its potential consequences because of the larger gene expression changes found in this structure after PCP treatment. We generated a mouse model enabling chemogenetic control of activity in cerebellar granule cells by crossing the floxed hM3Dq knock-in mouse model (68) with the NeuroD1Cre mouse line expressing the Cre recombinase in cerebellar granule cells (**Figure 4A**). To mimic the increased neuronal activity induced in the PCP model, Clozapine N-Oxide (CNO, 3 mg/kg), the synthetic ligand of hM3Dq, was injected at P7, P9 and P11. This protocol induced, as expected, a strong increase in *cFos* mRNA expression in the cerebellum of P11 double transgenic animals (**Figure 4B**). This increase was specific and the result of the combination of both the expression of hM3Dq and CNO administration, as it was absent in control mice not expressing the Cre recombinase or treated with vehicle instead of CNO (**Figure 4B**). Out of the three genes with the biggest misregulation in the PCP subchronic neonatal model **(Figure 3C**), only the increase of *Ctgf* expression was recapitulated by increasing neuronal activity in the cerebellum using chemogenetics (mean expression relative to *Rpl13a* ±SEM, ND1Cre/WT controls+CNO: 0,0092±0.0004, n=6, ND1Cre/HM3Dq + CNO: 0.0283±0.0021, n=4, Mann Whitney test: p=0,0095; **Figure 4B**). To determine whether this is sufficient to induce long-term synaptic defects similar to those induced with PCP, we then analyzed the morphology of CF/PC synapses using VGLUT2 immunolabeling, high resolution confocal imaging and 3D quantitative analysis. None of the parameters analyzed, density or volume of VGLUT2 clusters, were changed in the cerebellum of P30 CNO-treated animals compared to controls, regardless of the lobule analyzed (**Figure 4C**). Single molecule FISH experiments on sections from PCP-treated mice at P11 showed that *Ctgf* expression showed a trend for increase in the internal and external granular layers of the cerebellum, but that the biggest increase in expression was detected at the surface where meninges are located (**Figure S6**). Altogether, these results show that transient increased neuronal activity and *Ctgf* overexpression in the cerebellum during the second postnatal week are not sufficient to recapitulate the long-term cerebellar synaptic changes induced by neonatal PCP administration and that *Ctgf* can be considered as a biomarker for increased neuronal activity in this model.

Discussion

The last trimester of pregnancy and the first two postnatal years of human development constitute a period of intense synapse formation and network remodeling whose perturbations have been associated with diseases like schizophrenia. In the cerebellum, this period corresponds to the growth and maturation of the PC dendritic tree and its connectivity, and is equivalent to the second and third postnatal weeks of rodent development (69). Our study shows that neonatal administration of PCP during this sensitive period correlates with transient molecular changes in genes coding for the neuronal surfaceome in the cerebellum and leads to lasting deficits at the climbing fiber/Purkinje cell synapse in juvenile mice.

Activity-dependent and independent consequences of neonatal PCP administration

Cell adhesion molecules that are important for the development of synapses are regulated by neuronal activity (53, 70), and the development of neuronal circuits, including in the cerebellum, implicates activity-dependent mechanisms (71). PCP is a non-competitive NMDA antagonist, and thus will affect glutamatergic neurotransmission and neuronal activity. Indeed both previous data (67) and our results

show that PCP administration increases neuronal activity in the olivocerebellar network, as assessed by *cFos* mRNA expression. A direct consequence is the transient misregulation of a subset of genes coding for membrane or secreted proteins in the cerebellum. This misregulation occurs during the second postnatal week at a critical period for the development of the synaptic connectivity on cerebellar PCs (71). Our gene expression and pathway analysis pointed to the misregulation of two genes, *Gal* and *Ctgf,* with the most strongly misregulated gene coding for CTGF, an extracellular secreted matrix protein known for its implication in tissue repair, extracellular matrix remodeling, cell survival, cell adhesion, dendritogenesis, and the formation of the neuromuscular junction. CTGF is known to interact with several proteins that are associated with synapse elimination such as IGF1 (72–74), BMP4 (73, 75, 76) or TGF-β1 (77). Its pattern of expression during postnatal development also suggested *Ctgf* as a candidate for the regulation of circuit formation. Using chemogenetics, we showed that *Ctgf* increase in the cerebellum, induced by increased neuronal activity, is not enough to lead to long-term CF/PC synaptic changes. CTGF has been suggested as a plasmatic biomarker in schizophrenia (78, 79): our study indicates that it should be considered more as a biomarker of changes in neuronal activity rather than as a marker of the synaptopathy per se. Misregulation of other surfaceome genes, such as *Gal* the gene coding for the neuropeptide Galanin, are not recapitulated by increased neuronal activity in the cerebellum using chemogenetics and could be involved in the long-lasting PCP induced-changes in CF connectivity. These additional gene expression misregulations could thus be the result of other circuit effects of PCP, in neuronal or cell types other than granule cells, or the result of direct gene modulation via mechanisms independent of the PCP blockade of glutamatergic neurotransmission.

Deficits in climbing fiber/Purkinje cell synapses as a hallmark of neurodevelopmental disorders

The cerebellar cortex, in particular via the integration of multimodal informations by Purkinje cells, controls the fineness of various cognitive and motor tasks. The synapse between inferior olivary neurons and cerebellar PCs is key for cerebellar computation, as it provides error feedback to the cerebellar cortex and controls the direction of plasticity at PF/PC synapses (80). As such, any defect in this synapse would have profound implications for circuit function and adaptation. In the neonatal subchronic PCP model, the mean volume of CF/PC presynaptic boutons labeled using the VGLUT2 marker is reduced compared to control conditions, with no change in paired-pulse depression indicating no modifications of the short-term plasticity properties. Similar deficits have been described in models of early postnatal alcohol exposure (81), or genetic models of neurodevelopmental disorders (49, 56, 82). In particular, knockdown of *Bai3*, a gene associated with psychiatric symptoms including in schizophrenia (83–85), induces a reduction in the volume of VGLUT2 boutons. Climbing fiber synaptic defects could thus be a feature of several pathological conditions. In the PCP model, this volume reduction is not accompanied by a reduction in synapse density. On the contrary, an increase in the density of CF/PC boutons is found in juvenile mice treated neonatally with PCP, with a bigger effect in lobule VI than in lobule VIII. This lasting morphological change correlates with an increase in the charge transfer at the CF/PC synapses in a subpopulation of PCs, suggesting that the connectivity between a group of climbing fibers and their target PCs has been strengthened abnormally by the neonatal administration of PCP. One possible explanation would come from the fact that the cerebellum has an asynchronous development: for example dendritogenesis in lobules I and X occur earlier than in lobules VI, VII and VIII (86). In the neonatal PCP model, PCP is injected at P7, P9 and P11 and might perturb specific regions of the cerebellum because of their asynchronous maturation. Given that the olivocerebellar network is organized topographically, this lobule specific effect could have consequences on cerebellar computation in specific behavioral tasks. This is particularly relevant for neurodevelopmental disorders like schizophrenia that are not associated with a broad and homogeneous effect on behavior and cognition. Furthermore this type of selective deficits could render the system much more susceptible to secondary insults during circuit maturation leading to specific behavioral symptoms, in line with the multifactorial etiology of disorders such as schizophrenia. Synaptic deficits in postmortem tissues and genetic association with mutations in synaptic genes indicate that schizophrenia is a synaptopathy. While it is considered that schizophrenia has a developmental origin (87), little is known about the precise developmental mechanisms leading to synaptic deficits in this disease. While initially thought to be essentially a motor task-related structure, many studies highlight the role of the cerebellum in cognition (35, 36, 88–91). The cerebellum emerges now as a potential actor of psychiatric disorders, such as Autism Spectrum Disorders (92, 93) or schizophrenia (94). Together with our demonstration of CF deficits in the neonatal PCP model, this warrants the search for cerebellar synaptic deficits in postmortem tissue from schizophrenic patients and further studies of cerebellar involvement in the pathophysiology of this disease.

Materials and Methods

Animals
All animal protocols were approved by the *Comité Regional d'Ethique en Experimentation Animale* (#21815) and animals were housed in authorized facilities of the CIRB (# C75 05 12). Phencyclidine (Phencyclidine hydrochloride, #P3029, Merck KGaA, Darmstadt, 10mg/kg diluted in saline solution) or vehicle (saline solution) was injected subcutaneously at P7, P9 and P11 in C57BL6/J mice. The NeuroD1Cre mouse line (Tg(Neurod1-cre)RZ24Gsat/Mmucd) was obtained from Mary Beth Hatten, and transgene detection was performed using the following primers: 5'TAG GAT TAG GGA GAG GGA GCT GAA 3' and 5' CGG CAA ACG GAC AGA AGC ATT 3'. The hM3Dq DREADD mouse line was obtained from the Jackson laboratory *(B6N;129-Tg(CAG-CHRM3*,-mCitrine)1Ute/J)*, and transgene detection was performed using the following primers: 5' CAG GTC GGC TCC AGC ATT 3' and 5' TCA CCA GTC ATT TCT GCC TTT G 3'. NeuroD1cre homozygous mice were crossed with hM3Dq DREADD heterozygous mice in order to obtain NeuroD1cre -hM3Dq double heterozygous and NeuroD1cre heterozygous/hM3Dq control (WT) mice in the same litters. Mice from both sexes were used in our experiments.

Antibodies
The following primary antibodies were used: mouse monoclonal anti-CABP (1:1000; Swant, Switzerland, #300), rabbit polyclonal anti-CABP (1:1000; Swant, #CB38), guinea pig polyclonal anti VGLUT1 (1:5000; Millipore, Massachusetts, USA, #AB5905), guinea pig polyclonal anti-VGLUT2 (1:5000; Millipore, #AB2251), goat anti-foxP2 (1:2000, Abcam, Cambridge, United kingdom, #ab1307), chicken anti-GFP (1:1000; Abcam, #ab13970), mouse anti-Parvalbumin (1:1000: Swant, #PV235), rabbit (1:1000, Abcam, #ab6556), and mouse anti-GAD65 (1:500, Abcam, #ab26113).

The following secondary antibodies were used: donkey polyclonal anti-guinea pig Alexa Fluor 594 (2µg/mL; Invitrogen, California, USA, #A11076), donkey anti-mouse Alexa Fluor 488 (2µg/mL; Invitrogen, #R37114), donkey polyclonal anti-Mouse Alexa Fluor 568 (2µg/mL; Invitrogen, #A10037), donkey polyclonal anti-Rabbit Alexa Fluor 488 (2µg/mL; invitrogen, #A21206).

Immunohistochemistry
Brains were extracted after intracardiac perfusion of mice with 4% paraformaldehyde (PFA) in phosphate-buffered saline (PBS) solution. Brains were post-fixed in 4% PFA/PBS for one hour at 4°C, and then cryoprotected for 48h in a 30% sucrose/PBS solution at 4°C. After sectioning with a freezing microtome, 30µm-thick sections were washed and blocked with 4% normal donkey serum in PBS for 30 minutes at room temperature. The primary antibodies were diluted in PBS, 1% triton X-100, 1% donkey serum, and incubated overnight at 4°C under agitation. The sections were then washed three times for five minutes in PBS 1% triton X-100 and incubated for one hour at room temperature in the secondary antibody, diluted in PBS, 1% triton X-100, 1% donkey serum. The sections were then incubated for 15 minutes at room temperature with the nuclear marker Hoechst 33342 (0,2 mg/mL, Sigma, Gothenburg, Sweden, Cat#H6024) in PBS 0.2% triton. After washing, the sections were mounted with ProLong Gold Antifade Reagent (Invitrogen, #P36930).

Single molecule fluorescent in situ hybridization
Brains were extracted after intracardiac perfusion of mice with 4% paraformaldehyde (PFA) solution and post-fixed at 4°C for 24 hours. Brains were cryopreserved 24 hours in 10%, 20%, 30% sucrose/PBS at 4°C. Parasagittal sections were cut (30 µm-thick) using a freezing microtome and stored at -20°C in cryoprotectant until use. Slides mounted with sections were processed using the RNAscope Multiplex Fluorescent Assay (ACD, cat#323100) according to manufacturer instructions. SinglePlex *in situ* hybridization were done with the *Ctgf* RNAscope probe (ACD, cat# 314541). DAPI was used to stain nuclei and sections were mounted with Prolong Gold Antifade reagent. Images were taken using a spinning-disk confocal CSU-W1 microscope. Quantifications were performed using a custom-made java plugin for unbiased detection of individual RNA puncta inside each region of interest.

Image acquisition and quantifications
Images for global cerebellar morphology were acquired using a Zeiss Axiozoom V16 macroscope, equipped with a digital camera (AxioCam HRm) using a 10x objective (pixel size: 0,650µm).
Images for synaptic quantifications in the PCP experiment were acquired using a Leica SP5 upright confocal microscope, using a 63x objective (1.4 NA, WD: 0.1mm), pixel size 57x57nm. The pinhole aperture was set to one Airy Unit and a z-step of 200 nm was used. Laser intensity and photomultiplier tube (PMT) gain was set in order to occupy the full dynamic range of the detector. Images were acquired in 16-bit range.

Images for synaptic quantifications in the NeuroD1cre/hM3Dq experiment were taken using a Zeiss Axioobserver Z1 inverted spinning disk microscope with a CSUW11 scan head and a 63x objective (1.4NA, WD:0.1mm, pixel size 103x103nm)
All the quantifications were done in blind condition, with the Fiji opensource software (95).
For VGLUT2, GAD65, and PV neuron quantifications, all the images were normalized using the quantile-based normalization plugin of Fiji (https://www.longair.net/edinburgh/imagej/quantile-normalization/). The intensity distribution of the images has been normalized using 256 quantiles for each staining.
The synaptic boutons were extracted from the background using the 3D Weka Segmentation plugin (https://imagej.net/Trainable_Weka_Segmentation) after manual selection of signal and background samples. The Fiji built-in plugin 3D object counter was then used in order to count and measure every object (cluster of VGLUT2 or GAD65 positive signal, or a whole PV+ molecular layer interneuron).
For VGLUT1 quantification, the background of the whole image was subtracted using the Fiji built-in subtract background plugin. The signal measured was the raw integrated density (the sum of the values of the pixels in the selection) divided by the area in µm², thus providing a measure of the mean intensity per µm².

Gene expression analysis

Translational profiling of inferior olivary neurons

The RP23-454P8 bacterial artificial chromosome (BAC) driver was modified according to previously published protocols (96) to drive the expression of the *EGFPL10a* transgene under the regulatory elements of the *Cdk6* gene. The mouse line Cdk6-EGFPL10A was then generated by random transgenesis via injection of the modified BAC in FVB/N mouse oocytes (mouse oocyte injection performed at the SEAT (UPS44) CNRS, France).
The gene expression profile of inferior olivary neurons was identified using bacTRAP purification of EGFP-tagged polysomes from the Cdk6-EGFPL10A and S10010-EGFPL10A mouse lines according to previously published protocols (57). For each set, brainstems were dissected from twenty adult mice (both males and females). Four independent sets of immunopurification were performed for the Cdk6-EGFPL10A line and three sets for the S100A10-EGFPL10A line. RNA quantity and quality were determined with a Nanodrop spectrophotometer (Wilmington, DE) and Agilent 2100 Bioanalyzer (Foster City, CA). For each sample, total RNA was amplified with the Affymetrix two-cycle amplification kit and hybridized to Affymetrix 430 2.0 microarrays according to the manufacturer's instructions (for the Cdk6-EGFPL10A line at the Plateforme BIOPUCES et SEQUENCAGE, IGBMC, Illkirch, France; for the S100A10 -EGFPL10A line at the Rockefeller University facility, USA). Analysis was performed using the GeneSpringGX software (version 11.5). First, mRNAs expressed and enriched in IONs compared to the rest of the brainstem were identified by comparing immunoprecipitated mRNAs with the unbound fraction as described in (57, 97) using a threshold of 1.5 to obtain a baseline level of expression. Second, the immunoprecipitated fraction from IONs was compared to the immunoprecipitated fraction from the NeuroD1-EGFPL10A line (57) corresponding to the granule cells using a high threshold (≥ 5) to obtain a high level of input cell specificity. Both lists were then compared to identify common genes that constituted the final gene list for each cell type.

RNA extraction

The cerebellum and brainstem were dissected in cold Hanks balanced salt solution (HBSS). After removal of the meninges, the tissues were frozen in liquid nitrogen and stored at -80C°. Total RNA was extracted using the Qiagen RNeasy mini kit (Qiagen, Venlo, Netherlands, #74106) following tissue homogenization, according to manufacturer's instruction.

High throughput RTqPCR.

RNA quality and integrity were analyzed by capillary electrophoresis with the Fragment Analyzer (Agilent Technologies). The mean RNA Quality Number (defined on a scale ranging from 1 to 10) of the samples was 9.6. cDNAs were synthesized using 100ng total RNAs using Reverse Transcription Master Mix from Fluidigm™ on a Nexus Thermocycler (Eppendorf®) following the temperature protocol: 5min at 25°C, 30min at 42°C followed by heat-inactivation of the reverse transcriptase for 5min at 85°C and immediately cooled to 4°C. cDNA samples were diluted 5 times in low TE buffer [10mM Tris ; 0.1mM EDTA; pH = 8.0] (TEKNOVA®) and used for specific target multiplex pre-amplification using Fluidigm® PreAmp Master Mix and pooled TaqMan® Gene Expression assays (Life Technologies, ThermoFisher) with a final concentration of each assay of 180nM (temperature protocol: 95°C for 2min, followed by 18 cycles at 95°C for 15s and 60°C for 4min). Pre-designed Taqman Gene Expression assay are listed in Supplemental data 1. Quantitative PCR was performed using the high-throughput platform BioMark™ HD System and the 96.96 GE Dynamic Arrays (Fluidigm®). The expression of target genes was

quantified in the samples by quantitative PCR on 96.96 microfluidic chips. The 5 times diluted pre-amplified cDNAs and assays were mixed inside the chip using HX IFC controller (Fluidigm). The loaded Dynamic Array was transferred to the Biomark™ real-time PCR instrument and subjected to PCR experiment (25°C for 30min and 70°C for 60min for thermal mix; 50°C for 2min and 95°C for 10min for hot start; 40 cycles at 95°C for 15s and 60°C for 1min). The parameters of the thermocycler were set with ROX as passive reference and single probe FAM-MGB as fluorescent detector. To determine the quantification cycle Ct, data were processed by automatic threshold for each assay, with linear derivative baseline correction using BioMark Real-Time PCR Analysis Software 4.0.1 (Fluidigm). The quality threshold was set at the default setting of 0.65.
The raw data from gene expression analysis were extracted and analyzed using MATLAB. For the systematic fold change and statistical test analysis, a script was written using the R opensource software. For each dataset, a multiple t test comparison was performed on the 323 genes, assuming a normal distribution and the equality of variances. Benjamini-Hochberg procedure for multiple correction was performed. The delta Ct method (2−ΔCt) was used to determine the relative fold gene expression, using the formula $Q=2^{(deltaCT)}$, where (deltaCT) = CT(treated) - CT(untreated). The data were normalized to *Rpl13a*, which showed the most stable expression among all the samples.

Droplet Digital™ PCR (ddPCR™, BioRad)
Equivalent amounts of total RNA (100 ng) were reverse-transcribed using SuperScript® VILO™ cDNA Synthesis kit (Life Technologies, California, USA, Cat#11754-250), according to manufacturer's instructions. The cDNA samples diluted 5 times were mixed with the fluorescent probes FAM-labeled along with the VIC-labeled Rpl13a reference (pre-designed Taqman Gene Expression assay, Supplemental data 1) and ddPCR™ Supermix for Probes (No dUTP) (BioRad, California, USA Cat#1863023). The samples were then fractionated into >12.000 droplets in water–oil emulsion using the automatic droplet generator (Bio-Rad). The template molecules from each droplet were PCR amplified in a thermocycler (BioRad), following the protocol: one cycle of 95 °C for 10 minutes, 40 cycles of 94 °C for 30 seconds and 60 °C for one minute, and one cycle of 98 °C for 10 minutes. The fluorescence (FAM, VIC) in each droplet was then digitally counted using QX200 droplet reader (Bio-Rad). QuantaSoft analysis software (Bio-Rad) was used for data acquisition and analysis. For each assay, identical manual threshold was selected, and relative expression was determined doing the ratio of the number of copies of template molecules/µl of reaction to the number of copies of the reference/µl of reaction.

High density microelectrode array (MEA) analysis of Purkinje cell spiking
Acute cerebellar slices were obtained from P30 to P38 mice in artificial cerebrospinal fluid (ACSF) containing (in mM): NaCl 125, KCl 2.5, D(+)Glucose 25, $NaHCO_3$ 25, NaH_2PO_4 1.25, $CaCl_2$ 2, and $MgCl_2$ 1, gassed with 5% CO_2/95% O_2. Parasagittal slices (320 µm) were cut at 30°C with a Campden Ci 7000 smz microtome at an advance speed of 0.03 mm/s and vertical vibration set to 0.1–0.3 µm. Slices were then transferred to a chamber filled with oxygenated ACSF at 37°C and allowed to recover for 1 h before recordings.
For recordings, the slices were placed over a high-density MEA of 4096 electrodes (electrode size, 21×21 µm; pitch, 42 µm; 64 × 64 matrix; Biocam X, 3Brain, Wädenswil, Switzerland), and constantly perfused with oxygenated ACSF at 37C°. Extracellular activity was digitized at 17 kHz and data were analyzed with the SpyKING CIRCUS software (98). Data were automatically sorted into individual units using the following parameters: cut off = 200hz (cut-off frequency for the butterworth filter), spike threshold (threshold for spike detection) = 6, N_t (width of the template) = 5 cc_merge = 0.95 (merging if cross-correlation similarity > 0.95). We excluded units presenting more than 5% of refractory period violation (refractory period between two spikes set to 3 ms). Firing pattern variability, or regularity, is defined as a measure of the consistency of time intervals between spikes [interspike interval (ISI) = seconds]. To quantify the average variability in firing patterns, the coefficient of variance of the ISI (CV) was calculated as the ratio of the standard deviation (SD) of ISIs to the mean ISI of a given cell. To measure rhythmicity of cells, CV2 was calculated. CV2 measures firing pattern variability within a short period of two ISIs [$CV2 = 2|ISI_{n+1} - ISI_n|/(ISI_{n+1} + ISI_n)$] (47).

Patch-clamp recordings
Acute parasagittal cerebellar slices were obtained from PCP or vehicle-treated mice from P24 to P28. 200 µm-thick slices were cut at room temperature with a Campden Ci 7000 smz microtome in (in mM): Sucrose 120, NaCl 60, KCl 2.5, D(+)Glucose 25, $NaHCO_3$ 25, NaH_2PO_4 1.25, $CaCl_2$ 0.1, $MgCl_2$ 3, ascorbic acid 0.4, myo-inositol 3, NaPyruvate 2, pH=7.3-7.4. Slices were then transferred and allowed to recover for one hour at room temperature in the following solution (in mM): NaCl 125, KCl 2.5,

D(+)Glucose 25, $NaHCO_3$ 25, NaH_2PO_4 1.25, $CaCl_2$ 2, $MgCl_2$ 1, ascorbic acid 0.4, myo-inositol 3, NaPyruvate 2, pH=7.3-7.4, oxygenated. This solution was used to fill the stimulation pipette and, complemented with picrotoxin (100 μM) was used as external solution for recordings. Borosilicate glass pipettes with 2-5 MΩ resistance were used for recordings and filled with the following internal solution (in mM): CsCl2 155, Hepes 10, EDTA 5, QX314 5, pH=7.35 adjusted with CsOH. Responses to CF stimulation were recorded at a holding membrane potential of −10 mV in Purkinje cells of lobule VI using a MultiClamp 700B amplifier (Molecular Devices, CA) and acquired using the freeware WinWCP written by John Dempster (https://pureportal.strath.ac.uk/en/datasets/strathclyde-electrophysiology-software-winwcp-winedr). Series resistance was compensated by 80–90% and cells were discarded if significant changes were detected. CF-mediated responses were identified by the typical all-or-none response and strong depression displayed by the second response elicited during paired pulse stimulations (20 Hz). Electrophysiological data were analyzed using the software Clampfit 10.7 (Molecular Devices).

Statistical Analysis

Data were analyzed using GraphPad Prism for statistics. Values are given as mean± SEM.

Normality was estimated using the d'Agostino Pearson normality test. The means between two conditions were compared using unpaired Student's t test when both data sets followed a normal law and when the variances are not significantly different (F test to compare variance). When data were normally distributed but their variances were different, the Welch's t test was used. When the dataset didn't follow a normal law, the means were compared using a Mann Whitney nonparametric test. In order to identify and remove potential outliers in our data, we used the Robust regression and outlier removal (ROUT) test, with a Q fixed at 1%. One outlier was identified in the VGLUT2 volume quantification (indicated in the data file).

Acknowledgments

We would like to thank P. Marin, and B. Ducos for helpful discussions, E. Schmidt for the S100a10 mouse line and Mary Beth Hatten for the Neurod1Cre line. We also thank Pierre Yger for help with the SpyKING CIRCUS software, Philippe Mailly for the quantification plugin used for the RNAscope experiment, France Maloumian for some infographics and the personnel from the CIRB animal and imaging facilities. High throughput qPCR was carried out on the qPCR-HD-Genomic Paris Centre platform supported by grants from Région Ile-de-France.
This work was supported by funding from: Association Française du Syndrome de Rett, ATIP-AVENIR program (RSE11005JSA to FS), Idex PSL ANR-10-IDEX-0001-02 PSL*(FS), Fondation pour la Recherche Médicale Equipe FRM DEQ20150331748 (FS) and European Research Council ERC consolidator grant SynID 724601 (to FS), the ENS Labex MemoLife (ANR-10-LABX-54 MEMO LIFE, to KI and AU). KI was supported by a PhD grant from the Ecole des Neurosciences de Paris (ENP).

References

1. E. F. Domino, E. D. Luby, Phencyclidine/schizophrenia: One view toward the past, the other to the future. Schizophrenia Bulletin 38, 914–919 (2012).

2. D. Lodge, M. S. Mercier, Ketamine and phencyclidine: The good, the bad and the unexpected. British Journal of Pharmacology 172, 4254–4276 (2015).

3. C. Jones, D. Watson, K. Fone, Animal models of schizophrenia. British Journal of Pharmacology 164, 1162–1194 (2011).

4. C. Wang, et al., Long-term behavioral and neurodegenerative effects of perinatal phencyclidine administration: implications for schizophrenia. Neuroscience 107, 535–550 (2001).

5. A. Nakatani-Pawlak, K. Yamaguchi, Y. Tatsumi, H. Mizoguchi, Y. Yoneda, Neonatal Phencyclidine Treatment in Mice Induces Behavioral, Histological and Neurochemical Abnormalities in Adulthood. Biol. Pharm. Bull. 32, 1576–1583 (2009).

6. J.-P. Terranova, et al., SSR181507, a dopamine D2 receptor antagonist and 5-HT1A receptor agonist, alleviates disturbances of novelty discrimination in a social context in rats, a putative model of selective attention deficit. Psychopharmacology 181, 134–144 (2005).

7. J. Meffre, et al., 5-HT 6 receptor recruitment of mTOR as a mechanism for perturbed cognition in schizophrenia: 5-HT 6 receptors activate mTOR to control cognition. EMBO Molecular Medicine 4, 1043–1056 (2012).

8. N. E. Clifton, N. Morisot, S. Girardon, M. J. Millan, F. Loiseau, Enhancement of social novelty discrimination by positive allosteric modulators at metabotropic glutamate 5 receptors: adolescent administration prevents adult-onset deficits induced by neonatal treatment with phencyclidine. Psychopharmacology 225, 579–594 (2013).

9. N. C. Anastasio, K. M. Johnson, Atypical Antischizophrenic Drugs Prevent Changes in Cortical N-Methyl-D-Aspartate Receptors and Behavior Following Sub-chronic Phencyclidine Administration in Developing Rat Pups. Pharmacol Biochem Behav 90, 569–577 (2008).

10. C. Kjaerby, C. Bundgaard, K. Fejgin, U. Kristiansen, N. O. Dalby, Repeated potentiation of the metabotropic glutamate receptor 5 and the alpha 7 nicotinic acetylcholine receptor modulates behavioural and GABAergic deficits induced by early postnatal phencyclidine (PCP) treatment. Neuropharmacology 72, 157–168 (2013).

11. F. Rahbar, A. Fomufod, D. White, L. S. Westney, Impact of intrauterine exposure to phencyclidine (PCP) and cocaine on neonates. Journal of the National Medical Association 85, 349–352 (1993).

12. S. I. Deutsch, J. Mastropaolo, R. B. Rosse, Neurodevelopmental consequences of early exposure to phencyclidine and related drugs. Clinical Neuropharmacology 21, 320–332 (1998).

13. J. Rapoport, J. Giedd, N. Gogtay, Neurodevelopmental model of schizophrenia: update 2012. Mol Psychiatry 17, 1228–1238 (2012).

14. L. A. Glantz, D. A. Lewis, Reduction of Synaptophysin Immunoreactivity in the Prefrontal Cortex of Subjects With Schizophrenia: Regional and Diagnostic Specificity. Arch Gen Psychiatry 54, 660–669 (1997).

15. C. N. Karson, et al., Alterations in synaptic proteins and their encoding mRNAs in prefrontal cortex in schizophrenia: a possible neurochemical basis for 'hypofrontality.' Mol Psychiatry 4, 39–45 (1999).

16. S. L. Eastwood, P. J. Harrison, Decreased expression of vesicular glutamate transporter 1 and complexin II mRNAs in schizophrenia: further evidence for a synaptic pathology affecting glutamate neurons. Schizophrenia Research 73, 159–172 (2005).

17. E. Scarr, L. Gray, D. Keriakous, P. J. Robinson, B. Dean, Increased levels of SNAP-25 and synaptophysin in the dorsolateral prefrontal cortex in bipolar I disorder. Bipolar Disord 8, 133–143 (2006).

18. S. M. Purcell, et al., A polygenic burden of rare disruptive mutations in schizophrenia. Nature 506, 185–190 (2014).

19. S. Ripke, et al., Biological insights from 108 schizophrenia-associated genetic loci. Nature 511, 421–427 (2014).

20. E. F. Osimo, K. Beck, T. R. Marques, O. D. Howes, Synaptic loss in schizophrenia: a meta-analysis and systematic review of synaptic protein and mRNA measures. Mol Psychiatry 24, 549–561 (2019).

21. R. C. Roberts, L. A. Gaither, F. J. Peretti, B. Lapidus, D. J. Chute, Synaptic organization of the human striatum: A postmortem ultrastructural study. Journal of Comparative Neurology 374, 523–534 (1996).

22. L. A. Glantz, D. A. Lewis, Decreased Dendritic Spine Density on Prefrontal Cortical Pyramidal Neurons in Schizophrenia. Arch Gen Psychiatry 57, 65–73 (2000).

23. G. Rosoklija, et al., Structural Abnormalities of Subicular Dendrites in Subjects With Schizophrenia and Mood Disorders: Preliminary Findings. Arch Gen Psychiatry 57, 349–356 (2000).

24. G. P. Reynolds, Z. Abdul-Monim, J. C. Neill, Z.-J. Zhang, Calcium binding protein markers of GABA deficits in schizophrenia — post mortem studies and animal models. Neurotoxicity Research, 57–61 (2004).

25. T. A. Jenkins, M. K. Harte, C. E. McKibben, J. J. Elliott, G. P. Reynolds, Disturbances in social interaction occur along with pathophysiological deficits following sub-chronic phencyclidine administration in the rat. Behavioural Brain Research 194, 230–235 (2008).

26. A. Mouri, Y. Noda, T. Enomoto, T. Nabeshima, Phencyclidine animal models of schizophrenia: Approaches from abnormality of glutamatergic neurotransmission and neurodevelopment. Neurochemistry International 51, 173–184 (2007).

27. S. S. Kaalund, et al., Differential expression of parvalbumin in neonatal phencyclidine-treated rats and socially isolated rats. J. Neurochem. 124, 548–557 (2013).

28. B. Yu, C. Wang, J. Liu, K. M. Johnson, J. P. Gallagher, Adaptation to chronic PCP results in hyperfunctional NMDA and hypofunctional GABAA synaptic receptors. Neuroscience 113, 1–10 (2002).

29. T. Nomura, et al., Subchronic phencyclidine treatment in adult mice increases GABAergic transmission and LTP threshold in the hippocampus. Neuropharmacology 100, 90–97 (2016).

30. C. Kjaerby, B. V. Broberg, U. Kristiansen, N. O. Dalby, Impaired GABAergic Inhibition in the Prefrontal Cortex of Early Postnatal Phencyclidine (PCP)-Treated Rats. Cerebral Cortex 24, 2522–2532 (2014).

31. J. D. Schmahmann, An Emerging Concept: The Cerebellar Contribution to Higher Function. Archives of Neurology 48, 1178–1187 (1991).

32. C. J. Stoodley, J. D. Schmahmann, Evidence for topographic organization in the cerebellum of motor control versus cognitive and affective processing. Cortex 46, 831–844 (2010).

33. C. Rochefort, et al., Cerebellum Shapes Hippocampal Spatial Code. Science 334, 385–389 (2011).

34. X. Guell, F. Hoche, J. D. Schmahmann, Metalinguistic deficits in patients with cerebellar dysfunction: empirical support for the dysmetria of thought theory. Cerebellum 14, 50–58 (2015).

35. M. J. Wagner, T. H. Kim, J. Savall, M. J. Schnitzer, L. Luo, Cerebellar granule cells encode the expectation of reward. Nature 544, 96–100 (2017).

36. A. Badura, et al., Normal cognitive and social development require posterior cerebellar activity. eLife 7, e36401 (2018).

37. D. R. Weinberger, J. E. Kleinman, D. J. Luchins, L. B. Bigelow, R. J. Wyatt, Cerebellar pathology in schizophrenia: a controlled postmortem study. Am J Psychiatry 137, 359–361 (1980).

38. N. C. Andreasen, et al., Schizophrenia and cognitive dysmetria: a positron-emission tomography study of dysfunctional prefrontal-thalamic-cerebellar circuitry. Proceedings of the National Academy of Sciences 93, 9985–9990 (1996).

39. T. Moberget, et al., Cerebellar Gray Matter Volume Is Associated With Cognitive Function and Psychopathology in Adolescence. Biological Psychiatry, 65–75 (2019).

40. D. Hirjak, P. A. Thomann, K. M. Kubera, B. Stieltjes, R. C. Wolf, Cerebellar contributions to neurological soft signs in healthy young adults. Eur Arch Psychiatry Clin Neurosci 266, 35–41 (2016).

41. T. H. Wassink, N. C. Andreasen, P. Nopoulos, M. Flaum, Cerebellar morphology as a predictor of symptom and psychosocial outcome in schizophrenia. Biological Psychiatry 45, 41–48 (1999).

42. R. Prikryl, E. Ceskova, T. Kasparek, H. Kucerova, Neurological soft signs and their relationship to 1-year outcome in first-episode schizophrenia. European Psychiatry 22, 499–504 (2007).

43. H. Picard, I. Amado, S. Mouchet-Mages, J. P. Olié, M. O. Krebs, The role of the cerebellum in schizophrenia: An update of clinical, cognitive, and functional evidences. Schizophrenia Bulletin 34, 155–172 (2008).

44. R. O. Brady, et al., Cerebellar-Prefrontal Network Connectivity and Negative Symptoms in Schizophrenia. AJP 176, 512–520 (2019).

45. T. Moberget, R. B. Ivry, Prediction, Psychosis, and the Cerebellum. Biological Psychiatry: Cognitive Neuroscience and Neuroimaging 4, 820–831 (2019).

46. M. E. van der Heijden, et al., Maturation of Purkinje cell firing properties relies on neurogenesis of excitatory neurons. eLife 10, 1–37 (2021).

48. C. J. Stoodley, The Cerebellum and Cognition: Evidence from Functional Imaging Studies. The Cerebellum 11, 352–365 (2012).

49. B. Zhang, et al., Neuroligins Sculpt Cerebellar Purkinje-Cell Circuits by Differential Control of Distinct Classes of Synapses. Neuron 87, 781–796 (2015).

50. G. Gonzalez-Burgos, T. Hashimoto, D. A. Lewis, Alterations of Cortical GABA Neurons and Network Oscillations in Schizophrenia. Curr Psychiatry Rep 12, 335–344 (2010).

51. N. Radhu, et al., Evidence for inhibitory deficits in the prefrontal cortex in schizophrenia. Brain 138, 483–497 (2015).

52. A. Konnerth, I. Llanot, C. M. Armstrongt, Synaptic currents in cerebellar Purkinje cells. Neurobiology 87, 2662–2665 (1990).

53. D. H. Ebert, M. E. Greenberg, Activity-dependent neuronal signalling and autism spectrum disorder. Nature 493, 327–337 (2013).

54. H. Hirai, et al., Cbln1 is essential for synaptic integrity and plasticity in the cerebellum. Nat. Neurosci. 8, 1534–1541 (2005).

55. W. Kakegawa, et al., Anterograde C1ql1 signaling is required in order to determine and maintain a single-winner climbing fiber in the mouse cerebellum. Neuron 85, 316–329 (2015).

56. S. M. Sigoillot, et al., The Secreted Protein C1QL1 and Its Receptor BAI3 Control the Synaptic Connectivity of Excitatory Inputs Converging on Cerebellar Purkinje Cells. Cell Reports 10, 820–832 (2015).

57. J. P. Doyle, et al., Application of a Translational Profiling Approach for the Comparative Analysis of CNS Cell Types. Cell 135, 749–762 (2008).

58. E. F. Schmidt, et al., Identification of the cortical neurons that mediate antidepressant responses. Cell 149, 1152–1163 (2012).

59. C. S. L. Lai, D. Gerrelli, A. P. Monaco, S. E. Fisher, A. J. Copp, FOXP2 expression during brain development coincides with adult sites of pathology in a severe speech and language disorder. Brain 126, 2455–2462 (2003).

60. Y. Benjamini, Y. Hochberg, Controlling the False Discovery Rate: A Practical and Powerful Approach to Multiple Testing. Journal of the Royal Statistical Society. Series B (Methodological) 57, 289–300 (1995).

61. R. Ichikawa, et al., Territories of heterologous inputs onto Purkinje cell dendrites are segregated by mGluR1-dependent parallel fiber synapse elimination. Proc Natl Acad Sci USA 113, 2282–2287 (2016).

62. D. Szklarczyk, et al., The STRING database in 2017: quality-controlled protein-protein association networks, made broadly accessible. Nucleic Acids Res. 45, D362–D368 (2017).

63. M. Hoshijima, et al., CT domain of CCN2/CTGF directly interacts with fibronectin and enhances cell adhesion of chondrocytes through integrin α5β1. FEBS Letters 580, 1376–1382 (2006).

64. K. Khodosevich, et al., Connective Tissue Growth Factor Regulates Interneuron Survival and Information Processing in the Olfactory Bulb. Neuron 79, 1136–1151 (2013).

65. B. Ohkawara, et al., CTGF/CCN2 facilitates LRP4-mediated formation of the embryonic neuromuscular junction. EMBO reports n/a, e48462 (2020).

66. Y. Ramazani, et al., Connective tissue growth factor (CTGF) from basics to clinics. Matrix Biol. 68–69, 44–66 (2018).

67. R. Nakki, J. Koistinaho, F. Sharp, S. Sagar, Cerebellar toxicity of phencyclidine. The Journal of Neuroscience 15, 2097–2108 (1995).

68. G. M. Alexander, et al., Remote Control of Neuronal Activity in Transgenic Mice Expressing Evolved G Protein-Coupled Receptors. Neuron 63, 27–39 (2009).

69. N. Zecevic, P. Rakic, Differentiation of Purkinje cells and their relationship to other components of developing cerebellar cortex in man. Journal of Comparative Neurology 167, 27–47 (1976).

70. R. D. Fields, K. Itoh, Neural cell adhesion molecules in activity-dependent development and synaptic plasticity. Trends in Neurosciences 19, 473–480 (1996).

71. K. Hashimoto, M. Kano, Synapse elimination in the developing cerebellum. Cellular and Molecular Life Sciences 70, 4667–4680 (2013).

72. H.-S. Kim, et al., Identification of a family of low-affinity insulin-like growth factor binding proteins (IGFBPs): Characterization of connective tissue growth factor as a member of the IGFBP superfamily. PNAS 94, 12981–12986 (1997).

73. J. G. Abreu, N. I. Ketpura, B. Reversade, E. M. De Robertis, Connective-tissue growth factor (CTGF) modulates cell signalling by BMP and TGF-β. Nat Cell Biol 4, 599–604 (2002).

74. S. Kakizawa, K. Yamada, M. Iino, M. Watanabe, M. Kano, Effects of insulin-like growth factor I on climbing fibre synapse elimination during cerebellar development. European Journal of Neuroscience 17, 545–554 (2003).

75. A. Kalinovsky, et al., Development of Axon-Target Specificity of Ponto-Cerebellar Afferents. PLOS Biology 9, e1001013 (2011).

76. T. Higashi, S. Tanaka, T. Iida, S. Okabe, Synapse Elimination Triggered by BMP4 Exocytosis and Presynaptic BMP Receptor Activation. Cell Reports 22, 919–929 (2018).

77. A. R. Bialas, B. Stevens, TGF-β signaling regulates neuronal C1q expression and developmental synaptic refinement. Nat Neurosci 16, 1773–1782 (2013).

78. E. Schwarz, et al., Validation of a blood-based laboratory test to aid in the confirmation of a diagnosis of schizophrenia. Biomark Insights 5, 39–47 (2010).

79. Y. Li, et al., Biomarker Identification and Effect Estimation on Schizophrenia – A High Dimensional Data Analysis. Front Public Health 3 (2015).

80. J. L. Raymond, J. F. Medina, Computational Principles of Supervised Learning in the Cerebellum. Annu. Rev. Neurosci. 41, 233–253 (2018).

81. D. R. Pierce, A. Hayar, D. K. Williams, K. E. Light, Olivary Climbing Fiber Alterations in PN40 Rat Cerebellum Following Postnatal Ethanol Exposure. Brain Res 1378, 54–65 (2011).

82. H. L. Cha, et al., Deletion of the α subunit of the heterotrimeric Go protein impairs cerebellar cortical development in mice. Molecular Brain 12, 57 (2019).

83. P. DeRosse, et al., The Genetics of Symptom-Based Phenotypes: Toward a Molecular Classification of Schizophrenia. Schizophrenia Bulletin 34, 1047–1053 (2008).

84. H.-M. Liao, et al., Identification and characterization of three inherited genomic copy number variations associated with familial schizophrenia. Schizophrenia Research 139, 229–236 (2012).

85. the International Schizophrenia Consortium, et al., Functional gene group analysis identifies synaptic gene groups as risk factor for schizophrenia. Mol Psychiatry 17, 996–1006 (2012).

86. C. Sotelo, Cellular and genetic regulation of the development of the cerebellar system. Progress in Neurobiology 72, 295–339 (2004).

87. D. R. Weinberger, The neurodevelopmental origins of schizophrenia in the penumbra of genomic medicine. World Psychiatry 16, 225–226 (2017).

88. J. D. Schmahmann, The cerebellum and cognition. Neuroscience Letters 688, 62–75 (2019).

89. N. Sendhilnathan, A. E. Ipata, M. E. Goldberg, Neural Correlates of Reinforcement Learning in Mid-lateral Cerebellum. Neuron 106, 188-198.e5 (2020).

90. L. Rondi-Reig, A.-L. Paradis, J. M. Lefort, B. M. Babayan, C. Tobin, How the cerebellum may monitor sensory information for spatial representation. Front. Syst. Neurosci. 8 (2014).

91. I. Carta, C. H. Chen, A. L. Schott, S. Dorizan, K. Khodakhah, Cerebellar modulation of the reward circuitry and social behavior. Science 363, eaav0581–eaav0581 (2019).

92. E. B. E. Becker, C. J. Stoodley, “Chapter One - Autism Spectrum Disorder and the Cerebellum” in International Review of Neurobiology, Neurobiology of Autism., G. Konopka, Ed. (Academic Press, 2013), pp. 1–34.

93. S. S.-H. Wang, A. D. Kloth, A. Badura, The Cerebellum, Sensitive Periods, and Autism. Neuron 83, 518–532 (2014).

94. N. C. Andreasen, R. Pierson, The Role of the Cerebellum in Schizophrenia. Biol Psychiatry 64, 81–88 (2008).

95. J. Schindelin, et al., Fiji: an open-source platform for biological-image analysis. Nature Methods 9, 676–682 (2012).

96. S. Gong, L. Kus, N. Heintz, Rapid bacterial artificial chromosome modification for large-scale mouse transgenesis. Nat Protoc 5, 1678–1696 (2010).

97. J. D. Dougherty, E. F. Schmidt, M. Nakajima, N. Heintz, Analytical approaches to RNA profiling data for the identification of genes enriched in specific cells. Nucleic Acids Res 38, 4218–4230 (2010).

98. P. Yger, et al., A spike sorting toolbox for up to thousands of electrodes validated with ground truth recordings in vitro and in vivo. eLife 7, e34518 (2018).

99. G. R. Holt, J. Douglas, Comparison of Discharge Variability Visual Cortex Neurons. Journal of Neurophysiology 75, 1806–1814 (1996).

Figures

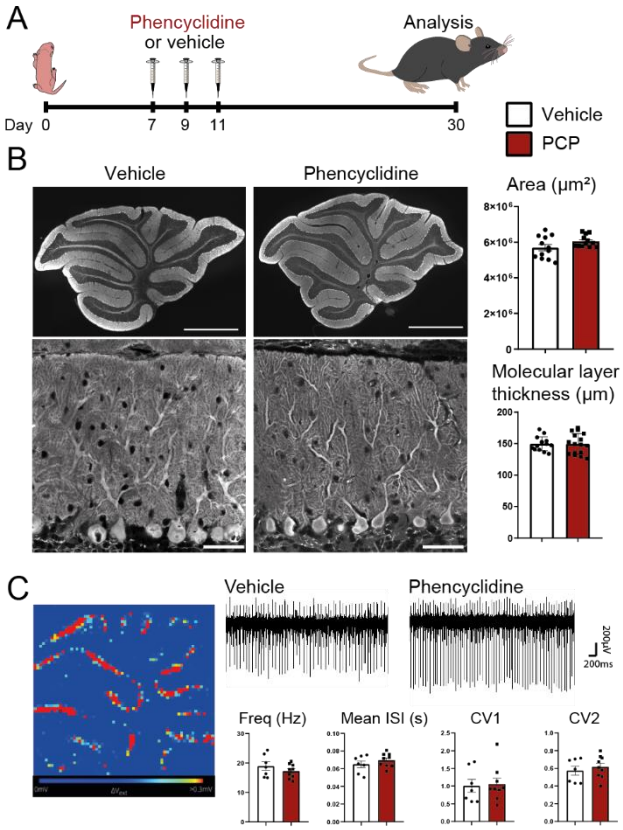

Figure 1. Neonatal Phencyclidine administration does not modify the cytoarchitecture of the cerebellum and the spontaneous activity of Purkinje cells.
(A) Experimental design. Phencyclidine (PCP, 10 mg/kg) or vehicle is injected sub-cutaneously in mouse pups at postnatal day 7 (P7), P9 and P11. Morphological and electrophysiological analysis is performed at P30.
(B) Parasagittal cerebellar sections from the vermis of P30 mice were immunolabeled with an anti-calbindin antibody, to stain Purkinje cells in their entirety and reveal cerebellar cytoarchitecture. Scale bars: Top: 1000 µm; bottom: 50 µm. Quantification of the mean area of cerebellar slices show no significant differences between the two conditions (Mean ± SEM. Vehicle: n=12 animals, PCP: n=12. Student t test p=0.0962). Representative images from Purkinje cells and their dendritic tree in lobule VI reveal similar morphology in sections from P30 vehicle- and PCP- treated animals. Quantification of the thickness of the molecular layer in the lobule VI, measured as the length from the beginning of the primary dendrite of Purkinje cells to the upper extremity of the molecular layer, reveals no significant difference between vehicle- and PCP-treated animals (lobule VI is shown here, Mean ± SEM. Vehicle: n=14 animals, PCP: n=16 animals. Unpaired Student's t test p=0.964).
(C) High density microelectrode arrays (MEA) were used to record Purkinje cell spontaneous spiking in acute cerebellar slices from P30 mice. An example of the recorded electrical activity in a cerebellar slice from a vehicle-treated mouse is shown with each pixel representing one channel, and units showing high activity in red, and low activity in blue. A representative trace of recordings from one channel is shown for each condition. Spike sorting using the SpyKING CIRCUS software allowed estimation of the mean firing rate, mean Inter Spike Interval (ISI), coefficient of variation of ISIs (CV) and CV2. No significant difference was detected in any of these parameters (Mean ± SEM. Vehicle: n=7 animals, PCP, n=9 animals. Unpaired Student's t test).

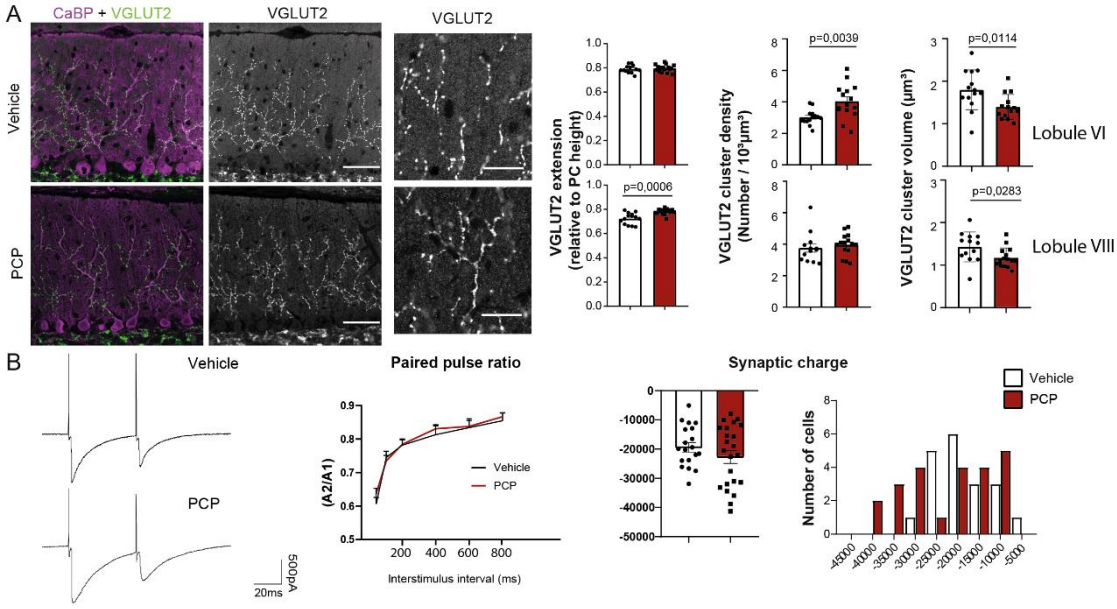

Figure 2. Neonatal phencyclidine administration leads to long lasting changes in climbing fiber/Purkinje cell connectivity.
(A) Climbing fiber presynaptic boutons were immunostained with an anti-VGLUT2 antibody (green), and Purkinje cells and their dendritic tree with an anti-calbindin antibody (magenta), in parasagittal cerebellar sections from P30 vehicle- and PCP-treated mice. Scale bar: 50 µm. High magnification image of VGLUT2 clusters are shown for both conditions. Scale bar: 20µm.
Quantifications of the extension of the climbing fiber synaptic territory, mean volume of the VGLUT2 puncta and their mean density were performed in lobules VI and VIII (Mean ± SEM are represented, with p values when they are significant; unpaired Student's t test for the volume, Welch's t test for the extension and density; vehicle n=13-14 animals, PCP: n=15-16 animals.
(B) Purkinje cell responses after climbing fiber stimulation were recorded using patch-clamp. Representative traces of responses obtained in Purkinje cells from lobule VI after paired pulse stimulation (50 ms interval) are shown for both conditions. No difference in the paired-pulse ratio (ratio between the amplitude of the second response and the first response A2/A1) was detected regardless of the stimuli interval between PCP mice and vehicle mice (Kolmogorov-Smirnov test). The mean synaptic charge after climbing fiber stimulation is not significantly different between the PCP and vehicle conditions (vehicle: n = 19 cells/ 9 mice and PCP: n = 23 cells/ 9 mice; unpaired Student's t test), but a change in the distribution is visible with a shift towards higher charges in the PCP condition.

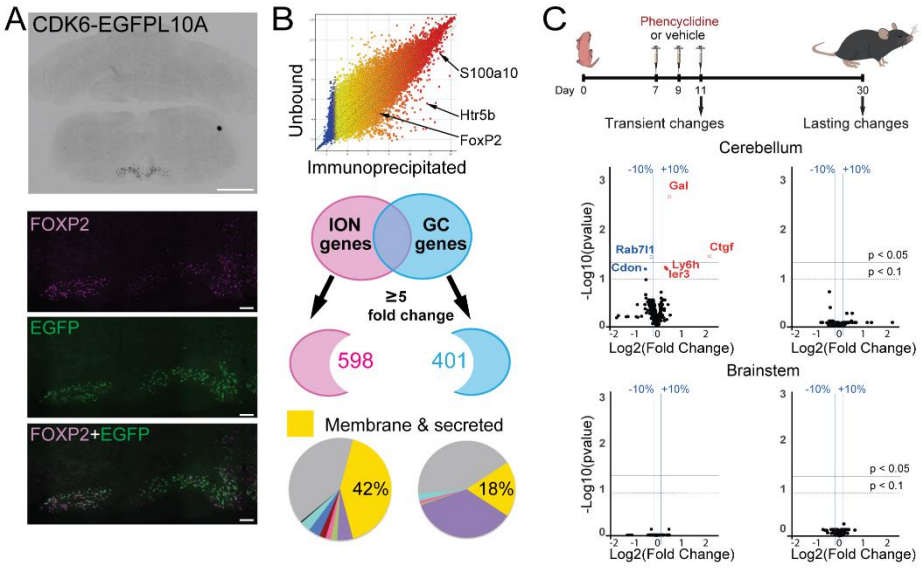

Figure 3. Neonatal Phencyclidine administration induces transient translatome changes in the cerebellum

(A) Translational profiling of inferior olivary neurons. The Cdk6 BAC driver was used to drive specifically EGFPL10A expression in inferior olivary neurons (IONs) of the brainstem in adult mice (CDK6-EGFPL10A, scale bar: 1 mm). Immunostaining with an antibody against Foxp2, an ION-specific transcription factor, confirmed the identity of EGFPL10A expressing neurons. Scale bar: 100 µm).

***(B)* ION-enriched mRNAs were identified by comparing the immunoprecipitated fraction with the unbound fraction. Known markers of IONs, FoxP2, Htr5b, S100A10, were identified in the immunoprecipitated fraction. The ION dataset was compared to the granule cell (GC) dataset previously identified (57) to identify input specific genes (with a threshold of five). DAVID bioinformatics was then used to classify these specific genes according to their cellular localization and to identify the genes coding for the surfaceome (membrane and secreted proteins).**

***(C)* Experimental design. PCP or vehicle is injected sub-cutaneously in neonatal mice at P7, P9 and P11. Gene expression changes were analyzed from both cerebellum and brainstem mRNA extracts at either P11, to detect immediate changes after PCP treatment, or at P30, to detect long-lasting changes. Volcano plots are used to represent the changes in gene expression detected in the four groups. Each dot represents the fold change for a gene and the corresponding corrected p value (using the Benjamini-Hochberg correction for multiple t test comparison (Benjamini and Hochberg, 1995)). Y axis: $-\log_{10}$ of corrected p values. X axis: Log_2 of gene fold change. The top black horizontal bar corresponds to a false discovery rate (FDR) threshold set to 5%, the bottom dotted bar corresponds to FDR set to 10%, and vertical blue bars correspond to a fold change in gene expression level of 10%. Genes with a FDR < 5% are represented with empty circles.**

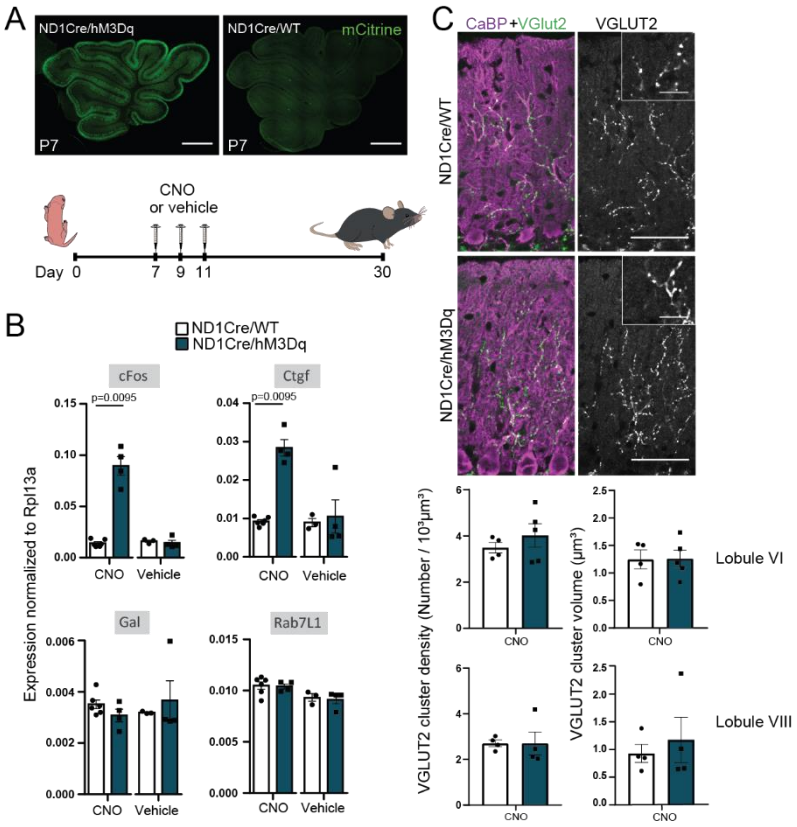

Figure 4. Increased neuronal activity in the cerebellum during postnatal development reproduces the transient increase in *Ctgf* expression, but not the long-lasting synaptic effects.
(A) A chemogenetic strategy was used to reproduce the PCP-induced increase in neuronal activity in the cerebellum during the second postnatal week. For this, knock-in mice with cre-dependent expression of the excitatory DREADD hM3Dq, along with mCitrine, were crossed with the NeuroD1CRE line that drives Cre recombinase expression in the cerebellar granule cell lineage (ND1Cre/ hM3Dq). Clozapine N-Oxide (CNO) or vehicle was injected intra-peritoneally at P7, P9 and P11, to reproduce the time course of neonatal PCP injections. Control littermates lacking hM3Dq expression in cerebellar granule cells were also analyzed (ND1Cre/WT). Inset: Expression of the DREADD hM3Dq was monitored using anti-GFP immunostaining to detect mCitrine in slices from the cerebellum of ND1Cre/hM3Dq mice at P7.
(B) ddPCR quantifications were used to monitor the gene expression changes induced by increased activity in cerebellar extracts from P11 animals. Subchronic CNO administration leads to a significant increase in *cFos* and *Ctgf* expression in extracts from ND1Cre/hM3Dq mice, but not in ND1Cre/WT littermates. *Gal* and *Rab7L1* expression levels remain unchanged. Vehicle treatment does not modify gene expression in either genotype. Gene expression is normalized to *Rpl13a*. Data are presented as Mean ±SEM. ND1Cre/WT + CNO: n = 6, ND1Cre/HM3Dq + CNO: n=4; ND1Cre/WT + vehicle: n = 3; ND1Cre/HM3Dq + vehicle: n=4. Mann Whitney U test.
(C) Top panel: Climbing fiber presynaptic boutons were immunostained with an anti-VGLUT2 antibody (green), and Purkinje cells and their dendritic tree with an anti-calbindin antibody (magenta), in parasagittal cerebellar sections from ND1Cre/hM3Dq and ND1Cre/WT control mice. All mice have been injected with CNO at P7, P9, and P11. Scale bars: 50 µm and 12.5 µm for the insert. Bottom panel: quantification of the mean density and the mean volume of VGLUT2 puncta revealed no difference in lobule VI and lobule VIII of ND1Cre/hM3Dq mice compared to control mice (Mean ± SEM. ND1Cre/WT: n=4 animals, ND1Cre/hM3Dq: n=4-5 animals. Unpaired Student's t-test).

PNAS
www.pnas.org

Supplementary Information for

Transient molecular changes and lasting synaptic effects in the cerebellum of the neonatal phencyclidine mouse model of schizophrenia.

Maxime Veleanu[1], Beetsi Urrieta-Chavez[1], Séverine M. Sigoillot[1], Maëla Paul[1], Alessia Usardi[1], Keerthana Iyer[1], Marine Delagrange[2], Joseph P. Doyle[3], Nathaniel Heintz[3], Carine Bécamel[4], Fekrije Selimi[1].
[1]Center for Interdisciplinary Research in Biology (CIRB), College de France, CNRS, INSERM, Université PSL, Paris, France
[2]Plateforme qPCR-HD-GPC, Institut de Biologie de l'Ecole Normale Supérieure, Paris, France
[3]Laboratory of Molecular Biology, Howard Hughes Medical Institute, The Rockefeller University, New York, NY, USA
[4]Institute for Functional Genomics (IGF), University of Montpellier, CNRS, INSERM, Montpellier, France

*corresponding authors: Fekrije Selimi and Nathaniel Heintz.
Email: fekrije.selimi@college-de-france.fr; heintz@rockefeller.edu

This PDF file includes:

Figures S1 to S6

Other supplementary materials for this manuscript include the following:

Dataset S1

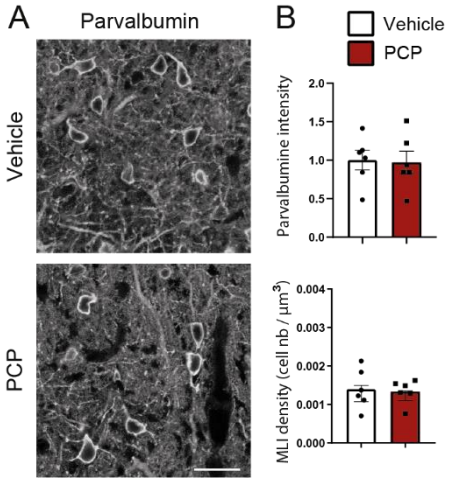

Fig. S1 Neonatal subchronic PCP treatment does not induce any changes in parvalbumin expression and molecular layer interneurons.
(A) Anti-parvalbumin immunostaining was used to reveal molecular layer interneurons (MLI) in cerebellar parasagittal sections of PCP-treated mice at P30. Scalebar = 20µm.
(B) Parvalbumin intensity, quantified using the ImageJ integrated density measurement (data normalized to vehicle), and MLI density are not changed in PCP mice compared to controls (Mean ± SEM; N= 6 per condition. Unpaired Student's t-test).

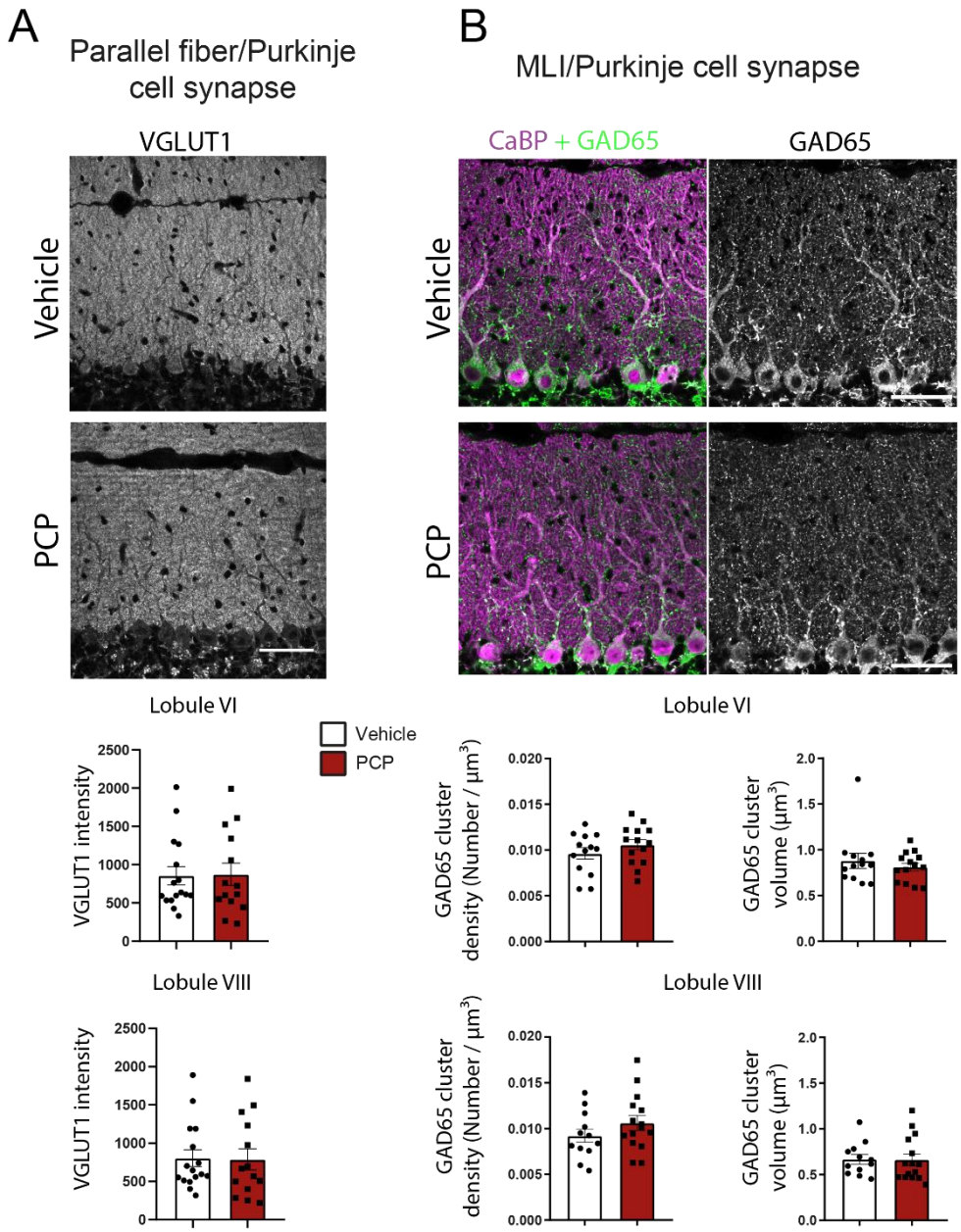

Fig. S2 Neonatal subchronic PCP treatment does not induce any changes in inhibitory synapses and parallel fiber synapses on cerebellar Purkinje cells.
(A) Parallel fiber presynaptic boutons were immunostained with an anti-VGLUT1 antibody, and an anti-calbindin antibody was used to stain Purkinje cells and its dendritic tree in parasagittal cerebellar sections from P30 vehicle and PCP mice. Scale bar: 50 µm.
Quantification of the mean VGLUT1 intensity in the molecular layer revealed no change in the PCP model, in both lobules VI and VIII (Mean ± SEM. Vehicle: n=16 animals, PCP n=14 animals. Unpaired Student's t test).
(B) Molecular layer interneurons (MLI) presynaptic boutons were immunostained with an anti-GAD65 antibody (green), and an anti-calbindin antibody (magenta) was used to stain Purkinje cells and its dendritic tree in parasagittal cerebellar sections from P30 vehicle and PCP mice. Scale bar: 50 µm.
Quantification of GAD65 puncta revealed normal presynaptic inhibitory boutons density and volumes in the molecular layer of lobules VI and VIII in PCP animals (Mean ± SEM. Vehicle: n=13 animals in lobule VI, n=14 in lobule VIII, PCP: n=14 in lobule VI, n=15 in lobule VIII. Unpaired Student's t-test for the density, and Welch's t test for the mean volume).

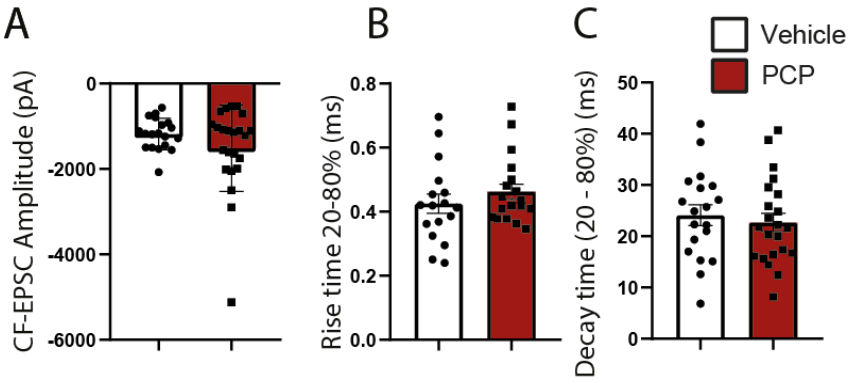

Fig. S3 Properties of climbing fiber/Purkinje cell transmission in PCP-treated mice.

(A) The mean amplitude of climbing fiber (CF)- elicited EPSC is not changed in PCP mice compared to vehicle. Note that the variance is increased in PCP treated animals (vehicle: n = 19 cells/ 9 mice; PCP n = 23 cells/ 9 mice. Welch's t test).
(B) Mean rise time (20 – 80%) is not changed in PCP mice compared to vehicle (vehicle: n = 17 cells/ 9 mice, PCP n = 19 cells/ 8 mice. Unpaired Student's t test).
(C) Decay time (20-80% is not changed in PCP mice compared to controls (vehicle: n = 17 cells/ 9 mice; PCP: n = 19 cells/ 8 mice; Unpaired Student's t test).

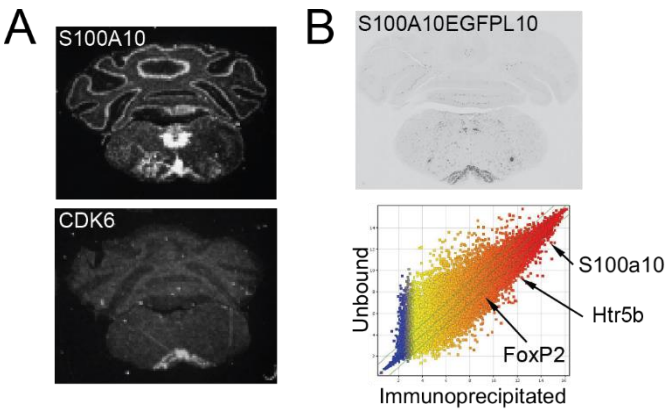

Fig S4 *S100a10* and *Cdk6* regulatory elements can be used as drivers for expression in inferior olivary neurons
(A) In situ hybridization for S100A10 and *Cdk6,* the two genes used as drivers for EGFPL10A in the bacTRAP experiments (BGEM data from gensat.org).
(B) EGFPL10A expression in the S100A10EGFPL10A line (data from gensat.org) and identification of known ION markers in the immunoprecipitated fraction after bacTRAP purification (enrichment shown compared to the unbound fraction).

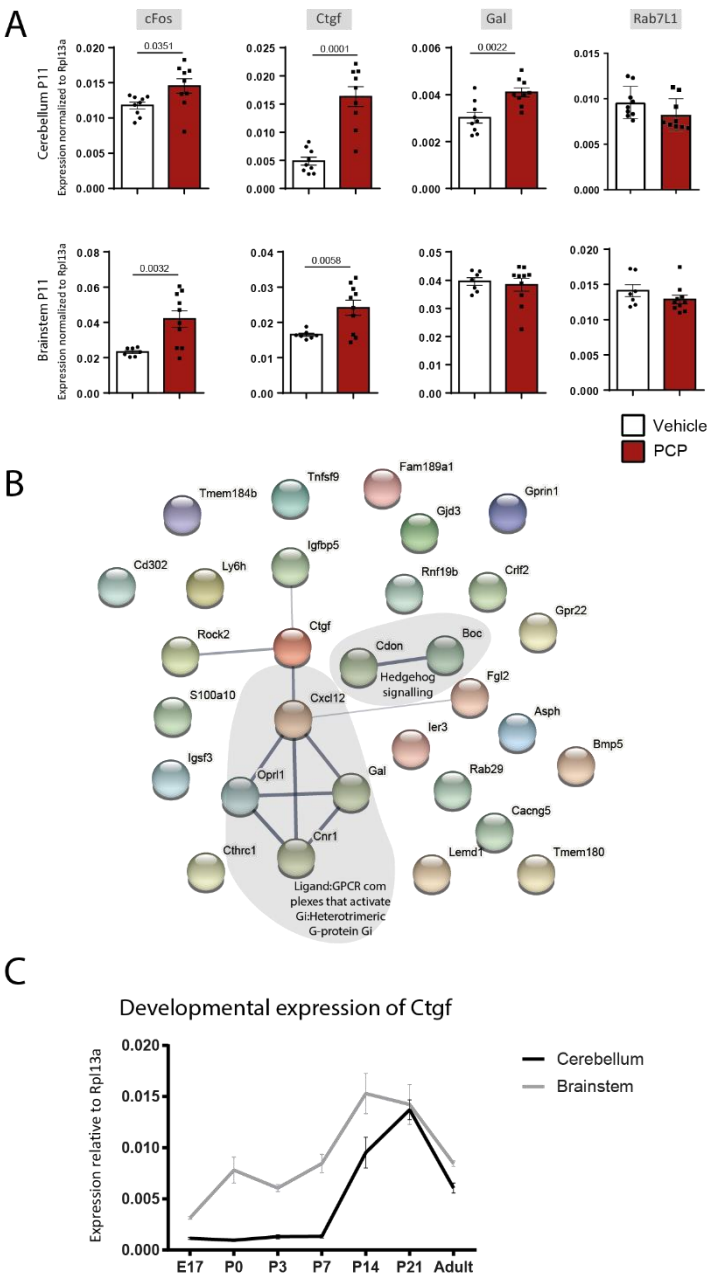

Fig. S5 *Ctgf* expression is increased by PCP and during postnatal development

(A) Molecular changes detected by high throughput RTqPCR in cerebellar and brainstem extracts were confirmed using ddPCR on mRNA extracts from P11 animals treated with PCP or vehicle at P7, P9 and P11. PCP treatment leads to a significant increase in *cFos* and *Ctgf* expression expression in both tissues, and to a significant increase in *Gal* expression in cerebellum but not brainstem tissue compared to vehicle treatment. Gene expression is normalized to *Rpl13a*. Data are presented as Mean ±SEM. Student's *t* test with Welsch's correction when variances are significantly different; Cerebellum: vehicle: n = 9, PCP: n=9; Brainstem: vehicle: n = 7; PCP: n=10. N=2 to 3 independent litters.
(B) The 30 genes found to be transiently misregulated at P11 in the cerebellum and brainstem were mapped in the String-database to represent known and predicted functional interactions between proteins. Line thickness indicates the strength of data support collected from curated databases,

extracted from PubMed abstracts or from gene fusion or co-expression databases. *Ctgf* is part of a network of several misregulated genes, including *Igfbp5*, *Rock2*, and *Cxcl12*.
(C) Expression of *Ctgf* was assessed at different stages of postnatal mouse brain development on mRNA extracts from brainstem and cerebellum. Gene expression is normalized to *Rpl13a*. Data are presented as Mean ±SEM; n= 3 to 4 animals per timepoint.

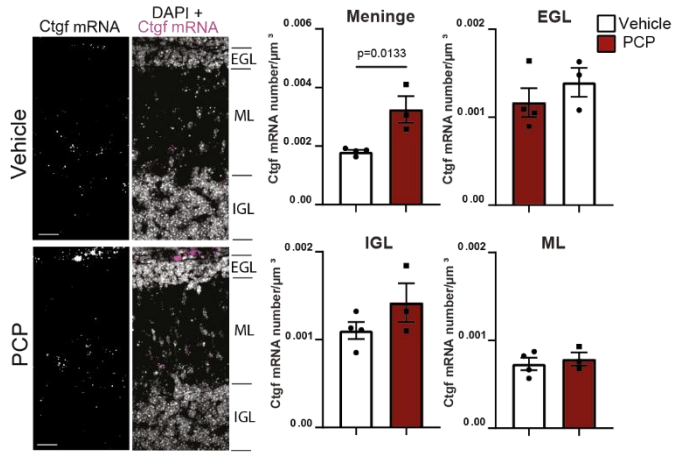

Fig. S6 Cellular expression of *Ctgf* mRNA in the cerebellum of vehicle- and PCP-treated mice.

SmFISH for *Ctgf* mRNA (*Ctgf*, magenta; DAPI, gray) in parasagittal cerebellar sections from vehicle- or PCP-treated mice at P11. Scale bar: 20µm. The number of fluorescent puncta per µm^3 were quantified in meninges (M), external granular layer (EGL), molecular layer (ML), internal granular layer (IGL) in lobule Vi and VIII (Mean ± SEM. Vehicle: n=4 animals, PCP: n=3 animals; 4 images per animals. Unpaired Student's t test).

Supplementary tables

Supplementary table 1: Fig3A-GCspecific genes-BacTRAP

	Probe Set ID	cdk6 (IP GC vs IP ION) FC	cdk6 (IP GC vs UB GC) FC	s100a10 (IP GC vs IP ION) FC	s100a10 (IP GC vs UB GC) FC	Gene
Membrane	1449903_at	-969,30884	1,8166343	-1526.1477	1.8166343	Crtam
	1428574_a_at	-206,49777	3,2506547	-67.747154	-1.1876626	Chn2
	1434673_at	-94,94498	1,6513175	-15.636596	1.6513175	Gpr22
	1439303_at	-76,55369	2,877505	-135.0198	2.877505	LOC100502679
	1439808_at	-74,77739	-1,3261086	-98.023224	-1.3261086	Ipcef1
	1433788_at	-48,995464	-1,1872914	-5.08849	-1.1872914	Nrxn3
	1441978_at	-48,52555	-1,041404	-91.22216	-1.041404	Aqp6
	1454939_at	-36,30144	1,8268837	-5.5377164	1.8268837	slc30a10
	1423592_at	-36,160316	-1,4455696	-5.72413	-1.4455696	Rock2
	1420401_a_at	-29,87695	3,6085851	-70.05258	3.6085851	Ramp3
	1456944_at	-26,292778	1,2310941	-7.954697	-1.2240206	Kcnc1
	1420884_at	-25,263685	7,287913	-29.121538	7.287913	Sln
	1457299_at	-23,11823	1,0910615	-15.631707	1.0910615	Grm4
	1452947_at	-21,248201	1,7705748	-76.855225	1.7705748	Gprc5c
	1450044_at	-21,06792	1,201468	-34.377872	1.201468	Fzd7
	1441280_at	-20,997166	2,9255443	-8.925743	2.9255443	Kcnk12
	1426869_at	-19,91993	-1,156014	-69.8785	-1.156014	Boc
	1434172_at	-17,978294	-1,4497621	-12.077083	-1.4497621	Cnr1
	1426283_at	-17,813671	1,1814297	-8.026098	1.1814297	Ntm
	1457156_at	-17,456852	1,0536102	-10.029701	1.0536102	Trhde
	1451935_a_at	-17,154842	1,3269916	-7.6259055	1.3269916	Spint2
	1450773_at	-15,895303	1,3377914	-13.56096	1.3377914	Kcnd2
	1428197_at	-14,862788	-1,1524189	-25.829494	-1.1524189	Tspan9
	1436405_at	-13,668936	1,2040209	-18.94814	1.2040209	Dock4
	1449228_at	-13,135283	1,7237887	-18.169718	1.7237887	Sh3gl2
	1424148_a_at	-11,434414	1,8150271	-9.322618	1.8150271	Stap2
	1437279_x_at	-11,090888	1,5691253	-6.9790955	1.5691253	Sdc1
	1419605_at	-10,859014	3,711838	-33.23906	3.711838	Clec10a
	1430301_at	-10,732347	-1,2258992	-6.5723996	-1.2258992	Stxbp5
	1455482_at	-10,70542	-1,0978092	-5.8576136	-1.0978092	Ap2a2
	1416012_at	-10,203089	1,1441418	-8.428408	1.412095	Ehd1
	1439669_at	-9,333114	1,3243548	-6.553746	1.3243548	6430571L13Rik
	1436082_at	-9,309461	1,273424	-10.870969	1.273424	slc24a5
	1424137_at	-8,69662	1,6216207	-30.917622	1.6216207	Gprin1
	1418602_at	-8,576852	1,3111744	-5.3343396	1.3111744	Cdh15
	1426436_at	-7,8791666	5,723027	-11.060807	5.723027	Tmem159
	1425275_at	-6,981617	-1,390801	-10.487118	-1.390801	Asph
	1419732_at	-6,960812	3,0350492	-6.5259233	3.0350492	Rtn4r
	1452784_at	-6,684033	1,134962	-7.47726	1.134962	Itgav
	1447559_at	-6,485429	2,1355171	-6.82797	2.1355171	Gpr25
	1458755_at	-6,415515	2,0417113	-6.6465545	2.0417113	Cdon
	1445194_at	-6,13347	1,1887363	-10.1613035	1.1887363	Cnksr2
	1432478_a_at	-5,567655	1,030012	-9.25929	1.030012	Rnf19b
	1424380_at	-5,5424647	1,3467699	-13.122235	1.3467699	Vps37b
	1445473_at	-5,4770956	2,0690675	-6.6592665	2.0690675	Diras2
	1446610_at	-5,311236	1,6424054	-6.8111453	1.7220502	Elmo1
	1422924_at	-5,257436	1,2926817	-5.802939	1.2926817	Tnfsf9
	1417121_at	-1552,7438	-1,2168518	-5815.1704	-1.2168518	Gabra6
	1449980_a_at	-195,77948	1,2674723	-356.29083	1.2674723	Gabrd
	1451499_at	-117,56467	1,1709421	-73.42671	1.1709421	Cadps2
	1437319_at	-67,10223	1,0361085	-77.6817	1.0361085	Unc13c
	1429105_at	-65,182205	-1,4704047	-89.44608	-1.4704047	Dlgap1
	1428986_at	-29,82594	3,095563	-15.989522	3.095563	Slc17a7
	1422878_at	-29,486862	1,1208067	-21.619844	1.1208067	Syt12
	1418984_at	-26,165714	1,8844339	-5.5006657	1.056455	Inadl
	1423322_at	-20,38082	1,0898577	-7.875043	1.0898577	Lin7c
	1457683_at	-9,130702	-1,0849253	-5.5832987	-1.0849253	Grik2
	1423258_at	-6,5673075	1,0520638	-6.743538	1.0520638	Syt9
	1426873_s_at	-6,4160905	1,7869399	-6.1616154	1.7869399	Jup
	1459105_at	-6,1857057	2,0704384	-6.3647003	2.0704384	Dlg4
	1423175_s_at	-6,1346297	1,3849128	-5.6629443	2.7586858	Pard6b
Secreted	1455445_at	-773,0212	-1,2142469	-829.1388	1.2473133	Cbln3
	1434802_s_at	-240,85023	3,8277757	-5.7138124	2.6028435	Ntf3
	1423367_at	-79,25514	1,2812445	-30.534428	1.2812445	Wnt7a
	1417391_a_at	-39,620262	1,6054308	-61.86002	1.6054308	Il16
	1452090_a_at	-25,599281	1,3354897	-5.877892	1.0330597	Olfm3
	1449234_at	-10,526747	-1,1181334	-14.2975855	-1.1181334	Car15 /// Dgcr2
	1423288_s_at	-10,468012	-1,0457915	-7.780201	-1.2102809	Cbln1
	1426566_s_at	-9,55311	1,4082711	-5.6837254	1.4082711	Il17re
	1455851_at	-8,111035	1,1535934	-61.42914	1.1535934	Bmp5
	1422313_a_at	-7,661543	3,4431353	-7.269742	-1.1870606	Igfbp5
	1418476_at	-5,7768364	2,2262187	-5.6576805	2.2262187	Crlf1
	1419527_at	-5,261447	1,0320052	-19.907871	1.0320052	Comp
	1450388_s_at	-5,0062685	-1,3625851	-5.237893	-1.3625851	Twsg1

Gene	Gene Name
Crtam	cytotoxic and regulatory T cell molecule
Chn2	chimerin (chimaerin) 2
Gpr22	G protein-coupled receptor 22
LOC100502679	neuronal growth regulator 1
Ipcef1	interaction protein for cytohesin exchange factors 1
Nrxn3	neurexin III
Aqp6	aquaporin 6
slc30a10	solute carrier family 30, member 10
Rock2	Rho-associated coiled-coil containing protein kinase 2
Ramp3	receptor (calcitonin) activity modifying protein 3; similar to receptor activity modifying protein 3
Kcnc1	potassium voltage gated channel, Shaw-related subfamily, member 1
Sln	sarcolipin
Grm4	glutamate receptor, metabotropic 4
Gprc5c	G protein-coupled receptor, family C, group 5, member C; similar to G protein-coupled receptor, family C, group 5, member C
Fzd7	frizzled homolog 7 (Drosophila)
Kcnk12	potassium channel, subfamily K, member 12
Boc	biregional cell adhesion molecule-related/down-regulated by oncogenes (Cdon) binding protein
Cnr1	cannabinoid receptor 1 (brain)
Ntm	neurotrimin
Trhde	TRH-degrading enzyme
Spint2	serine protease inhibitor, Kunitz type 2
Kcnd2	potassium voltage-gated channel, Shal-related family, member 2
Tspan9	tetraspanin 9
Dock4	dedicator of cytokinesis 4
Sh3gl2	SH3-domain GRB2-like 2
Stap2	signal transducing adaptor family member 2
Sdc1	syndecan 1
Clec10a	macrophage galactose N-acetyl-galactosamine specific lectin 1
Stxbp5	syntaxin binding protein 5 (tomosyn)
Ap2a2	hypothetical protein LOC100044229; adaptor protein complex AP-2, alpha 2 subunit
Ehd1	EH-domain containing 1
6430571L13Rik	RIKEN cDNA 6430571L13 gene
slc24a5	solute carrier family 24, member 5
Gprin1	G protein-regulated inducer of neurite outgrowth 1
Cdh15	cadherin 15
Tmem159	transmembrane protein 159
Asph	aspartate-beta-hydroxylase
Rtn4r	reticulon 4 receptor
Itgav	integrin alpha V
Gpr25	G protein-coupled receptor 25
Cdon	cell adhesion molecule-related/down-regulated by oncogenes
Cnksr2	connector enhancer of kinase suppressor of Ras 2
Rnf19b	ring finger protein 19B
Vps37b	vacuolar protein sorting 37B (yeast)
Diras2	DIRAS family, GTP-binding RAS-like 2
Elmo1	engulfment and cell motility 1, ced-12 homolog (C. elegans)
Tnfsf9	tumor necrosis factor (ligand) superfamily, member 9
Gabra6	gamma-aminobutyric acid (GABA) A receptor, subunit alpha 6
Gabrd	gamma-aminobutyric acid (GABA) A receptor, subunit delta
Cadps2	Ca2+-dependent activator protein for secretion 2
Unc13c	unc-13 homolog C (C. elegans)
Dlgap1	discs, large (Drosophila) homolog-associated protein 1
Slc17a7	solute carrier family 17 (sodium-dependent inorganic phosphate cotransporter), member 7
Syt12	synaptotagmin XII
Inadl	InaD-like (Drosophila)
Lin7c	lin-7 homolog C (C. elegans)
Grik2	glutamate receptor, ionotropic, kainate 2 (beta 2)
Syt9	synaptotagmin IX
Jup	junction plakoglobin
Dlg4	discs, large homolog 4 (Drosophila)
Pard6b	par-6 (partitioning defective 6) homolog beta (C. elegans)
Cbln3	cerebellin 3 precursor protein
Ntf3	neurotrophin 3
Wnt7a	wingless-related MMTV integration site 7A
Il16	interleukin 16
Olfm3	olfactomedin 3
Car15 /// Dgcr2	carbonic anhydrase 15
Cbln1	cerebellin 1 precursor protein; similar to precerebellin-1
Il17re	interleukin 17 receptor E
Bmp5	bone morphogenetic protein 5
Igfbp5	insulin-like growth factor binding protein 5
Crlf1	cytokine receptor-like factor 1
Comp	cartilage oligomeric matrix protein
Twsg1	twisted gastrulation homolog 1 (Drosophila)

Supplementary table 2: Fig3C-TaqMan Probe - HTqPCR

Supplemental data 1

List of selected genes and corresponding pre-formulated TaqMan Assay (TaqMan MGB probe labeled with FAM* and, forward ar

* For ddPCR, Rpl13a TaqMan MGB probe was labeled with VIC allowing analysis of both gene of interest (TaqMan MGB probe

Genes enriched in the ION
Genes enriched in the GC

Gene Symbol	Gene name	Assay ID
6430571L13Rik	RIKEN cDNA 6430571L13 gene	Mm01230602_m1
Abcg2	ATP-binding cassette, sub-family G (WHITE), member 2	Mm00496364_m1
Ache	Acetylcholinesterase	Mm00477274_g1
Acsl5	Acyl-CoA synthetase long-chain family member 5	Mm01261083_m1
Adam11	A disintegrin and metallopeptidase domain 11	Mm00477288_m1
Adam23	A disintegrin and metallopeptidase domain 23	Mm00478606_m1
Adcy2	Adenylate cyclase 2	Mm00467874_m1
Adcyap1	Adenylate cyclase activating polypeptide 1	Mm00437433_m1
Ajap1	Adherens junction associated protein 1	Mm01263771_m1
Alox5ap	Arachidonate 5-lipoxygenase activating protein	Mm01218551_m1
Amhr2	Anti-Mullerian hormone type 2 receptor	Mm00513847_m1
Anxa2	Annexin A2	Mm01150673_m1
Ap2a2	Adaptor-related protein complex 2, alpha 2 subunit	Mm01279159_m1
Aqp6	Aquaporin 6	Mm00558232_m1
Arhgap15	Rho GTPase activating protein 15	Mm00464309_m1
Armcx2	Armadillo repeat containing, X-linked 2	Mm00482835_g1
asap1	ArfGAP with SH3 domain, ankyrin repeat and PH domain1	Mm00802434_m1
Asph	Aspartate-beta-hydroxylase	Mm01211480_m1
Atp13a2	ATPase type 13A2	Mm00661379_m1
Atp1b1	ATPase, Na+/K+ transporting, beta 1 polypeptide	Mm00437612_m1
B2m	Beta-2 microglobulin	Mm00437762_m1
Bai1	Brain-specific angiogenesis inhibitor 1	Mm01195143_m1
BC048546	A2ml1 / Ovostatin homolog	Mm01184514_m1
Bgn	Biglycan	Mm01191753_m1
Bmp5	Bone morphogenetic protein 5	Mm00432091_m1
Boc	Biregional cell adhesion molecule-related/down-regulated by oncogenes (Cdon) binding protein	Mm00552906_m1
Btbd11	BTB (POZ) domain containing 11	Mm00955650_m1
C1ql1	Complement component 1, q subcomponent-like 1	Mm00657289_m1
C3	Complement component 3	Mm00437838_m1
Cacna1g	Calcium channel, voltage-dependent, T type, alpha 1G subunit	Mm00486572_m1
Cacng5	Calcium channel, voltage-dependent, gamma subunit 5	Mm00519145_m1
Cadps2	Ca2+-dependent activator protein for secretion 2	Mm01137059_m1
Cartpt	CART (Cocaine- and amphetamine-regulated transcript) prepropeptide	Mm04210469_m1
Casc4	Cancer susceptibility candidate 4	Mm01269365_g1
Cbln1	Cerebellin 1 precursor protein / precerebellin-1	Mm01247194_g1
Cbln3	Cerebellin 3 precursor protein	Mm00490772_g1
Cbln4	Cerebellin 4 precursor protein	Mm00558663_m1
Ccl5	Chemokine (C-C motif) ligand 5	Mm01302427_m1
Cd151	CD151 antigen	Mm01275946_g1
Cd164l2	CD164 sialomucin-like 2	Mm03031105_s1
Cd24a	CD24a antigen	Mm00782538_sH
Cd302	CD302 antigen	Mm01329153_m1
Cdh13	Cadherin 13	Mm01247310_m1
Cdh15	Cadherin 15	Mm00483191_m1
Cdh9	Cadherin 9	Mm03412730_m1
Cdon	Cell adhesion molecule-related/down-regulated by oncogenes	Mm00491185_m1
Cgref1	Cell growth regulator with EF hand domain 1	Mm01217835_m1
Chid1	Chitinase domain containing 1	Mm00471522_m1
Chn2	Chimerin (chimaerin) 2	Mm01326532_m1
Cklf	Chemokine-like factor	Mm00459364_m1
Clec10a	Macrophage galactose N-acetyl-galactosamine specific lectin 1	Mm00546125_g1
Clu	Clusterin	Mm01197002_m1
Cnih3	Cornichon homolog 3 (Drosophila)	Mm01319298_m1
Cnksr2	Connector enhancer of kinase suppressor of Ras 2	Mm00625046_m1
Cnr1	Cannabinoid receptor 1	Mm01212171_s1
Cntnap2	Contactin associated protein-like 2	Mm01163304_m1
Comp	Cartilage oligomeric matrix protein	Mm00489490_m1
Copz2	Coatomer protein complex, subunit zeta 2	Mm04203911_m1
Crh	Corticotropin releasing hormone	Mm01293920_s1
Crlf1	Cytokine receptor-like factor 1	Mm00517026_m1
Crlf2	Cytokine receptor-like factor 2	Mm00497362_m1
Crtac1	Cartilage acidic protein 1	Mm00513940_m1
Crtam	Cytotoxic and regulatory T cell molecule	Mm00490300_m1
Crtap	Cartilage associated protein	Mm00517335_m1
Ctgf	Connective tissue growth factor	Mm01192933_g1
Cthrc1	Collagen triple helix repeat containing 1	Mm01163611_m1

Ctla2a	Cytotoxic T lymphocyte-associated protein 2 alpha	Mm00484032_g1
Ctla2b	Cytotoxic T lymphocyte-associated protein 2 beta	Mm01621586_s1
Ctxn1	Cortexin 1	Mm01217030_g1
Ctxn2	Cortexin 2	Mm03990522_m1
Cx3cl1	Chemokine (C-X3-C motif) ligand 1	Mm00436454_m1
Cxcl12	Chemokine (C-X-C motif) ligand 12	Mm00445553_m1
Cxcr7	Chemokine (C-X-C motif) receptor 7	Mm02619632_s1
Cyb561	Cytochrome b-561	Mm00514474_m1
Cyb561d2	Cytochrome b-561 domain containing 2	Mm00498085_m1
Dgcr2	DiGeorge syndrome critical region gene 2	Mm00438417_m1
Diras2	DIRAS family, GTP-binding RAS-like 2	Mm02763326_s1
Dlg4	Discs, large homolog 4 (Drosophila) / Postsynaptic density protein 95 (PSD95) / SAP-90	Mm00492193_m1
Dlgap1	Discs, large (Drosophila) homolog-associated protein 1	Mm00510688_m1
Dnaja4	DnaJ (Hsp40) homolog, subfamily A, member 4	Mm00445390_m1
Dnajc15	DnaJ (Hsp40) homolog, subfamily C, member 15	Mm00481271_m1
Dner	Delta/notch-like EGF-related receptor	Mm00548872_m1
Dock4	Dedicator of cytokinesis 4	Mm00555659_m1
Dos	Downstream of Stk11	Mm01150067_m1
Dusp15	Dual specificity phosphatase-like 15	Mm00521352_m1
E130311K13Rik	RIKEN cDNA E130311K13 gene	Mm00625778_m1
Ecel1	Endothelin converting enzyme-like 1	Mm00469610_m1
Efna3	Ephrin A3	Mm01212723_g1
Egfl7	EGF-like domain 7	Mm00618004_m1
Ehd1	EH-domain containing 1	Mm01236839_m1
Elmo1	Engulfment and cell motility 1, ced-12 homolog (C. elegans)	Mm00519109_m1
Epha4	Eph receptor A4	Mm00433056_m1
Evc2	Ellis van Creveld syndrome 2 homolog (human)	Mm00507589_m1
F2r	Coagulation factor II (thrombin) receptor	Mm00438851_m1
Fam174b	Family with sequence similarity 174, member B	Mm01311071_m1
Fam189a1	Family with sequence similarity 189, member A1	Mm00812955_m1
Fam19a1	Family with sequence similarity 19, member A1	Mm00805384_m1
Fam20c	Family with sequence similarity 20, member C	Mm00504210_m1
Fam210b /// 2010011I20Rik	Family with sequence similarity 210, member B	Mm00508881_m1
Fam3c	Family with sequence similarity 3, member C	Mm00506842_m1
Fgl2	Fibrinogen-like protein 2	Mm00433327_m1
Fos	FBJ osteosarcoma oncogene / cFos	Mm00487425_m1
Fstl1	Follistatin-like 1	Mm00433371_m1
Fuca2	Fucosidase, alpha-L- 2, plasma	Mm00482088_m1
Fxyd1	FXYD domain-containing ion transport regulator 1	Mm00444674_m1
Fxyd7	FXYD domain-containing ion transport regulator 7	Mm00469666_m1
Fzd7	Frizzled homolog 7 (Drosophila)	Mm00433409_s1
Gab2	GRB2(Growth factor receptor bound protein 2)-associated-binding protein 2	Mm00839698_m1
Gabra4	Gamma-aminobutyric acid (GABA) A receptor, subunit alpha 4	Mm00802631_m1
Gabra5	Gamma-aminobutyric acid (GABA) A receptor, subunit alpha 5	Mm00621092_m1
Gabra6	Gamma-aminobutyric acid (GABA) A receptor, subunit alpha 6	Mm01227754_m1
Gabrd	Gamma-aminobutyric acid (GABA) A receptor, subunit delta	Mm01266203_g1
Gabrg1	Gamma-aminobutyric acid (GABA) A receptor, subunit gamma 1	Mm00439047_m1
Gal	Galanin	Mm00439056_m1
Gjd2	Gap junction protein, delta 2	Mm00439121_m1
Gm4980	Predicted gene 4980 / Trophoblast glycoprotein-like	Mm01280246_s1
Gm5868 /// Slc10a4-ps	Solute carrier family 10 (sodium/bile acid cotransporter family), member 4, pseudogene	Mm02766599_sH
Gng4	Guanine nucleotide binding protein (G protein), gamma 4	Mm00772342_m1
Gng5	Guanine nucleotide binding protein (G protein), gamma 45	Mm02601703_g1
Gp1bb	Glycoprotein Ib, beta polypeptide	Mm00494713_s1
Gpr123 /// Adgra1	G protein-coupled receptor 123 /// Adhesion G protein-coupled receptor A1	Mm00624275_m1
Gpr125 /// Adgra3	G protein-coupled receptor 125 /// Adhesion G protein-coupled receptor A3	Mm00475185_m1
Gpr137b	G protein-coupled receptor 137B /// Integral membrane protein GPR137B (lysosome)	Mm04213549_g1
Gpr137b-ps	G protein-coupled receptor 137B, pseudogene	Mm01620949_s1
Gpr176	G protein-coupled receptor 176	Mm01277657_m1
Gpr22	G protein-coupled receptor 22	Mm01291487_m1
Gpr25	G protein-coupled receptor 25	Mm02621666_s1
Gpr26	G protein-coupled receptor 26	Mm01165717_m1
Gpr45	G protein-coupled receptor 45	Mm00446398_s1
Gpr64 /// ADGRG2	G protein-coupled receptor 64 /// Adhesion G-protein coupled receptor G2	Mm00724548_m1
Gpr88	G-protein coupled receptor 88	Mm02620353_s1
Gprc5c	G protein-coupled receptor, family C, group 5, member C	Mm00548863_m1
Gprin1	G protein-regulated inducer of neurite outgrowth 1	Mm01721902_s1
Gpx3	Glutathione peroxidase 3	Mm00492427_m1
Grid1	Glutamate receptor, ionotropic, delta 1	Mm01222210_m1
Grik2	Glutamate receptor, ionotropic, kainate 2 (beta 2)	Mm00599860_m1
Grin3a	Glutamate receptor ionotropic, NMDA3A	Mm01341723_m1
Grm4	Glutamate receptor, metabotropic 4	Mm01306128_m1
H2-Aa	Histocompatibility 2, class II antigen A, alpha	Mm00439211_m1
H2-T10	histocompatibility 2, T region locus 10	Mm02393404_gH
Htr5b	5-hydroxytryptamine (serotonin) receptor 5B	Mm00439389_m1

Ier3	Immediate early response 3	Mm00519290_g1
Ifi27l1=Ifi27	Interferon, alpha-inducible protein 27 (like 1)	Mm00835449_g1
Ifitm1	Interferon induced transmembrane protein 1	Mm00850040_g1
Ifngr2	Interferon gamma receptor 2	Mm00492626_m1
Igf1	Insulin-like growth factor 1	Mm00439560_m1
Igfbp3	Insulin-like growth factor binding protein 3	Mm01187817_m1
Igfbp5	Insulin-like growth factor binding protein 5	Mm00516037_m1
Igsf3	Immunoglobulin superfamily, member 3	Mm01302155_m1
Il10rb	Interleukin 10 receptor, beta	Mm00434157_m1
Il16	Interleukin 16	Mm00516039_m1
Il17re	Interleukin 17 receptor E	Mm01189488_m1
Inadl	InaD-like (Drosophila)	Mm00483318_m1
Ipcef1	Interaction protein for cytohesin exchange factors 1	Mm01179956_m1
Itgav	Integrin alpha V	Mm00434486_m1
Itm2a	Integral membrane protein 2A	Mm00515208_m1
Jakmip1	Janus kinase and microtubule interacting protein 1	Mm01220342_m1
Jup	Junction plakoglobin	Mm00550256_m1
Kcna6	Potassium voltage-gated channel, shaker-related, subfamily, member 6	Mm00496625_s1
Kcnc1	Potassium voltage gated channel, Shaw-related subfamily, member 1	Mm00657708_m1
Kcnd2	Potassium voltage-gated channel, Shal-related family, member 2	Mm01161732_m1
Kcng1	Potassium voltage-gated channel, subfamily G, member 1	Mm01249536_m1
Kcnh2	Similar to potassium channel erg1a; potassium voltage-gated channel, subfamily H (eag-related), member 2	Mm00465377_mH
Kcnip2	Kv channel-interacting protein 2	Mm00518915_g1
Kcnk12	Potassium channel, subfamily K, member 12	Mm02344857_m1
Kcnq2	Potassium voltage-gated channel, subfamily Q, member 2	Mm00440080_m1
Kcnq5	Potassium voltage-gated channel, subfamily Q, member 5	Mm01226041_m1
Kit	Tyrosine-protein kinase Kit	Mm00445212_m1
Laptm4b	Lysosomal-associated protein transmembrane 4B	Mm00835799_g1
Lcn2	Lipocalin 2	Mm01324470_m1
Lemd1	LEM domain containing 1	Mm01290780_m1
Leprot	Leptin receptor overlapping transcript	Mm00838516_g1
Lgals3	Lectin, galactose binding, soluble 3	Mm01322955_m1
Lgi2	Leucine-rich repeat LGI family, member 2	Mm00523552_m1
Lhfpl5	Lipoma HMGIC fusion partner-like 5 (HFPL tetraspan subfamily member 5 protein)	Mm00509660_m1
Lin7c	Lin-7 homolog C (C. elegans)	Mm00457063_m1
Lphn2 /// Adgrl2	Calcium-independent alpha-latrotoxin receptor homolog 2 /// Adhesion G protein-coupled receptor L2	Mm01320597_m1
Lpl	Lipoprotein lipase	Mm00434764_m1
Lrfn5	Leucine rich repeat and fibronectin type III domain containing 5	Mm00724566_m1
Ly6h	Lymphocyte antigen 6 complex, locus H	Mm00522014_g1
Lypd1	Ly6/Plaur domain containing 1	Mm00513929_m1
Lypd6	LY6/PLAUR domain containing 6	Mm00622636_m1
Lypd6b	LY6/PLAUR domain containing 6B	Mm01340107_m1
Lyz1	Lysozyme 1	Mm00657323_m1
March11	Membrane-associated ring finger (C3HC4) 11	Mm00617023_m1
Masp1	Mannan-binding lectin serine peptidase 1	Mm00434830_m1
Mbl2	Mannose-binding lectin (protein C) 2	Mm01207555_m1
Mboat7	Membrane bound O-acyltransferase domain containing 7	Mm00513220_m1
Mfsd6	Major facilitator superfamily domain containing 6	Mm00505561_m1
Mgp	Matrix Gla protein	Mm00485009_m1
Minar2 /// A730017C20Rik	Major intrinsically disordered NOTCH2-binding receptor 1-like homolog	Mm00620529_m1
Mmp15	Matrix metallopeptidase 15	Mm00485062_m1
Mrvi1	MRV integration site 1	Mm00456785_m1
Nat8l	N-acetyltransferase 8-like	Mm01217217_m1
Ndnf /// A930038C07Rik	Neuron-derived neurotrophic factor	Mm00549567_m1
Nell1	NEL-like 1 (chicken)	Mm01203866_m1
Nell2	NEL-like 2 (chicken)	Mm00479405_m1
Ninj1	Ninjurin 1	Mm00479014_m1
Npc2	Niemann Pick type C2 (intracellular cholesterol transporter)	Mm00499230_m1
Npnt	Nephronectin	Mm00473794_m1
Nptx2	Neuronal pentraxin-2	Mm00479438_m1
Nrcam	Neuron-glia-CAM-related cell adhesion molecule	Mm00663607_m1
Nrsn2	Neurensin 2	Mm01251252_m1
Nrxn3	Neurexin 3	Mm04279482_m1
Ntf3	Neurotrophin 3	Mm00435413_s1
Ntm	Neurotrimin	Mm01169379_m1
Odz3=Tenm2	Odd Oz/ten-m homolog 3 (Drosophila)	Mm00496219_m1
Olfm2	Olfactomedin 2	Mm00620619_m1
Olfm3	Olfactomedin 3	Mm00462529_m1
Oprl1	Opioid receptor-like 1	Mm00440563_m1
Oscp1	Organic solute carrier partner 1	Mm00554628_m1
Panx1	Pannexin 1	Mm00450900_m1
Pard6b	Par-6 (partitioning defective 6) homolog beta (C. elegans)	Mm00480520_m1
Pcdh20	Protocadherin 20	Mm00724499_m1
Pcolce	Procollagen C-endopeptidase enhancer protein	Mm00453052_m1
Pcsk5	Proprotein convertase subtilisin/kexin type 5	Mm01206130_m1

Pde2a	Phosphodiesterase 2A, cGMP-stimulated	Mm01136644_m1
Pex5l	Peroxisomal biogenesis factor 5-like	Mm00458088_m1
Plp2	Proteolipid protein 2; predicted gene 13669	Mm02342686_g1
Plxdc1	Plexin domain containing 1	Mm00511436_m1
Pmepa1	Prostate transmembrane protein, androgen induced 1 /// Nedd4 WW binding protein 4	Mm00452230_g1
Popdc3	Popeye domain containing 3	Mm00712331_m1
Ppap2c	Phosphatidic acid phosphatase type 2C	Mm01147288_m1
Prmt8	Protein arginine N-methyltransferase 8	Mm01182914_m1
Prss23	Protease, serine, 23	Mm01972869_s1
Ptn	Pleiotrophin	Mm01132688_m1
Ptplad2 /// Hdacd4	Protein tyrosine phosphatase-like A domain containing 2 /// 3-hydroxyacyl-CoA dehydratase 4	Mm01267670_m1
Ptprn	Protein tyrosine phosphatase, receptor type, N	Mm01258989_m1
Pvrl2	Poliovirus receptor-related 2	Mm00436144_m1
Qpctl	Glutaminyl-peptide cyclotransferase-like	Mm00482770_m1
Rab6b	RAB6B, member RAS oncogene family	Mm00620652_m1
Rab7l1 /// Rab29	RAB7, member RAS oncogene family-like 1 /// RAB29, member RAS oncogene family	Mm00523103_m1
Ramp3	Receptor (calcitonin) activity modifying protein 3	Mm00840142_m1
Rasgrp2	RAS, guanyl releasing protein 2	Mm01231708_m1
Rell2	RELT-like 2	Mm00464175_m1
Resp18	Regulated endocrine-specific protein 18	Mm00485697_m1
Rgs19	Regulator of G-protein signaling 19	Mm01215219_g1
Rhbdd2	Rhomboid domain containing 2	Mm00524533_m1
Rnaset2a	Ribonuclease T2A	Mm02601904_m1
Rnaset2b	Ribonuclease T2B	Mm03931873_m1
Rnf19b	Ring finger protein 19B	Mm01188000_m1
Rock2	Rho-associated coiled-coil containing protein kinase 2	Mm01270843_m1
RPL13A	60S ribosomal protein L13a	Mm01612986_gH
Rtn4r	Reticulon 4 receptor	Mm00452228_m1
Rtn4rl2	Reticulon 4 receptor-like 2	Mm01336368_g1
S100a10	S100 calcium binding protein A10 (calpactin)	Mm00501458_g1
S100a4	S100 calcium binding protein A4	Mm00803372_g1
S100a6	S100 calcium binding protein A6 (calcyclin)	Mm00771682_g1
S1pr3	Sphingosine-1-phosphate receptor 3	Mm02620181_s1
Scarb1	Scavenger receptor class B, member 1	Mm00450234_m1
Scn3a	Sodium channel, voltage-gated, type III, alpha	Mm00658167_m1
Scn3b	Sodium channel, voltage-gated, type III, beta	Mm00463369_m1
Sdc1	Syndecan 1	Mm00448918_m1
Sema4a	Sema domain, immunoglobulin domain (Ig), transmembrane domain (TM) and short cytoplasmic domain, (semaphorin) 4A	Mm00443140_m1
Sema4f	Sema domain, immunoglobulin domain (Ig), transmembrane domain (TM) and short cytoplasmic domain, (semaphorin) 4F	Mm01181885_m1
Serpinf1	Serine (or cysteine) peptidase inhibitor, clade F, member 1	Mm00441270_m1
Sh3gl2	SH3-domain GRB2-like 2 /// Endophilin-A1	Mm00490393_m1
Shisa4	Shisa homolog 4 (Xenopus laevis)	Mm00723565_m1
Shisal1 /// 1810041L15Rik	Shisa-like-1	Mm01303852_m1
Slc10a4	Solute carrier family 10 member 4	Mm00557788_m1
Slc17a7	Solute carrier family 17 (sodium-dependent inorganic phosphate cotransporter), member 7	Mm00812886_m1
Slc1a4	Solute carrier family 1 (glutamate/neutral amino acid transporter), member 4	Mm01223875_m1
Slc20a1	Solute carrier family 20, member 1	Mm00489378_m1
Slc22a23	Solute carrier family 22, member 23	Mm01339800_m1
Slc24a3	Solute carrier family 24 (sodium/potassium/calcium exchanger), member 3	Mm00446428_m1
slc24a5	Solute carrier family 24, member 5	Mm00558210_m1
Slc25a1	Solute carrier family 25 (mitochondrial carrier, citrate transporter), member 1	Mm00467666_m1
slc30a10	Solute carrier family 30, member 10	Mm01315481_m1
Slc4a2	Solute carrier family 4 (anion exchanger), member 2	Mm00436617_m1
Sln	Sarcolipin	Mm00481536_m1
Smpdl3a	Sphingomyelin phosphodiesterase, acid-like 3A	Mm00480407_m1
Spint2	Serine protease inhibitor, Kunitz type 2	Mm01169253_m1
Spns2	Spinster homolog 2 (Drosophila)	Mm01249328_m1
Srgn	Serglycin	Mm01169070_m1
Stap2	Signal transducing adaptor family member 2	Mm00521540_m1
Stbd1	Starch binding domain 1	Mm00612997_m1
Stx1a	Syntaxin 1A (brain)	Mm00444008_m1
Stxbp5	Syntaxin binding protein 5 (tomosyn)	Mm01180425_m1
Susd4	Sushi domain containing 4	Mm01312134_m1
Syngr3	Synaptogyrin 3	Mm00448921_m1
Syt12	Synaptotagmin XII	Mm00506619_m1
Syt9	Synaptotagmin IX	Mm00502475_m1
Sytl2	Synaptotagmin-like 2	Mm01317927_m1
Tctn2	Tectonic family member 2	Mm00471430_m1
Tgfbi	Transforming growth factor, beta induced	Mm00493634_m1
Tgfbr2	Transforming growth factor, beta receptor II	Mm03024091_m1
Thy1	Thymus cell antigen 1, theta	Mm00493681_m1
Timp2	Tissue inhibitor of metalloproteinase 2	Mm00441825_m1
Tm6sf1	Transmembrane 6 superfamily member 1	Mm00461004_m1
Tmed10	Transmembrane emp24-like trafficking protein 10 (yeast)	Mm00728199_s1
Tmeff1	Transmembrane protein with EGF-like and two follistatin-like domains 1	Mm01345571_m1
Tmem14a	Transmembrane protein 14A	Mm00512678_g1

Tmem159	Transmembrane protein 159	Mm01281245_m1
Tmem179	Transmembrane protein 179	Mm00626884_m1
Tmem179b	Transmembrane protein 179B	Mm00471111_m1
Tmem180	Transmembrane protein 180	Mm00551419_m1
Tmem184b	Transmembrane protein 184b	Mm01300246_m1
Tmem19	Transmembrane protein 19	Mm00504986_m1
Tmem191c	Transmembrane protein 191C	Mm00462071_g1
Tmem204	Transmembrane protein 204	Mm01301186_m1
Tmem205	Transmembrane protein 205	Mm00724248_m1
Tmem248 /// 0610007L01Rik	Transmembrane protein 248	Mm01201805_m1
Tmem42	transmembrane protein 42	Mm01352328_m1
Tmie	Transmembrane inner ear	Mm00461584_m1
Tnfrsf11b	Tumor necrosis factor receptor superfamily, member 11b (osteoprotegerin)	Mm00435454_m1
Tnfrsf21	Tumor necrosis factor receptor superfamily, member 21	Mm00446361_m1
Tnfsf9	Tumor necrosis factor (ligand) superfamily, member 9	Mm00437155_m1
Trhde	TRH-degrading enzyme	Mm00455443_m1
Tspan12	Tetraspanin 12	Mm00557112_m1
Tspan31	Tetraspanin 31	Mm00482543_m1
Tspan6	Tetraspanin 6	Mm00451045_m1
Tspan9	Tetraspanin 9	Mm00615105_m1
Twsg1	Twisted gastrulation homolog 1 (Drosophila)	Mm00452254_m1
Unc13c	Unc-13 homolog C (C. elegans)	Mm00463432_m1
Vasn	Vasorin	Mm00454838_m1
Vegfb	Vascular endothelial growth factor B	Mm00442102_m1
Vps37b	Vacuolar protein sorting 37B (yeast)	Mm01196801_m1
Vstm2a	V-set and transmembrane domain containing 2A	Mm00461304_m1
Vstm2b	V-set and transmembrane domain containing 2B	Mm00480489_m1
Vstm2l	V-set and transmembrane domain containing 2-like	Mm01246628_m1
Vstm5 /// 2200002K05Rik	V-set and transmembrane domain containing 5	Mm01176177_g1
Wnt7a	Wingless-related MMTV integration site 7A	Mm00437354_m1
Zdhhc22	Zinc finger, DHHC-type containing 22	Mm01308190_m1
Znrf2	Zinc and ring finger 2	Mm01326476_m1

2. A molecularly-defined non-redundant subpopulation of OPCs controls the generation of myelinating oligodendrocytes during postnatal development

Title: A molecularly-defined non-redundant subpopulation of OPCs controls the generation of myelinating oligodendrocytes during postnatal development.

Authors:

Shayan Moghimyfiroozabad[1,2,3], Maela Paul[1,3], Lea Bellenger[3], Fekrije Selimi[1]

Affiliations:

[1]Center for Interdisciplinary Research in Biology (CIRB), College de France, CNRS, INSERM, Université PSL, Paris, France

[2]Ecole des neurosciences de Paris, Paris, France

[3]Sorbonne Universite, Paris, France

Abstract:

Oligodendrocyte precursor cells (OPCs) are a class of glial cells that uniformly tiles the whole central nervous system. They play several key functions across the brain including the generation of oligodendrocytes and the control of myelination. Whether the functional diversity of OPCs is the result of genetically defined subpopulations or of their regulation by external factors has not been definitely established. We discovered that a subpopulation of OPCs found across the brain is defined by the expression of *C1ql1*, a gene previously described for its synaptic function in neurons. This subpopulation starts to appear during the first postnatal week in the mouse brain. Ablation of *C1ql1*-expressing OPCs in the mouse is not compensated by the remaining OPCs, and results in a massive lack of oligodendrocytes and myelination in many brain regions. Therefore, *C1ql1* is a molecular marker of a functionally non-redundant subpopulation of OPCs, which controls the generation of myelinating oligodendrocytes.

3. Mapping and targeting of *C1ql1*-expressing cells in the mouse

Title: Mapping and targeting of *C1ql1*-expressing cells in the mouse

Authors:

Shayan Moghimyfiroozabad[1], Maëla A. Paul[1], Séverine M. Sigoillot[1†*], Fekrije Selimi[1†*]

Affiliations:

[1]Center for Interdisciplinary Research in Biology (CIRB), College de France, CNRS, INSERM, Université PSL, Paris, France

[†] These authors contributed equally to this work

*corresponding authors: Fekrije Selimi and Séverine M. Sigoillot

Abstract:

The C1Q complement protein C1QL1 is highly conserved in mammals where it is expressed in various tissues including the brain. It interacts with Brain-specific Angiogenesis Inhibitor 3, BAI3/ADGRB3, and controls synapse formation and maintenance. *C1ql1* is expressed in the inferior olivary neurons that send projections to cerebellar Purkinje cells, but its expression in the rest of the brain is less documented. To map *C1ql1* expression in the brain and enable the specific targeting of *C1ql1*-expressing cells, we characterized a knockin mouse model expressing the Cre recombinase under the *C1ql1* promoter. We characterized the capacity of the Cre to recombine in the brain and mapped its expression pattern in various neuron types using Cre-dependent reporter mouse lines. Using an intersectional strategy with viral particle injections, we show that this line can be used to target specific afferents of Purkinje cells. As *C1ql1* is also expressed in other regions of the brain, as well as in other tissues such as adrenal glands, placenta, colon and testis, our mouse model could be used to target *C1ql1*-expressing cells in a broad variety of tissues.

BIBLIOGRAPHY

-A-

Agi E, Kulkarni A, Hiesinger PR. 2020. Neuronal strategies for meeting the right partner during brain wiring. Current Opinion in Neurobiology. 63:1–8. https://doi.org/10.1016/j.conb.2020.01.002

Akin O, Zipursky SL. 2020. Activity regulates brain development in the fly. Current Opinion in Genetics & Development. 65:8–13. https://doi.org/10.1016/j.gde.2020.04.005

Altman J. 1972. Postnatal development of the cerebellar cortex in the rat. I. The external germinal layer and the transitional molecular layer. Journal of Comparative Neurology. 145(3):353–397. https://doi.org/10.1002/cne.901450305

Altman J, Bayer SA. 1987. Development of the precerebellar nuclei in the rat: I. The precerebellar neuroepithelium of the rhombencephalon. J Comp Neurol. 257(4):477–489. https://doi.org/10.1002/cne.902570402

Andjus PR, Zhu L, Cesa R, Carulli D, Strata P. 2003. A change in the pattern of activity affects the developmental regression of the Purkinje cell polyinnervation by climbing fibers in the rat cerebellum. Neuroscience. 121(3):563–572. https://doi.org/10.1016/s0306-4522(03)00556-6

Ango F, Cristo G di, Higashiyama H, Bennett V, Wu P, Huang ZJ. 2004. Ankyrin-Based Subcellular Gradient of Neurofascin, an Immunoglobulin Family Protein, Directs GABAergic Innervation at Purkinje Axon Initial Segment. Cell. 119(2):257–272. https://doi.org/10.1016/j.cell.2004.10.004

Ango F, Wu C, Van der Want JJ, Wu P, Schachner M, Huang ZJ. 2008. Bergmann Glia and the Recognition Molecule CHL1 Organize GABAergic Axons and Direct Innervation of Purkinje Cell Dendrites.Ghosh A, editor. PLoS Biol. 6(4):e103. https://doi.org/10.1371/journal.pbio.0060103

Antón-Bolaños N, Sempere-Ferràndez A, Guillamón-Vivancos T, Martini FJ, Pérez-Saiz L, Gezelius H, Filipchuk A, Valdeolmillos M, López-Bendito G. 2019. Prenatal activity from thalamic neurons governs the emergence of functional cortical maps in mice. Science. 364(6444):987–990. https://doi.org/10.1126/science.aav7617

Aoto J, Martinelli DC, Malenka RC, Tabuchi K, Südhof TC. 2013. Presynaptic Neurexin-3 Alternative Splicing trans-Synaptically Controls Postsynaptic AMPA Receptor Trafficking. Cell. 154(1):75–88. https://doi.org/10.1016/j.cell.2013.05.060

Apóstolo N, Smukowski SN, Vanderlinden J, Condomitti G, Rybakin V, ten Bos J, Trobiani L, Portegies S, Vennekens KM, Gounko NV, et al. 2020. Synapse type-specific proteomic dissection identifies IgSF8 as a hippocampal CA3 microcircuit organizer. Nat Commun. 11(1):5171. https://doi.org/10.1038/s41467-020-18956-x

Apóstolo N, de Wit J. 2019. Compartmentalized distributions of neuronal and glial cell-surface proteins pattern the synaptic network. Current Opinion in Neurobiology. 57:126–133. https://doi.org/10.1016/j.conb.2019.01.025

Arce KP, Ribic A, Chowdhury D, Watters K, Thompson GJ, Sanganahalli BG, Lippard ETC, Rohlmann A, Strittmatter SM, Missler M, et al. 2023. Concerted roles of LRRTM1 and SynCAM 1 in organizing prefrontal cortex synapses and cognitive functions. Nat Commun. 14(1):459. https://doi.org/10.1038/s41467-023-36042-w

Armengol JA, Sotelo C. 1991. Early dendritic development of Purkinje cells in the rat cerebellum. A light and electron microscopic study using axonal tracing in “in vitro” slices. Brain Res Dev Brain Res. 64(1–2):95–114. https://doi.org/10.1016/0165-3806(91)90213-3

Auguste YSS, Ferro A, Kahng JA, Xavier AM, Dixon JR, Vrudhula U, Nichitiu A-S, Rosado D, Wee T-L, Pedmale UV, Cheadle L. 2022. Oligodendrocyte precursor cells engulf synapses during circuit remodeling in mice. Nat Neurosci. 25(10):1273–1278. https://doi.org/10.1038/s41593-022-01170-x

-B-

Baines RA, Landgraf M. 2021. Neural development: The role of spontaneous activity. Current Biology. 31(23):R1513–R1515. https://doi.org/10.1016/j.cub.2021.10.026

Balaskas N, Abbott LF, Jessell TM, Ng D. 2019. Positional Strategies for Connection Specificity and Synaptic Organization in Spinal Sensory-Motor Circuits. Neuron. 102(6):1143-1156.e4. https://doi.org/10.1016/j.neuron.2019.04.008

BaptistaMary E.Hatten CA, Blazeski R, Mason CA. 1994. Cell-cell interactions influence survival and differentiation of purified purkinje cells in vitro. Neuron. 12(2):243–260. https://doi.org/10.1016/0896-6273(94)90268-2

Barbour B. 1993. Synaptic currents evoked in purkinje cells by stimulating individual granule cells. Neuron. 11(4):759–769. https://doi.org/10.1016/0896-6273(93)90085-6

Basu R, Duan X, Taylor MR, Martin EA, Muralidhar S, Wang Y, Gangi-Wellman L, Das SC, Yamagata M, West PJ, et al. 2017. Heterophilic Type II Cadherins Are Required for High-Magnitude Synaptic Potentiation in the Hippocampus. Neuron. 96(1):160-176.e8. https://doi.org/10.1016/j.neuron.2017.09.009

Batchelor AM, Madge DJ, Garthwaite J. 1994. Synaptic activation of metabotropic glutamate receptors in the parallel fibre-Purkinje cell pathway in rat cerebellar slices. Neuroscience. 63(4):911–915. https://doi.org/10.1016/0306-4522(94)90558-4

Baudouin S, Scheiffele P. 2010. SnapShot: Neuroligin-neurexin complexes. Cell. 141(5):908, 908.e1. https://doi.org/10.1016/j.cell.2010.05.024

Bennett MR. 1999. The early history of the synapse: from plato to sherrington. Brain Research Bulletin. 50(2):95–118. https://doi.org/10.1016/S0361-9230(99)00094-5

Bernard C, Exposito-Alonso D, Selten M, Sanalidou S, Hanusz-Godoy A, Aguilera A, Hamid F, Oozeer F, Maeso P, Allison L, et al. 2022. Cortical wiring by synapse type–specific control of local protein synthesis. Science. 378(6622):eabm7466. https://doi.org/10.1126/science.abm7466

Blockus H, Polleux F. 2021a. Developmental mechanisms underlying circuit wiring: Novel insights and challenges ahead. Current Opinion in Neurobiology. 66:205–211. https://doi.org/10.1016/j.conb.2020.12.013
Blockus H, Polleux F. 2021b. Developmental mechanisms underlying circuit wiring: Novel insights and challenges ahead. Current Opinion in Neurobiology. 66:205–211. https://doi.org/10.1016/j.conb.2020.12.013

Blockus H, Rolotti SV, Szoboszlay M, Peze-Heidsieck E, Ming T, Schroeder A, Apostolo N, Vennekens KM, Katsamba PS, Bahna F, et al. 2021. Synaptogenic activity of the axon guidance molecule Robo2 underlies hippocampal circuit function. Cell Reports. 37(3):109828. https://doi.org/10.1016/j.celrep.2021.109828

Bolliger MF, Martinelli DC, Südhof TC. 2011. The cell-adhesion G protein-coupled receptor BAI3 is a high-affinity receptor for C1q-like proteins. Proc Natl Acad Sci U S A. 108(6):2534–2539. https://doi.org/10.1073/pnas.1019577108

Bourrat F, Sotelo C. 1983. Postnatal development of the inferior olivary complex in the rat. I. An electron microscopic study of the medial accessory olive. Developmental Brain Research. 8(2):291–310. https://doi.org/10.1016/0165-3806(83)90013-5

Bourrat F, Sotelo C. 1988. Migratory pathways and neuritic differentiation of inferior olivary neurons in the rat embryo. Axonal tracing study using the in vitro slab technique. Brain Res. 467(1):19–37. https://doi.org/10.1016/0165-3806(88)90064-8

Bourrat F, Sotelo C. 1991. Relationships between neuronal birthdates and cytoarchitecture in the rat inferior olivary complex. J Comp Neurol. 313(3):509–521. https://doi.org/10.1002/cne.903130311

Bravin M, Morando L, Vercelli A, Rossi F, Strata P. 1999. Control of spine formation by electrical activity in the adult rat cerebellum. Proc Natl Acad Sci USA. 96(4):1704–1709. https://doi.org/10.1073/pnas.96.4.1704

Brochu G, Maler L, Hawkes R. 1990. Zebrin II: A polypeptide antigen expressed selectively by purkinje cells reveals compartments in rat and fish cerebellum. Journal of Comparative Neurology. 291(4):538–552. https://doi.org/10.1002/cne.902910405

Brown AM, Arancillo M, Lin T, Catt DR, Zhou J, Lackey EP, Stay TL, Zuo Z, White JJ, Sillitoe RV. 2019. Molecular layer interneurons shape the spike activity of cerebellar Purkinje cells. Sci Rep. 9(1):1742. https://doi.org/10.1038/s41598-018-38264-1

Buckner RL. 2013. The Cerebellum and Cognitive Function: 25 Years of Insight from Anatomy and Neuroimaging. Neuron. 80(3):807–815. https://doi.org/10.1016/j.neuron.2013.10.044

Buckner RL, Krienen FM, Castellanos A, Diaz JC, Yeo BTT. 2011. The organization of the human cerebellum estimated by intrinsic functional connectivity. J Neurophysiol. 106(5):2322–2345. https://doi.org/10.1152/jn.00339.2011

-C-

Cadwell CR, Scala F, Fahey PG, Kobak D, Mulherkar S, Sinz FH, Papadopoulos S, Tan ZH, Johnsson P, Hartmanis L, et al. 2020. Cell type composition and circuit organization of clonally related excitatory neurons in the juvenile mouse neocortex.West AE, Behrens TE, Hevner R, Fishell G, editors. eLife. 9:e52951. https://doi.org/10.7554/eLife.52951

Cajal SRY. 1909. Histology of the nervous system of man and vertebrates. In: Vol. 1 & 2. Oxford University Press. New york.

Calvo I. 2018. Sushi domain proteins during the life of the excitatory synapse in the olivocerebellar network.

Cavalieri D, Angelova A, Islah A, Lopez C, Bocchio M, Bollmann Y, Baude A, Cossart R. 2021. CA1 pyramidal cell diversity is rooted in the time of neurogenesis.Huguenard JR, Capogna M, editors. eLife. 10:e69270. https://doi.org/10.7554/eLife.69270

Caviness VS, So DK, Sidman RL. 1972. The Hybrid Reeler Mouse. Journal of Heredity. 63(5):241–246. https://doi.org/10.1093/oxfordjournals.jhered.a108286

Cesa R, Morando L, Strata P. 2003. Glutamate Receptor δ2 Subunit in Activity-Dependent Heterologous Synaptic Competition. J Neurosci. 23(6):2363–2370. https://doi.org/10.1523/JNEUROSCI.23-06-02363.2003

Cesa R, Premoselli F, Renna A, Ethell IM, Pasquale EB, Strata P. 2011. Eph Receptors Are Involved in the Activity-Dependent Synaptic Wiring in the Mouse Cerebellar Cortex. PLOS ONE. 6(4):e19160. https://doi.org/10.1371/journal.pone.0019160

Cesa R, Scelfo B, Strata P. 2007. Activity-Dependent Presynaptic and Postsynaptic Structural Plasticity in the Mature Cerebellum. Journal of Neuroscience. 27(17):4603–4611. https://doi.org/10.1523/JNEUROSCI.5617-06.2007

Cesa R, Strata P. 2009. Axonal competition in the synaptic wiring of the cerebellar cortex during development and in the mature cerebellum. Neuroscience. 162(3):624–632. https://doi.org/10.1016/j.neuroscience.2009.02.061

Chaillet JR. 1994. Genomic imprinting: Lessons from mouse transgenes. Mutation Research/Fundamental and Molecular Mechanisms of Mutagenesis. 307(2):441–449. https://doi.org/10.1016/0027-5107(94)90255-0

Changeux J-P, Danchin A. 1976. Selective stabilisation of developing synapses as a mechanism for the specification of neuronal networks. Nature. 264(5588):705–712. https://doi.org/10.1038/264705a0

Chédotal A, Bloch-Gallego E, Sotelo C. 1997. The embryonic cerebellum contains topographic cues that guide developing inferior olivary axons. Development. 124(4):861–870. https://doi.org/10.1242/dev.124.4.861

Chédotal A, Pourquié O, Ezan F, San Clemente H, Sotelo C. 1996. BEN As a Presumptive Target Recognition Molecule during the Development of the Olivocerebellar System. J Neurosci. 16(10):3296–3310. https://doi.org/10.1523/JNEUROSCI.16-10-03296.1996

Chedotal A, Sotelo C. 1992. Early Development of Olivocerebellar Projections in the Fetal Rat Using CGRP Immunocytochemistry. European Journal of Neuroscience. 4(11):1159–1179. https://doi.org/10.1111/j.1460-9568.1992.tb00142.x

Chedotal A, Sotelo C. 1993. The “creeper stage” in cerebellar climbing fiber synaptogenesis precedes the ’pericellular nest’--ultrastructural evidence with parvalbumin immunocytochemistry. Brain Res Dev Brain Res. 76(2):207–220. https://doi.org/10.1016/0165-3806(93)90209-s

Cheng D, Hoogenraad CC, Rush J, Ramm E, Schlager MA, Duong DM, Xu P, Wijayawardana SR, Hanfelt J, Nakagawa T, et al. 2006. Relative and Absolute Quantification of Postsynaptic Density Proteome Isolated from Rat Forebrain and Cerebellum*S. Molecular & Cellular Proteomics. 5(6):1158–1170. https://doi.org/10.1074/mcp.D500009-MCP200

Cheng M-C, Chien W-H, Huang Y-S, Fang T-H, Chen C-H. 2021. Translational Study of Copy Number Variations in Schizophrenia. Int J Mol Sci. 23(1):457. https://doi.org/10.3390/ijms23010457

Chih B, Gollan L, Scheiffele P. 2006. Alternative splicing controls selective trans-synaptic interactions of the neuroligin-neurexin complex. Neuron. 51(2):171–178. https://doi.org/10.1016/j.neuron.2006.06.005

Cioni J-M, Telley L, Saywell V, Cadilhac C, Jourdan C, Huber AB, Huang JZ, Jahannault-Talignani C, Ango F. 2013. SEMA3A Signaling Controls Layer-Specific Interneuron Branching in the Cerebellum. Current Biology. 23(10):850–861. https://doi.org/10.1016/j.cub.2013.04.007

Coesmans M, Weber JT, Zeeuw CID, Hansel C. 2004. Bidirectional Parallel Fiber Plasticity in the Cerebellum under Climbing Fiber Control. Neuron. 44(4):691–700. https://doi.org/10.1016/j.neuron.2004.10.031

Collins MO, Husi H, Yu L, Brandon JM, Anderson CNG, Blackstock WP, Choudhary JS, Grant SGN. 2006. Molecular characterization and comparison of the components and

multiprotein complexes in the postsynaptic proteome. J Neurochem. 97 Suppl 1:16–23. https://doi.org/10.1111/j.1471-4159.2005.03507.x

Crepel F. 1974. Excitatory and inhibitory processes acting upon cerebellar Purkinje cells during maturation in the rat; Influence of hypothyroidism. Exp Brain Res [Internet]. [accessed 2023 Feb 13] 20(4). https://doi.org/10.1007/BF00237384

Crepel F, Delhaye-Bouchaud N, Dupont JL. 1981. Fate of the multiple innervation of cerebellar Purkinje cells by climbing fibers in immature control, X-irradiated and hypothyroid rats. Developmental Brain Research. 1(1):59–71. https://doi.org/10.1016/0165-3806(81)90094-8

Crepel F, Delhaye-Bouchaud N, Guastavino JM, Sampaio I. 1980. Multiple innervation of cerebellar Purkinje cells by climbing fibres in staggerer mutant mouse. Nature. 283(5746):483–484. https://doi.org/10.1038/283483a0

Crepel F, Mariani J. 1976. Multiple innervation of purkinje cells by climbing fibers in the cerebellum of the weaver mutant mouse. Journal of Neurobiology. 7(6):579–582. https://doi.org/10.1002/neu.480070610

-D-

Dai J, Aoto J, Südhof TC. 2019. Alternative Splicing of Presynaptic Neurexins Differentially Controls Postsynaptic NMDA and AMPA Receptor Responses. Neuron. 102(5):993-1008.e5. https://doi.org/10.1016/j.neuron.2019.03.032

Dai J, Patzke C, Liakath-Ali K, Seigneur E, Südhof TC. 2021. GluD1 is a signal transduction device disguised as an ionotropic receptor. Nature. 595(7866):261–265. https://doi.org/10.1038/s41586-021-03661-6

Davie JT, Clark BA, Häusser M. 2008. The origin of the complex spike in cerebellar Purkinje cells. J Neurosci. 28(30):7599–7609. https://doi.org/10.1523/JNEUROSCI.0559-08.2008

De Robertis E, De Iraldi AP, Rodriguez G, Gomez CJ. 1961. ON THE ISOLATION OF NERVE ENDINGS AND SYNAPTIC VESICLES. The Journal of Biophysical and Biochemical Cytology. 9(1):229–235. https://doi.org/10.1083/jcb.9.1.229

Deguchi Y, Donato F, Galimberti I, Cabuy E, Caroni P. 2011. Temporally matched subpopulations of selectively interconnected principal neurons in the hippocampus. Nat Neurosci. 14(4):495–504. https://doi.org/10.1038/nn.2768

DeRosse P, Lencz T, Burdick KE, Siris SG, Kane JM, Malhotra AK. 2008. The genetics of symptom-based phenotypes: toward a molecular classification of schizophrenia. Schizophr Bull. 34(6):1047–1053. https://doi.org/10.1093/schbul/sbn076

Dos Reis R, Kornobis E, Pereira A, Tores F, Carrasco J, Gautier C, Jahannault-Talignani C, Nitschké P, Muchardt C, Schlosser A, et al. 2022. Complex regulation of Gephyrin splicing is a determinant of inhibitory postsynaptic diversity. Nat Commun. 13:3507. https://doi.org/10.1038/s41467-022-31264-w

Doust C, Fontanillas P, Eising E, Gordon SD, Wang Z, Alagöz G, Molz B, 23andMe Research Team, Aslibekyan S, Auton A, et al. 2022. Discovery of 42 genome-wide significant loci associated with dyslexia. Nat Genet. 54(11):1621–1629. https://doi.org/10.1038/s41588-022-01192-y

Duan X, Krishnaswamy A, De la Huerta I, Sanes JR. 2014. Type II Cadherins Guide Assembly of a Direction-Selective Retinal Circuit. Cell. 158(4):793–807. https://doi.org/10.1016/j.cell.2014.06.047

Duman JG, Tu Y-K, Tolias KF. 2016. Emerging Roles of BAI Adhesion-GPCRs in Synapse Development and Plasticity. Neural Plasticity. 2016:e8301737. https://doi.org/10.1155/2016/8301737

-E-

Ea M, Ma S, G G, Tg G, P R, E F, S A, A C, Sa M, P L, et al. 2022. Schizophrenia-associated somatic copy number variants from 12,834 cases reveal contribution to risk and recurrent,

isoform-specific NRXN1 disruptions [Internet]. [accessed 2023 Apr 1]. https://doi.org/10.1101/2021.12.24.21268385

Eccles JC. 2013. The Cerebellum as a Neuronal Machine. [place unknown]: Springer Science & Business Media.
Eccles JC, Llinás R, Sasaki K. 1966. The excitatory synaptic action of climbing fibres on the Purkinje cells of the cerebellum. The Journal of Physiology. 182(2):268–296. https://doi.org/10.1113/jphysiol.1966.sp007824

Espinosa JS, Luo L. 2008. Timing Neurogenesis and Differentiation: Insights from Quantitative Clonal Analyses of Cerebellar Granule Cells. J Neurosci. 28(10):2301–2312. https://doi.org/10.1523/JNEUROSCI.5157-07.2008

Essrich C, Lorez M, Benson JA, Fritschy JM, Lüscher B. 1998. Postsynaptic clustering of major GABAA receptor subtypes requires the gamma 2 subunit and gephyrin. Nat Neurosci. 1(7):563–571. https://doi.org/10.1038/2798

-F-

Favuzzi E, Deogracias R, Marques-Smith A, Maeso P, Jezequel J, Exposito-Alonso D, Balia M, Kroon T, Hinojosa AJ, F. Maraver E, Rico B. 2019. Distinct molecular programs regulate synapse specificity in cortical inhibitory circuits. Science. 363(6425):413–417. https://doi.org/10.1126/science.aau8977

Finch EA, Augustine GJ. 1998. Local calcium signalling by inositol-1,4,5-trisphosphate in Purkinje cell dendrites. Nature. 396(6713):753–756. https://doi.org/10.1038/25541

Fossati M, Assendorp N, Gemin O, Colasse S, Dingli F, Arras G, Loew D, Charrier C. 2019. Trans-Synaptic Signaling through the Glutamate Receptor Delta-1 Mediates Inhibitory Synapse Formation in Cortical Pyramidal Neurons. Neuron. 104(6):1081-1094.e7. https://doi.org/10.1016/j.neuron.2019.09.027

Foster M, Sherrington CS. 1897. A textbook of physiology. With C.S. Sherrington. Part 3. The central nervous system [Internet]. 7th ed. London: Macmillan; [accessed 2023 Feb 9]. https://archive.org/details/b21271458

Fritschy J-M. 2006. Differential Dependence of Axo-Dendritic and Axo-Somatic GABAergic Synapses on GABAA Receptors Containing the 1 Subunit in Purkinje Cells. Journal of Neuroscience. 26(12):3245–3255. https://doi.org/10.1523/JNEUROSCI.5118-05.2006

Fu JM, Satterstrom FK, Peng M, Brand H, Collins RL, Dong S, Wamsley B, Klei L, Wang L, Hao SP, et al. 2022. Rare coding variation provides insight into the genetic architecture and phenotypic context of autism. Nat Genet. 54(9):1320–1331. https://doi.org/10.1038/s41588-022-01104-0

Fukata Y, Lovero KL, Iwanaga T, Watanabe A, Yokoi N, Tabuchi K, Shigemoto R, Nicoll RA, Fukata M. 2010. Disruption of LGI1-linked synaptic complex causes abnormal synaptic transmission and epilepsy. Proc Natl Acad Sci U S A. 107(8):3799–3804. https://doi.org/10.1073/pnas.0914537107

-G-

Garey L. 1999. Cortex: Statistics and Geometry of Neuronal Connectivity, 2nd edn. By V. BRAITENBERG and A. SCHÜZ. (Pp. xiii+249; 90 figures; ISBN 3 540 63816 4). Berlin: Springer. 1998. Journal of Anatomy. 194(1):153–157. https://doi.org/10.1046/j.1469-7580.1999.194101535.x

Gomez AM, Traunmüller L, Scheiffele P. 2021. Neurexins: molecular codes for shaping neuronal synapses. Nat Rev Neurosci. 22(3):137–151. https://doi.org/10.1038/s41583-020-00415-7

González-Calvo I, Iyer K, Carquin M, Khayachi A, Giuliani FA, Sigoillot SM, Vincent J, Séveno M, Veleanu M, Tahraoui S, et al. 2021. Sushi domain-containing protein 4 controls synaptic plasticity and motor learning.Carey MR, Westbrook GL, editors. eLife. 10:e65712. https://doi.org/10.7554/eLife.65712

Graf ER, Zhang X, Jin S-X, Linhoff MW, Craig AM. 2004. Neurexins induce differentiation of GABA and glutamate postsynaptic specializations via neuroligins. Cell. 119(7):1013–1026. https://doi.org/10.1016/j.cell.2004.11.035

Grant SGN. 2019. Synapse diversity and synaptome architecture in human genetic disorders. Hum Mol Genet. 28(R2):R219–R225. https://doi.org/10.1093/hmg/ddz178

Gray E, Whittaker V. 1962. The isolation of nerve endings from brain: an electron microscopic study of cell fragments derived by homogenization and centrifugation. Journal of anatomy. 96(Pt 1):79.

Gray EG. 1959. Axo-somatic and axo-dendritic synapses of the cerebral cortex: an electron microscope study. Journal of anatomy. 93(Pt 4):420.
Gray EG. 1960. The isolation of synaptic vesicles from the central nervous system. J Physiol. 153:35–37.

Guastavino J-M, Sotelo C, Damez-Kinselle I. 1990. Hot-foot murine mutation: behavioral effects and neuroanatomical alterations. Brain Research. 523(2):199–210. https://doi.org/10.1016/0006-8993(90)91488-3

Gutman-Wei AY, Brown SP. 2021. Mechanisms Underlying Target Selectivity for Cell Types and Subcellular Domains in Developing Neocortical Circuits. Frontiers in Neural Circuits [Internet]. [accessed 2022 Dec 17] 15. https://www.frontiersin.org/articles/10.3389/fncir.2021.728832

-H-

Han P, She Y, Yang Z, Zhuang M, Wang Q, Luo X, Yin C, Zhu J, Jaffrey SR, Ji S-J. 2022. Cbln1 regulates axon growth and guidance in multiple neural regions. PLOS Biology. 20(11):e3001853. https://doi.org/10.1371/journal.pbio.3001853

Harvey RJ, Napper RMA. 1991. Quantitatives studies on the mammalian cerebellum. Progress in Neurobiology. 36(6):437–463. https://doi.org/10.1016/0301-0082(91)90012-P

Hasegawa S, Hamada S, Kumode Y, Esumi S, Katori S, Fukuda E, Uchiyama Y, Hirabayashi T, Mombaerts P, Yagi T. 2008. The protocadherin-alpha family is involved in axonal coalescence of olfactory sensory neurons into glomeruli of the olfactory bulb in mouse. Mol Cell Neurosci. 38(1):66–79. https://doi.org/10.1016/j.mcn.2008.01.016

Hashimoto Kouichi, Ichikawa R, Kitamura K, Watanabe M, Kano M. 2009. Translocation of a “Winner” Climbing Fiber to the Purkinje Cell Dendrite and Subsequent Elimination of “Losers” from the Soma in Developing Cerebellum. Neuron. 63(1):106–118. https://doi.org/10.1016/j.neuron.2009.06.008

Hashimoto K, Kano M. 1998. Presynaptic origin of paired-pulse depression at climbing fibre–Purkinje cell synapses in the rat cerebellum. J Physiol. 506(Pt 2):391–405. https://doi.org/10.1111/j.1469-7793.1998.391bw.x

Hashimoto K, Kano M. 2003. Functional Differentiation of Multiple Climbing Fiber Inputs during Synapse Elimination in the Developing Cerebellum. Neuron. 38(5):785–796. https://doi.org/10.1016/S0896-6273(03)00298-8

Hashimoto K, Tsujita M, Miyazaki T, Kitamura K, Yamazaki M, Shin H-S, Watanabe M, Sakimura K, Kano M. 2011. Postsynaptic P/Q-type Ca2+ channel in Purkinje cell mediates synaptic competition and elimination in developing cerebellum. Proc Natl Acad Sci U S A. 108(24):9987–9992. https://doi.org/10.1073/pnas.1101488108

Hashimoto K, Watanabe M, Kurihara H, Offermanns S, Jiang H, Wu Y, Jun K, Shin H-S, Inoue Y, Wu D, et al. 2000. Climbing fiber synapse elimination during postnatal cerebellar development requires signal transduction involving Gαq and phospholipase Cβ4. In: Progress in Brain Research [Internet]. Vol. 124. [place unknown]: Elsevier; [accessed 2023 Jan 19]; p. 31–48. https://doi.org/10.1016/S0079-6123(00)24006-5

Hashimoto K., Yoshida T, Sakimura K, Mishina M, Watanabe M, Kano M. 2009. Influence of parallel fiber-Purkinje cell synapse formation on postnatal development of climbing fiber-Purkinje cell synapses in the cerebellum. Neuroscience. 162(3):601–611. https://doi.org/10.1016/j.neuroscience.2008.12.037

Heller EA, Zhang W, Selimi F, Earnheart JC, Ślimak MA, Santos-Torres J, Ibañez-Tallon I, Aoki C, Chait BT, Heintz N. 2012. The Biochemical Anatomy of Cortical Inhibitory Synapses. PLOS ONE. 7(6):e39572. https://doi.org/10.1371/journal.pone.0039572

Hensch TK. 2005. Critical period plasticity in local cortical circuits. Nat Rev Neurosci. 6(11):877–888. https://doi.org/10.1038/nrn1787

Herculano-Houzel S. 2012. The remarkable, yet not extraordinary, human brain as a scaled-up primate brain and its associated cost. Proceedings of the National Academy of Sciences. 109(supplement_1):10661–10668. https://doi.org/10.1073/pnas.1201895109

Hirai H, Pang Z, Bao D, Miyazaki T, Li L, Miura E, Parris J, Rong Y, Watanabe M, Yuzaki M, Morgan JI. 2005. Cbln1 is essential for synaptic integrity and plasticity in the cerebellum. Nat Neurosci. 8(11):1534–1541. https://doi.org/10.1038/nn1576

Hirano A, Dembitzer HM. 1973. Cerebellar alterations in the weaver mouse. J Cell Biol. 56(2):478–486. https://doi.org/10.1083/jcb.56.2.478

Hubel DH, Wiesel TN. 1970. The period of susceptibility to the physiological effects of unilateral eye closure in kittens. The Journal of Physiology. 206(2):419–436. https://doi.org/10.1113/jphysiol.1970.sp009022

Humeau Y, Doussau F, Grant NJ, Poulain B. 2000. How botulinum and tetanus neurotoxins block neurotransmitter release. Biochimie. 82(5):427–446. https://doi.org/10.1016/s0300-9084(00)00216-9

Hunt CA, Schenker LJ, Kennedy MB. 1996. PSD-95 is associated with the postsynaptic density and not with the presynaptic membrane at forebrain synapses. J Neurosci. 16(4):1380–1388. https://doi.org/10.1523/JNEUROSCI.16-04-01380.1996

-I-

Ibata K, Kono M, Narumi S, Motohashi J, Kakegawa W, Kohda K, Yuzaki M. 2019. Activity-Dependent Secretion of Synaptic Organizer Cbln1 from Lysosomes in Granule Cell Axons. Neuron. 102(6):1184-1198.e10. https://doi.org/10.1016/j.neuron.2019.03.044

Ichikawa R, Hashimoto K, Miyazaki T, Uchigashima M, Yamasaki M, Aiba A, Kano M, Watanabe M. 2016. Territories of heterologous inputs onto Purkinje cell dendrites are segregated by mGluR1-dependent parallel fiber synapse elimination. Proc Natl Acad Sci USA. 113(8):2282–2287. https://doi.org/10.1073/pnas.1511513113

Ichikawa R, Miyazaki T, Kano M, Hashikawa T, Tatsumi H, Sakimura K, Mishina M, Inoue Y, Watanabe M. 2002. Distal Extension of Climbing Fiber Territory and Multiple Innervation Caused by Aberrant Wiring to Adjacent Spiny Branchlets in Cerebellar Purkinje Cells Lacking Glutamate Receptor δ2. J Neurosci. 22(19):8487–8503. https://doi.org/10.1523/JNEUROSCI.22-19-08487.2002

Ichikawa R, Yamasaki M, Miyazaki T, Konno K, Hashimoto K, Tatsumi H, Inoue Y, Kano M, Watanabe M. 2011. Developmental Switching of Perisomatic Innervation from Climbing Fibers to Basket Cell Fibers in Cerebellar Purkinje Cells. J Neurosci. 31(47):16916–16927. https://doi.org/10.1523/JNEUROSCI.2396-11.2011

Iijima T, Wu K, Witte H, Hanno-Iijima Y, Glatter T, Richard S, Scheiffele P. 2011. SAM68 Regulates Neuronal Activity-Dependent Alternative Splicing of Neurexin-1. Cell. 147(7):1601–1614. https://doi.org/10.1016/j.cell.2011.11.028

Iino M, Goto K, Kakegawa W, Okado H, Sudo M, Ishiuchi S, Miwa A, Takayasu Y, Saito I, Tsuzuki K, Ozawa S. 2001. Glia-Synapse Interaction Through Ca2+-Permeable AMPA Receptors in Bergmann Glia. Science. 292(5518):926–929. https://doi.org/10.1126/science.1058827

Imai T, Yamazaki T, Kobayakawa R, Kobayakawa K, Abe T, Suzuki M, Sakano H. 2009. Pre-Target Axon Sorting Establishes the Neural Map Topography. Science. 325(5940):585–590. https://doi.org/10.1126/science.1173596

Isope P, Barbour B. 2002. Properties of Unitary Granule Cell→Purkinje Cell Synapses in Adult Rat Cerebellar Slices. J Neurosci. 22(22):9668–9678. https://doi.org/10.1523/JNEUROSCI.22-22-09668.2002

Ito S, Takeichi M. 2009. Dendrites of cerebellar granule cells correctly recognize their target axons for synaptogenesis in vitro. Proceedings of the National Academy of Sciences. 106(31):12782–12787. https://doi.org/10.1073/pnas.0906653106

Ito-Ishida A, Miyazaki T, Miura E, Matsuda K, Watanabe M, Yuzaki M, Okabe S. 2012. Presynaptically Released Cbln1 Induces Dynamic Axonal Structural Changes by Interacting with GluD2 during Cerebellar Synapse Formation. Neuron. 76(3):549–564. https://doi.org/10.1016/j.neuron.2012.07.027

Ito-Ishida A, Okabe S, Yuzaki M. 2014. The role of Cbln1 on Purkinje cell synapse formation. Neuroscience Research. 83:64–68. https://doi.org/10.1016/j.neures.2014.01.009

-J-

J A. 1997. Development of the Cerebellar System. Relation to its Evolution, Structure, and Functions [Internet]. [accessed 2023 Mar 16]. https://cir.nii.ac.jp/crid/1573668924978289792

Joo J-Y, Lee S-J, Uemura T, Yoshida T, Yasumura M, Watanabe M, Mishina M. 2011. Differential interactions of cerebellin precursor protein (Cbln) subtypes and neurexin variants for synapse formation of cortical neurons. Biochem Biophys Res Commun. 406(4):627–632. https://doi.org/10.1016/j.bbrc.2011.02.108

-K-

Kaiser N, Pätz C, Brachtendorf S, Eilers J, Bechmann I. 2020. Undisturbed climbing fiber pruning in the cerebellar cortex of CX3CR1-deficient mice. Glia. 68(11):2316–2329. https://doi.org/10.1002/glia.23842

Kakegawa W, Mitakidis N, Miura E, Abe M, Matsuda K, Takeo YH, Kohda K, Motohashi J, Takahashi A, Nagao S, et al. 2015. Anterograde C1ql1 Signaling Is Required in Order to Determine and Maintain a Single-Winner Climbing Fiber in the Mouse Cerebellum. Neuron. 85(2):316–329. https://doi.org/10.1016/j.neuron.2014.12.020

Kakegawa W, Miyazaki T, Emi K, Matsuda K, Kohda K, Motohashi J, Mishina M, Kawahara S, Watanabe M, Yuzaki M. 2008. Differential regulation of synaptic plasticity and cerebellar motor learning by the C-terminal PDZ-binding motif of GluRdelta2. J Neurosci. 28(6):1460–1468. https://doi.org/10.1523/JNEUROSCI.2553-07.2008

Kakegawa W, Miyazaki T, Kohda K, Matsuda K, Emi K, Motohashi J, Watanabe M, Yuzaki M. 2009. The N-terminal domain of GluD2 (GluRdelta2) recruits presynaptic terminals and

regulates synaptogenesis in the cerebellum in vivo. J Neurosci. 29(18):5738–5748. https://doi.org/10.1523/JNEUROSCI.6013-08.2009

Kakizawa S, Miyazaki T, Yanagihara D, Iino M, Watanabe M, Kano M. 2005. Maintenance of presynaptic function by AMPA receptor-mediated excitatory postsynaptic activity in adult brain. Proc Natl Acad Sci U S A. 102(52):19180–19185. https://doi.org/10.1073/pnas.0504359103

Kalinovsky A, Boukhtouche F, Blazeski R, Bornmann C, Suzuki N, Mason CA, Scheiffele P. 2011. Development of Axon-Target Specificity of Ponto-Cerebellar Afferents.Polleux F, editor. PLoS Biol. 9(2):e1001013. https://doi.org/10.1371/journal.pbio.1001013

Kano M, Hashimoto K, Chen C, Abeliovich A, Aiba A, Kurihara H, Watanabe M, Inoue Y, Tonegawa S. 1995. Impaired synapse elimination during cerebellar development in PKC gamma mutant mice. Cell. 83(7):1223–1231. https://doi.org/10.1016/0092-8674(95)90147-7

Kano M, Hashimoto K, Kurihara H, Watanabe M, Inoue Y, Aiba A, Tonegawa S. 1997. Persistent multiple climbing fiber innervation of cerebellar Purkinje cells in mice lacking mGluR1. Neuron. 18(1):71–79. https://doi.org/10.1016/s0896-6273(01)80047-7

Kano M, Watanabe M. 2019. Synaptogenesis and Synapse Elimination. In: Manto M, Gruol D, Schmahmann J, Koibuchi N, Sillitoe R, editors. Handbook of the Cerebellum and Cerebellar Disorders [Internet]. Cham: Springer International Publishing; [accessed 2023 Mar 16]; p. 1–24. https://doi.org/10.1007/978-3-319-97911-3_14-2

Kano M, Watanabe T. 2017. Type-1 metabotropic glutamate receptor signaling in cerebellar Purkinje cells in health and disease. F1000Res. 6:416. https://doi.org/10.12688/f1000research.10485.1

Kano M, Watanabe T. 2019. Developmental synapse remodeling in the cerebellum and visual thalamus [Internet]. [accessed 2023 Jan 16]. https://doi.org/10.12688/f1000research.18903.1

Kashiwabuchi N, Ikeda K, Araki K, Hirano T, Shibuki K, Takayama C, Inoue Y, Kutsuwada T, Yagi T, Kang Y. 1995. Impairment of motor coordination, Purkinje cell synapse formation,

and cerebellar long-term depression in GluR delta 2 mutant mice. Cell. 81(2):245–252. https://doi.org/10.1016/0092-8674(95)90334-8

Katz LC, Shatz CJ. 1996. Synaptic Activity and the Construction of Cortical Circuits. Science, New Series. 274(5290):1133–1138.

Kawakami Y, Kurihara Y, Saito Y, Fujita Y, Yamashita T, Takei K. 2018. The Soluble Form of LOTUS inhibits Nogo Receptor-Mediated Signaling by Interfering with the Interaction Between Nogo Receptor Type 1 and p75 Neurotrophin Receptor. J Neurosci. 38(10):2589–2604. https://doi.org/10.1523/JNEUROSCI.0953-17.2018

Kawamura Y, Nakayama H, Hashimoto K, Sakimura K, Kitamura K, Kano M. 2013. Spike timing-dependent selective strengthening of single climbing fibre inputs to Purkinje cells during cerebellar development. Nat Commun. 4(1):2732. https://doi.org/10.1038/ncomms3732

Kennedy MB. 2000. Signal-Processing Machines at the Postsynaptic Density. Science. 290(5492):750–754. https://doi.org/10.1126/science.290.5492.750

Kerjan G, Dolan J, Haumaitre C, Schneider-Maunoury S, Fujisawa H, Mitchell K, Chedotal A. 2005. The transmembrane semaphorin Sema6A controls cerebellar granule cell migration. Nature neuroscience. 8:1516–24. https://doi.org/10.1038/nn1555

Kerschensteiner D, Morgan JL, Parker ED, Lewis RM, Wong ROL. 2009. Neurotransmission selectively regulates synapse formation in parallel circuits in vivo. Nature. 460(7258):1016–1020. https://doi.org/10.1038/nature08236

Kiral FR, Linneweber GA, Mathejczyk T, Georgiev SV, Wernet MF, Hassan BA, von Kleist M, Hiesinger PR. 2020. Autophagy-dependent filopodial kinetics restrict synaptic partner choice during Drosophila brain wiring. Nat Commun. 11(1):1325. https://doi.org/10.1038/s41467-020-14781-4

Kishimoto Y, Kawahara S, Suzuki M, Mori H, Mishina M, Kirino Y. 2001. Classical eyeblink conditioning in glutamate receptor subunit δ2 mutant mice is impaired in the delay paradigm but not in the trace paradigm. European Journal of Neuroscience. 13(6):1249–1253.
Kita Y, Tanaka K, Murakami F. 2015. Specific labeling of climbing fibers shows early synaptic interactions with immature Purkinje cells in the prenatal cerebellum. Developmental Neurobiology. 75(9):927–934. https://doi.org/10.1002/dneu.22259

Ko H, Cossell L, Baragli C, Antolik J, Clopath C, Hofer SB, Mrsic-Flogel TD. 2013. The emergence of functional microcircuits in visual cortex. Nature. 496(7443):96–100. https://doi.org/10.1038/nature12015

Komuro H, Yacubova E, Yacubova E, Rakic P. 2001. Mode and tempo of tangential cell migration in the cerebellar external granular layer. J Neurosci. 21(2):527–540. https://doi.org/10.1523/JNEUROSCI.21-02-00527.2001

Konnerth A, Llano I, Armstrong CM. 1990. Synaptic currents in cerebellar Purkinje cells. Proceedings of the National Academy of Sciences. 87(7):2662–2665. https://doi.org/10.1073/pnas.87.7.2662

Kornau H-C, Schenker LT, Kennedy MB, Seeburg PH. 1995. Domain Interaction Between NMDA Receptor Subunits and the Postsynaptic Density Protein PSD-95. Science. 269(5231):1737–1740. https://doi.org/10.1126/science.7569905

Kurihara H, Hashimoto K, Kano M, Takayama C, Sakimura K, Mishina M, Inoue Y, Watanabe M. 1997. Impaired Parallel Fiber→Purkinje Cell Synapse Stabilization during Cerebellar Development of Mutant Mice Lacking the Glutamate Receptor δ2 Subunit. J Neurosci. 17(24):9613–9623. https://doi.org/10.1523/JNEUROSCI.17-24-09613.1997

Kuwako K, Nishimoto Y, Kawase S, Okano HJ, Okano H. 2014. Cadherin-7 Regulates Mossy Fiber Connectivity in the Cerebellum. Cell Reports. 9(1):311–323. https://doi.org/10.1016/j.celrep.2014.08.063

Kwon O, Feng L, Druckmann S, Kim J. 2018. Schaffer Collateral Inputs to CA1 Excitatory and Inhibitory Neurons Follow Different Connectivity Rules. J Neurosci. 38(22):5140–5152. https://doi.org/10.1523/JNEUROSCI.0155-18.2018

-L-

Lainé J, Axelrad H. 1994. The candelabrum cell: a new interneuron in the cerebellar cortex. J Comp Neurol. 339(2):159–173. https://doi.org/10.1002/cne.903390202

Landsend AS, Amiry-Moghaddam M, Matsubara A, Bergersen L, Usami S, Wenthold RJ, Ottersen OP. 1997. Differential localization of delta glutamate receptors in the rat cerebellum: coexpression with AMPA receptors in parallel fiber-spine synapses and absence from climbing fiber-spine synapses. J Neurosci. 17(2):834–842. https://doi.org/10.1523/JNEUROSCI.17-02-00834.1997

Langley JN. 1895. Note on Regeneration of Præ-Ganglionic Fibres of the Sympathetic. J Physiol. 18(3):280–284.

Lanoue V, Usardi A, Sigoillot SM, Talleur M, Iyer K, Mariani J, Isope P, Vodjdani G, Heintz N, Selimi F. 2013. The adhesion-GPCR BAI3, a gene linked to psychiatric disorders, regulates dendrite morphogenesis in neurons. Mol Psychiatry. 18(8):943–950. https://doi.org/10.1038/mp.2013.46

Larramendi LHM. 1969. Analysis of synaptogenesis in the cerebellum of the mouse. Neurobiology of cerebellar evolution and development.

Le Vay S, Wiesel TN, Hubel DH. 1980. The development of ocular dominance columns in normal and visually deprived monkeys. Journal of Comparative Neurology. 191(1):1–51. https://doi.org/10.1002/cne.901910102

LeBlanc JJ, Fagiolini M. 2011. Autism: A “Critical Period” Disorder? Neural Plasticity. 2011:1–17. https://doi.org/10.1155/2011/921680

Levenes C, Daniel H, Jaillard D, Conquet F, Crépel F. 1997. Incomplete regression of multiple climbing fibre innervation of cerebellar Purkinje cells in mGLuR1 mutant mice. Neuroreport. 8(2):571–574. https://doi.org/10.1097/00001756-199701200-00038

Lévi S, Chesnoy-Marchais D, Sieghart W, Triller A. 1999. Synaptic Control of Glycine and GABAA Receptors and Gephyrin Expression in Cultured Motoneurons. J Neurosci. 19(17):7434–7449. https://doi.org/10.1523/JNEUROSCI.19-17-07434.1999

Li Y, Lu H, Cheng P, Ge S, Xu H, Shi S-H, Dan Y. 2012. Clonally related visual cortical neurons show similar stimulus feature selectivity. Nature. 486(7401):118–121. https://doi.org/10.1038/nature11110

Lips ES, Cornelisse LN, Toonen RF, Min JL, Hultman CM, Holmans PA, O'Donovan MC, Purcell SM, Smit AB, Verhage M, et al. 2012. Functional gene group analysis identifies synaptic gene groups as risk factor for schizophrenia. Mol Psychiatry. 17(10):996–1006. https://doi.org/10.1038/mp.2011.117

Liu Q-R, Drgon T, Johnson C, Walther D, Hess J, Uhl GR. 2006. Addiction molecular genetics: 639,401 SNP whole genome association identifies many "cell adhesion" genes. Am J Med Genet B Neuropsychiatr Genet. 141B(8):918–925. https://doi.org/10.1002/ajmg.b.30436

Llorca A, Deogracias R. 2022. Origin, Development, and Synaptogenesis of Cortical Interneurons. Frontiers in Neuroscience [Internet]. [accessed 2023 Jan 9] 16. https://www.frontiersin.org/articles/10.3389/fnins.2022.929469

Lorenzetto E, Caselli L, Feng G, Yuan W, Nerbonne JM, Sanes JR, Buffelli M. 2009. Genetic perturbation of postsynaptic activity regulates synapse elimination in developing cerebellum. Proc Natl Acad Sci USA. 106(38):16475–16480. https://doi.org/10.1073/pnas.0907298106

Lowery RL, Tremblay M-E, Hopkins BE, Majewska AK. 2017. The microglial fractalkine receptor is not required for activity-dependent plasticity in the mouse visual system. Glia. 65(11):1744–1761. https://doi.org/10.1002/glia.23192

Luhmann HJ, Sinning A, Yang J-W, Reyes-Puerta V, Stüttgen MC, Kirischuk S, Kilb W. 2016. Spontaneous Neuronal Activity in Developing Neocortical Networks: From Single Cells to Large-Scale Interactions. Frontiers in Neural Circuits [Internet]. [accessed 2023 Jan 11] 10. https://www.frontiersin.org/articles/10.3389/fncir.2016.00040

Luo L, Ambrozkiewicz MC, Benseler F, Chen C, Dumontier E, Falkner S, Furlanis E, Gomez AM, Hoshina N, Huang W-H, et al. 2020. Optimizing Nervous System-Specific Gene Targeting with Cre Driver Lines: Prevalence of Germline Recombination and Influencing Factors. Neuron. 106(1):37-65.e5. https://doi.org/10.1016/j.neuron.2020.01.008

-M-

Malenka RC, Bear MF. 2004. LTP and LTD: an embarrassment of riches. Neuron. 44(1):5–21. https://doi.org/10.1016/j.neuron.2004.09.012

Malik AN, Vierbuchen T, Hemberg M, Rubin AA, Ling E, Couch CH, Stroud H, Spiegel I, Farh KK-H, Harmin DA, Greenberg ME. 2014. Genome-wide identification and characterization of functional neuronal activity–dependent enhancers. Nat Neurosci. 17(10):1330–1339. https://doi.org/10.1038/nn.3808

Marcassa G, Dascenco D, de Wit J. 2023. Proteomics-based synapse characterization: From proteins to circuits. Current Opinion in Neurobiology. 79:102690. https://doi.org/10.1016/j.conb.2023.102690

Martinelli DC, Chew KS, Rohlmann A, Lum MY, Ressl S, Hattar S, Brunger AT, Missler M, Südhof TC. 2016. Expression of C1ql3 in Discrete Neuronal Populations Controls Efferent Synapse Numbers and Diverse Behaviors. Neuron. 91(5):1034–1051. https://doi.org/10.1016/j.neuron.2016.07.002

Mason CA, Christakos S, Catalano SM. 1990a. Early climbing fiber interactions with Purkinje cells in the postnatal mouse cerebellum. J Comp Neurol. 297(1):77–90. https://doi.org/10.1002/cne.902970106

Mason CA, Christakos S, Catalano SM. 1990b. Early climbing fiber interactions with Purkinje cells in the postnatal mouse cerebellum. J Comp Neurol. 297(1):77–90. https://doi.org/10.1002/cne.902970106

Mason CA, Gregory E. 1984. Postnatal maturation of cerebellar mossy and climbing fibers: transient expression of dual features on single axons. J Neurosci. 4(7):1715–1735. https://doi.org/10.1523/JNEUROSCI.04-07-01715.1984

Matsuda K, Miura E, Miyazaki T, Kakegawa W, Emi K, Narumi S, Fukazawa Y, Ito-Ishida A, Kondo T, Shigemoto R, et al. 2010a. Cbln1 is a ligand for an orphan glutamate receptor delta2, a bidirectional synapse organizer. Science. 328(5976):363–368. https://doi.org/10.1126/science.1185152

Matsuda K, Miura E, Miyazaki T, Kakegawa W, Emi K, Narumi S, Fukazawa Y, Ito-Ishida A, Kondo T, Shigemoto R, et al. 2010b. Cbln1 is a ligand for an orphan glutamate receptor delta2, a bidirectional synapse organizer. Science (New York, NY). 328(5976):363–368.

McCarthy MJ, Nievergelt CM, Kelsoe JR, Welsh DK. 2012. A Survey of Genomic Studies Supports Association of Circadian Clock Genes with Bipolar Disorder Spectrum Illnesses and Lithium Response. PLOS ONE. 7(2):e32091. https://doi.org/10.1371/journal.pone.0032091

McLaughlin T, Torborg CL, Feller MB, O'Leary DDM. 2003. Retinotopic Map Refinement Requires Spontaneous Retinal Waves during a Brief Critical Period of Development. Neuron. 40(6):1147–1160. https://doi.org/10.1016/S0896-6273(03)00790-6

Miale IL, Sidman RL. 1961. An autoradiographic analysis of histogenesis in the mouse cerebellum. Experimental Neurology. 4(4):277–296. https://doi.org/10.1016/0014-4886(61)90055-3

Millard SS, Lu Z, Zipursky SL, Meinertzhagen IA. 2010. Drosophila Dscam Proteins Regulate Postsynaptic Specificity at Multiple-Contact Synapses. Neuron. 67(5):761–768. https://doi.org/10.1016/j.neuron.2010.08.030

Miyazaki T, Fukaya M, Shimizu H, Watanabe M. 2003. Subtype switching of vesicular glutamate transporters at parallel fibre–Purkinje cell synapses in developing mouse cerebellum. European Journal of Neuroscience. 17(12):2563–2572. https://doi.org/10.1046/j.1460-9568.2003.02698.x

Miyazaki T, Hashimoto K, Shin H-S, Kano M, Watanabe M. 2004. P/Q-Type Ca2+ Channel α1A Regulates Synaptic Competition on Developing Cerebellar Purkinje Cells. J Neurosci. 24(7):1734–1743. https://doi.org/10.1523/JNEUROSCI.4208-03.2004

Miyazaki T, Yamasaki M, Hashimoto K, Kohda K, Yuzaki M, Shimamoto K, Tanaka K, Kano M, Watanabe M. 2017. Glutamate transporter GLAST controls synaptic wrapping by Bergmann glia and ensures proper wiring of Purkinje cells. Proceedings of the National Academy of Sciences. 114(28):7438–7443. https://doi.org/10.1073/pnas.1617330114

Miyazaki T, Yamasaki M, Takeuchi T, Sakimura K, Mishina M, Watanabe M. 2010. Ablation of Glutamate Receptor GluRδ2 in Adult Purkinje Cells Causes Multiple Innervation of Climbing Fibers by Inducing Aberrant Invasion to Parallel Fiber Innervation Territory. J Neurosci. 30(45):15196–15209. https://doi.org/10.1523/JNEUROSCI.0934-10.2010

Motta A, Berning M, Boergens KM, Staffler B, Beining M, Loomba S, Hennig P, Wissler H, Helmstaedter M. 2019. Dense connectomic reconstruction in layer 4 of the somatosensory cortex. Science. 366(6469):eaay3134. https://doi.org/10.1126/science.aay3134

-N-

Nakashima A, Ihara N, Shigeta M, Kiyonari H, Ikegaya Y, Takeuchi H. 2019. Structured spike series specify gene expression patterns for olfactory circuit formation. Science. 365(6448):eaaw5030. https://doi.org/10.1126/science.aaw5030

Nakayama H, Abe M, Morimoto C, Iida T, Okabe S, Sakimura K, Hashimoto K. 2018. Microglia permit climbing fiber elimination by promoting GABAergic inhibition in the developing cerebellum. Nature Communications. 9(1). https://doi.org/10.1038/s41467-018-05100-z

Nakayama H, Miyazaki T, Kitamura K, Hashimoto K, Yanagawa Y, Obata K, Sakimura K, Watanabe M, Kano M. 2012. GABAergic Inhibition Regulates Developmental Synapse Elimination in the Cerebellum. Neuron. 74(2):384–396. https://doi.org/10.1016/j.neuron.2012.02.032

Narushima M, Uchigashima M, Yagasaki Y, Harada T, Nagumo Y, Uesaka N, Hashimoto K, Aiba A, Watanabe M, Miyata M, Kano M. 2016. The Metabotropic Glutamate Receptor Subtype 1 Mediates Experience-Dependent Maintenance of Mature Synaptic Connectivity in the Visual Thalamus. Neuron. 91(5):1097–1109. https://doi.org/10.1016/j.neuron.2016.07.035

Nguyen T-M, Schreiner D, Xiao L, Traunmüller L, Bornmann C, Scheiffele P. 2016. An alternative splicing switch shapes neurexin repertoires in principal neurons versus interneurons in the mouse hippocampus.Nelson SB, editor. eLife. 5:e22757. https://doi.org/10.7554/eLife.22757

Nishida K, Flanagan JG, Nakamoto M. 2002. Domain-specific olivocerebellar projection regulated by the EphA-ephrin-A interaction. Development. 129(24):5647–5658. https://doi.org/10.1242/dev.00162

-O-

Offermanns S, Hashimoto K, Watanabe M, Sun W, Kurihara H, Thompson RF, Inoue Y, Kano M, Simon MI. 1997. Impaired motor coordination and persistent multiple climbing fiber innervation of cerebellar Purkinje cells in mice lacking Galphaq. Proc Natl Acad Sci U S A. 94(25):14089–14094. https://doi.org/10.1073/pnas.94.25.14089

Ohtsuki G, Nishiyama M, Yoshida T, Murakami T, Histed M, Lois C, Ohki K. 2012. Similarity of Visual Selectivity among Clonally Related Neurons in Visual Cortex. Neuron. 75(1):65–72. https://doi.org/10.1016/j.neuron.2012.05.023

Okawa H, Hoon M, Yoshimatsu T, Della Santina L, Wong ROL. 2014. Illuminating the multifaceted roles of neurotransmission in shaping neuronal circuitry. Neuron. 83(6):1303–1318. https://doi.org/10.1016/j.neuron.2014.08.029

Osorno T, Rudolph S, Nguyen T, Kozareva V, Nadaf NM, Norton A, Macosko EZ, Lee W-CA, Regehr WG. 2022. Candelabrum cells are ubiquitous cerebellar cortex interneurons with specialized circuit properties. Nat Neurosci. 25(6):702–713. https://doi.org/10.1038/s41593-022-01057-x

Osterhout JA, Josten N, Yamada J, Pan F, Wu S, Nguyen PL, Panagiotakos G, Inoue YU, Egusa SF, Volgyi B, et al. 2011. Cadherin-6 Mediates Axon-Target Matching in a Non-Image-Forming Visual Circuit. Neuron. 71(4):632–639. https://doi.org/10.1016/j.neuron.2011.07.006

-P-

Pakozdy A, Patzl M, Zimmermann L, Jokinen T s., Glantschnigg U, Kelemen A, Hasegawa D. 2015. LGI Proteins and Epilepsy in Human and Animals. Journal of Veterinary Internal Medicine. 29(4):997–1005. https://doi.org/10.1111/jvim.12610

Palade GE. 1954. Electron microscope observations of interneuronal and neuromuscular synapses. Anat Rec. 118:335–336.

Palay SL. 1958. The morphology of synapses in the central nervous system. Exp Cell Res. 14(Suppl 5):275–293.

Palay SL, Palade GE. 1955. The fine structure of neurons. The Journal of biophysical and biochemical cytology. 1(1):69.

Paolicelli RC, Bolasco G, Pagani F, Maggi L, Scianni M, Panzanelli P, Giustetto M, Ferreira TA, Guiducci E, Dumas L, et al. 2011. Synaptic Pruning by Microglia Is Necessary for Normal Brain Development. Science. 333(6048):1456–1458. https://doi.org/10.1126/science.1202529

Park H, Kim T, Kim J, Yamamoto Y, Tanaka-Yamamoto K. 2019. Inputs from Sequentially Developed Parallel Fibers Are Required for Cerebellar Organization. Cell Reports. 28(11):2939-2954.e5. https://doi.org/10.1016/j.celrep.2019.08.010

Park WJ, Fine I. 2020. New insights into cortical development and plasticity: from molecules to behavior. Current Opinion in Physiology. 16:50–60. https://doi.org/10.1016/j.cophys.2020.06.004

Pätz C, Brachtendorf S, Eilers J. 2019. Developmental Easing of Short-Term Depression in "Winner" Climbing Fibers. Frontiers in Cellular Neuroscience [Internet]. [accessed 2023 Feb 12] 13. https://www.frontiersin.org/articles/10.3389/fncel.2019.00183

Paul MA, Sigoillot SM, Marti L, Delagrange M, Mailly P, Selimi F. 2023. Stepwise molecular specification of excitatory synapse diversity on a target neuron [Internet]. [accessed 2023 Feb 22]:2023.01.03.521946. https://doi.org/10.1101/2023.01.03.521946
Pellegrino LJ, Altman J. Effects of Differential Interference With Postnatal Gerebellar Neurogenesis on Motor Performance, Activity Level, and Maze Learning of Rats: A Developmental Study.

Peng J, Kim MJ, Cheng D, Duong DM, Gygi SP, Sheng M. 2004. Semiquantitative proteomic analysis of rat forebrain postsynaptic density fractions by mass spectrometry. J Biol Chem. 279(20):21003–21011. https://doi.org/10.1074/jbc.M400103200

Penn AA, Riquelme PA, Feller MB, Shatz CJ. 1998. Competition in Retinogeniculate Patterning Driven by Spontaneous Activity. Science. 279(5359):2108–2112. https://doi.org/10.1126/science.279.5359.2108

Petanjek Z, Judaš M, Šimić G, Rašin MR, Uylings HBM, Rakic P, Kostović I. 2011. Extraordinary neoteny of synaptic spines in the human prefrontal cortex. Proceedings of the National Academy of Sciences. 108(32):13281–13286. https://doi.org/10.1073/pnas.1105108108

Peters A, Feldman ML. 1976. The projection of the lateral geniculate nucleus to area 17 of the rat cerebral cortex. I. General description. J Neurocytol. 5(1):63–84. https://doi.org/10.1007/BF01176183

Petit-Pedrol M, Sell J, Planagumà J, Mannara F, Radosevic M, Haselmann H, Ceanga M, Sabater L, Spatola M, Soto D, et al. 2018. LGI1 antibodies alter Kv1.1 and AMPA receptors changing synaptic excitability, plasticity and memory. Brain. 141(11):3144–3159. https://doi.org/10.1093/brain/awy253

Petrinovic MM, Hourez R, Aloy EM, Dewarrat G, Gall D, Weinmann O, Gaudias J, Bachmann LC, Schiffmann SN, Vogt KE, Schwab ME. 2013. Neuronal Nogo-A negatively regulates dendritic morphology and synaptic transmission in the cerebellum. Proceedings of the National Academy of Sciences. 110(3):1083–1088. https://doi.org/10.1073/pnas.1214255110

Pignatelli M, Rockland KS. 2020. Organization and development of hippocampal circuits. In: Neural Circuit and Cognitive Development [Internet]. [place unknown]: Elsevier; [accessed 2022 Dec 28]; p. 201–219. https://doi.org/10.1016/B978-0-12-814411-4.00009-3

-R-

Rakic P, Bourgeois J-P, Eckenhoff MF, Zecevic N, Goldman-Rakic PS. 1986. Concurrent Overproduction of Synapses in Diverse Regions of the Primate Cerebral Cortex. Science. 232(4747):232–235. https://doi.org/10.1126/science.3952506

Rakic P, Sidman RL. 1973. Organization of cerebellar cortex secondary to deficit of granule cells in weaver mutant mice. J Comp Neurol. 152(2):133–161. https://doi.org/10.1002/cne.901520203

Redolfi N, Lodovichi C. 2021. Spontaneous Afferent Activity Carves Olfactory Circuits. Frontiers in Cellular Neuroscience [Internet]. [accessed 2023 Jan 13] 15. https://www.frontiersin.org/articles/10.3389/fncel.2021.637536

Reeber S, White J, George-Jones N, Sillitoe R. 2013. Architecture and development of olivocerebellar circuit topography. Frontiers in Neural Circuits [Internet]. [accessed 2023 Feb 24] 6. https://www.frontiersin.org/articles/10.3389/fncir.2012.00115

Rees CL, Moradi K, Ascoli GA. 2017. Weighing the Evidence in Peters' Rule: Does Neuronal Morphology Predict Connectivity? Trends Neurosci. 40(2):63–71. https://doi.org/10.1016/j.tins.2016.11.007

Ressl S, Vu BK, Vivona S, Martinelli DC, Südhof TC, Brunger AT. 2015. Structures of C1q-like Proteins Reveal Unique Features among the C1q/TNF Superfamily. Structure. 23(4):688–699. https://doi.org/10.1016/j.str.2015.01.019

Roche KW, Ly CD, Petralia RS, Wang YX, McGee AW, Bredt DS, Wenthold RJ. 1999. Postsynaptic density-93 interacts with the delta2 glutamate receptor subunit at parallel fiber synapses. J Neurosci. 19(10):3926–3934. https://doi.org/10.1523/JNEUROSCI.19-10-03926.1999

Rossi F, Strata P. 1995. Reciprocal trophic interactions in the adult climbing fibre-Purkinje cell system. Prog Neurobiol. 47(4–5):341–369.

Roussos P, Guennewig B, Kaczorowski DC, Barry G, Brennand KJ. 2016. Activity-Dependent Changes in Gene Expression in Schizophrenia Human-Induced Pluripotent Stem Cell Neurons. JAMA Psychiatry. 73(11):1180–1188. https://doi.org/10.1001/jamapsychiatry.2016.2575

Rozic-Kotliroff G, Zisapel N. 2007. Ca2+ -dependent splicing of neurexin IIalpha. Biochem Biophys Res Commun. 352(1):226–230. https://doi.org/10.1016/j.bbrc.2006.11.008
Sakurai T. 2012. The role of NrCAM in neural development and disorders--beyond a simple glue in the brain. Mol Cell Neurosci. 49(3):351–363. https://doi.org/10.1016/j.mcn.2011.12.002

-S-

Sanders SJ, He X, Willsey AJ, Ercan-Sencicek AG, Samocha KE, Cicek AE, Murtha MT, Bal VH, Bishop SL, Dong S, et al. 2015. Insights into Autism Spectrum Disorder Genomic Architecture and Biology from 71 Risk Loci. Neuron. 87(6):1215–1233. https://doi.org/10.1016/j.neuron.2015.09.016

Sando R, Bushong E, Zhu Y, Huang M, Considine C, Phan S, Ju S, Uytiepo M, Ellisman M, Maximov A. 2017. Assembly of Excitatory Synapses in the Absence of Glutamatergic Neurotransmission. Neuron. 94(2):312-321.e3. https://doi.org/10.1016/j.neuron.2017.03.047

Sando R, Jiang X, Südhof TC. 2019. Latrophilin GPCRs direct synapse specificity by coincident binding of FLRTs and teneurins. Science. 363(6429):eaav7969. https://doi.org/10.1126/science.aav7969

Sato Y, Iketani M, Kurihara Y, Yamaguchi M, Yamashita N, Nakamura F, Arie Y, Kawasaki T, Hirata T, Abe T, et al. 2011. Cartilage Acidic Protein–1B (LOTUS), an Endogenous Nogo Receptor Antagonist for Axon Tract Formation. Science. 333(6043):769–773. https://doi.org/10.1126/science.1204144

Scale of the Human Brain. 2015. AI Impacts [Internet]. [accessed 2023 Mar 27]. https://aiimpacts.org/scale-of-the-human-brain/

Schafer DP, Lehrman EK, Kautzman AG, Koyama R, Mardinly AR, Yamasaki R, Ransohoff RM, Greenberg ME, Barres BA, Stevens B. 2012. Microglia Sculpt Postnatal Neural Circuits in an Activity and Complement-Dependent Manner. Neuron. 74(4):691–705. https://doi.org/10.1016/j.neuron.2012.03.026

Scheiffele P, Fan J, Choih J, Fetter R, Serafini T. 2000. Neuroligin Expressed in Nonneuronal Cells Triggers Presynaptic Development in Contacting Axons. Cell. 101(6):657–669. https://doi.org/10.1016/S0092-8674(00)80877-6

Schiavo G, Benfenati F, Poulain B, Rossetto O, Polverino de Laureto P, DasGupta BR, Montecucco C. 1992. Tetanus and botulinum-B neurotoxins block neurotransmitter release by proteolytic cleavage of synaptobrevin. Nature. 359(6398):832–835. https://doi.org/10.1038/359832a0

Schmahmann JD. 1997. Rediscovery of an early concept. Int Rev Neurobiol. 41:3–27. https://doi.org/10.1016/s0074-7742(08)60345-1

Schmahmann JD. 1998. Dysmetria of thought: clinical consequences of cerebellar dysfunction on cognition and affect. Trends in Cognitive Sciences. 2(9):362–371. https://doi.org/10.1016/S1364-6613(98)01218-2

Schmahmann JD, Sherman JC. 1998. The cerebellar cognitive affective syndrome. Brain. 121 (Pt 4):561–579. https://doi.org/10.1093/brain/121.4.561

Schmucker D, Clemens JC, Shu H, Worby CA, Xiao J, Muda M, Dixon JE, Zipursky SL. 2000. Drosophila Dscam Is an Axon Guidance Receptor Exhibiting Extraordinary Molecular Diversity. Cell. 101(6):671–684. https://doi.org/10.1016/S0092-8674(00)80878-8

Schnell E, Sizemore M, Karimzadegan S, Chen L, Bredt DS, Nicoll RA. 2002. Direct interactions between PSD-95 and stargazin control synaptic AMPA receptor number. Proceedings of the National Academy of Sciences. 99(21):13902–13907. https://doi.org/10.1073/pnas.172511199

Schreiner D, Nguyen T-M, Russo G, Heber S, Patrignani A, Ahrné E, Scheiffele P. 2014. Targeted combinatorial alternative splicing generates brain region-specific repertoires of neurexins. Neuron. 84(2):386–398. https://doi.org/10.1016/j.neuron.2014.09.011

Schroeder A, Vanderlinden J, Vints K, Ribeiro LF, Vennekens KM, Gounko NV, Wierda KD, de Wit J. 2018. A Modular Organization of LRR Protein-Mediated Synaptic Adhesion Defines Synapse Identity. Neuron. 99(2):329-344.e7. https://doi.org/10.1016/j.neuron.2018.06.026

Seigneur E, Südhof TC. 2018. Genetic Ablation of All Cerebellins Reveals Synapse Organizer Functions in Multiple Regions Throughout the Brain. J Neurosci. 38(20):4774–4790. https://doi.org/10.1523/JNEUROSCI.0360-18.2018

Selimi F, Cristea IM, Heller E, Chait BT, Heintz N. 2009. Proteomic Studies of a Single CNS Synapse Type: The Parallel Fiber/Purkinje Cell Synapse. PLOS Biology. 7(4):e1000083. https://doi.org/10.1371/journal.pbio.1000083

Seppälä EH, Jokinen TS, Fukata M, Fukata Y, Webster MT, Karlsson EK, Kilpinen SK, Steffen F, Dietschi E, Leeb T, et al. 2011. LGI2 truncation causes a remitting focal epilepsy in dogs. PLoS Genet. 7(7):e1002194. https://doi.org/10.1371/journal.pgen.1002194

Shuster SA, Wagner MJ, Pan-Doh N, Ren J, Grutzner SM, Beier KT, Kim TH, Schnitzer MJ, Luo L. 2021. The relationship between birth timing, circuit wiring, and physiological response properties of cerebellar granule cells. Proc Natl Acad Sci U S A. 118(23):e2101826118. https://doi.org/10.1073/pnas.2101826118

Sigler A, Oh WC, Imig C, Altas B, Kawabe H, Cooper BH, Kwon H-B, Rhee J-S, Brose N. 2017. Formation and Maintenance of Functional Spines in the Absence of Presynaptic Glutamate Release. Neuron. 94(2):304-311.e4. https://doi.org/10.1016/j.neuron.2017.03.029

Sigoillot SM, Iyer K, Binda F, González-Calvo I, Talleur M, Vodjdani G, Isope P, Selimi F. 2015. The Secreted Protein C1QL1 and Its Receptor BAI3 Control the Synaptic Connectivity of Excitatory Inputs Converging on Cerebellar Purkinje Cells. Cell Reports. 10(5):820–832. https://doi.org/10.1016/j.celrep.2015.01.034

Sillitoe RV, Marzban H, Larouche M, Zahedi S, Affanni J, Hawkes R. 2005. Conservation of the architecture of the anterior lobe vermis of the cerebellum across mammalian species. In: Progress in Brain Research [Internet]. Vol. 148. [place unknown]: Elsevier; [accessed 2023 Feb 26]; p. 283–297. https://doi.org/10.1016/S0079-6123(04)48022-4

Slezak M, Grosche A, Niemiec A, Tanimoto N, Pannicke T, Münch TA, Crocker B, Isope P, Härtig W, Beck SC, et al. 2012. Relevance of Exocytotic Glutamate Release from Retinal Glia. Neuron. 74(3):504–516. https://doi.org/10.1016/j.neuron.2012.03.027

Somogyu P, Hámori J. 1976. A quantitative electron microscopic study of the purkinje cell axon initial segment. Neuroscience. 1(5):361-IN3. https://doi.org/10.1016/0306-4522(76)90127-5

Sotelo C. 1975. Anatomical, physiological and biochemical studies of the cerebellum from mutant mice. II. Morphological study of cerebellar cortical neurons and circuits in the weaver mouse. Brain Res. 94(1):19–44. https://doi.org/10.1016/0006-8993(75)90874-4

Sotelo C. 1978. Purkinje Cell Ontogeny: Formation and Maintenance of Spines. In: Corner MA, Baker RE, Vandepoll NE, Swaab DF, Uylings HBM, editors. Progress in Brain Research [Internet]. Vol. 48. [place unknown]: Elsevier; [accessed 2023 Jan 16]; p. 149–170. https://doi.org/10.1016/S0079-6123(08)61021-3

Sotelo C. 1990. Cerebellar synaptogenesis: what we can learn from mutant mice. Journal of Experimental Biology. 153(1):225–249. https://doi.org/10.1242/jeb.153.1.225

Sotelo C. 2004. Cellular and genetic regulation of the development of the cerebellar system. Progress in Neurobiology. 72(5):295–339. https://doi.org/10.1016/j.pneurobio.2004.03.004

Sotelo C. 2008. Development of "Pinceaux" formations and dendritic translocation of climbing fibers during the acquisition of the balance between glutamatergic and γ-aminobutyric acidergic inputs in developing Purkinje cells. Journal of Comparative Neurology. 506(2):240–262. https://doi.org/10.1002/cne.21501

Sotelo C. 2020. The History of the Synapse. The Anatomical Record. 303(5):1252–1279. https://doi.org/10.1002/ar.24392

Sotelo C, Rossi F. 2013. Purkinje Cell Migration and Differentiation. In: Manto M, Schmahmann JD, Rossi F, Gruol DL, Koibuchi N, editors. Handbook of the Cerebellum and Cerebellar Disorders [Internet]. Dordrecht: Springer Netherlands; [accessed 2023 Feb 13]; p. 147–178. https://doi.org/10.1007/978-94-007-1333-8_9

Sperry RW. 1943. Visuomotor coordination in the newt (triturus viridescens) after regeneration of the optic nerve. Journal of Comparative Neurology. 79(1):33–55. https://doi.org/10.1002/cne.900790104

Sperry RW. 1944. Optic nerve regeneration with return of vision in anurans. Journal of Neurophysiology. 7(1):57–69. https://doi.org/10.1152/jn.1944.7.1.57

Sperry RW. 1963. CHEMOAFFINITY IN THE ORDERLY GROWTH OF NERVE FIBER PATTERNS AND CONNECTIONS*. Proc Natl Acad Sci U S A. 50(4):703–710.

Stepanyants A, Chklovskii DB. 2005. Neurogeometry and potential synaptic connectivity. Trends in Neurosciences. 28(7):387–394. https://doi.org/10.1016/j.tins.2005.05.006

Stevens B, Allen NJ, Vazquez LE, Howell GR, Christopherson KS, Nouri N, Micheva KD, Mehalow AK, Huberman AD, Stafford B, et al. 2007. The Classical Complement Cascade Mediates CNS Synapse Elimination. Cell. 131(6):1164–1178. https://doi.org/10.1016/j.cell.2007.10.036

Stoessel MB, Majewska AK. 2021. Little cells of the little brain: microglia in cerebellar development and function. Trends in Neurosciences. 44(7):564–578. https://doi.org/10.1016/j.tins.2021.04.001

Stoodley CJ. 2012. The cerebellum and cognition: evidence from functional imaging studies. Cerebellum. 11(2):352–365. https://doi.org/10.1007/s12311-011-0260-7

Stoodley CJ, Schmahmann JD. 2009. Functional topography in the human cerebellum: a meta-analysis of neuroimaging studies. Neuroimage. 44(2):489–501. https://doi.org/10.1016/j.neuroimage.2008.08.039

Strata P. 2002. Dendritic spines in Purkinje cells. Cerebellum. 1(4):230–232. https://doi.org/10.1080/147342202320883533

Straub I, Witter L, Eshra A, Hoidis M, Byczkowicz N, Maas S, Delvendahl I, Dorgans K, Savier E, Bechmann I, et al. 2020. Gradients in the mammalian cerebellar cortex enable Fourier-like transformation and improve storing capacity.Nelson SB, Shinn-Cunningham BG, Nelson SB, editors. eLife. 9:e51771. https://doi.org/10.7554/eLife.51771

Stroud H, Yang MG, Tsitohay YN, Davis CP, Sherman MA, Hrvatin S, Ling E, Greenberg ME. 2020. An Activity-Mediated Transition in Transcription in Early Postnatal Neurons. Neuron. 107(5):874-890.e8. https://doi.org/10.1016/j.neuron.2020.06.008

Südhof TC. 2008. Neuroligins and neurexins link synaptic function to cognitive disease. Nature. 455(7215):903–911. https://doi.org/10.1038/nature07456

Südhof TC. 2017. Synaptic Neurexin Complexes: A Molecular Code for the Logic of Neural Circuits. Cell. 171(4):745–769. https://doi.org/10.1016/j.cell.2017.10.024

Südhof TC. 2018. Towards an Understanding of Synapse Formation. Neuron. 100(2):276–293. https://doi.org/10.1016/j.neuron.2018.09.040

Südhof TC. 2021. The cell biology of synapse formation. Journal of Cell Biology. 220(7):e202103052. https://doi.org/10.1083/jcb.202103052

Sugihara I. 2005. Microzonal projection and climbing fiber remodeling in single olivocerebellar axons of newborn rats at postnatal days 4-7. J Comp Neurol. 487(1):93–106. https://doi.org/10.1002/cne.20531

Sugihara I, Shinoda Y. 2004. Molecular, Topographic, and Functional Organization of the Cerebellar Cortex: A Study with Combined Aldolase C and Olivocerebellar Labeling. J Neurosci. 24(40):8771–8785. https://doi.org/10.1523/JNEUROSCI.1961-04.2004

Sugihara I, Shinoda Y. 2007. Molecular, Topographic, and Functional Organization of the Cerebellar Nuclei: Analysis by Three-Dimensional Mapping of the Olivonuclear Projection and Aldolase C Labeling. J Neurosci. 27(36):9696–9710. https://doi.org/10.1523/JNEUROSCI.1579-07.2007

Sugihara I, Wu H-S, Shinoda Y. 2001. The Entire Trajectories of Single Olivocerebellar Axons in the Cerebellar Cortex and their Contribution to Cerebellar Compartmentalization. J Neurosci. 21(19):7715–7723. https://doi.org/10.1523/JNEUROSCI.21-19-07715.2001

-T-

Takayama C, Nakagawa S, Watanabe M, Mishina M, Inoue Y. 1995. Light- and electron-microscopic localization of the glutamate receptor channel delta 2 subunit in the mouse Purkinje cell. Neurosci Lett. 188(2):89–92. https://doi.org/10.1016/0304-3940(95)11403-j

Takechi H, Eilers J, Konnerth A. 1998. A new class of synaptic response involving calcium release in dendritic spines. Nature. 396(6713):757–760. https://doi.org/10.1038/25547

Takeda T, Maekawa K. 1989. Transient direct connection of vestibular mossy fibers to the vestibulocerebellar Purkinje cells in early postnatal development of kittens. Neuroscience. 32(1):99–111. https://doi.org/10.1016/0306-4522(89)90110-3

Takeichi M. 2007. The cadherin superfamily in neuronal connections and interactions. Nat Rev Neurosci. 8(1):11–20. https://doi.org/10.1038/nrn2043

Takemura Shin-ya, Xu CS, Lu Z, Rivlin PK, Parag T, Olbris DJ, Plaza S, Zhao T, Katz WT, Umayam L, et al. 2015. Synaptic circuits and their variations within different columns in the visual system of Drosophila. Proceedings of the National Academy of Sciences. 112(44):13711–13716. https://doi.org/10.1073/pnas.1509820112

Telley L, Cadilhac C, Cioni J-M, Saywell V, Jahannault-Talignani C, Huettl RE, Sarrailh-Faivre C, Dayer A, Huber AB, Ango F. 2016. Dual Function of NRP1 in Axon Guidance and Subcellular Target Recognition in Cerebellum. Neuron. 91(6):1276–1291. https://doi.org/10.1016/j.neuron.2016.08.015

Thomas R, Favell K, Morante-Redolat J, Pool M, Kent C, Wright M, Daignault K, Ferraro GB, Montcalm S, Durocher Y, et al. 2010. LGI1 Is a Nogo Receptor 1 Ligand that Antagonizes Myelin-Based Growth Inhibition. J Neurosci. 30(19):6607–6612. https://doi.org/10.1523/JNEUROSCI.5147-09.2010

Thomas RA, Gibon J, Chen CXQ, Chierzi S, Soubannier VG, Baulac S, Séguéla P, Murai K, Barker PA. 2018. The Nogo Receptor Ligand LGI1 Regulates Synapse Number and Synaptic Activity in Hippocampal and Cortical Neurons. eNeuro. 5(4):ENEURO.0185-18.2018. https://doi.org/10.1523/ENEURO.0185-18.2018

Trinidad JC, Thalhammer A, Specht CG, Lynn AJ, Baker PR, Schoepfer R, Burlingame AL. 2008. Quantitative analysis of synaptic phosphorylation and protein expression. Mol Cell Proteomics. 7(4):684–696. https://doi.org/10.1074/mcp.M700170-MCP200

Tyssowski KM, DeStefino NR, Cho J-H, Dunn CJ, Poston RG, Carty CE, Jones RD, Chang SM, Romeo P, Wurzelmann MK, et al. 2018. Different Neuronal Activity Patterns Induce

Different Gene Expression Programs. Neuron. 98(3):530-546.e11. https://doi.org/10.1016/j.neuron.2018.04.001

-U-

Uemura T, Lee S-J, Yasumura M, Takeuchi T, Yoshida T, Ra M, Taguchi R, Sakimura K, Mishina M. 2010. Trans-synaptic interaction of GluRdelta2 and Neurexin through Cbln1 mediates synapse formation in the cerebellum. Cell. 141(6):1068–1079. https://doi.org/10.1016/j.cell.2010.04.035

Uemura T, Mori H, Mishina M. 2004. Direct interaction of GluRdelta2 with Shank scaffold proteins in cerebellar Purkinje cells. Mol Cell Neurosci. 26(2):330–341. https://doi.org/10.1016/j.mcn.2004.02.007

Uesaka N, Uchigashima M, Mikuni T, Nakazawa T, Nakao H, Hirai H, Aiba A, Watanabe M, Kano M. 2014. Retrograde semaphorin signaling regulates synapse elimination in the developing mouse brain. Science. 344(6187):1020–1023. https://doi.org/10.1126/science.1252514

Uezu A, Kanak DJ, Bradshaw TWA, Soderblom EJ, Catavero CM, Burette AC, Weinberg RJ, Soderling SH. 2016. Identification of an elaborate complex mediating postsynaptic inhibition. Science. 353(6304):1123–1129. https://doi.org/10.1126/science.aag0821

Uezu A, Soderling S. 2019. Identifying Synaptic Proteins by In Vivo BioID from Mouse Brain. In: Sunbul M, Jäschke A, editors. Proximity Labeling: Methods and Protocols [Internet]. New York, NY: Springer; [accessed 2023 Mar 16]; p. 107–119. https://doi.org/10.1007/978-1-4939-9537-0_9

-V-

Valdes-Aleman J, Fetter RD, Sales EC, Heckman EL, Venkatasubramanian L, Doe CQ, Landgraf M, Cardona A, Zlatic M. 2021. Comparative Connectomics Reveals How Partner Identity, Location, and Activity Specify Synaptic Connectivity in Drosophila. Neuron. 109(1):105-122.e7. https://doi.org/10.1016/j.neuron.2020.10.004

Valera AM, Doussau F, Poulain B, Barbour B, Isope P. 2012. Adaptation of granule cell to Purkinje cell synapses to high-frequency transmission. J Neurosci. 32(9):3267–3280. https://doi.org/10.1523/JNEUROSCI.3175-11.2012

Van Der Loos H, Glaser EM. 1972. Autapses in neocortex cerebri: synapses between a pyramidal cell's axon and its own dendrites. Brain Research. 48:355–360. https://doi.org/10.1016/0006-8993(72)90189-8

Varoqueaux F, Sigler A, Rhee J-S, Brose N, Enk C, Reim K, Rosenmund C. 2002. Total arrest of spontaneous and evoked synaptic transmission but normal synaptogenesis in the absence of Munc13-mediated vesicle priming. Proc Natl Acad Sci U S A. 99(13):9037–9042. https://doi.org/10.1073/pnas.122623799

Veleanu M, Urrieta-Chávez B, Sigoillot Séverine M, Paul MA, Usardi A, Iyer K, Delagrange M, Doyle JP, Heintz N, Bécamel C, Selimi F. 2022. Modified climbing fiber/Purkinje cell synaptic connectivity in the cerebellum of the neonatal phencyclidine model of schizophrenia. Proceedings of the National Academy of Sciences. 119(21):e2122544119–e2122544119. https://doi.org/10.1073/pnas.2122544119

Veleanu M, Urrieta-Chávez B, Sigoillot Séverine M., Paul MA, Usardi A, Iyer K, Delagrange M, Doyle JP, Heintz N, Bécamel C, Selimi F. 2022. Modified climbing fiber/Purkinje cell synaptic connectivity in the cerebellum of the neonatal phencyclidine model of schizophrenia. Proc Natl Acad Sci U S A. 119(21):e2122544119. https://doi.org/10.1073/pnas.2122544119

Verhage M, Maia AS, Plomp JJ, Brussaard AB, Heeroma JH, Vermeer H, Toonen RF, Hammer RE, van den Berg TK, Missler M, et al. 2000. Synaptic assembly of the brain in the absence of neurotransmitter secretion. Science. 287(5454):864–869. https://doi.org/10.1126/science.287.5454.864

-W-

Walsh T, McClellan JM, McCarthy SE, Addington AM, Pierce SB, Cooper GM, Nord AS, Kusenda M, Malhotra D, Bhandari A, et al. 2008. Rare structural variants disrupt multiple genes in neurodevelopmental pathways in schizophrenia. Science. 320(5875):539–543. https://doi.org/10.1126/science.1155174

Wang F, Nemes A, Mendelsohn M, Axel R. 1998. Odorant Receptors Govern the Formation of a Precise Topographic Map. Cell. 93(1):47–60. https://doi.org/10.1016/S0092-8674(00)81145-9

Wang J, Zugates CT, Liang IH, Lee C-HJ, Lee T. 2002. Drosophila Dscam Is Required for Divergent Segregation of Sister Branches and Suppresses Ectopic Bifurcation of Axons. Neuron. 33(4):559–571. https://doi.org/10.1016/S0896-6273(02)00570-6

Wang Jie, Miao Y, Wicklein R, Sun Z, Wang Jinzhao, Jude KM, Fernandes RA, Merrill SA, Wernig M, Garcia KC, Südhof TC. 2021. RTN4/NoGo-receptor binding to BAI adhesion-GPCRs regulates neuronal development. Cell. 184(24):5869-5885.e25. https://doi.org/10.1016/j.cell.2021.10.016

Wess J, Nakajima K, Jain S. 2013. Novel designer receptors to probe GPCR signaling and physiology. Trends Pharmacol Sci. 34(7):385–392. https://doi.org/10.1016/j.tips.2013.04.006

White JJ, Arancillo M, Stay TL, George-Jones NA, Levy SL, Heck DH, Sillitoe RV. 2014. Cerebellar Zonal Patterning Relies on Purkinje Cell Neurotransmission. J Neurosci. 34(24):8231–8245. https://doi.org/10.1523/JNEUROSCI.0122-14.2014

White JJ, Sillitoe RV. 2017. Genetic silencing of olivocerebellar synapses causes dystonia-like behaviour in mice. Nat Commun. 8(1):14912. https://doi.org/10.1038/ncomms14912
Whittaker VP. 1993. Thirty years of synaptosome research. J Neurocytol. 22(9):735–742. https://doi.org/10.1007/BF01181319

Wiegert JS, Mahn M, Prigge M, Printz Y, Yizhar O. 2017. Silencing Neurons: Tools, Applications, and Experimental Constraints. Neuron. 95(3):504–529. https://doi.org/10.1016/j.neuron.2017.06.050

Wiesel TN, Hubel DH. 1963. Single-cell responses in striate cortex of kittens deprived of vision in one eye. Journal of Neurophysiology. 26(6):1003–1017. https://doi.org/10.1152/jn.1963.26.6.1003

Wilhelm BG, Mandad S, Truckenbrodt S, Kröhnert K, Schäfer C, Rammner B, Koo SJ, Claßen GA, Krauss M, Haucke V, et al. 2014. Composition of isolated synaptic boutons reveals the amounts of vesicle trafficking proteins. Science. 344(6187):1023–1028. https://doi.org/10.1126/science.1252884

Williams ME, Wilke SA, Daggett A, Davis E, Otto S, Ravi D, Ripley B, Bushong EA, Ellisman MH, Klein G, Ghosh A. 2011. Cadherin-9 Regulates Synapse-Specific Differentiation in the Developing Hippocampus. Neuron. 71(4):640–655. https://doi.org/10.1016/j.neuron.2011.06.019

Wills ZP, Mandel-Brehm C, Mardinly AR, McCord AE, Giger RJ, Greenberg ME. 2012. The nogo receptor family restricts synapse number in the developing hippocampus. Neuron. 73(3):466–481. https://doi.org/10.1016/j.neuron.2011.11.029

Willyard C. 2018. New human gene tally reignites debate. Nature. 558(7710):354–355. https://doi.org/10.1038/d41586-018-05462-w

Wilms CD, Häusser M. 2015. Reading out a spatiotemporal population code by imaging neighbouring parallel fibre axons in vivo. Nat Commun. 6(1):6464. https://doi.org/10.1038/ncomms7464

Wojtowicz WM, Wu W, Andre I, Qian B, Baker D, Zipursky SL. 2007. A vast repertoire of Dscam binding specificities arises from modular interactions of variable Ig domains. Cell. 130(6):1134–1145. https://doi.org/10.1016/j.cell.2007.08.026

Wu Q-F, Yang L, Li S, Wang Q, Yuan X-B, Gao X, Bao L, Zhang X. 2012. Fibroblast growth factor 13 is a microtubule-stabilizing protein regulating neuronal polarization and migration. Cell. 149(7):1549–1564. https://doi.org/10.1016/j.cell.2012.04.046

-Y-

Yap E-L, Greenberg ME. 2018. Activity-regulated transcription: Bridging the gap between neural activity and behavior. Neuron. 100(2):330–348. https://doi.org/10.1016/j.neuron.2018.10.013

Yu CR, Power J, Barnea G, O'Donnell S, Brown HEV, Osborne J, Axel R, Gogos JA. 2004. Spontaneous Neural Activity Is Required for the Establishment and Maintenance of the Olfactory Sensory Map. Neuron. 42(4):553–566. https://doi.org/10.1016/S0896-6273(04)00224-7

Yu Y-C, Bultje RS, Wang X, Shi S-H. 2009. Specific synapses develop preferentially among sister excitatory neurons in the neocortex. Nature. 458(7237):501–504. https://doi.org/10.1038/nature07722

Yu Y-C, He S, Chen S, Fu Y, Brown KN, Yao X-H, Ma J, Gao KP, Sosinsky GE, Huang K, Shi S-H. 2012. Preferential electrical coupling regulates neocortical lineage-dependent microcircuit assembly. Nature. 486(7401):113–117. https://doi.org/10.1038/nature10958

-Z-

Zhan X-L, Clemens JC, Neves G, Hattori D, Flanagan JJ, Hummel T, Vasconcelos ML, Chess A, Zipursky SL. 2004. Analysis of Dscam Diversity in Regulating Axon Guidance in Drosophila Mushroom Bodies. Neuron. 43(5):673–686. https://doi.org/10.1016/j.neuron.2004.07.020

Zhang H, Tang X, Feng C, Gao Y, Hong Q, Zhang J, Zhang X, Zheng Q, Lin J, Liu X, Shen L. 2023. The use of data independent acquisition based proteomic analysis and machine learning to reveal potential biomarkers for autism spectrum disorder. Journal of Proteomics. 278:104872. https://doi.org/10.1016/j.jprot.2023.104872

Zhang L, Goldman JE. 1996. Generation of cerebellar interneurons from dividing progenitors in white matter. Neuron. 16(1):47–54. https://doi.org/10.1016/s0896-6273(00)80022-7

Zhao H-M, Wenthold RJ, Petralia RS. 1998. Glutamate Receptor Targeting to Synaptic Populations on Purkinje Cells Is Developmentally Regulated. J Neurosci. 18(14):5517–5528. https://doi.org/10.1523/JNEUROSCI.18-14-05517.1998

Zhu F, Cizeron M, Qiu Z, Benavides-Piccione R, Kopanitsa MV, Skene NG, Koniaris B, DeFelipe J, Fransén E, Komiyama NH, Grant SGN. 2018. Architecture of the Mouse Brain Synaptome. Neuron. 99(4):781-799.e10. https://doi.org/10.1016/j.neuron.2018.07.007

Zipursky SL, Sanes JR. 2010. Chemoaffinity Revisited: Dscams, Protocadherins, and Neural Circuit Assembly. Cell. 143(3):343–353. https://doi.org/10.1016/j.cell.2010.10.009

Zong H, Espinosa JS, Su HH, Muzumdar MD, Luo L. 2005. Mosaic Analysis with Double Markers in Mice. Cell. 121(3):479–492. https://doi.org/10.1016/j.cell.2005.02.012

SUMMARY

Brain function is based on the establishment of highly stereotyped neuronal networks through precise and diverse synaptic contacts. Understanding what controls synapse specificity and identity is thus mandatory not only to understand brain functions but also the etiology of synaptopathies such as autism spectrum disorders or schizophrenia. While Sperry postulated the chemo-affinity hypothesis in the 1960s, implying a molecular combination for each synapse type in the assembly of neural circuits, the existence and nature of these combinations have not been demonstrated. To address this question, I focused on the olivo-cerebellar network involved in the control of motor function and cognitive processes. In this well characterized circuit, two different excitatory inputs, the climbing fibers and the parallel fibers, connect the same target neuron, the Purkinje cell, initially on the same territory and then on distinct and non-overlapping territories in the mature stage. It is therefore an ideal model to study the molecular basis of synapse identity. Based on previous data from our laboratory and others, the expression of a specific C1Q-related protein in each input is necessary, but not sufficient, for proper formation of climbing fibers and parallel fibers synapses on Purkinje cells. Loss of function of the specific C1Q-related protein at each input, CBLN1 at the parallel fibers and C1QL1 at the climbing fiber, result in the loss of about half of the respective synapses, suggesting the involvement of other molecules. Thus, I searched for the nature of this molecular combination, focusing on identifying the one coding for climbing fiber/Purkinje cell synapse identity. I combined neuron-specific transcriptomics and bioinformatics analyses followed by neuron-specific loss of function using genome editing *in vivo* during mouse development. I have identified a combination of presynaptic secreted molecules underlying the identity of the climbing fiber/Purkinje cell synapses. Surprisingly, I have also discovered that this specific code is generated, during postnatal development, in an afferent-specific manner starting from a common code. Climbing fibers actively and gradually specify their synaptic molecular identity while parallel fibers rely on the “original common code”. This result suggests that synapse molecular diversification follows input-specific molecular rules. Finally, I am currently testing whether the specification of the molecular code is regulated by neuronal activity during postnatal development. This study represents an unprecedented dissection of the mechanisms controlling circuit development at a single neuron type level with important consequences for our understanding of the etiology of neurodevelopmental disorders.